

Physics and Astronomy

**History and characterization of atmospheric
black carbon in the Anthropocene**

Aja Anne Ellis

This thesis is presented for the Degree of

**Doctor of Philosophy
of
Curtin University**

February 2017

Declaration

To the best of my knowledge and belief this thesis contains no material previously published by any other person except where due acknowledgment has been made. This thesis contains no material that has been accepted for the award of any other degree or diploma in any university

A handwritten signature in black ink, appearing to read 'Aja Ellis', written over a faint circular stamp.

Aja Ellis

14 February, 2017

Abstract

Black carbon aerosols (BC) are emitted by biomass burning and fossil fuel combustion and are present throughout the troposphere and the stratosphere. These aerosols have substantial direct and indirect effects on the atmosphere and climate and contribute to climate sensitivity and future climate change estimate uncertainties. Tropospheric BC has a relatively short residence time in the atmosphere (days to weeks) and exhibits large spatial and temporal gradients associated with emission sources, atmospheric transport, aging, and wet deposition. Once emitted, BC absorbs solar radiation warming the surrounding atmosphere and altering atmospheric circulation and cloud properties. Deposited to snowfields, ice caps, and alpine glaciers, BC reduces surface albedo and enhances surface melt, changing the energy balance of the glacier. Before the advent of fossil fuel combustion, BC emissions were from biomass burning due to both human activity and natural variability. Past BC emissions and the resulting atmospheric distribution are largely unconstrained. Greater knowledge of past BC is required to reduce uncertainties in climate sensitivity estimates. This thesis investigates long-range transported BC in the Southern Hemisphere using the Antarctic ice cap as an archive for BC from the recent past to the late 19th Century. The deposition rates and characteristics of BC in Australian rainfall were also studied to investigate wet removal rates and latitudinal differences in wet deposited BC particle morphology, chemical composition, and insoluble coatings.

Mass concentrations of BC in Antarctic snow and ice are extremely low, typically at the parts-per-trillion level. Detailed analysis of individual BC particles required the development of new methods to concentrate and isolate BC for analysis by electron microscopy. This investigation resulted in the first elemental analysis of BC in Antarctic ice and revealed new information on tropical and Antarctic BC size, morphology and chemical impurities from ice core samples spanning the industrial revolution. As part of the International Roosevelt Island Climate Evolution Project (RICE), an annual BC deposition time series spanning 1887 to 2012 CE was reconstructed to investigate spatial and temporal variability. The time series included BC concentrations from two overlapping ice cores and two snow pits. The ice core and snow pit records revealed a significant increase in BC deposition to Roosevelt Island, West Antarctica, from 1990 CE through 2013 CE, likely due to a change in BC emissions combined with changes in atmospheric circulation. Comparison with previously published BC data from the West Antarctic Ice Sheet Divide (WAIS) ice core revealed that decadal

variability in concentration and deposition to the two sites is inversely correlated. We conclude that the inverse correlation between the two records is likely due to decadal shifts in the location and intensity of the Amundsen Sea Low in response to El Niño-Southern Oscillation.

Acknowledgements

Great thanks to my advisor Ross Edwards for the opportunity to work on such an interesting and significant project, and for his support and supervision. This project would have been impossible without the steadfast support and funding from Curtin University Physics and Astronomy, Office for Research, the School of Science, the TRACE facility and the Curtin University Microscopy & Microanalysis Facility. Invaluable scientific and technical assistance was received from Australian Microscopy & Microanalysis Research Facility at the Centre for Microscopy, Characterisation & Analysis, University of Western Australia. Funding for the project included Australian Antarctic Science grant 4144 (to R. Edwards), Australian Research Council LIEF grant LE130100029 (to R. Edwards.), Curtin University Senior Research Fellowships RES-SE-DAP-AW-47679-1 and RES-52688 (both to R. Edwards). Postgraduate scholarship funding was from Curtin University and the Agilent Foundation and Australian Antarctic Science grant 4144 (to R. Edwards).

I would like to acknowledge the thoughtful contributions and advice from committee members, R. Subramanian, Rajan Chakrabarty, and Arie van Riessen, and to Brendan McGann for the unwavering support over the years. I extend particular thanks to Subu for the immense and continuing support.

Special thanks to Nancy Bertler and the entire RICE team for the opportunity of a lifetime, and the great pleasure of working with such an inspiring group.

To my colleague and friend Holly Winton, for our many academic and non-academic conversations and for bringing the sunshine to the lab.

Thanks to my family for all the love and support, and to Taylor and Nick.

And finally, to Emily.

Table of Contents

Declaration.....	ii
Abstract.....	iii
Acknowledgements	v
Table of Contents	vi
List of publications included as part of this thesis	x
List of additional publications and conference proceedings relevant to this thesis.....	xi
Fieldwork completed as part of this thesis	xii
List of Abbreviations	xiii
List of Figures.....	xv
List of Tables	xxii
Chapter 1. Introduction	1
1.1 Significance and Rationale – Black carbon in the Southern Hemisphere	1
1.2 Research Objectives.....	1
1.3 Thesis Structure	3
1.4 References.....	4
Chapter 2. Literature review	5
2.1 Introduction.....	5
2.2 Black Carbon in the atmosphere	6
2.2.1 Sources of black carbon	6
2.2.2 Measurement techniques.....	7
2.2.3 Behavior in the atmosphere: BC particle evolution.....	8
2.2.4 Behavior in the atmosphere: transport, distribution, and removal.....	9
2.3 Black carbon in the cryosphere.....	12
2.3.1 Transport to the Antarctic atmosphere.....	13
2.3.2 Ice cores	15
2.3.3 Historical records of atmospheric black carbon.....	16
2.4 Global significance	17
2.4.1 Role of black carbon in global climate models.....	17

2.4.2	Black carbon in the changing climate	19
	References.....	21
Chapter 3. Characterizing black carbon in rain and ice cores using coupled tangential flow filtration and transmission electron microscopy		
		31
	Abstract.....	31
3.1	Introduction.....	32
3.2	Methodology	34
3.2.1	Clean room laboratory environment	34
3.2.2	Reagents and materials	35
3.2.3	Instrumentation	35
3.2.4	Samples	36
3.2.5	Decontamination and concentration method	37
3.2.6	Particle characterization using electron microscopy.....	40
3.2.7	Testing the cleanliness of the system.....	40
3.3	Results and Discussion	41
3.3.1	Blanks	41
3.3.2	Tangential flow filtration	41
3.3.3	Transmission electron microscopy	43
3.4	Conclusion	47
	Acknowledgements.....	48
	References.....	49
	Supplementary Information	53
Chapter 4. Individual particle morphology, coatings, and impurities of black carbon aerosols in Antarctic ice and tropical rainfall		
		55
	Abstract.....	55
4.1	Introduction.....	56
4.2	Materials and Methods.....	58
4.2.1	Ice core samples	58
4.2.2	Rain samples	58
4.2.3	Ice core decontamination and liquid preconcentration	58
4.2.4	TEM characterization.....	59
4.3	Results.....	59

4.4	Conclusions.....	67
	Acknowledgments, Samples, and Data.....	68
	References.....	69
	Supplementary Information	73
Chapter 5. Roosevelt Island Climate Evolution Project: Black carbon deposition to Roosevelt Island, West Antarctica approaches Arctic levels.....		94
	Abstract.....	94
5.1	Introduction.....	95
5.2	Methods.....	97
5.2.1	Ice core and snow pit samples	97
5.2.2	Sample analysis.....	98
5.2.3	Ice core and snow pit timescales.....	99
5.2.4	Flux calculations	99
5.3	Results and Discussion	100
5.3.1	Correlation of rBC concentrations across snow pits and ice cores.....	100
5.3.2	Comparison of snow pits and ice core records with GFED 4.1 fire emission estimates.....	102
5.3.3	RICE Ice core 20 th Century trend.	103
5.3.4	Potential causes of increase in rBC deposition to Roosevelt Island	105
5.4	Conclusions.....	107
	Acknowledgements.....	108
	References.....	109
	Supplementary Information	114
Chapter 6. Black carbon in rain: case studies from northern and western Australia .117		
	Abstract.....	117
6.1	Introduction.....	118
6.2	Methods.....	120
6.2.1	Sample collection and handling.....	120
6.2.2	TEM imaging	122
6.2.3	SP2 analysis	122
6.2.4	Uncertainty.....	122
6.3	Results and Discussion	123

6.3.1	Black carbon wet deposition in Darwin, Northern Territory and Perth, Western Australia	123
6.3.2	Particle characterization using electron microscopy.....	128
6.4	Conclusions.....	132
	Acknowledgements.....	133
	References.....	134
	Supplementary Information	137
Chapter 7. Thesis summary and conclusions		149
7.1	Summary and significance.....	149
7.2	Future work.....	151
Chapter 8. Bibliography		152
Appendix A. Statements of Co-Author Contributions		169
	Appendix A1: Statement of contribution for paper 1	169
	Appendix A2: Statement of contribution for paper 2	171
Appendix B. Copyright agreements for published papers.....		173
Appendix C. Reprinted published papers		174
Appendix D. Permissions to reproduce figures.....		175

List of publications included as part of this thesis

This thesis compiles a collection of research papers that are published or in preparation at the time of submission. The objectives of the papers are detailed in the introductory chapter, and connections and contextual integration of the research presented in each paper is detailed in the concluding chapter. A statement of co-authorship for each published paper is in Appendix A. Published papers 1 and 2 are reprinted in Appendix C. Published papers and manuscripts include:

1. **Ellis, A.**, Edwards, R., Saunders, M., Chakrabarty, R. K., Subramanian, R., van Riessen, A., Smith, A. M., Lambrinidis, D., Nunes, L. J., Vallelonga, P., Goodwin, I. D., Moy, A. D., Curran, M. A. J., and van Ommen, T. D. (2015). Characterizing black carbon in rain and ice cores using coupled tangential flow filtration and transmission electron microscopy. *Atmospheric Measurement Techniques*, 8(9), 3959-3969.
2. **Ellis, A.**, Edwards, R., Saunders, M., Chakrabarty, R. K., Subramanian, N. E. Timms, R., van Riessen, A., Smith, A. M., Lambrinidis, D., Nunes, L. J., Vallelonga, P., Goodwin, I. D., Moy, A. D., Curran, M. A. J., and van Ommen, T. D. (2016). Individual particle morphology, coatings, and impurities of black carbon aerosols in Antarctic ice, *Geophysical Research Letters*, 43(22), 11,875–11,883.
3. **Ellis, A.**, Edwards, R. Roosevelt Island Climate Evolution Project: Black carbon deposition to Roosevelt Island, West Antarctica approaches Arctic levels (in preparation, to be submitted to *Journal of Geophysical Research: Atmospheres*).
4. **Ellis, A.**, Edwards, R. Black carbon in rain: case studies from northern and western Australia (in preparation, to be submitted to *Journal of Geophysical Research: Atmospheres*).

List of additional publications and conference proceedings relevant to this thesis

A list of additional publications and conference proceedings are included below but not included as part of this thesis, as I was not the lead author on the study or because it is a conference abstract.

1. Winton, V. H. L., Edwards, R., Delmonte, B., **Ellis, A.**, Andersson, P. S., Bowie, A., Bertler, N. A. N., Neff, P., & Tuohy, A. (2016). Multiple sources of soluble atmospheric iron to Antarctic waters. *Global Biogeochemical Cycles*, 30(3), 421-437.

This paper details the sources of soluble iron deposition in the Ross Sea using snow pit samples from Roosevelt Island on the Ross Ice Shelf. Additional data from this field campaign is included in Chapter 5 of this thesis. I assisted with the analysis and interpretation of the black carbon record included in this paper.

2. **Ellis, A.**, Edwards, R., Bertler, N., Winton, V.H.L., Goodwin, I., Neff, P., Touhy, A., Proemse, B., Hogan, C., Feiteng, W. “RICE ice core: Black Carbon reflects climate variability at Roosevelt Island, West Antarctica.” Abstract EGU2015-8367, European Geophysical Union General Assembly, Vienna, 12 April 2015.

This is a poster presentation regarding the work detailed in Chapter 5.

3. **Ellis, A.**, Edwards, R., Van Riessen, A., Saunders, M., Smith, A. M., Curran, M. A., Goodwin, I. D., Feiteng, W. “Characterization of insoluble nanoparticles in Antarctic ice cores” Abstract C43B-0665, American Geophysical Union Fall Meeting, San Francisco, 9 December 2013.

This is a poster presentation regarding the work detailed in Chapter 4.

4. **Ellis, A.**, Edwards, R., Van Riessen, A., Saunders, M., Smith, A. M., Curran, M. A., Goodwin, I. D., Feiteng, W. “Characterization of insoluble nanoparticles in ice cores from Law Dome, East Antarctic.” Poster presentation at Strategic Science in Antarctica conference, Hobart, 24 June 2013.

This is a poster presentation regarding the work detailed in Chapter 3.

Fieldwork completed as part of this thesis

Several field campaigns were conducted to obtain or analyze samples for the purpose of this thesis, detailed below:

1. August – September 2012, CFA Ice Core Analysis, Roosevelt Island Climate Evolution (RICE) project, Wellington, NZ

I participated in an ice core analysis campaign conducted at GNS Science in Wellington, NZ, to analyze the top portion of the RICE ice core drilled during the austral 2011/2012 Antarctic field season. Data obtained during this analysis campaign is included in Chapter 5.

2. October 2012 – January 2013, Antarctica deep fieldwork, Roosevelt Island Climate Evolution (RICE) project

I participated in an extended field season involving drilling and processing of an ice core and conducting snow pit and fresh snow sampling as part of the RICE research team. Samples resulting from this field season were analyzed at Curtin University, Western Australia, and GNS Science, Wellington, NZ. Snow pit and ice core data from this field season are included in Chapter 5.

3. 2012 –2015, Rainwater sampling, Perth, Western Australia and Darwin, Northern Territory, Australia.

This fieldwork included project design and management, rainwater sampling, and laboratory analysis in order to study black carbon nanoparticles. Results from this field project are included in Chapters 3, 4, and 5.

List of Abbreviations

$\delta_{18}\text{O}$	Oxygen isotope ratio
ASL	Above sea level
ASL	Amundsen Sea low
AWS	Automatic weather station
b_{abs}	Aerosol absorption coefficient
BC	Black carbon
BOM	Bureau of Meteorology
CE	Common Era
CFA	Continuous flow analysis
ENSO	El Niño-Southern Oscillation
EELS	Electron energy loss spectrometry
EC	Elemental carbon
EDS	Energy-dispersive X-ray spectrometry
FINN	Fire Inventory from NCAR
GFED	Global Fire Emission Database
HC	Hadley circulation
HAADF	High-angle annular dark-field
HYSPLIT	Hybrid Single-Particle Lagrangian Integrated Trajectory
ICP-MS	Inductively-coupled plasma mass spectrometry
LDPE	Low-density polyethylene
MAC	Mass absorption coefficient
MAAP	Multi-Angle absorption photometer
nssS	Non-sea salt sulfur
NH	Northern Hemisphere
OC	Organic carbon
PDO	Pacific Decadal Oscillation
ppb	Parts per billion
ppm	Parts per million
ppt	Parts per trillion
PAS	Photoacoustic Spectrometer

rBC	Refractory black carbon
RICE	Roosevelt Island Climate Evolution
SEM	Scanning electron microscopy
STEM	Scanning transmission electron microscopy
SST	Sea surface temperature
SOA	Secondary organic aerosol
SP2	Single particle soot photometer
SAM	Southern Annular Mode
SH	Southern Hemisphere
TFF	Tangential flow filtration
TOA	Thermal-Optical Analysis
TOC	Total organic carbon
TRACE	Trace Research Advanced Clean Air Environment
TEM	Transmission electron microscopy
UP	Ultra-pure
WEQ	Water equivalent
WAIS	West Antarctic Ice Sheet

List of Figures

- Figure 2.1: The atmospheric evolution of a BC aggregate after emission, including (a) the uncoated, freshly emitted BC aggregate, (b) the addition of an organic matter coating to the aggregate, (c) the incorporation of sulfate aerosols into and around the coated aggregate, and (d) a 3-D reconstruction of the aged aerosol. Black, blue, and red are BC (“soot” in the original text), organic matter, and sulfate, respectively. Source: Adachi et al. (2010), reproduced with permission.9
- Figure 2.2 Black carbon emissions from (a) fossil and biofuels combustion (data from 1996), and (b) annual average of open biomass burning. Color scale is logarithmic, and units are $\text{ng m}^{-2} \text{s}^{-2}$. Source: Bond et al. (2004), reproduced with permission. 11
- Figure 2.3 Black carbon emissions by latitude and source type, showing the dramatic difference between BC sources in the Northern and Southern hemispheres, with the Northern Hemisphere consisting of predominantly industrial and residential fuel combustion, while the Southern Hemisphere is dominated by biomass burning. Source: Bond et al. (2013), reproduced with permission. 14
- Figure 3.1: Tangential flow filtration setup for concentration of rain or melted ice core sample H_2O . Water sample recirculates through the hollow fiber filter, with H_2O and dissolved species removed through open side port of filter cartridge.38
- Figure 3.2: Backflush of hollow fiber filter membrane setup, performed by stopping the peristaltic pump and injecting 1 mL of ultrapure water into the open side port using a syringe.39
- Figure 3.3: SEM image of PSL spheres from concentration method test on SiO_2/SiO coated grid surface, concentrated from $1 \mu\text{g}/\text{kg}$ to $\sim 667 \mu\text{g}/\text{kg}$ using TFF.....42
- Figure 3.4: An example of a BC aggregate with nitrogen and oxygen coating and aluminum-rich silicate inclusions from Law Dome, Antarctica ice core dated to 1759 CE. a) STEM image, scale bar = 300 nm. b-f) a series of STEM EDS maps for C, N, O, Si and Al, respectively. Element maps shown are from same field of view as image a.....43

Figure 3.5: TEM image of a particle from Darwin rain sample collected 11 April 2014, with accompanying STEM EDS maps of carbon, silicon, and aluminum. Element maps are from the same field of view as the TEM image.....	44
Figure 3.6: Examples of particles concentrated from a Law Dome, Antarctica ice core dated to 1930 CE. a) TEM image and b) EFTEM map of a complex aggregate particle where red is iron, blue is silicon, and yellow is carbon.....	45
Figure 3.7: Aged superaggregate from Darwin rain sample collected 08 April 2014. Inset is of an enlarged section of aggregate, showing individual BC sphere structure.	46
Figure S3.1: SEM image of Anopore filter after filtering 1 L of ice core melt water, and backflushing the filter to remove filtered particles.....	54
Figure 4.1: Black carbon nanospheres in Antarctic ice dated to 1838 CE: a) single BC nanosphere showing concentric ring structure with short-range internal structure, b) enlarged section of a), showing the concentric layers with 0.34 nm spacing between layers, c) BC particle with two spherules, arrows indicating spheres, and d) BC particle with three spherules, arrows indicating spheres. Additional examples of single spheres from 1759 CE and 1930 CE are included in the supporting information.....	61
Figure 4.2: TEM images and STEM-EDS maps to show compositional complexity of a black carbon aggregate, from ice dated to 1838 CE, with EDS maps taken from the same field of view as a). a) TEM image of BC aggregate, with tar ball incorporated into the aggregate, b) STEM-EDS map overlay of carbon and iron, to highlight the iron particle connected with a carbon coating, c) carbon map, d) nitrogen map, e) various aluminum-rich inclusions within the BC aggregate, f) iron map.....	63
Figure 4.3: Dust particle and BC aggregate dated to 1838 CE, with aluminum and iron dust particles incorporated within the BC aggregate, and EDS maps taken from the same field of view as a). a) TEM image, b) carbon, nitrogen, and iron STEM-EDS maps, overlaid to show the connection of the iron particles to the BC aggregate with a nitrogen-rich coating, c-f) carbon, nitrogen, aluminum, and iron STEM-EDS maps, respectively.....	64
Figure 4.4: Large silica-rich dust particle from ice dated to 1838 CE, with BC attached and mixed into the silica structure, with all components connected with thin (<5 nm), amorphous	

carbon and nitrogen rich coating, with EDS maps taken from the same field of view as a). a) TEM image, b) carbon, silicon, and nitrogen STEM-EDS maps overlaid to show connection of silicon and BC aggregates, with nitrogen-rich coating, c-f) carbon, silicon, nitrogen, and aluminum STEM-EDS maps, respectively. 65

Figure 4.5: BC aggregate from ice dated to 1930 CE attached to aluminosilicate and iron particles with nitrogen-rich coating, with EDS map taken from the same field of view as a). a) High-angle annular dark-field (HAADF) image of the particle, b) energy-dispersive x-ray spectroscopy (EDS) maps of C, Al, Fe, and N, indicating the aluminosilicate and iron particles are attached to the black carbon aggregate with a nitrogen-rich coating. 66

Figure 4.6: a) High-angle annular dark-field (HAADF) image of a tar ball from ice dated to 1838 CE with BC aggregate attached, b) EDS map of carbon from the same field of view as a). Additional EDS maps are included in the supporting information. 67

Figure S4.1: Additional image of a single BC spheres found in an ice core dated to 1759 CE 74

Figure S4.2: Additional image of a single BC sphere found in a rain sample collected in Darwin, Northern Territory, Australia on April 11, 2014. 75

Figure S4.3: Additional HAADF image for Figure 4.2. 76

Figure S4.4: Additional STEM-EDS maps for Figure 4.2. 77

Figure S4.5: Additional HAADF image for Figure 4.3. 78

Figure S4.6: Additional STEM-EDS maps for Figure 4.3. 79

Figure S4.7: Additional HAADF image for Figure 4.4. 80

Figure S4.8. Additional STEM-EDS maps for Figure 4.4. 81

Figure S4.9: Additional STEM-EDS map for Figure 4.5. 82

Figure S4.10: Additional STEM-EDS maps for Figure 4.6. 83

Figure S4.11: Additional STEM-EDS maps for Figure 4.6. 84

Figure S4.12: HYSPLIT back-trajectories of air-mass transport to Darwin, Northern Territories, Australia for April 4, 2014 for a final atmospheric height of 500 m above ground level.....	85
Figure S4.13: HYSPLIT back-trajectories of air-mass transport to Darwin, Northern Territories, Australia for April 4, 2014 for a final atmospheric height of 1000 m above ground level.....	86
Figure S4.14: HYSPLIT back-trajectories of air-mass transport to Darwin, Northern Territories, Australia for April 4, 2014 for a final atmospheric height of 2000 m above ground level.....	87
Figure S4.15: HYSPLIT back-trajectories of air-mass transport to Darwin, Northern Territories, Australia for April 8, 2014 for a final atmospheric height of 500 m above ground level.....	88
Figure S4.16: HYSPLIT back-trajectories of air-mass transport to Darwin, Northern Territories, Australia for April 8, 2014 for a final atmospheric height of 1000 m above ground level.....	89
Figure S4.17: HYSPLIT back-trajectories of air-mass transport to Darwin, Northern Territories, Australia for April 8, 2014 for a final atmospheric height of 2000 m above ground level.....	90
Figure S4.18: HYSPLIT back-trajectories of air-mass transport to Darwin, Northern Territories, Australia for April 11, 2014 for a final atmospheric height of 500 m above ground level.....	91
Figure S4.19: HYSPLIT back-trajectories of air-mass transport to Darwin, Northern Territories, Australia for April 11, 2014 for a final atmospheric height of 1000 m above ground level.	92
Figure S4.20: HYSPLIT back-trajectories of air-mass transport to Darwin, Northern Territories, Australia for April 4, April 8, and April 22, 2014 for final atmospheric heights of 500 m, 1000 m, and 2000 m above ground level.....	93

Figure 5.1 Map of Antarctica, with location of Roosevelt Island noted on the Ross Ice Shelf, West Antarctica. Another prominent ice core location, WAIS Divide on the West Antarctic Ice Sheet, is also noted for comparison.96

Figure 5.2 RICE BC records RICE ice core (black) and snow pit records (Winton snow pit blue and Ellis snow pit red). RICE ice core has been resampled to monthly resolution. Snow pit records have not been resampled. 100

Figure 5.3. RICE ice core and snow pit BC records and GFED 4.1 fire emissions. (a) RICE ice core (black) and snow pit records (Winton pit red and Ellis pit blue); (b) Central and eastern Australia GFED fire emissions as Tg carbon; (c) Southwestern Africa GFED fire emissions; and (d) Southeastern Australia GFED fire emissions. 102

Figure 5.4. RICE ice core and snow pit BC concentration and atmospheric flux. (a) RICE ice core (black) and snow pit records (Winton snow pit red and Ellis snow pit blue); (b) RICE ice core annual BC atmospheric flux; and (c) RICE BC atmospheric flux trend (black) and WAIS ice core BC atmospheric flux trend (red)..... 105

Figure S5.1 Configuration of RICE field camp (with generator), drill site for the main ice core (11/12A), the shallow core (12/13B) and two snow pits. 114

Figure S5.2 Depth-age scale for the shallow core 12/13B, from Ross Edwards (personal communication). 115

Figure S5.3 A comparison of monthly BC concentration (a) and annual BC flux (b) from the ice core record at Roosevelt Island. Underlying trends in both the BC flux and the monthly BC concentration are nearly identical, suggesting that annual snow accumulation variability is less of a contribution to flux than the BC concentration inter-annual variability..... 116

Figure 6.1 A map of Australia, with sampling locations marked in Perth, Western Australia, and Darwin, Northern Territory. Perth is located on the Indian Ocean with predominant winds from the West. Darwin is in close proximity to seasonal biomass burning in northern Australia and Indonesia..... 120

Figure 6.2 HYSPLIT back trajectory for the Darwin sampling site for the samples collected on 20 Feb 2015. Air mass transport was predominately over the Northern Territory, Queensland, and Western Australia before deposition in Darwin. Additional trajectories for a

starting airmass height of 500 m and 2000 m are included in the Supplementary Information.	126
Figure 6.3 HYSPLIT back trajectory for 14 March 2015, for the Perth sampling site, demonstrating transport from Western Australia mobilized by Cyclone Olwyn which passed southward along the west coast on the continent. Additional trajectories for a starting airmass height of 500 m and 2000 m are included in the Supplementary Information.	127
Figure 6.4 HYSPLIT back trajectory for 16 March 2015, for the Perth sampling site, demonstrating long-range remote transport from the Indian Ocean, a common weather pattern in Perth. Additional trajectories for a starting airmass height of 500 m and 2000 m are included in the Supplementary Information.	128
Figure 6.5 Black carbon superaggregates were found in Darwin rain, many of which are larger than the SP2 detection size range. This superaggregate was also attached to a large aluminosilicate dust particle, and contained iron spherules incorporated into the carbon aggregate (inset).....	129
Figure 6.6 A black carbon aggregate from Darwin rain with multiple distinct carbon morphologies present and iron spherules attached to the carbon aggregate (bottom-right)..	130
Figure 6.7 HAADF image of the black carbon aggregate in Figure 6.5 (top), along with STEM-EDS spectra maps of carbon (bottom-left) and iron (bottom-right).	131
Figure S6.1 HYSPLIT back trajectory for Perth, 14 March 2015 with starting height of 500 m.	137
Figure S6.2 HYSPLIT back trajectory for Perth, 14 March 2015 with starting height of 2000 m.	138
Figure S6.3 HYSPLIT back trajectory for Perth, 15 March 2015 with starting height of 500 m.	139
Figure S6.4 HYSPLIT back trajectory for Perth, 15 March 2015 with starting height of 1000 m.	140
Figure S6.5 HYSPLIT back trajectory for Perth, 15 March 2015 with starting height of 2000 m.	141

Figure S6.6 HYSPLIT back trajectory for Perth, 16 March 2015 with starting height of 2000 m.	142
Figure S6.7 HYSPLIT back trajectory for Darwin, 25 November 2014 with starting height of 1000 m.	143
Figure S6.8 HYSPLIT back trajectory for Darwin, 23 November 2014 with starting height of 1000 m.	144
Figure S6.9 HYSPLIT back trajectory for Darwin, 30 January 2015 with starting height of 1000 m.	145
Figure S6.10 HYSPLIT back trajectory for Darwin, 23 February 2015 with starting height of 1000 m.	146
Figure S6.11 HYSPLIT back trajectory for Darwin, 24 February 2015 with starting height of 1000 m.	147

List of Tables

Table 6.1 rBC concentrations and deposition rates from individual rain events collected in Darwin, Northern Territory and Perth, Western Australia.	125
Table 6.2 rBC concentrations from individual rain events and extrapolated deposition rates calculated from 24-hour rainfall measurements in Darwin, Northern Territory and Perth, Western Australia.....	125

Chapter 1. Introduction

1.1 Significance and Rationale – Black carbon in the Southern Hemisphere

Black carbon aerosol particles (BC) affect the climate in multiple ways, including optical absorption, snow albedo reduction, and atmospheric chemistry effects. BC is produced by biomass burning and fossil fuel combustion, and is irregularly distributed in the atmosphere. While there are a growing number of modeling studies regarding the atmospheric transport and climate forcing of these particles, models are limited by the lack of spatially distributed data of depositional flux (Bond et al., 2013). The interaction of BC with water and its removal from the atmosphere by wet deposition is crucial to understanding BC residence times in the atmosphere, and consequently its variability in the atmosphere. However, there is a distinct lack of knowledge on BC particles in snow and rain. Consequently, the models poorly represent the temporal evolution of BC particles and deposition rates during atmospheric transport. The Southern Hemisphere is distinct from the Northern Hemisphere in that emissions are dominated by biomass burning (Lamarque et al., 2010). Little is known regarding the recent history of BC aerosols in the atmosphere of the Southern Hemisphere. Ice caps contain the only reliable record of BC in the past atmosphere.

1.2 Research Objectives

This thesis aims to investigate the history and physical characteristics of black carbon aerosols in the southern hemisphere from the late 19th century to the near-present. This is achieved by studying past precipitation in the form of Antarctic snow and ice, as well as modern rain samples from two different Australian sites.

The following outline describes the primary objections of this research, sample selection, and employed techniques.

1. Develop a method to isolate and characterize black carbon aerosols present in trace concentrations in rainwater, snow, and ice samples (Chapter 3);

- a. Sample selection: Archived ice core samples previously drilled on Law Dome, East Antarctica during the 2005/2006 austral summer (collected by A. Smith, 2005-2006).
 - b. Isolate ultra-trace concentrations of black carbon aerosols in Australian rain and Antarctic ice.
 - c. Validate the method using electron microscopy.
2. Characterize historical black carbon particles in Antarctic ice dated to pre- to post-industrialization of the Southern Hemisphere and in modern precipitation (Chapter 4);
 - a. Sample selection: Archived ice core samples previously drilled on Law Dome, East Antarctica during the 2005/2006 austral summer (collected by A. Smith, 2005-2006). Australian rain samples were collected for this study in Darwin, Northern Territories.
 - b. Using the method described in Chapter 3, identify and characterize black carbon particles using electron microscopy, detailing the variability in black carbon particles found in historic ice core samples from 1759, 1838, and 1930 CE as well as modern rainwater samples.
3. Investigate the record of black carbon deposition in West Antarctica and identify the variables in long-range transported particle deposition over the 20th century (Chapter 5);
 - a. Sample selection: Ross Ice Shelf ice, firn, and snow pit samples collected during the 2011/2012 and 2012/2013 austral summers as part of the Roosevelt Island Climate Evolution (RICE) project.
 - b. Quantify BC concentrations from 1890 CE to 2013 CE using the single-particle soot photometer (SP2).
4. Investigate deposition of black carbon particles in rain, including particle morphology and flux (Chapter 6).
 - a. Sample selection: Australian rain samples were collected for this project in Darwin, Northern Territories and Perth, Western Australia.
 - b. Study the wet deposition of black carbon in rain through flux measurements using the SP2 and particle characterization using the methods developed in Chapters 1 and 2.

1.3 Thesis Structure

This main body of this thesis is presented as a series of manuscripts, including one published paper, one submitted paper, and two papers in preparation for submission. Due to the format of this thesis as a collection of intended publications, there is some repetition of concepts within the text.

Chapter 1: Introduction

This chapter introduces the topic of black carbon in the southern hemisphere, describes the research objectives, and outlines the structure of this thesis.

Chapter 2: Literature Review

This chapter provides a review of the role of black carbon in the atmosphere and the variety of methods used to quantify it.

Chapter 3: Paper 1

Ellis, A., R. Edwards, M. Saunders, R. K. Chakrabarty, R. Subramanian, A. van Riessen, A. M. Smith, D. Lambrinidis, L. J. Nunes, P. Vallelonga, I. D. Goodwin, A. D. Moy, M. A. J. Curran and T. D. van Ommen (2015). Characterizing black carbon in rain and ice cores using coupled tangential flow filtration and transmission electron microscopy, *Atmospheric Measurement Techniques*, 8(9), 3959-3969. doi:10.5194/amt-8-3959-2015

Chapter 4: Paper 2

Ellis, A., Edwards, R., Saunders, M., Chakrabarty, R. K., Subramanian, R., Timms, N. E., van Riessen, A., Smith, A. M., Lambrinidis, D., Nunes, L. J., Vallelonga, P., Goodwin, I. D., Moy, A. D., Curran, M. A. J., & van Ommen, T. D. (2016). Individual particle morphology, coatings, and impurities of black carbon aerosols in Antarctic ice and tropical rainfall. *Geophysical Research Letters*, 43(22), 11,875-811,883. doi:10.1002/2016GL071042

Chapter 5: Paper 3

Roosevelt Island Climate Evolution Project: Black carbon deposition to Roosevelt Island, West Antarctica approaches Arctic levels (to be submitted to *Journal of Geophysical Research: Atmospheres*).

Chapter 6: Paper 4

Black carbon in rain: case studies from northern and western Australia (to be submitted to *Journal of Geophysical Research: Atmospheres*).

Chapter 7: Conclusions

This chapter describes and connects the results of the studies detailed in Chapters 3-6, and addresses the objectives outlined above. These results are also placed in the greater context of black carbon literature.

Chapter 8: Bibliography

Copyright agreements were obtained in order to reproduce publications, text, and images from publications resulting from this thesis. Copyright agreements can be found in Appendix B.

1.4 References

Bond, T. C., Doherty, S. J., Fahey, D. W., Forster, P. M., Berntsen, T., DeAngelo, B. J., Flanner, M. G., Ghan, S., Kärcher, B., Koch, D., Kinne, S., Kondo, Y., Quinn, P. K., Sarofim, M. C., Schultz, M. G., Schulz, M., Venkataraman, C., Zhang, H., Zhang, S., Bellouin, N., Guttikunda, S. K., Hopke, P. K., Jacobson, M. Z., Kaiser, J. W., Klimont, Z., Lohmann, U., Schwarz, J. P., Shindell, D., Storelvmo, T., Warren, S. G., & Zender, C. S. (2013). Bounding the role of black carbon in the climate system: A scientific assessment. *Journal of Geophysical Research: Atmospheres*, 118(11), 5380-5552.

Lamarque, J. F., Bond, T. C., Eyring, V., Granier, C., Heil, A., Klimont, Z., Lee, D., Liousse, C., Mieville, A., Owen, B., Schultz, M. G., Shindell, D., Smith, S. J., Stehfest, E., Van Aardenne, J., Cooper, O. R., Kainuma, M., Mahowald, N., McConnell, J. R., Naik, V., Riahi, K., & van Vuuren, D. P. (2010). Historical (1850–2000) gridded anthropogenic and biomass burning emissions of reactive gases and aerosols: methodology and application. *Atmos. Chem. Phys.*, 10(15), 7017-7039.

Chapter 2. Literature review

2.1 Introduction

Black carbon nanoparticles (BC) pervade the Earth system and are present throughout the atmosphere, soils and sediments, and terrestrial waters. They are formed through incomplete combustion of fuel sources, including human use of fossil fuels and solid fuels and biomass burning (Murr, 2008). BC is transported as atmospheric aerosols and are found in high concentrations in the urban environment. It constitutes a substantial portion of particulate matter (PM) in the <2.5 nm particle diameter range, and has been linked to significant health risks in urban environments (IPCC, 2013; Janssen et al., 2011).

BC can be transported on a hemispheric scale in the troposphere and globally in the stratosphere (Koch et al., 2007; Koch & Hansen, 2005), and is found in both remote deep ocean sediments and glacial snow and ice (Schmidt & Noack, 2000; Warren & Clarke, 1990). The presence of BC in the atmosphere influences regional and global climate (Bond et al., 2013; Ramanathan & Carmichael, 2008). These aerosol particles impact the radiative, physical, and chemical properties of the atmosphere, affecting climate directly due to solar radiation absorption and indirectly through changes in cloud formation and structure (Hansen et al., 2000; Jacobson, 2000; McFiggans et al., 2006). When deposited to snow and ice, BC decreases surface albedo and contributes to surface melting (Flanner et al., 2007; Hansen & Nazarenko, 2004; Quinn et al., 2008). Historic records of BC are needed to understand past emissions, atmospheric distribution, and deposition, and ice cores contain those records.

The global climate forcing impact of BC is studied using General Circulation Models (GCMs). However, there are large uncertainties associated with these studies due to incomplete understanding of BC emissions, physical and chemical processes in the atmosphere, and removal rates (Koch et al., 2007; Reddy & Boucher, 2007; Stier et al., 2007). Small changes in the BC characteristics used by particle-resolved models can have large effects on model results (Fierce et al., 2016; Hodnebrog et al., 2014), suggesting that accurate particle studies in both local and remote environments are critical to understanding the global significance of BC.

2.2 Black Carbon in the atmosphere

2.2.1 Sources of black carbon

Black carbon is composed of primary particles formed from the gaseous products of incomplete combustion. Primary particles are comprised of ~30 nm concentric-layered, semi-graphitic carbon spherules joined into larger, semi-fractal aggregates (Li et al., 2003). Combustion sources include fossil fuels, solid fuels, and biomass burning. Fuel source, combustion temperature, oxygen availability, and atmospheric turbulence can all affect the characteristics of primary BC particles and the extent of graphitization of the carbon spheres (Murr, 2008).

Black carbon is a common component of 'soot,' though both have various definitions in the literature (Bond et al., 2013). Ramanathan and Carmichael (2008) describe soot as the combination of BC (light-absorbing elemental carbon particles) and various organics condensed from the gas phase.

There has been some inconsistency in the history of naming and identification of black carbon, so in this text we adopt the criteria listed in (Bond et al., 2013), namely that:

- the primary particles are refractory, with a vaporization temperature of 4000 K;
- the primary spheres cluster into larger aggregate particles;
- aggregates are insoluble in organic solvents as well as water;
- aggregates have strong absorption of visible light of at least $5 \text{ m}^2 \text{ g}^{-1}$ at 550 nm (Bond & Bergstrom, 2006);
- the refractive index of BC is constant across the visible spectrum.

The lack of consistency with BC terminology has limited the ability to compare measurements and modeling results, as studies have often included a broader range of particles than this definition.

2.2.2 Measurement techniques

There have been many methods used to measure BC concentrations in the atmosphere, including optical absorption, thermal-optical analysis, laser-induced incandescence, photoacoustic spectrometry, and aerosol mass spectrometry (Moosmuller et al., 2009; Slowik et al., 2007). BC has also been quantified in the atmosphere using optical depth measured by absorption photometers (Sato et al., 2003). As these methods measure different properties of BC, quantitative intercomparison of different study results must consider potentially large discrepancies in measurements (Slowik et al., 2007).

Thermal-optical analysis (TOA) is a quartz filter-based technique to measure the organic carbon (OC) and elemental carbon (EC) fractions of aerosol samples (Birch & Cary, 1996; Chow et al., 2007; Jeong et al., 2004). Optical absorption instruments measure the aerosol absorption coefficient (b_{abs}) by depositing aerosols on a quartz filter and optically measuring the change in transmittance through the filter. Instruments include the aethalometer and the Multi-Angle Absorption Photometer (MAAP). This method is limited, however, in converting optical measurements to BC mass by the conversion factor used in instrument calibration.

The radiative impact of BC is often discussed in terms of mixing state, or how the BC aggregate has been incorporated into or onto complex aerosol particles including sulfates and organic material. Mixing state and coating can have substantial effects on BC absorption, thereby affecting the resulting concentrations from optical measurement techniques such as the aethalometer and MAAP (Knox et al., 2009).

Single particle mass concentration and particle size can be measured in real-time by single particle intra-cavity laser-induced incandescence (SP2, Droplet Measurement Technologies, Boulder, Colorado; Baumgardner et al., 2004; Stephens et al., 2003). Single particle measurements using the SP2 can detect very low concentrations of BC in the atmosphere ($\sim 10 \text{ ng m}^{-3}$). These measurements are limited by the particle size detection range of the SP2 ($\sim 100 \text{ nm}$ to 650 nm mass-equivalent diameter), but this size range represents approximately 90% of the accumulation mode of BC (Schwarz et al., 2010a). The SP2 has been used to measure BC abundance (as number and mass concentrations) in the atmosphere (Schwarz et al., 2006).

BC aggregates are small and their structure complex; therefore, the study of the individual aggregate particles has been imperative to understand their optical effects. Imaging and spectroscopy of individual particles has been facilitated by electron microscopy techniques such as scanning electron microscopy (SEM) and transmission electron microscopy (TEM). Electron microscopy technology has already shown to be a valuable resource for the study of atmospheric nanoparticles (Adachi et al., 2010), and has historically been used to characterize individual BC particles (Pósfai et al., 1999).

Transmission electron microscopy (TEM) coupled with electron energy loss spectrometry (EELS) and energy-dispersive X-ray spectrometry (EDS) have been used to determine the size, morphological, and elemental characteristics of atmospheric aerosols (Pósfai et al., 1999). Scanning transmission electron microscopy (STEM) coupled with EDS has been used to study aerosol particles (Utsunomiya & Ewing, 2003), with high-resolution imaging and STEM EDS mapping revealing nano-scale inclusions in larger aerosols that would go unnoticed with traditional TEM imaging. A recent study has also used synchrotron-generated x-rays to study the organic and inorganic composition and mixing state of urban aerosols, including BC (O'Brien et al., 2015).

Although there is substantial variation in BC aggregate morphology, there appears to be some consistency in particle formation. The atomic structure of graphitic carbon bonds, particularly the extent of sp^2 orbital hybridization, determine its strong light absorption properties (Andreae and Gelencsér, 2006). Laboratory-generated BC from fossil fuel combustion was studied using various electron microscopy methods, indicating that the average sp^2 hybridization state of the carbon atoms was consistent for coal, oil, and diesel fuels (Chen et al., 2005).

2.2.3 Behavior in the atmosphere: BC particle evolution

The physical and chemical properties of BC are highly dynamic, and evolve rapidly in the atmosphere in response to atmospheric conditions, formation conditions, and co-emitted species (Browne et al., 2015; Shen et al., 2014; Wang et al., 2014). In the atmosphere, the black carbon aggregates are mixed and coated with various organic materials, including hydrophilic coatings (Figure 2.1). The coatings and particle mixing states have a direct effect on global climate forcing through the absorption of solar radiation (Jacobson, 2001), and an indirect effect through nucleation of ice and water particles (DeMott et al., 1999; Lammel &

Novakov, 1995). Particle mixing can occur rapidly at some locations, within a few hours of emission (Moffet & Prather, 2009; Moteki et al., 2007), and can amplify the mass absorption coefficient (MAC) by a factor of up to 2.9 (Jacobson, 2012). Coatings become thicker the higher up in the atmosphere BC has travelled from the emission source, and these coatings can affect the light absorption of the atmospheric column by more than 30% (Schwarz et al., 2008).

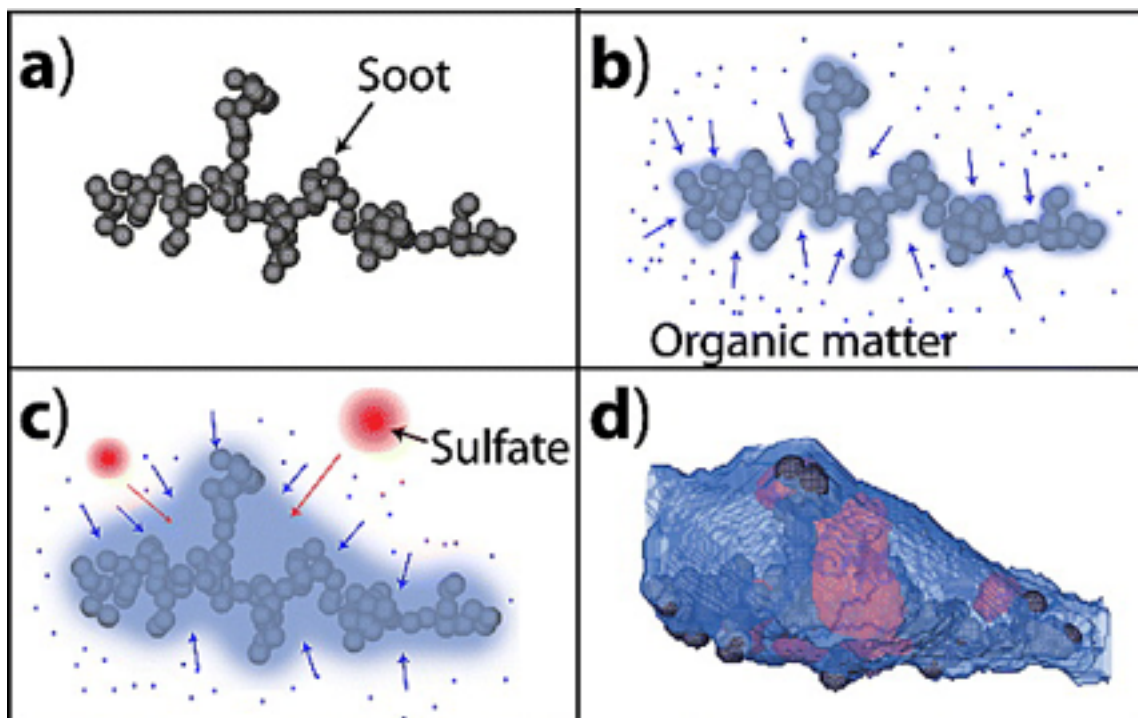


Figure 2.1: The atmospheric evolution of a BC aggregate after emission, including (a) the uncoated, freshly emitted BC aggregate, (b) the addition of an organic matter coating to the aggregate, (c) the incorporation of sulfate aerosols into and around the coated aggregate, and (d) a 3-D reconstruction of the aged aerosol. Black, blue, and red are BC (“soot” in the original text), organic matter, and sulfate, respectively. Source: Adachi et al. (2010), reproduced with permission.

2.2.4 Behavior in the atmosphere: transport, distribution, and removal

Once emitted, atmospheric nanoparticles such as BC can stay suspended from days to weeks in the troposphere and for over a year in the stratosphere (Bauer et al., 2013; Buseck & Adachi, 2008) while being transported hemispherically and globally. It is important to understand the behavior of BC in the remote atmosphere in order to better inform general

circulation models, as model estimates often vary widely from observations (Hodnebrog et al., 2014; Koch et al., 2009). Recent SP2 studies of BC aerosol loading in the atmosphere over the remote Pacific indicated significant latitudinal and vertical variability (Schwarz et al., 2010b). Additionally, modeling of the BC aging timescale constrained by observations from Schwarz et al. (2010b) indicates that different source regions have significantly different lifetimes in the atmosphere, likely due to the prevalence and composition of co-emitted species (Zhang et al., 2015).

BC particles are irregularly distributed in the atmosphere, further contributing to uncertainties in model parameters of atmospheric loading. Figure 2.2 demonstrates the strong regional variability, with large emissions from biofuels in Southeast Asia, India, Europe, and the United States (Bond et al., 2004; Ramanathan & Carmichael, 2008). In contrast, BC emissions from biomass burning dominate in the Southern Hemisphere, with seasonal bush and forest fires in South America, Africa and Australia.

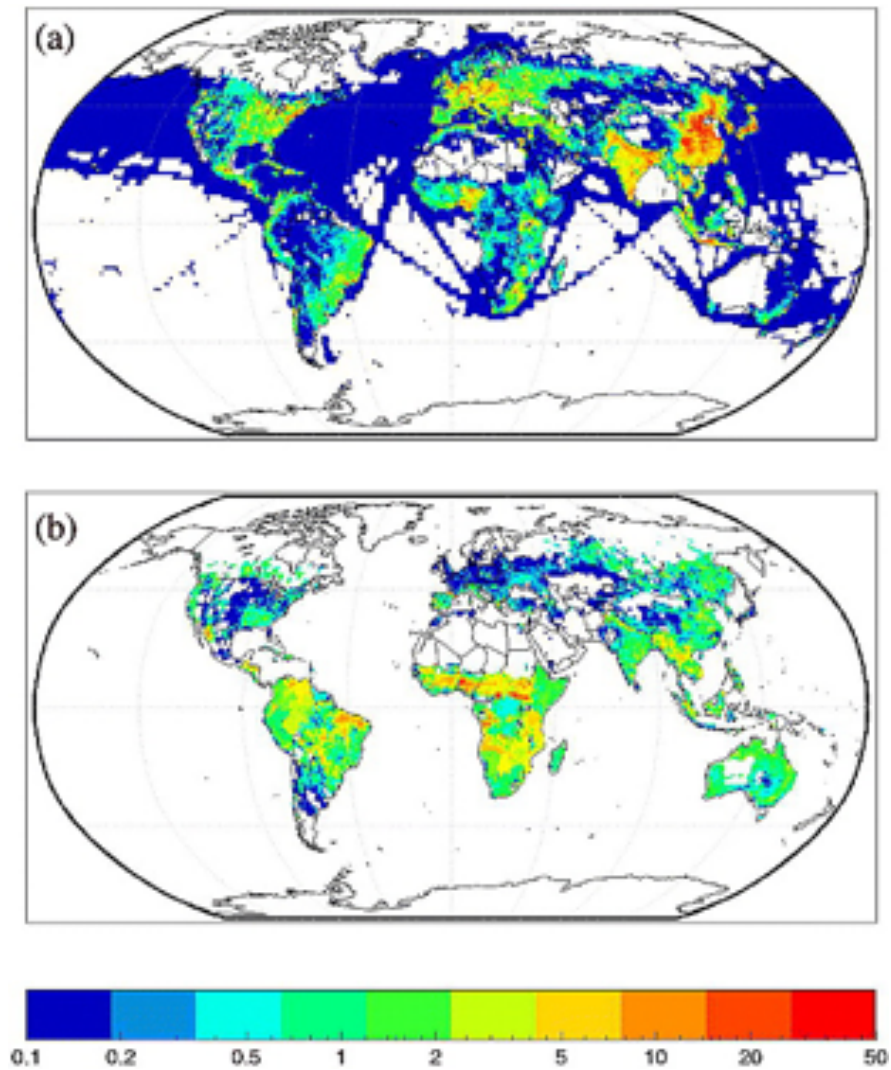


Figure 2.2 Black carbon emissions from (a) fossil and biofuels combustion (data from 1996), and (b) annual average of open biomass burning. Color scale is logarithmic, and units are $\text{ng m}^{-2} \text{s}^{-2}$. Source: Bond et al. (2004), reproduced with permission.

Carbonaceous aerosols and other particles in the accumulation mode (particle size between 100 nm and 1 μm) are removed from the atmosphere by wet and dry deposition processes. Dry deposition processes generally governing BC aerosols include gravitational sedimentation, impaction, and Brownian diffusion, whereas wet deposition describes particles removed from the atmosphere through scavenging by precipitation such as rain and snow (Seinfeld & Pandis, 2016). BC particles also function as cloud and ice nuclei (Koehler et al., 2009), providing a mechanism for nucleation scavenging. The worldwide dry deposition of BC accounts for approximately 0.46% of the total BC deposition, indicating that the overwhelming majority of BC particles are wet deposited (Jacobson, 2012). There are a

number of critical uncertainties in studying the effect of BC on the global climate, due in part to uncertainties in atmospheric removal through wet removal processes (Vignati et al., 2010).

While there are a growing number of modeling studies regarding the atmospheric transport of these particles, there is a lack of field measurement data characterizing removal rates from the atmosphere, or wet deposition flux. As a result, the models are largely unconstrained with respect to removal rates (Bauer et al., 2013). The removal of BC from the atmosphere and deposition in rain and snow has a significant effect on global climate models, as it is crucial to understanding BC residence times in the atmosphere, and consequently its influence on climate forcing (Bond et al., 2013). Deposition of BC to the ocean has also been modeled but not conclusively measured, which could be significantly aided by a study of BC in rainwater over the oceans (Jurado et al., 2008).

The ultrasonic nebulizer coupled to the SP2 system has been used in the past to measure BC particles wet deposited in rain and melted snow samples, though the effectiveness of the measurement drops substantially with larger particle size (>500 nm, Ohata et al., 2011). Consequently, studies suggest that SP2 methods to measure BC in rainwater consistently underestimate BC mass (Ohata et al., 2011; Torres et al., 2013), but systematic loss can be controlled for by using aqueous BC standards.

2.3 Black carbon in the cryosphere

Black carbon has been measured in snow packs around the world, including remote locations far from source emissions and as far as the South Pole (Hansen et al., 1988; Hegg et al., 2009; Warren & Clarke, 1990). BC plays an important and distinct role in the cryosphere, including seasonal snow packs and glaciated regions such as the Arctic, Antarctica, and alpine regions such as the Himalayas. When deposited to reflective surfaces such as snow, BC decreases the albedo of the surface, thereby absorbing heat and contributing to climate forcing (Hansen & Nazarenko, 2004; McConnell et al., 2007). Studies have suggested that BC snow concentrations as low as 10 ppb are enough to decrease snow albedo by 1%, accelerating melting (Flanner et al., 2007; Hadley & Kirchstetter, 2012; Hansen & Nazarenko, 2004), but these concentrations are unlikely in Antarctica where BC in snow has been measured in the parts-per-trillion (ppt) range (Bisiaux et al., 2012).

The IPCC Fifth Assessment Report review suggests that BC has a net climate forcing of $+0.4 \text{ W m}^{-2}$, with BC-induced darkening of snow and ice around the globe contributing an estimated $+0.04 \text{ W m}^{-2}$ (IPCC, 2013), though there are distinct regional variations in the climate forcing estimations, with one model reporting that emissions from Southeast Asia induced forcing of up to 20 W m^{-2} in regions of the Tibetan plateau (Flanner et al., 2007).

2.3.1 Transport to the Antarctic atmosphere

Latitudinal gradients are particularly pronounced in the Southern Hemisphere (SH, Figure 2.3), with emissions dominated by austral dry season fires in the tropical belt (Dwyer et al., 1998). Emissions in the lower latitudes (potential source regions for Antarctica) are also primarily from biomass burning (Lamarque et al., 2010). Biomass burning is also one of the largest sources of insoluble nanoparticle emissions in the SH (Crutzen & Andreae, 1990; Reddington et al., 2016).

Pósfai et al. (2003) detailed the complexity of particles generated by biomass burning in Southern Africa, a potential source of BC to Antarctica. The study found BC, tar balls (amorphous, carbon-rich spheres emitted from smoldering fires), and other organic aerosols in smoke plumes. Pósfai et al. (1999) conducted TEM characterization of BC aerosol particles collected in the remote Southern Ocean troposphere, near Antarctica. These particles were predominately internally mixed with sulfate aerosols and show significant atmospheric aging, as expected for long-range transported particles.

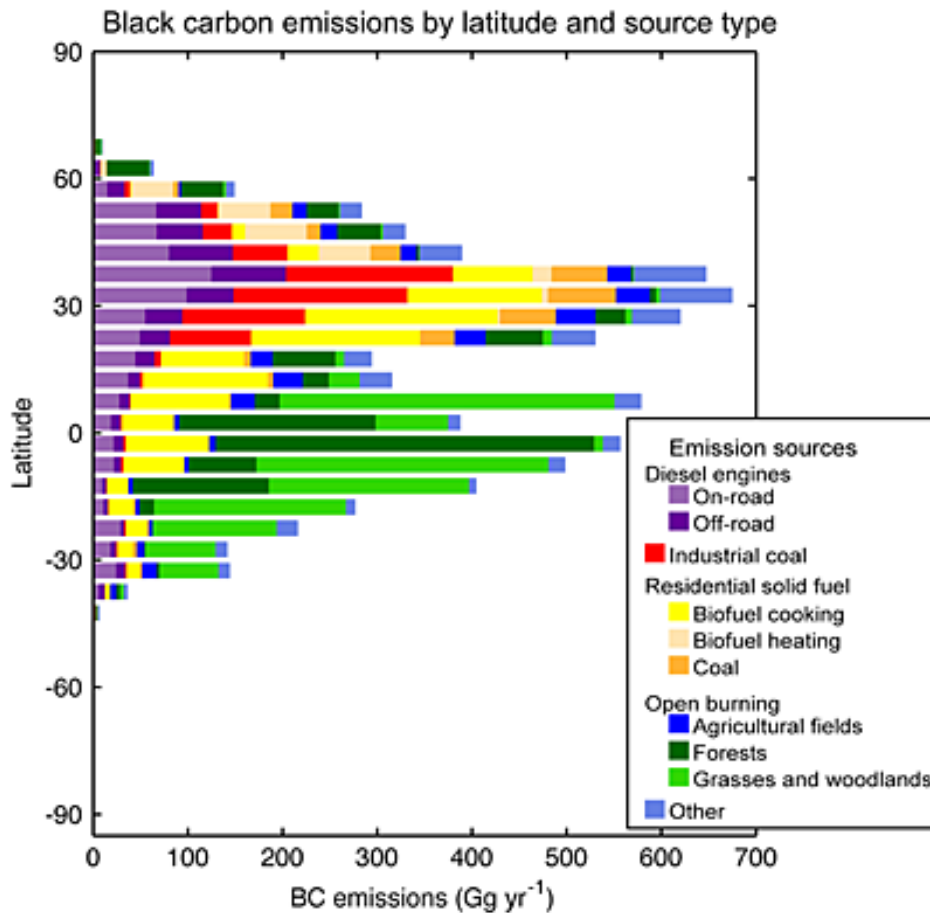


Figure 2.3 Black carbon emissions by latitude and source type, showing the dramatic difference between BC sources in the Northern and Southern hemispheres, with the Northern Hemisphere consisting of predominantly industrial and residential fuel combustion, while the Southern Hemisphere is dominated by biomass burning. Source: Bond et al. (2013), reproduced with permission.

Once emitted, atmospheric transport mechanisms carry the particles to Antarctica where the particles are deposited in snow and preserved in the ice caps (Fiebig et al., 2009). Meridional transport from the SH to Antarctica is governed by the cyclonic systems that circle the Southern Ocean as well as the Southern Annular Mode (SAM; Abram et al., 2014; Wang & Cai, 2013). SAM governs the latitudinal expansion and contraction of subpolar westerly winds and is the main contributor to variability in atmospheric circulation patterns around Antarctica (Marshall, 2003). A large factor in meridional transport efficiency of aerosols to Antarctica is distance – while Africa and South America dominate in BC emissions, Australia contributes a disproportionate amount of BC to Antarctica simply due to its proximity (Stohl & Sodemann, 2010).

Several atmospheric aerosol studies of BC in Antarctica have identified strong seasonality in coastal BC aerosol concentrations, in both East and West Antarctica (Caiazzo et al., 2017; Weller et al., 2013; Wolff & Cachier, 1998). These papers reported primary peaks in BC concentration in the austral winter/spring, a period associated with dry-season biomass burning on nearby continents. One record on the Ekström Ice Shelf in Dronning Maud Land contained secondary peaks in BC concentration during the austral summer (Weller et al., 2013). High-temporal resolution ice core studies found similar seasonality in West and East Antarctic ice concentrations during the past 200 years (Bisiaux et al., 2012). The seasonality of BC deposition to Antarctica and atmospheric meridional transport suggests that biomass burning emissions from the SH are the primary source of BC in Antarctica (Bisiaux et al., 2012; Stohl & Sodemann, 2010).

2.3.2 Ice cores

Ice cores recovered from glaciers around the world have provided invaluable records of the past atmosphere and climate on Earth. Ice cores have been particularly instrumental to demonstrating the impact of human activities on the climate (Legrand & Mayewski, 1997; Lorius et al., 1990). Ice cores are atmospheric record keepers: ambient air samples are preserved in the small bubbles trapped in the ice for hundreds of thousands of years. The data stored in the ice and bubbles allows us to reconstruct atmospheric conditions: a landmark 420 kyr ice core record from Antarctica contained the evidence that modern methane and carbon dioxide levels are unprecedented in the last four glacial cycles (Petit et al., 1999). This was later reinforced by the longer European Project for Ice Coring in Antarctica (EPICA) Dome C record, extending the record of atmospheric methane and carbon dioxide to 650 kyr before present (Luthi et al., 2008; Spahni et al., 2005).

Ice core drilling sites are selected by parameters such as glacier stability, bedrock topography, and snow accumulation rate (Legrand & Mayewski, 1997). The low accumulation rate at sites such as Vostok and Dome C on the East Antarctic Ice Sheet contributes to records that span 800 kyr but with low temporal resolution, such that annual and seasonal patterns are difficult or impossible to distinguish (EPICA Community Members, 2004; Petit et al., 1999). Conversely, the high accumulation rate at Roosevelt Island on the Ross Ice Shelf allows for sub-annual time resolution but a substantially shorter record (Tuohy et al., 2015). Additionally, ice core records are spatially limited and reflect highly variable atmospheric transport conditions. As such, many different records are needed

to build robust conclusions (Bauer et al., 2013; Masson-Delmotte et al., 2011; Sigl et al., 2015).

Ice core records are reconstructed by developing a depth-age comparison. Seasonal cycles in the water isotope fractionation (ratio of stable isotopes ^{18}O and ^{16}O , or $\delta^{18}\text{O}$), non-sea salt sulfur (nssS), hydrogen peroxide from summer photochemistry, and sodium from sea salt allow for annual layer counting of the ice core record (Legrand & Mayewski, 1997). Sulfate aerosols from volcanic events can provide age-scale validation for ice core records as they represent absolute time horizons. Due to the global transport of some eruptions, volcanic events can also facilitate intercomparison between ice core locations around the world (Sigl et al., 2015). Nevertheless, there can be significant uncertainties in ice core dating due to several factors, including inaccurate layer counting (i.e. questionable layers, missing layers), ice core loss during core processing, and insufficient instrument and sampling resolution (Rasmussen et al., 2006).

Many modern ice core studies have moved away from time-intensive discrete sampling procedures involving manual partitioning and decontamination, and now use a continuous-flow analysis (CFA) system that allows for high-resolution sampling (Bigler et al., 2011; Hiscock et al., 2013; McConnell et al., 2002; Röthlisberger et al., 2000). A CFA system usually consists of mounting the ice core vertically on top of a heated plate, or melting plate, and pumping the melt-water from the clean center of the ice core directly to instrument analysis.

2.3.3 Historical records of atmospheric black carbon

Ice cores can provide significantly longer records of atmospheric BC than direct observation and measurement in the atmosphere. Human activity has had a significant and ongoing effect on atmospheric black carbon, through fossil fuel combustion, contained burning of biomass, and increased land use activities affecting biomass burning patterns (Marlon et al., 2008). Greenland ice cores reveal a dramatic shift to coal burning in the northern hemisphere in the mid-1800s (McConnell et al., 2007), and ice cores from the Tibetan Plateau suggest an increased deposition of BC corresponding to increasing industrial activity in the 1990s in Southeast Asia, with BC concentrations accelerating melting of the glaciers (Xu et al., 2009).

Black carbon has been measured in the atmosphere in Antarctica (Warren & Clarke, 1990; Weller et al., 2013), and snow and ice cores from these regions have recently been used to

reconstruct century scale records of black carbon at several sites (Bisiaux et al., 2012). The deposition of biomass burning BC in Antarctica varies on decadal to millennial time scales and is affected by climate variability and meteorological conditions such as the El Niño-Southern Oscillation, or ENSO (Bisiaux et al., 2012).

Ice cores provide a unique opportunity to study the properties of historical BC particles that have been long-range transported in the atmosphere and deposited in Antarctica. Though numerous studies exist on individual aerosol particle morphology and composition, a single study was found that investigates the morphology of carbonaceous aerosols in global precipitation. Murr et al. (2004) used TEM to image particles in ice cores from the Greenland ice cap by depositing the ice core melt-water on a TEM grid, but this study did not identify BC aggregates.

2.4 Global significance

2.4.1 Role of black carbon in global climate models

The global climate forcing impact of BC is studied using numerous General Circulation Models (GCMs), using variables such as emissions rate, atmospheric lifetime, vertical distribution, internal vs external mixing state, mass absorption coefficient (MAC), and aerosol optical depth (AOD, Bond et al., 2013). Uncertainties in the characteristics, distribution, and lifetime of BC, as well as its historical variability, impairs our ability to model and forecast its contribution to climate change. Global climate models (GCMs) rely on a detailed understanding of the physical and chemical nature of the particles, their atmospheric effects, and past records of climate variability and forcings. Climate forcing due to aerosols represents a major uncertainty in both our understanding of past climate variability and our ability to model future climate change scenarios (IPCC, 2013). This is particularly true of aerosols emitted by biomass burning, which are modulated on decadal scales by hydroclimate variability and human land use activity (Marlon et al., 2008).

A comprehensive analysis of the treatment of BC in GCMs is available in Bond et al. (2013), including various iterations of the NCAR Community Atmosphere Model (CAM; Allen et al., 2012; Ban-Weiss et al., 2012; Collins et al., 2004; Hodnebrog et al., 2014; Neale et al., 2010) the Reading Intermediate General-Circulation Model (IGCM, Cook & Highwood, 2004), the

Canadian Centre for Climate modeling and analysis (CCCma) model (Croft et al., 2005), and the Goddard Institute for Space Studies (GISS) modelE2 (Bauer et al., 2013). However, there are large uncertainties associated with these studies due to incomplete understanding of BC emissions, physical and chemical processes in the atmosphere, and removal rates (Koch et al., 2007; Reddy & Boucher, 2007; Stier et al., 2007). Changes in BC characteristic such as particle coating used by particle-resolved models can have large effects on model results (Fierce et al., 2016; Hodnebrog et al., 2014).

The Industrial Revolution brought about a marked change in aerosol composition and chemistry due to the introduction of anthropogenically emitted inorganic aerosol precursors and secondary organic aerosol (SOA) formation (Tsigaridis et al., 2006). A shift in particle emissions has also altered climate forcing in the arctic in the 20th century through deposition of industrial BC on the snow surface (McConnell et al., 2007). To understand the influence of BC on climate change on a global scale and to validate model simulations, it is critical to account for the past variability of atmospheric BC using ice core records.

2.4.1.1 Black carbon particle treatment in models

Gustav Mie published a method in 1908 to estimate the optical absorption of aerosol particles through scattering of an electromagnetic wave on a simplified, homogeneous sphere (Mie, 1908). Mie theory has since been regularly used to model the optical absorption and consequent radiative forcing of BC (Bond & Bergstrom, 2006; Lack & Cappa, 2010). More complex models use fractal morphology for the BC particles rather than a spherical approximation. Simulation results of the radiative forcing using fractal morphology indicates that the radiative impact of aggregate models can be up to twice as high as the homogenous sphere method (Kahnert & Devasthale, 2011). Consequently, non-spherical corrections are beginning to appear in aggregate absorption and scattering models of BC (Liou et al., 2011). The light absorption of aerosol particles has been modeled based on particle size and wavelength, using spherical and spherically symmetric core-shell particle models (Moosmuller et al., 2009). Scattering and absorption of atmospheric BC is often calculated using the fractal dimensions of the particles, which change as the aggregates collapse and are mixed with other species in the atmosphere (Chakrabarty et al., 2007).

Some field studies support substantial increases in BC absorption relative to coating thickness (Liu et al., 2015), whereas others have shown that coating thickness has limited impact on

absorption (Cappa et al., 2012). The most recent evidence suggests that changes in individual particle composition and diversity of the population has a large effect on global estimates of BC climate forcing potential, reinforcing the need to understand the composition and morphology of BC (Fierce et al., 2016). Regardless, there are insufficient experimental measurements of BC to determine the spatial variability of internal mixing in atmosphere (Bond et al., 2013).

2.4.2 Black carbon in the changing climate

BC has a complicated relationship with climate, as it is both influenced by climate change and a climate forcer itself. Global sedimentary charcoal records, a measure of past biomass burning, suggest that anthropogenic effects have had a marked influence on global biomass burning (Marlon et al., 2008). There are also many indications of the direct impact of aerosol emissions on synoptic and global scales, including the Australian climate, a significant source region for Antarctica. Recent modeling work has suggested that aerosols may have a comparable climate forcing effect to greenhouse gases in Australia (Rotstayn et al., 2009). Indeed, the recent increase in northwest Australia rainfall and continental cloudiness appear to be linked to the increase in aerosols generated in the Northern Hemisphere (Rotstayn et al., 2007; Shi et al., 2008). BC emissions may have already contributed to large-scale changes in atmospheric circulation, with models suggesting that the Northern Hemisphere tropics expand linearly with increasing radiative forcing from BC emissions (Allen et al., 2012; Kovilakam & Mahajan, 2015).

The Australian continent is particularly sensitive to climate variations, with historical peaks in the charcoal record closely coordinated with maximum El Niño and La Niña frequency (Lynch et al., 2007). Variability associated with ENSO may drive a ‘boom and bust’ cycle in Australia, characterized by heavy rainfall during La Niña years causing significant fuel loading, followed by dry conditions where the new growth is subject to severe bushfires (Letnic & Dickman, 2006). Climate change may amplify drought conditions in Australia (Nicholls, 2004), and models suggest an increasing risk for extreme bushfires in Australia with rising temperatures and lower relative humidity (Pitman et al., 2007). Southern Africa, another strong emissions source region for Antarctica, has also experienced a drying trend since the 1950s, although it is likely caused by natural climate variability (Hoerling et al., 2006).

Recent studies have shown a likely increase in frequency of La Niña events, coupled with an increase in frequency of El Niño events, and a more frequent oscillation between the two (Cai et al., 2015). Southeast Australia has been affected by persistent drought from 1997 to 2010 known as the ‘Big Dry,’ potentially influenced by the positive phase of the southern annular mode (SAM) and subsequent amplification of ENSO events (Verdon-Kidd & Kiem, 2009).

In a rapidly changing environment, it is increasingly important to understand the long-term effects of climate change on the generation and transport of atmospheric BC in the Southern Hemisphere.

References

- Abram, N. J., Mulvaney, R., Vimeux, F., Phipps, S. J., Turner, J., & England, M. H. (2014). Evolution of the Southern Annular Mode during the past millennium. *Nature Clim. Change*, *4*(7), 564-569.
- Adachi, K., Chung, S. H., & Buseck, P. R. (2010). Shapes of soot aerosol particles and implications for their effects on climate. *Journal of Geophysical Research: Atmospheres*, *115*
- Allen, R. J., Sherwood, S. C., Norris, J. R., & Zender, C. S. (2012). Recent Northern Hemisphere tropical expansion primarily driven by black carbon and tropospheric ozone. *Nature*, *485*(7398), 350-354.
- Andreae, M. O., & Gelencsér, A. (2006). Black carbon or brown carbon? The nature of light-absorbing carbonaceous aerosols. *Atmos. Chem. Phys.*, *6*(10), 3131-3148.
- Ban-Weiss, G. A., Cao, L., Bala, G., & Caldeira, K. (2012). Dependence of climate forcing and response on the altitude of black carbon aerosols. *Climate Dynamics*, *38*(5), 897-911.
- Bauer, S. E., Bausch, A., Nazarenko, L., Tsigaridis, K., Xu, B., Edwards, R., Bisiaux, M., & McConnell, J. (2013). Historical and future black carbon deposition on the three ice caps: Ice core measurements and model simulations from 1850 to 2100. *Journal of Geophysical Research: Atmospheres*, *118*(14), 7948-7961.
- Baumgardner, D., Kok, G., & Raga, G. (2004). Warming of the Arctic lower stratosphere by light absorbing particles. *Geophysical Research Letters*, *31*(6), L06117.
- Bigler, M., Svensson, A., Kettner, E., Vallelonga, P., Nielsen, M. E., & Steffensen, J. P. (2011). Optimization of High-Resolution Continuous Flow Analysis for Transient Climate Signals in Ice Cores. *Environmental Science & Technology*, *45*(10), 4483-4489.
- Birch, M. E., & Cary, R. A. (1996). Elemental Carbon-Based Method for Monitoring Occupational Exposures to Particulate Diesel Exhaust. *Aerosol Science and Technology*, *25*(3), 221-241.
- Bisiaux, M. M., Edwards, R., McConnell, J. R., Curran, M. A. J., Van Ommen, T. D., Smith, A. M., Neumann, T. A., Pasteris, D. R., Penner, J. E., & Taylor, K. (2012). Changes in black carbon deposition to Antarctica from two high-resolution ice core records, 1850–2000 AD. *Atmos. Chem. Phys.*, *12*(9), 4107-4115.
- Bond, T. C., & Bergstrom, R. W. (2006). Light absorption by carbonaceous particles: An investigative review. *Aerosol Science and Technology*, *40*(1), 27-67.
- Bond, T. C., Doherty, S. J., Fahey, D. W., Forster, P. M., Berntsen, T., DeAngelo, B. J., Flanner, M. G., Ghan, S., Kärcher, B., Koch, D., Kinne, S., Kondo, Y., Quinn, P. K., Sarofim, M. C., Schultz, M. G., Schulz, M., Venkataraman, C., Zhang, H., Zhang, S., Bellouin, N., Guttikunda, S. K., Hopke, P. K., Jacobson, M. Z., Kaiser, J. W., Klimont, Z., Lohmann, U., Schwarz, J. P., Shindell, D., Storelvmo, T., Warren, S. G., & Zender, C. S. (2013). Bounding the role of black carbon in the climate system: A scientific assessment. *Journal of Geophysical Research: Atmospheres*, *118*(11), 5380-5552.

- Bond, T. C., Streets, D. G., Yarber, K. F., Nelson, S. M., Woo, J.-H., & Klimont, Z. (2004). A technology-based global inventory of black and organic carbon emissions from combustion. *Journal of Geophysical Research: Atmospheres*, *109*(D14)
- Browne, E. C., Franklin, J. P., Canagaratna, M. R., Massoli, P., Kirchstetter, T. W., Worsnop, D. R., Wilson, K. R., & Kroll, J. H. (2015). Changes to the Chemical Composition of Soot from Heterogeneous Oxidation Reactions. *The Journal of Physical Chemistry A*, *119*(7), 1154-1163.
- Buseck, P. R., & Adachi, K. (2008). Nanoparticles in the Atmosphere. *Elements*, *4*(6), 389-394.
- Cai, W., Wang, G., Santoso, A., McPhaden, M. J., Wu, L., Jin, F.-F., Timmermann, A., Collins, M., Vecchi, G., Lengaigne, M., England, M. H., Dommenges, D., Takahashi, K., & Gouilly, E. (2015). Increased frequency of extreme La Nina events under greenhouse warming. *Nature Clim. Change*, *5*(2), 132-137.
- Caiazza, L., Baccolo, G., Barbante, C., Becagli, S., Bertò, M., Ciardini, V., Crotti, I., Delmonte, B., Dreossi, G., Frezzotti, M., Gabrieli, J., Giardi, F., Han, Y., Hong, S. B., Hur, S. D., Hwang, H., Kang, J. H., Narcisi, B., Proposito, M., Scarchilli, C., Selmo, E., Severi, M., Spolaor, A., Stenni, B., Traversi, R., & Udisti, R. (2017). Prominent features in isotopic, chemical and dust stratigraphies from coastal East Antarctic ice sheet (Eastern Wilkes Land). *Chemosphere*, *176*, 273-287.
- Cappa, C. D., Onasch, T. B., Massoli, P., Worsnop, D. R., Bates, T. S., Cross, E. S., Davidovits, P., Hakala, J., Hayden, K. L., Jobson, B. T., Kolesar, K. R., Lack, D. A., Lerner, B. M., Li, S.-M., Mellon, D., Nuaaman, I., Olfert, J. S., Petäjä, T., Quinn, P. K., Song, C., Subramanian, R., Williams, E. J., & Zaveri, R. A. (2012). Radiative Absorption Enhancements Due to the Mixing State of Atmospheric Black Carbon. *Science*, *337*(6098), 1078-1081.
- Chakrabarty, R. K., Moosmüller, H., Arnott, W. P., Garro, M. A., Slowik, J. G., Cross, E. S., Han, J.-H., Davidovits, P., Onasch, T. B., & Worsnop, D. R. (2007). Light scattering and absorption by fractal-like carbonaceous chain aggregates: comparison of theories and experiment. *Applied Optics*, *46*(28), 6990-7006.
- Chen, Y., Shah, N., Braun, A., Huggins, F. E., & Huffman, G. P. (2005). Electron Microscopy Investigation of Carbonaceous Particulate Matter Generated by Combustion of Fossil Fuels. *Energy & Fuels*, *19*(4), 1644-1651.
- Chow, J. C., Watson, J. G., Chen, L. W. A., Chang, M. C. O., Robinson, N. F., Trimble, D., & Kohl, S. (2007). The IMPROVE_A Temperature Protocol for Thermal/Optical Carbon Analysis: Maintaining Consistency with a Long-Term Database. *Journal of the Air & Waste Management Association*, *57*(9), 1014-1023.
- Collins, W. D., Rasch, P. J., Boville, B. A., Hack, J. J., McCaa, J. R., Williamson, D. L., Kiehl, J. T., Briegleb, B., Bitz, C., & Lin, S. (2004). Description of the NCAR community atmosphere model (CAM 3.0). *NCAR Tech. Note NCAR/TN-464+ STR*, 226

- Cook, J., & Highwood, E. J. (2004). Climate response to tropospheric absorbing aerosols in an intermediate general-circulation model. *Quarterly Journal of the Royal Meteorological Society*, 130(596), 175-191.
- Croft, B., Lohmann, U., & von Salzen, K. (2005). Black carbon ageing in the Canadian Centre for Climate modeling and analysis atmospheric general circulation model. *Atmos. Chem. Phys.*, 5(7), 1931-1949.
- Crutzen, P. J., & Andreae, M. O. (1990). Biomass Burning in the Tropics - Impact on Atmospheric Chemistry and Biogeochemical Cycles. *Science*, 250(4988), 1669-1678.
- DeMott, P. J., Chen, Y., Kreidenweis, S. M., Rogers, D. C., & Sherman, D. E. (1999). Ice formation by black carbon particles. *Geophysical Research Letters*, 26(16), 2429-2432.
- Dwyer, E., Gregoire, J. M., & Malingreau, J. P. (1998). A global analysis of vegetation fires using satellite images: Spatial and temporal dynamics. *Ambio*, 27(3), 175-181.
- EPICA Community Members (2004). Eight glacial cycles from an Antarctic ice core. *Nature*, 429(6992), 623-628.
- Fiebig, M., Lunder, C. R., & Stohl, A. (2009). Tracing biomass burning aerosol from South America to Troll Research Station, Antarctica. *Geophysical Research Letters*, 36
- Fierce, L., Bond, T. C., Bauer, S. E., Mena, F., & Riemer, N. (2016). Black carbon absorption at the global scale is affected by particle-scale diversity in composition. *Nature Communications*, 7, 12361.
- Flanner, M. G., Zender, C. S., Randerson, J. T., & Rasch, P. J. (2007). Present-day climate forcing and response from black carbon in snow. *Journal of Geophysical Research: Atmospheres*, 112(D11)
- Hadley, O. L., & Kirchstetter, T. W. (2012). Black-carbon reduction of snow albedo. *Nature Clim. Change*, 2(6), 437-440.
- Hansen, A. D. A., Bodhaine, B. A., Dutton, E. G., & Schnell, R. C. (1988). Aerosol black carbon measurements at the South Pole: Initial results, 1986-1987. *Geophysical Research Letters*, 15(11), 1193-1196.
- Hansen, J., & Nazarenko, L. (2004). Soot climate forcing via snow and ice albedos. *Proceedings of the National Academy of Sciences of the United States of America*, 101(2), 423-428.
- Hansen, J., Sato, M., Ruedy, R., Lacis, A., & Oinas, V. (2000). Global warming in the twenty-first century: An alternative scenario. *Proceedings of the National Academy of Sciences*, 97(18), 9875-9880.
- Hegg, D. A., Warren, S. G., Grenfell, T. C., Doherty, S. J., Larson, T. V., & Clarke, A. D. (2009). Source Attribution of Black Carbon in Arctic Snow. *Environmental Science & Technology*, 43(11), 4016-4021.

- Hiscock, W. T., Fischer, H., Bigler, M., Gfeller, G., Leuenberger, D., & Mini, O. (2013). Continuous Flow Analysis of Labile Iron in Ice-Cores. *Environmental Science & Technology*, 47(9), 4416-4425.
- Hodnebrog, Ø., Myhre, G., & Samset, B. H. (2014). How shorter black carbon lifetime alters its climate effect. *Nat Commun*, 5(6065)
- Hoerling, M., Hurrell, J., Eischeid, J., & Phillips, A. (2006). Detection and Attribution of Twentieth-Century Northern and Southern African Rainfall Change. *Journal of Climate*, 19(16), 3989-4008.
- IPCC. (2013). *Climate Change 2013: the physical science basis, in: Contribution of Working Group I to the Fifth Assessment Report of the Intergovernmental Panel on Climate Change*. Cambridge, United Kingdom and New York, NY, USA: Cambridge University Press.
- Jacobson, M. Z. (2000). Physically-based treatment of elemental carbon optics: Implications for global direct forcing of aerosols. *Geophysical Research Letters*, 27(2), 217-220.
- Jacobson, M. Z. (2001). Strong radiative heating due to the mixing state of black carbon in atmospheric aerosols. *Nature*, 409(6821), 695-697.
- Jacobson, M. Z. (2012). Investigating cloud absorption effects: Global absorption properties of black carbon, tar balls, and soil dust in clouds and aerosols. *Journal of Geophysical Research: Atmospheres*, 117(D6)
- Janssen, N. A. H., Hoek, G., Simic-Lawson, M., Fischer, P., van Bree, L., ten Brink, H., Keuken, M., Atkinson, R. W., Anderson, H. R., Brunekreef, B., & Cassee, F. R. (2011). Black Carbon as an Additional Indicator of the Adverse Health Effects of Airborne Particles Compared with PM(10) and PM(2.5). *Environmental Health Perspectives*, 119(12), 1691-1699.
- Jeong, C.-H., Hopke, P. K., Kim, E., & Lee, D.-W. (2004). The comparison between thermal-optical transmittance elemental carbon and Aethalometer black carbon measured at multiple monitoring sites. *Atmospheric Environment*, 38(31), 5193-5204.
- Jurado, E., Dachs, J., Duarte, C. M., & Simó, R. (2008). Atmospheric deposition of organic and black carbon to the global oceans. *Atmospheric Environment*, 42(34), 7931-7939.
- Kahnert, M., & Devasthale, A. (2011). Black carbon fractal morphology and short-wave radiative impact: a modeling study. *Atmospheric Chemistry and Physics*, 11(22), 11745-11759.
- Knox, A., Evans, G. J., Brook, J. R., Yao, X., Jeong, C. H., Godri, K. J., Sabaliauskas, K., & Slowik, J. G. (2009). Mass Absorption Cross-Section of Ambient Black Carbon Aerosol in Relation to Chemical Age. *Aerosol Science and Technology*, 43(6), 522-532.
- Koch, D., Bond, T. C., Streets, D., Unger, N., & van der Werf, G. R. (2007). Global impacts of aerosols from particular source regions and sectors. *Journal of Geophysical Research: Atmospheres*, 112(D2)

Koch, D., & Hansen, J. (2005). Distant origins of Arctic black carbon: A Goddard Institute for Space Studies ModelE experiment. *Journal of Geophysical Research: Atmospheres*, *110*(D4), D04204.

Koch, D., Schulz, M., Kinne, S., McNaughton, C., Spackman, J. R., Balkanski, Y., Bauer, S., Bernsten, T., Bond, T. C., Boucher, O., Chin, M., Clarke, A., De Luca, N., Dentener, F., Diehl, T., Dubovik, O., Easter, R., Fahey, D. W., Feichter, J., Fillmore, D., Freitag, S., Ghan, S., Ginoux, P., Gong, S., Horowitz, L., Iversen, T., Kirkev, aring, g, A., Klimont, Z., Kondo, Y., Krol, M., Liu, X., Miller, R., Montanaro, V., Moteki, N., Myhre, G., Penner, J. E., Perlwitz, J., Pitari, G., Reddy, S., Sahu, L., Sakamoto, H., Schuster, G., Schwarz, J. P., Seland, Ø., Stier, P., Takegawa, N., Takemura, T., Textor, C., van Aardenne, J. A., & Zhao, Y. (2009). Evaluation of black carbon estimations in global aerosol models. *Atmos. Chem. Phys.*, *9*(22), 9001-9026.

Koehler, K. A., DeMott, P. J., Kreidenweis, S. M., Popovicheva, O. B., Petters, M. D., Carrico, C. M., Kireeva, E. D., Khokhlova, T. D., & Shonija, N. K. (2009). Cloud condensation nuclei and ice nucleation activity of hydrophobic and hydrophilic soot particles. *Physical Chemistry Chemical Physics*, *11*(36), 7906-7920.

Kovilakam, M., & Mahajan, S. (2015). Black carbon aerosol-induced Northern Hemisphere tropical expansion. *Geophysical Research Letters*, *42*(12), 4964-4972.

Lack, D. A., & Cappa, C. D. (2010). Impact of brown and clear carbon on light absorption enhancement, single scatter albedo and absorption wavelength dependence of black carbon. *Atmos. Chem. Phys.*, *10*(9), 4207-4220.

Lamarque, J. F., Bond, T. C., Eyring, V., Granier, C., Heil, A., Klimont, Z., Lee, D., Liousse, C., Mieville, A., Owen, B., Schultz, M. G., Shindell, D., Smith, S. J., Stehfest, E., Van Aardenne, J., Cooper, O. R., Kainuma, M., Mahowald, N., McConnell, J. R., Naik, V., Riahi, K., & van Vuuren, D. P. (2010). Historical (1850–2000) gridded anthropogenic and biomass burning emissions of reactive gases and aerosols: methodology and application. *Atmos. Chem. Phys.*, *10*(15), 7017-7039.

Lammel, G., & Novakov, T. (1995). Water nucleation properties of carbon black and diesel soot particles. *Atmospheric Environment*, *29*(7), 813-823.

Legrand, M., & Mayewski, P. (1997). Glaciochemistry of polar ice cores: A review. *Reviews of Geophysics*, *35*(3), 219-243.

Letnic, M., & Dickman, C. (2006). Boom means bust: interactions between the El Niño/Southern Oscillation (ENSO), rainfall and the processes threatening mammal species in arid Australia. *Biodiversity & Conservation*, *15*(12), 3847-3880.

Li, J., Anderson, J. R., & Buseck, P. R. (2003). TEM study of aerosol particles from clean and polluted marine boundary layers over the North Atlantic. *Journal of Geophysical Research-Atmospheres*, *108*(D6)

Liou, K. N., Takano, Y., & Yang, P. (2011). Light absorption and scattering by aggregates: Application to black carbon and snow grains. *Journal of Quantitative Spectroscopy & Radiative Transfer*, *112*(10), 1581-1594.

- Liu, S., Aiken, A. C., Gorkowski, K., Dubey, M. K., Cappa, C. D., Williams, L. R., Herndon, S. C., Massoli, P., Fortner, E. C., Chhabra, P. S., Brooks, W. A., Onasch, T. B., Jayne, J. T., Worsnop, D. R., China, S., Sharma, N., Mazzoleni, C., Xu, L., Ng, N. L., Liu, D., Allan, J. D., Lee, J. D., Fleming, Z. L., Mohr, C., Zotter, P., Szidat, S., & Prévôt, A. S. H. (2015). Enhanced light absorption by mixed source black and brown carbon particles in UK winter. *Nature Communications*, *6*, 8435.
- Lorius, C., Jouzel, J., Raynaud, D., Hansen, J., & Treut, H. L. (1990). The ice-core record: climate sensitivity and future greenhouse warming. *Nature*, *347*(6289), 139-145.
- Luthi, D., Le Floch, M., Bereiter, B., Blunier, T., Barnola, J.-M., Siegenthaler, U., Raynaud, D., Jouzel, J., Fischer, H., Kawamura, K., & Stocker, T. F. (2008). High-resolution carbon dioxide concentration record 650,000-800,000 years before present. *Nature*, *453*(7193), 379-382.
- Lynch, A. H., Beringer, J., Kershaw, P., Marshall, A., Mooney, S., Tapper, N., Turney, C., & Kaars, S. V. D. (2007). Using the Paleorecord to Evaluate Climate and Fire Interactions in Australia. *Annual Review of Earth and Planetary Sciences*, *35*(1), 215-239.
- Marlon, J. R., Bartlein, P. J., Carcaillet, C., Gavin, D. G., Harrison, S. P., Higuera, P. E., Joos, F., Power, M. J., & Prentice, I. C. (2008). Climate and human influences on global biomass burning over the past two millennia. *Nature Geoscience*, *1*(10), 697-702.
- Marshall, G. J. (2003). Trends in the Southern Annular Mode from Observations and Reanalyses. *Journal of Climate*, *16*(24), 4134-4143.
- Masson-Delmotte, V., Buiron, D., Ekaykin, A., Frezzotti, M., Gallée, H., Jouzel, J., Krinner, G., Landais, A., Motoyama, H., Oerter, H., Pol, K., Pollard, D., Ritz, C., Schlosser, E., Sime, L. C., Sodemann, H., Stenni, B., Uemura, R., & Vimeux, F. (2011). A comparison of the present and last interglacial periods in six Antarctic ice cores. *Clim. Past*, *7*(2), 397-423.
- McConnell, J. R., Edwards, R., Kok, G. L., Flanner, M. G., Zender, C. S., Saltzman, E. S., Banta, J. R., Pasteris, D. R., Carter, M. M., & Kahl, J. D. W. (2007). 20th-century industrial black carbon emissions altered arctic climate forcing. *Science*, *317*(5843), 1381-1384.
- McConnell, J. R., Lamorey, G. W., Lambert, S. W., & Taylor, K. C. (2002). Continuous Ice-Core Chemical Analyses Using Inductively Coupled Plasma Mass Spectrometry. *Environmental Science & Technology*, *36*(1), 7-11.
- McFiggans, G., Artaxo, P., Baltensperger, U., Coe, H., Facchini, M. C., Feingold, G., Fuzzi, S., Gysel, M., Laaksonen, A., Lohmann, U., Mentel, T. F., Murphy, D. M., O'Dowd, C. D., Snider, J. R., & Weingartner, E. (2006). The effect of physical and chemical aerosol properties on warm cloud droplet activation. *Atmos. Chem. Phys.*, *6*(9), 2593-2649.
- Moffet, R. C., & Prather, K. A. (2009). In-situ measurements of the mixing state and optical properties of soot with implications for radiative forcing estimates. *Proceedings of the National Academy of Sciences*, *106*(29), 11872-11877.
- Moosmuller, H., Chakrabarty, R. K., & Arnott, W. P. (2009). Aerosol light absorption and its measurement: A review. *Journal of Quantitative Spectroscopy & Radiative Transfer*, *110*(11), 844-878.

- Moteki, N., Kondo, Y., Miyazaki, Y., Takegawa, N., Komazaki, Y., Kurata, G., Shirai, T., Blake, D. R., Miyakawa, T., & Koike, M. (2007). Evolution of mixing state of black carbon particles: Aircraft measurements over the western Pacific in March 2004. *Geophysical Research Letters*, *34*(11)
- Murr, L. (2008). Microstructures and Nanostructures for Environmental Carbon Nanotubes and Nanoparticulate Soots. *International Journal of Environmental Research and Public Health*, *5*(5), 321.
- Neale, R. B., Chen, C.-C., Gettelman, A., Lauritzen, P. H., Park, S., Williamson, D. L., Conley, A. J., Garcia, R., Kinnison, D., & Lamarque, J.-F. (2010). Description of the NCAR community atmosphere model (CAM 5.0). *NCAR Tech. Note NCAR/TN-486+ STR*,
- Nicholls, N. (2004). The Changing Nature of Australian Droughts. *Climatic Change*, *63*(3), 323-336.
- O'Brien, R. E., Wang, B., Laskin, A., Riemer, N., West, M., Zhang, Q., Sun, Y., Yu, X.-Y., Alpert, P., Knopf, D. A., Gilles, M. K., & Moffet, R. C. (2015). Chemical imaging of ambient aerosol particles: Observational constraints on mixing state parameterization. *Journal of Geophysical Research: Atmospheres*, *120*(18), 9591-9605.
- Ohata, S., Moteki, N., & Kondo, Y. (2011). Evaluation of a Method for Measurement of the Concentration and Size Distribution of Black Carbon Particles Suspended in Rainwater. *Aerosol Science and Technology*, *45*(11), 1326-1336.
- Petit, J. R., Jouzel, J., Raynaud, D., Barkov, N. I., Barnola, J. M., Basile, I., Bender, M., Chappellaz, J., Davis, M., Delaygue, G., Delmotte, M., Kotlyakov, V. M., Legrand, M., Lipenkov, V. Y., Lorius, C., Pepin, L., Ritz, C., Saltzman, E., & Stievenard, M. (1999). Climate and atmospheric history of the past 420,000 years from the Vostok ice core, Antarctica. *Nature*, *399*(6735), 429-436.
- Pitman, A. J., Narisma, G. T., & McAneney, J. (2007). The impact of climate change on the risk of forest and grassland fires in Australia. *Climatic Change*, *84*(3-4), 383-401.
- Pósfai, M., Anderson, J. R., Buseck, P. R., & Sievering, H. (1999). Soot and sulfate aerosol particles in the remote marine troposphere. *Journal of Geophysical Research: Atmospheres*, *104*(D17), 21685-21693.
- Pósfai, M., Simonics, R., Li, J., Hobbs, P. V., & Buseck, P. R. (2003). Individual aerosol particles from biomass burning in southern Africa: 1. Compositions and size distributions of carbonaceous particles. *Journal of Geophysical Research: Atmospheres*, *108*(D13), 8483.
- Quinn, P. K., Bates, T. S., Baum, E., Doubleday, N., Fiore, A. M., Flanner, M., Fridlind, A., Garrett, T. J., Koch, D., Menon, S., Shindell, D., Stohl, A., & Warren, S. G. (2008). Short-lived pollutants in the Arctic: their climate impact and possible mitigation strategies. *Atmos. Chem. Phys.*, *8*(6), 1723-1735.
- Ramanathan, V., & Carmichael, G. (2008). Global and regional climate changes due to black carbon. *Nature Geoscience*, *1*(4), 221-227.
- Rasmussen, S. O., Andersen, K. K., Svensson, A. M., Steffensen, J. P., Vinther, B. M., Clausen, H. B., Siggaard-Andersen, M. L., Johnsen, S. J., Larsen, L. B., Dahl-Jensen, D.,

Bigler, M., Röthlisberger, R., Fischer, H., Goto-Azuma, K., Hansson, M. E., & Ruth, U. (2006). A new Greenland ice core chronology for the last glacial termination. *Journal of Geophysical Research: Atmospheres*, *111*(D6), D06102.

Reddington, C. L., Spracklen, D. V., Artaxo, P., Ridley, D. A., Rizzo, L. V., & Arana, A. (2016). Analysis of particulate emissions from tropical biomass burning using a global aerosol model and long-term surface observations. *Atmos. Chem. Phys.*, *16*(17), 11083-11106.

Reddy, M. S., & Boucher, O. (2007). Climate impact of black carbon emitted from energy consumption in the world's regions. *Geophysical Research Letters*, *34*(11)

Röthlisberger, R., Bigler, M., Hutterli, M., Sommer, S., Stauffer, B., Junghans, H. G., & Wagenbach, D. (2000). Technique for Continuous High-Resolution Analysis of Trace Substances in Firn and Ice Cores. *Environmental Science & Technology*, *34*(2), 338-342.

Rotstayn, L. D., Cai, W. J., Dix, M. R., Farquhar, G. D., Feng, Y., Ginoux, P., Herzog, M., Ito, A., Penner, J. E., Roderick, M. L., & Wang, M. H. (2007). Have Australian rainfall and cloudiness increased due to the remote effects of Asian anthropogenic aerosols? *Journal of Geophysical Research-Atmospheres*, *112*(D9)

Rotstayn, L. D., Keywood, M. D., Forgan, B. W., Gabric, A. J., Galbally, I. E., Gras, J. L., Luhar, A. K., McTainsh, G. H., Mitchell, R. M., & Young, S. A. (2009). Possible impacts of anthropogenic and natural aerosols on Australian climate: a review. *International Journal of Climatology*, *29*(4), 461-479.

Sato, M., Hansen, J., Koch, D., Lacis, A., Ruedy, R., Dubovik, O., Holben, B., Chin, M., & Novakov, T. (2003). Global atmospheric black carbon inferred from AERONET. *Proceedings of the National Academy of Sciences*, *100*(11), 6319-6324.

Schmidt, M. W. I., & Noack, A. G. (2000). Black carbon in soils and sediments: Analysis, distribution, implications, and current challenges. *Global Biogeochemical Cycles*, *14*(3), 777-793.

Schwarz, J. P., Spackman, J. R., Fahey, D. W., Gao, R. S., Lohmann, U., Stier, P., Watts, L. A., Thomson, D. S., Lack, D. A., Pfister, L., Mahoney, M. J., Baumgardner, D., Wilson, J. C., & Reeves, J. M. (2008). Coatings and their enhancement of black carbon light absorption in the tropical atmosphere. *Journal of Geophysical Research-Atmospheres*, *113*(D3)

Schwarz, J. P., Spackman, J. R., Gao, R. S., Perring, A. E., Cross, E., Onasch, T. B., Ahern, A., Wrobel, W., Davidovits, P., Olfert, J., Dubey, M. K., Mazzoleni, C., & Fahey, D. W. (2010a). The Detection Efficiency of the Single Particle Soot Photometer. *Aerosol Science and Technology*, *44*(8), 612-628.

Schwarz, J. P., Spackman, J. R., Gao, R. S., Watts, L. A., Stier, P., Schulz, M., Davis, S. M., Wofsy, S. C., & Fahey, D. W. (2010b). Global-scale black carbon profiles observed in the remote atmosphere and compared to models. *Geophysical Research Letters*, *37*(18)

Seinfeld, J. H., & Pandis, S. N. (2016). *Atmospheric chemistry and physics: from air pollution to climate change*: John Wiley & Sons.

- Shen, Z., Liu, J., Horowitz, L., Henze, D., Fan, S., Mauzerall, D., Lin, J.-T., & Tao, S. (2014). Analysis of transpacific transport of black carbon during HIPPO-3: implications for black carbon aging. *Atmospheric Chemistry and Physics*, *14*(12), 6315-6327.
- Shi, G., Cai, W. J., Cowan, T., Ribbe, J., Rotstayn, L., & Dix, M. (2008). Variability and trend of North West Australia rainfall: Observations and coupled climate modeling. *Journal of Climate*, *21*(12), 2938-2959.
- Sigl, M., Winstrup, M., McConnell, J. R., Welten, K. C., Plunkett, G., Ludlow, F., Buntgen, U., Caffee, M., Chellman, N., Dahl-Jensen, D., Fischer, H., Kipfstuhl, S., Kostick, C., Maselli, O. J., Mekhaldi, F., Mulvaney, R., Muscheler, R., Pasteris, D. R., Pilcher, J. R., Salzer, M., Schupbach, S., Steffensen, J. P., Vinther, B. M., & Woodruff, T. E. (2015). Timing and climate forcing of volcanic eruptions for the past 2,500 years. *Nature*, *523*(7562), 543-549.
- Slowik, J. G., Cross, E. S., Han, J. H., Davidovits, P., Onasch, T. B., Jayne, J. T., Williams, L. R., Canagaratna, M. R., Worsnop, D. R., Chakrabarty, R. K., Moosmuller, H., Arnott, W. P., Schwarz, J. P., Gao, R. S., Fahey, D. W., Kok, G. L., & Petzold, A. (2007). An inter-comparison of instruments measuring black carbon content of soot particles. *Aerosol Science and Technology*, *41*(3), 295-314.
- Spahni, R., Chappellaz, J., Stocker, T. F., Louergue, L., Hausammann, G., Kawamura, K., Flückiger, J., Schwander, J., Raynaud, D., Masson-Delmotte, V., & Jouzel, J. (2005). Atmospheric Methane and Nitrous Oxide of the Late Pleistocene from Antarctic Ice Cores. *Science*, *310*(5752), 1317-1321.
- Stephens, M., Turner, N., & Sandberg, J. (2003). Particle identification by laser-induced incandescence in a solid-state laser cavity. *Applied Optics*, *42*(19), 3726-3736.
- Stier, P., Seinfeld, J. H., Kinne, S., & Boucher, O. (2007). Aerosol absorption and radiative forcing. *Atmos. Chem. Phys.*, *7*(19), 5237-5261.
- Stohl, A., & Sodemann, H. (2010). Characteristics of atmospheric transport into the Antarctic troposphere. *Journal of Geophysical Research-Atmospheres*, *115*
- Torres, A., Bond, T. C., Lehmann, C. M. B., Subramanian, R., & Hadley, O. L. (2013). Measuring Organic Carbon and Black Carbon in Rainwater: Evaluation of Methods. *Aerosol Science and Technology*, *48*(3), 239-250.
- Tsigaridis, K., Krol, M., Dentener, F. J., Balkanski, Y., Lathiere, J., Metzger, S., Hauglustaine, D. A., & Kanakidou, M. (2006). Change in global aerosol composition since preindustrial times. *Atmospheric Chemistry and Physics*, *6*, 5143-5162.
- Tuohy, A., Bertler, N., Neff, P., Edwards, R., Emanuelsson, D., Beers, T., & Mayewski, P. (2015). Transport and deposition of heavy metals in the Ross Sea Region, Antarctica. *Journal of Geophysical Research: Atmospheres*, *120*(20), 10,996-911,011.
- Utsunomiya, S., & Ewing, R. C. (2003). Application of High-Angle Annular Dark Field Scanning Transmission Electron Microscopy, Scanning Transmission Electron Microscopy-Energy Dispersive X-ray Spectrometry, and Energy-Filtered Transmission Electron Microscopy to the Characterization of Nanoparticles in the Environment. *Environmental Science & Technology*, *37*(4), 786-791.

- Verdon-Kidd, D. C., & Kiem, A. S. (2009). Nature and causes of protracted droughts in southeast Australia: Comparison between the Federation, WWII, and Big Dry droughts. *Geophysical Research Letters*, *36*(22)
- Vignati, E., Karl, M., Krol, M., Wilson, J., Stier, P., & Cavalli, F. (2010). Sources of uncertainties in modeling black carbon at the global scale. *Atmos. Chem. Phys.*, *10*(6), 2595-2611.
- Wang, G., & Cai, W. (2013). Climate-change impact on the 20th-century relationship between the Southern Annular Mode and global mean temperature. *Scientific Reports*, *3*, 2039.
- Wang, X., Heald, C. L., Ridley, D. A., Schwarz, J. P., Spackman, J. R., Perring, A. E., Coe, H., Liu, D., & Clarke, A. D. (2014). Exploiting simultaneous observational constraints on mass and absorption to estimate the global direct radiative forcing of black carbon and brown carbon. *Atmos. Chem. Phys.*, *14*(20), 10989-11010.
- Warren, S. G., & Clarke, A. D. (1990). Soot in the atmosphere and snow surface of Antarctica. *Journal of Geophysical Research: Atmospheres*, *95*(D2), 1811-1816.
- Weller, R., Minikin, A., Petzold, A., Wagenbach, D., & König-Langlo, G. (2013). Characterization of long-term and seasonal variations of black carbon (BC) concentrations at Neumayer, Antarctica. *Atmos. Chem. Phys.*, *13*(3), 1579-1590.
- Wolff, E. W., & Cachier, H. (1998). Concentrations and seasonal cycle of black carbon in aerosol at a coastal Antarctic station. *Journal of Geophysical Research*, *103*(D9), 11033-11041.
- Xu, B., Cao, J., Hansen, J., Yao, T., Joswita, D. R., Wang, N., Wu, G., Wang, M., Zhao, H., Yang, W., Liu, X., & He, J. (2009). Black soot and the survival of Tibetan glaciers. *Proceedings of the National Academy of Sciences*, *106*(52), 22114-22118.
- Zhang, J., Liu, J., Tao, S., & Ban-Weiss, G. A. (2015). Long-range transport of black carbon to the Pacific Ocean and its dependence on aging timescale. *Atmos. Chem. Phys.*, *15*(20), 11521-11535.

Chapter 3. Characterizing black carbon in rain and ice cores using coupled tangential flow filtration and transmission electron microscopy

This chapter been published in *Atmospheric Measurement Techniques*. Co-author contributions can be found in Appendix A1.

This article is published as:

Ellis, A., Edwards, R., Saunders, M., Chakrabarty, R. K., Subramanian, R., van Riessen, A., Smith, A. M., Lambrinidis, D., Nunes, L. J., Vallelonga, P., Goodwin, I. D., Moy, A. D., Curran, M. A. J., and van Ommen, T. D.: Characterizing black carbon in rain and ice cores using coupled tangential flow filtration and transmission electron microscopy, *Atmos. Meas. Tech.*, 8, 3959-3969, doi:10.5194/amt-8-3959-2015, 2015.

Abstract

Antarctic ice cores have been used to study the history of black carbon (BC), but little is known with regards to the physical and chemical characteristics of these particles in the remote atmosphere. Characterization remains limited by ultra-trace concentrations in ice core samples and the lack of adequate methods to isolate the particles unaltered from the melt water. To investigate the physical and chemical characteristics of these particles, we have developed a tangential flow filtration (TFF) method combined with transmission electron microscopy (TEM). Tests using ultrapure water and polystyrene latex particle standards resulted in excellent blanks and significant particle recovery. This approach has been applied to melt water from Antarctic ice cores as well as tropical rain from Darwin, Australia with successful results: TEM analysis revealed a variety of BC particle morphologies, insoluble coatings, and the attachment of BC to mineral dust particles. The TFF-based concentration of these particles has proven to give excellent results for TEM studies of BC particles in Antarctic ice cores and can be used for future studies of insoluble aerosols in rainwater and ice core samples.

3.1 Introduction

Carbonaceous aerosols emitted by combustion processes are comprised of black carbon (BC) and organic matter. These aerosols can stay suspended from days to weeks in the troposphere and for over a year in the stratosphere (Buseck and Adachi, 2008; Stohl and Sodemann, 2010). They impact the radiative, physical, and chemical properties of the atmosphere, affecting climate through direct optical effects and indirectly through changes in cloud formation and structure (Johnson et al., 2004). The contribution of BC to radiative forcing is significantly affected by particle shape, size, and mixing state, which is in turn affected by emission source and aging in the atmosphere (Jacobson, 2001; Moffet and Prather, 2009). Understanding the behavior of BC and other carbonaceous aerosols in the remote atmosphere is important for validating aerosol parameterization in general circulation models (Koch et al., 2009). Wet deposition through rain and snow is the primary removal process of BC from the atmosphere (Bond et al., 2013), and has a large impact on BC's atmospheric residence time and distribution (Hodnebrog et al., 2014). Furthermore, when deposited to highly reflective surfaces such as snow, the presence of BC can decrease surface albedo and accelerate melting (Flanner et al., 2007; Hansen and Nazarenko, 2004; McConnell et al., 2007). Therefore, studies of BC in modern and historic rain, snow, and ice samples are needed to understand their modern atmospheric distribution and their presence in the paleo-atmosphere, and in turn to study their impact on paleoclimate forcing and future climate change.

Several methods exist for determining BC concentrations in the atmosphere, such as optical absorption methods, thermo-optical analysis, photoacoustic absorption spectroscopy, and aerosol mass spectrometry (Slowik et al., 2007). Single particle mass concentration and particle size can be measured in real-time by single particle intracavity laser-induced incandescence (SP2, Droplet Measurement Technologies, Boulder, Colorado). Black carbon particles can also be characterized individually using electron microscopy (Pósfai et al., 1999). Many studies have measured BC abundance (as number and mass concentrations) in the atmosphere (Schwarz et al., 2006). Transmission electron microscopy (TEM) coupled with electron energy loss spectrometry (EELS) and energy-dispersive X-ray spectrometry (EDS) have long been used to determine the size, morphological, and elemental characteristics of atmospheric aerosols (Pósfai et al., 1999). Scanning transmission electron microscopy (STEM) coupled with EDS has been used to study aerosol particles (Utsunomiya

and Ewing, 2003), with high resolution imaging and STEM EDS mapping revealing nanoscale inclusions in larger aerosols that would go unnoticed with traditional TEM imaging.

Previous studies have investigated BC mass concentrations in rainwater (Ohata et al., 2011; Torres et al., 2013), snow packs (Hegg et al., 2009; Warren and Clarke, 1990), and ice cores (Bisiaux et al., 2012; McConnell et al., 2007), but little data exists regarding the morphology, chemical composition, and insoluble coatings of BC particles in rain and snow. This is particularly true of aged, long-range transported particles that have been deposited at the polar ice caps.

To the best of our knowledge, only one study has previously studied the morphology of carbonaceous aerosols in precipitation. Murr et al. (2004) analyzed particles in ice cores from the Greenland ice cap by melting the ice and depositing 180 mL of sample on a 5 mm TEM grid, a few microliters at a time. As evident by this process, isolating these particles for characterization is technically challenging, especially in ultra-clean Antarctic ice where their abundance is often less than $0.1 \mu\text{g kg}^{-1}$ (Bisiaux et al., 2012). As Antarctic ice cores have substantially lower BC concentrations than that observed in Greenland ice, larger sample volumes (>1 L melt water) are necessary to acquire sufficient particles for characterization, making this drop-by-drop method impractical. Salts and other dissolved species cause additional problems with the drop-by-drop method because they are also deposited on the grid, coating it with large amounts of unwanted material. When concentrated on TEM grids, these precipitated particles can hinder the detection and analysis of BC simply by obscuring particle morphology, especially when BC is present in ultra-trace concentrations.

An ideal preconcentration method for insoluble BC particles in polar ice should be reasonably quick, concentrate large volumes of ice melt water, remove salts, and keep the particles in motion to limit aggregation. Tangential flow filtration (TFF) is a technique that uses a continuous flow of solution tangentially across a filter membrane to avoid sample build-up on the surface of the membrane (and subsequent sample loss). Hollow fiber filters have been employed to concentrate environmental water samples (Benner et al., 1997; Giovannoni et al., 1990) as well as nanoparticles for pharmaceutical applications (Dalwadi et al., 2005). TFF has a high particle recovery, can concentrate large sample volumes (>1 L) without membrane fouling, does not cause nanoparticle aggregation, and can preserve fragile aerosol structures (Benner et al., 1997; Dalwadi et al., 2005). An important benefit of TFF to

the study of BC particles is that it can concentrate particles whilst removing dissolved salts and other species, depending on the pore size of the filter.

To study individual BC particles and other carbonaceous aerosols in global precipitation, we investigated the use of TFF to concentrate BC prior to analysis by TEM. Particle recovery rates and blanks were investigated using polystyrene latex (PSL) particle standards and ultrapure water. Test samples included tropical rainwater from Darwin, Australia as well as Antarctic ice cores. The rainwater provided an example of equatorial wet deposition of particles, whereas Antarctic ice provides both a modern example of polar deposition as well as a historical record of these particles in the global atmosphere.

3.2 Methodology

3.2.1 Clean room laboratory environment

Sample preparation and cleaning of laboratory and field equipment was performed in the Trace Research and Advanced Clean Environment (TRACE) laboratory at Curtin University. The TRACE facility is a 450 square meter clean-air laboratory facility described by Burn et al. (2009). The facility includes a large positive pressure clean-air exclusion space (ISO Class 5) housing five smaller clean-air laboratory modules (ISO Class 4) including a cold laboratory module. With the exception of the cold laboratory module, the modules draw clean air from the exclusion space through a series of high-efficiency particle air (HEPA) filters in the module roof. Module air passes through the floor and either recirculates back into the module and the exclusion space or is exhausted through the base of clean air hood. Air inside the cold laboratory module is filtered by a recirculating cryogenic air filtration HEPA system. The BC concentration in the exclusion space air was determined using an Single-Particle Soot Photometer (SP2) and found to be less than 1 BC particle / m³ STP for particles with a mass equivalent diameter range of 70 to 700 nm (assuming a constant density of 1.8 g/cc as in Schwarz et al. (2013)).

Mechanical decontamination of ice core samples was conducted in the TRACE cold laboratory module at -12° C. All other sample preparation and TEM grid preparation activities were conducted in a clean-air bench inside a laboratory module.

The modules are fitted with an ultrapure water (UP, $\rho > 18.2 \text{ m}\Omega$) system fed by a laboratory-wide reverse osmosis and deionized water supply. This water was used for cleaning all laboratory benches, fittings, tubing, and plastic ware. Melted samples were kept in Teflon or low-density polyethylene (LDPE) bottles, filled and rinsed multiple times with UP water. All surfaces were cleaned with UP water prior to sample decontamination.

3.2.2 Reagents and materials

Blanks: The entirety of this concentration method was blank-tested with laboratory-made UP ice. The blank ice was made by freezing UP water in a cleaned 3 L perfluoro alkoxyalkane container (PFA, Savillex). The ice was removed from the container, cut into rectangles on a clean band saw in the cold laboratory module, and bagged in plastic layflat bags. This was to mimic the condition and treatment of the Antarctic ice core samples.

Polystyrene latex particles: 200 nm polystyrene latex (PSL) spheres (SPI) were used to test the filtration and microscopy method, as they can be suspended in water and are readily identified on TEM grids.

Filters: 50 kD pore size mPES Hollow Fiber Filters (HFF, Spectrum Laboratories, California) with 20 cm² membrane surface area, gamma irradiated for sterility, were used to concentrate samples. The 50 kD (~10 nm) pore size was selected to retain as many particles as possible while minimizing filtration time. Any soluble species or particulates smaller than 10 nm are removed from the solution during filtration, including dissolved salts.

Grids: The TEM grids used for the study were SPI™ 300-mesh gold grids with a continuous (non-porous) SiO₂/SiO support film. Gold was selected due to its resistance to corrosive UP water. Additionally, the carbon coating on the traditional copper TEM grids had irregularities that made distinguishing the actual carbonaceous sample difficult, and silicon dioxide coatings did not interfere with identification of carbonaceous particles using EDS spectra.

3.2.3 Instrumentation

A scanning electron microscope (SEM) was used to look at TEM grids prior to TEM analysis, to verify that sufficient particles were present on the grid. Scanning electron microscopy was performed with a Zeiss Neon 40EsB FIBSEM operated at 5 kV, located at Curtin University's Microscopy & Microanalysis Facility.

The transmission electron microscopy was performed on a FEI Titan G2 80-200 TEM/STEM with ChemiSTEM Technology, which incorporates scanning transmission electron microscopy (STEM) with ~1 nm resolution EDS mapping. Samples were imaged using both TEM and STEM, both operating at 80 kV. This instrument is located at the University of Western Australia. Additional imaging and spectroscopy was performed on a JEOL 2100 TEM operated at 120 kV and equipped with a GATAN Tridiem energy filter for EELS and energy filtered transmission electron microscopy (EFTEM) work.

3.2.4 Samples

Ice core samples:

The DSS0506 ice core samples used in this study were collected in the 2005-2006 austral summer from Law Dome, East Antarctica. The ice core drilling location was at Dome Summit South (DSS), and provides overlapping ice core to the main DSS ice core (66°46'11" S, 112°48'25" E, 1,370 m elevation). Ice and snow from this site have been the subjects of a large number of studies (Burn-Nunes et al., 2011; Curran et al., 1998; Etheridge et al., 1996; Palmer et al., 2001; Pedro et al., 2012; Vallelonga et al., 2002; van Ommen and Morgan, 1996; van Ommen and Morgan, 2010). The flux of BC deposition at the same sampling site in Law Dome, East Antarctica has been quantified using an SP2 (Bisiaux et al., 2012). The ice core used in this study was cut longitudinally into two parallel sections, 1 m long with a 5 cm by 5 cm cross-section. One section was used for measuring trace ion chemicals and stable isotopes, and the matching section was transported to the TRACE facility at Curtin University for BC studies. The ice was dated by matching the dissolved ion chemistry and water stable isotope records ($\delta^{18}\text{O}$) to the main DSS ice core record to produce a depth age scale for DSS0506. The main DSS ice core record was dated using annual layer counting and identification of volcanic horizons (Plummer et al., 2012). The cores used in this study are DSS0506-38U from 70.5 m and dated to 1930 CE, DSS0506-69U from 131.5 m and dated to 1838 CE, and DSS0506-93U from 178.3 m and dated to 1759 CE. Approximately 1 cm of ice was removed from all sides during decontamination, resulting in ~1.5 to 2 L of melt water.

Rain samples:

Monsoon rain samples were collected in Darwin, in tropical northern Australia. The region experiences a dry season (May-November) and a monsoonal wet season in the summer

months (December-March) (Holland, 1986; Kaars et al., 2000), and is in close proximity to equatorial Asian biomass burning as well as annually occurring northern Australian bushfires. The samples used to test this method were collected on 08 April 2014 and 11 April 2014, during the end of the wet period in Darwin when large volumes of rain could be collected in short periods of time. Rain was collected using an UP water cleaned Teflon funnel with a 1 L cleaned low density polyethylene bottle (LDPE, Nalgene) attached via a threaded cap. The funnel was placed on a bucket in an open field, with no overhead obstructions.

3.2.5 Decontamination and concentration method

The ice core decontamination procedure was adapted from the methods of Burn et al. (2009), Candelone et al. (1994), and Edwards et al. (2006), using materials described in Section 2.1 of this paper.

Ice core sections were placed on a cleaned plastic covered surface in the TRACE facility cold laboratory module. The exterior of the ice core was progressively removed and discarded using an acid-cleaned stainless steel chisel. The chisel was cleaned with 2% nitric acid before use and rinsed with UP water in between different ice core samples. Approximately 5 mm were removed from all surfaces of the ice using the chisel. After removing the exterior, the ice samples were transferred into an acid-cleaned colander made from a 3 L fluorinated high-density polyethylene bottle with large holes drilled into the bottom. The colander was cleaned in 10% nitric acid and rinsed with UP water before use. The ice samples were then rinsed with large amounts of UP water to remove a further ~5 mm from all surfaces. Finally the samples were removed from the colander with acid-cleaned polypropylene tongs and transferred into a 3 L perfluoro alkoxyalkane container. Ice pieces were added periodically to the perfluoro alkoxyalkane melt water container over the course of the filtration, as to keep the sample cold while filtering to avoid possible aggregation. Rain samples were filtered directly from the sampling container (1 L LDPE Nalgene bottle).

The TFF setup consisted of a recirculating HFF connected to a multichannel peristaltic pump (Ismatec IPC pump, IDEX Health & Science), detailed in Figure 3.1. Samples were pumped through filters with standard PVC two-stop pump tubing and PFA tubing.

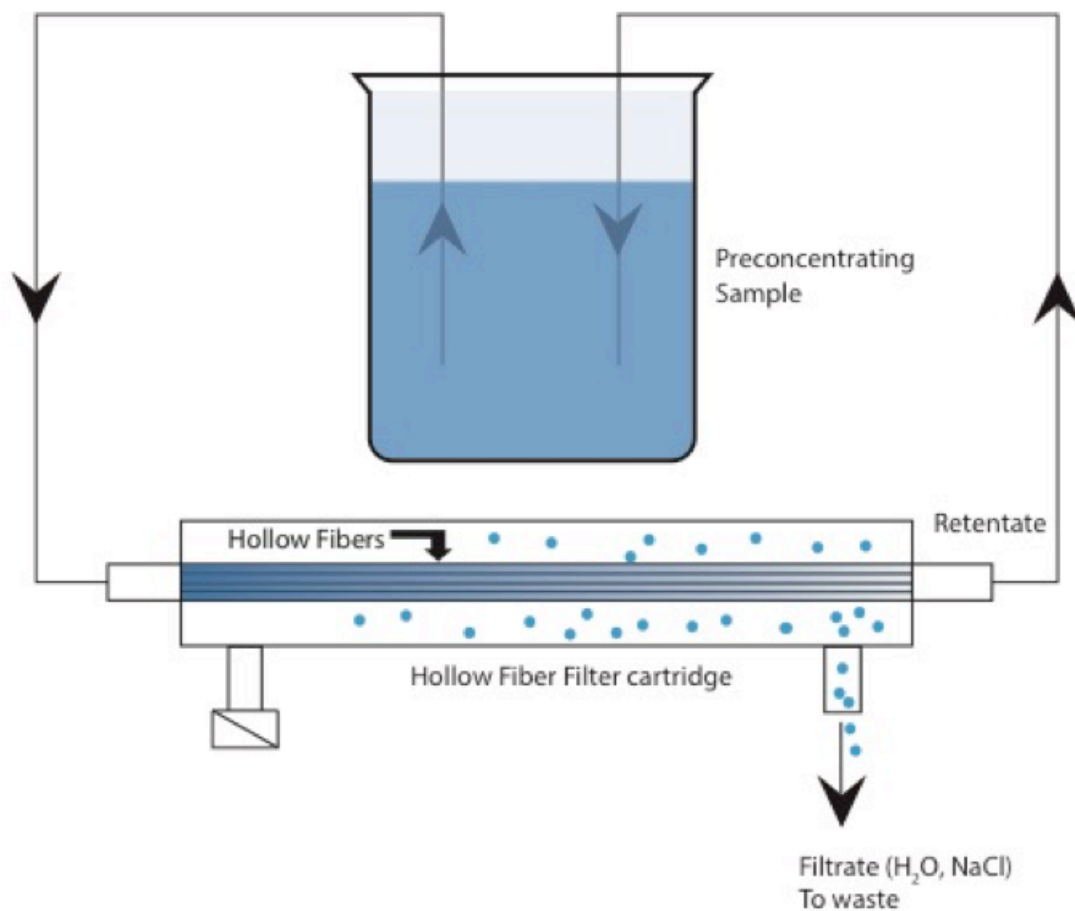


Figure 3.1: Tangential flow filtration setup for concentration of rain or melted ice core sample H₂O. Water sample recirculates through the hollow fiber filter, with H₂O and dissolved species removed through open side port of filter cartridge.

During concentration, sample water was recirculated from the bottle using the peristaltic pump, through a HFF, and then back into the sample bottle. One of two side ports on the HFF was left open over a waste container to allow filtrate to be removed with little backpressure, as backpressure on the filtrate removal line would have slowed the filtration rate. The sample bottle was elevated above the filter, and the height difference between filter and sample bottle was used to increase or decrease backpressure on the filter, speeding or slowing filtrate removal as required. Filtrate was removed at 250 mL/hour, resulting in a concentration of 2 L to 1.5 mL in approximately 8 hours.

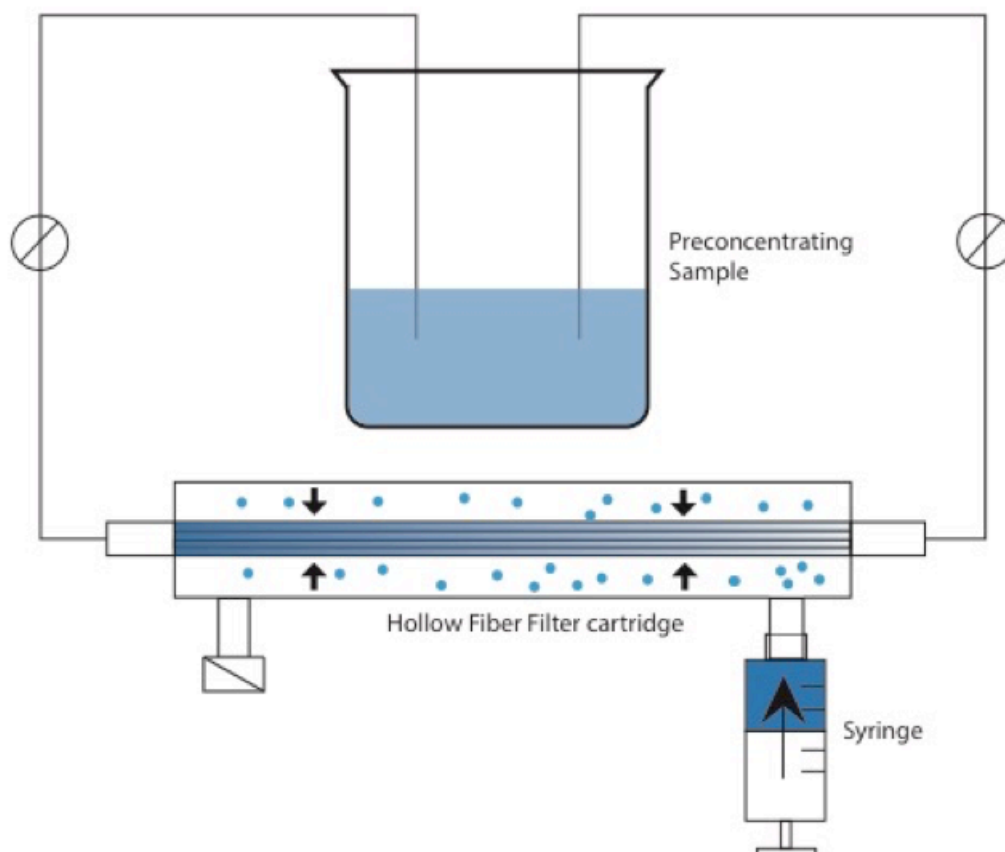


Figure 3.2: Backflush of hollow fiber filter membrane setup, performed by stopping the peristaltic pump and injecting 1 mL of ultrapure water into the open side port using a syringe.

The pump direction was periodically reversed, with the sample moving backwards through the filter, for ~5 seconds to avoid particle build-up on the membrane surface. The filter is also backflushed immediately prior to collecting the final concentrated sample with 1 mL of water (Figure 3.2) to remove any additional particles from the membrane. Samples were concentrated to 1.5 mL in the sample bottle, transferred to a cleaned polypropylene centrifuge vial, and gently shaken to avoid particle size separation. Concentrated samples were then deposited on 5mm TEM grids, 30 μ L at a time using a clean PP pipette tip. The TEM grid was held elevated off the laboratory bench surface by SPI stainless steel tweezers in the TRACE module clean air hood at room temperature ($\sim 22^\circ$ C) while the sample was evaporating down. Each 30 μ L drop was left to evaporate fully between drops, depositing particles on the surface of the grid. To avoid particle separation in the solution, the sample vial was shaken immediately before each deposition. The sample vial was stored at 2° C between drops. Approximately 0.18 mL of sample was deposited to each grid.

3.2.6 Particle characterization using electron microscopy

Insoluble particles were characterized using electron microscopy, initially to check for sample recovery, and eventually for quantification of particle size, morphology, and composition. During recovery method development, secondary electron imaging in the SEM was used to look for particles remaining on filters as well as for inspecting TEM grids for particles recovered through filtration.

The silicon-coated grid exhibited some charging effects under the electron beam, and damaged squares of film (i.e. holes from handling with tweezers) could collapse completely when imaged in normal TEM mode. Often, spreading the beam out over a large section of grid and waiting a few minutes before imaging at higher magnification could prevent sample jumping. Film squares with large objects, such as bacteria or dust particles $>10\ \mu\text{m}$, were more susceptible to complete collapse from charging.

On the TEM, the entire area of each grid was initially surveyed at 200-500x magnification to locate particles, which were then imaged at higher magnifications and EELS/EDS spectra were acquired to characterize particle types. Particles were imaged at $\sim 10,000\text{x}$ magnification for complex, larger aggregates, and 100,000-200,000x magnification for fine structure and individual particle morphology. Seemingly empty portions of the grid were also surveyed at higher magnification, to verify that potential deposits of smaller particles were not overlooked.

BC was identified using various TEM results, including spherule aggregate structure, the presence of carbon peaks in EDS or EELS spectra, size of primary spherules ($\sim 30\ \text{nm}$), and ‘onion-ring’ structure of spherules. STEM imaging and EDS were used to preserve beam-sensitive structures, such as coatings on the particles. EFTEM elemental maps were acquired using the traditional three-window technique using energy windows adjusted to provide optimum signal-to-noise (Brydson, 2001).

3.2.7 Testing the cleanliness of the system

As the concentration method will concentrate both sample and contaminants, blanks were tested on each major step of the procedure to exclude the possibility of procedural contamination. Unused TEM grids were scanned prior to use for sampling. To test the cleanliness of the water, blank UP water was concentrated and deposited on TEM grids for

imaging. Laboratory-made UP water blank ice was decontaminated and concentrated using the method in section 2.5. The TEM samples were prepared from the concentrated solution.

3.3 Results and Discussion

3.3.1 Blanks

No BC was found on any of the unused TEM grids or in any of the UP water tests. An UP water blank on the hollow fiber filter after filtering a rain sample was inspected on the TEM, and there was little evidence of cross contamination. Three, ~500 nm alumina silicate dust particles were found on the entire grid, surveying at 500x magnification.

3.3.2 Tangential flow filtration

Using TFF, the ice core samples were concentrated from an average initial volume of ~2 L to a final volume of 1.5 ± 0.1 mL, a factor of ~1300. The concentration factor varied slightly due to the initial volume of the ice core melt water, which was different for each ice core sample used. This was due to variations in the size of each ice core.

The TFF method was tested with polystyrene latex (PSL) spheres (200 nm diameter). A prepared standard of 1 L of $1 \mu\text{g kg}^{-1}$ (1 ppb) PSL particles was concentrated from 1 L to ~1.5 mL using the method in Section 2.5, resulting in a final concentration of $\sim 670 \mu\text{g kg}^{-1}$. This concentrated standard was then deposited on a SiO_2/SiO coated TEM grid. SEM images of the prepared sample grid showed significant sample recovery for characterization, with areas of the grid completely obscured with spheres (Figure 3.3).

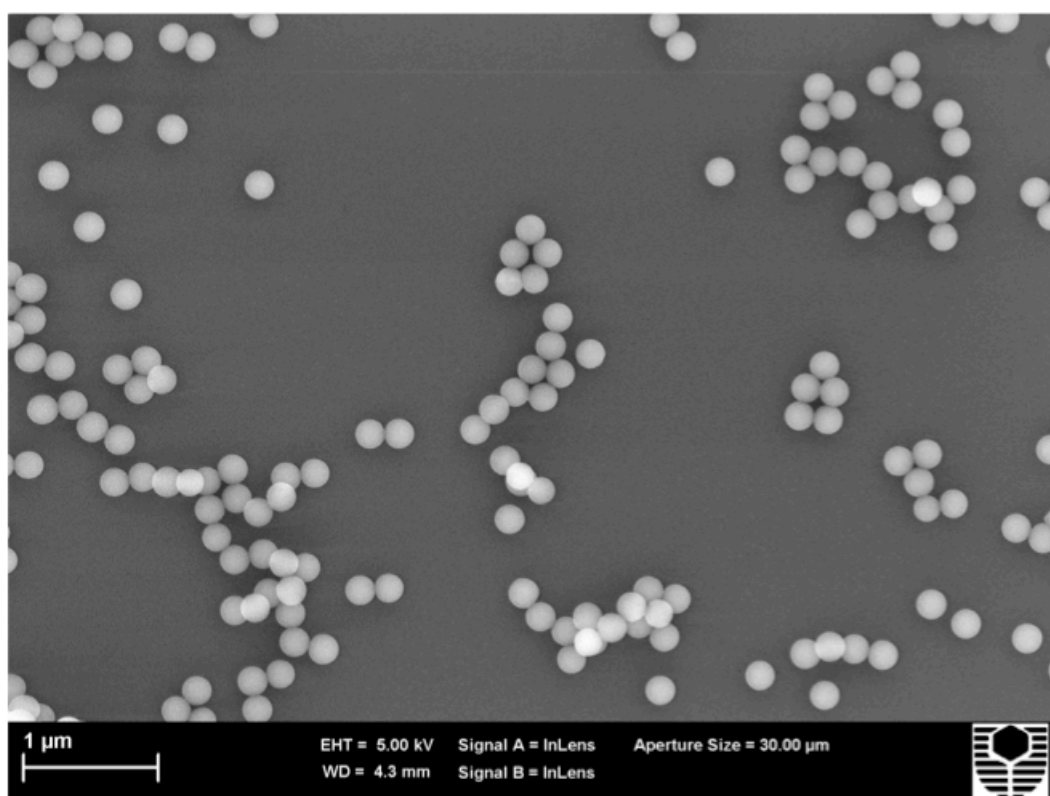


Figure 3.3: SEM image of PSL spheres from concentration method test on SiO₂/SiO coated grid surface, concentrated from 1 μg kg⁻¹ to ~667 μg kg⁻¹ using TFF.

Using an average BC concentration of 0.08 μg kg⁻¹ from the same Law Dome location in Antarctica (Bisiaux et al., 2012) and a concentration ratio of 2 L to 1.5 mL, the final BC concentration of the ice core samples was ~100 μg kg⁻¹. A number of methods were tested to extract particles from water samples in this study, and these methods are detailed in the Supplementary Information. Comparison of this TFF method with the ‘failed’ methods in Supplementary Information indicate that particle recovery from TFF is more effective at both concentrating particles and keeping particles suspended in a solution, which can then be deposited on a TEM grid for characterization. Given that the melting of snow samples does not affect the size distribution of BC aerosols (Schwarz et al., 2013), the only information lost in the melting of the ice core would be any possible soluble constituents of the BC aerosols, such as soluble coatings.

3.3.3 Transmission electron microscopy

Results presented from this study pertaining to the relative and absolute abundance of different particle types are qualitative only, because a statistically rigorous survey of all particles on the grid was not completed. Nevertheless, the images included in this paper have been chosen to be representative of particles commonly seen while scanning the grid.

Sample charging on the SiO₂/SiO-coated grids caused difficulty with TEM and STEM imaging, as the grid would periodically shift abruptly while collecting an image. The silicon and oxygen provided a useful background when looking for carbon in EDS and EELS spectra, but a carbon-coated grid would be more stable for high-resolution imaging on the nanometer scale.

Black carbon aggregates were readily identified by their onion structure and morphology on TEM grids from both rain samples and ice core samples. In addition, STEM EDS revealed coatings and inclusions in the aggregates that would have otherwise been overlooked. STEM EDS also preserved beam-sensitive sample, including nitrogen and oxygen coatings up to 5 nm thick on the BC aggregates (Figure 3.4).

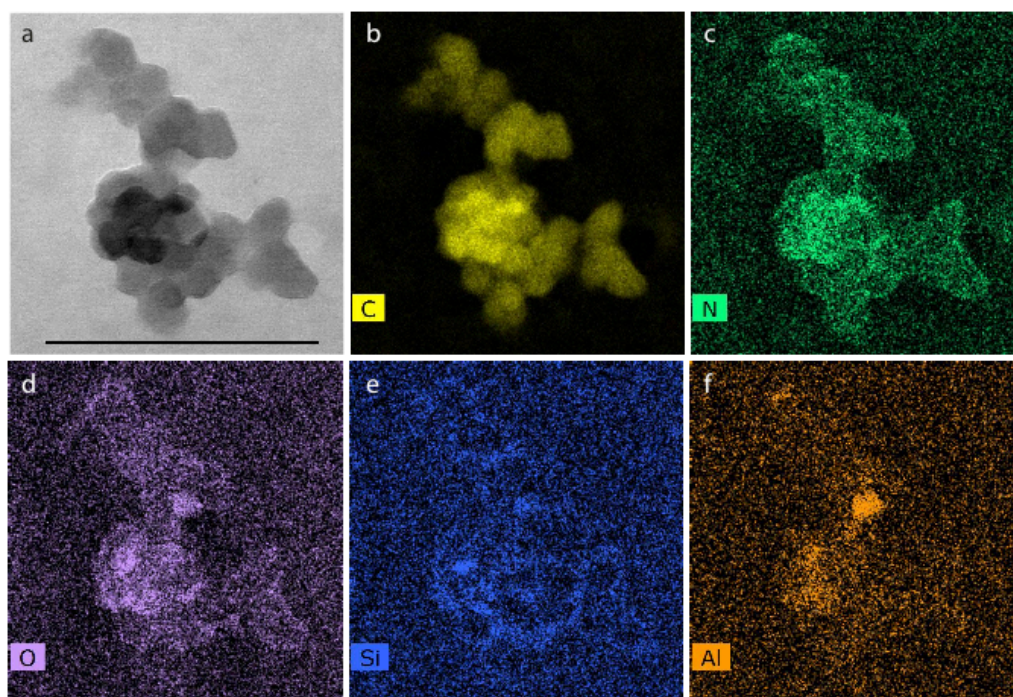


Figure 3.4: An example of a BC aggregate with nitrogen and oxygen coating and aluminum-rich silicate inclusions from Law Dome, Antarctica ice core dated to 1759 CE. a) STEM image, scale bar = 300 nm. b-f) a series of STEM EDS maps for C, N, O, Si and Al, respectively. Element maps shown are from same field of view as image a.

Various mineral dust particles were also successfully identified in both sample suites via imaging coupled with EELS and EDS analysis (Figures 3.5 and 3.6) and EELS and EFTEM analysis helped characterize complex dust particles containing Al, Si, Fe, and C (Figure 3.6). The mixing of BC and other particulates shown in Figures 3.5-3.7 is significant, as internal mixing of BC with other particles such as dust can affect their radiative forcing (Clarke et al., 2004; Scarnato et al., 2015). STEM-EDS can distinguish variations in BC composition that may routinely be overlooked.

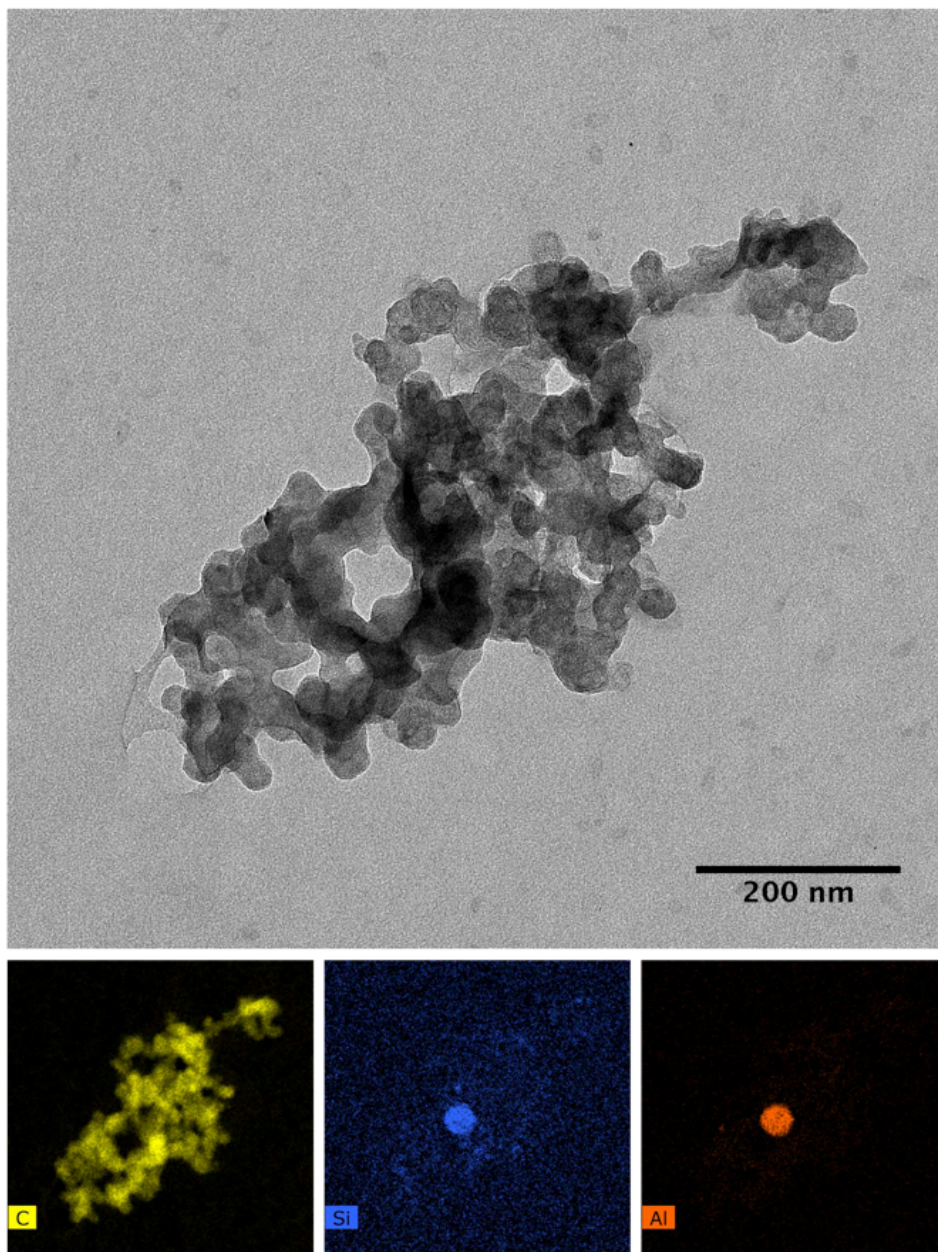


Figure 3.5: TEM image of a particle from Darwin rain sample collected 11 April 2014, with accompanying STEM EDS maps of carbon, silicon, and aluminum. Element maps are from the same field of view as the TEM image.

Both the rain and ice cores had a large quantity of BC particles, with graphitic carbon ‘onions’ of ~30 nm in diameter aggregated into larger particles of ~80 to >1000 nm in diameter. These particles often showed association with aluminosilicate dust particles (Figure 3.5). Black carbon particles in both the rain and ice cores appeared to be significantly aged in the atmosphere as indicated by the collapsed structure of the carbon spherules (Figures 3.4-3.7).

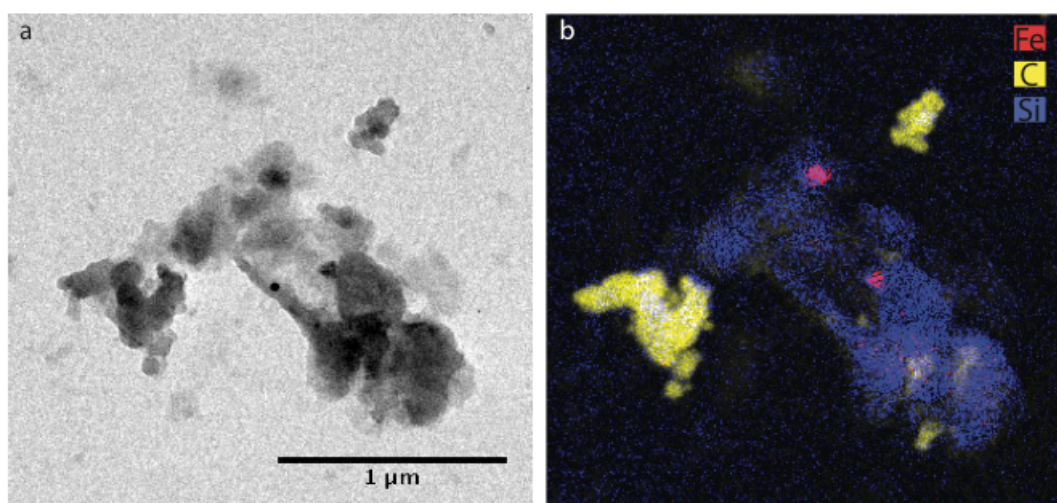


Figure 3.6: Examples of particles concentrated from a Law Dome, Antarctica ice core dated to 1930 CE. a) TEM image and b) EFTEM map of a complex aggregate particle where red is iron, blue is silicon, and yellow is carbon.

The surveys in this study permitted qualitative comparisons between samples. For example, in general, the rain samples had many larger BC aggregates (>200 nm) whereas BC aggregates found in the ice cores were significantly smaller (~100 nm) and displayed a much more compact structure. Rain samples also contained numerous superaggregates as described in Chakrabarty et al., 2014. These superaggregates were >1 μm in diameter and were absent in the ice cores (Figure 3.7). Given the high particle yields from the TFF concentration method, it is anticipated that more systematic TEM surveys could facilitate more statistically robust data on particle type and size distributions. However, this is beyond the scope of this study.

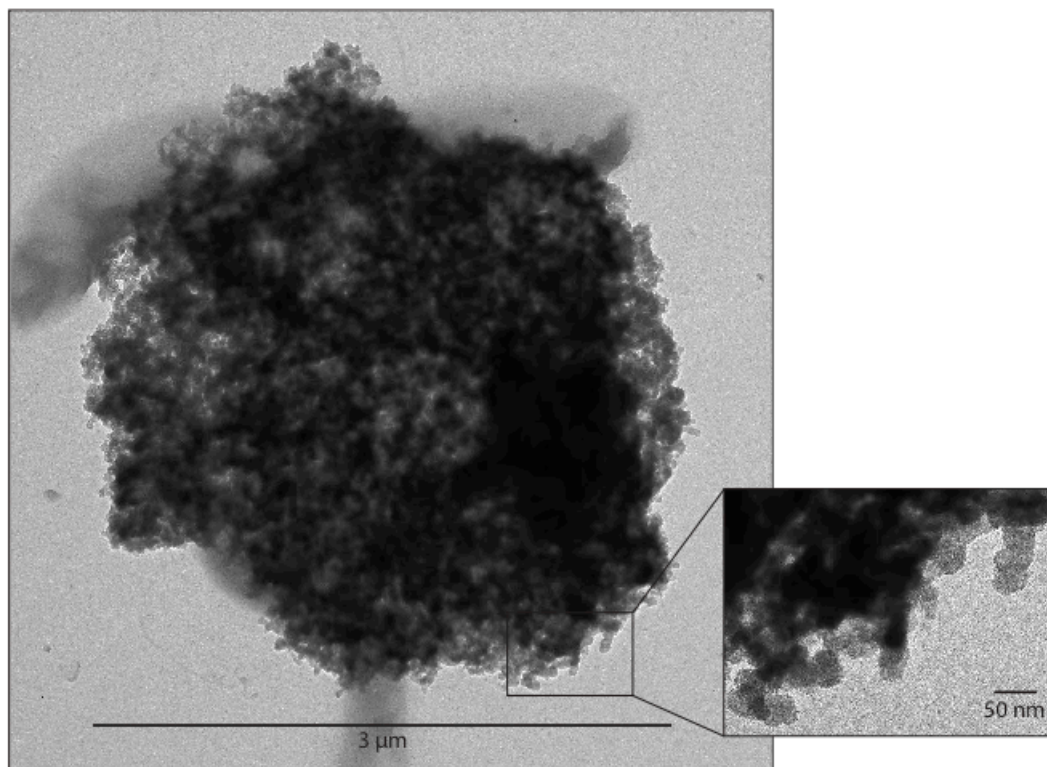


Figure 3.7: Aged superaggregate from Darwin rain sample collected 08 April 2014. Inset is of an enlarged section of aggregate, showing individual BC sphere structure.

The tangential flow filtration concentration method has been used to preserve fragile structures of particles and to avoid aggregation of nanoparticles. Nevertheless, disaggregation, aggregation, and aggregate collapse are still possible outcomes of the method. However, we see no obvious evidence that these factor significantly into the results.

Tests of bond strength between carbon spheres in BC show that aggregates are unlikely to fragment into smaller units (Rothenbacher et al., 2008). Hence, disaggregation from this method is unlikely. Additionally, both the rain samples and the ice core melt water samples were processed in an identical way, including the filtration technique to concentrate the samples and the evaporation technique to deposit particles on the TEM grids. Both rain and ice core samples contained significant variations in particle size, including large amounts of smaller BC aggregates (~100 nm). This variety suggests that method-induced aggregation did not result in significant changes to the particle population.

The collapsed structure of the black carbon aggregates seen in the ice core samples is supported by reports of BC aging in the atmosphere (Johnson et al., 1991; Li et al., 2003;

Martins et al., 1998). The BC contained in Antarctic ice cores has aged significantly from emission to deposition and would therefore likely contain collapsed aggregates. As BC is wet deposited in the rain samples, the particles are likely hydrophilic. The transition from hydrophobic to hydrophilic is a result of atmospheric aging (Stier et al., 2006), suggesting that the BC in rain has also aged significantly before deposition and will contain collapsed aggregates as well.

While post-deposition processes within the glacier cannot be ruled out, volume equivalent diameters of BC particles found in the ice (Bisiaux et al., 2012) are similar to those determined over the remote Southern Ocean by the HIPPO project (Schwarz et al., 2010). Snow densification and ice metamorphosis are more likely to aggregate BC particles into crystal junctions. If this were significant, larger particles would be expected rather than smaller ones. The differences between the BC found in rain and Antarctic ice likely reflect the loss of large aggregates during long-distance transport to Antarctica.

3.4 Conclusion

The results presented herein clearly show that the combination of tangential flow filtration and transmission electron microscopy methods provides an effective way to characterize both centuries-old atmospheric aerosols preserved in Antarctic ice and modern aerosols in rainwater. Using a clean decontamination procedure and tangential flow filtration method, aerosols in rain and Antarctic ice have been concentrated by a factor of ~1300. Tangential flow filtration method tests with polystyrene latex particle standards have shown sufficient particle recovery for transmission electron microscopy characterization, and blank tests with ultrapure laboratory ice indicate that this process does not introduce any measureable contaminants. The results in this paper indicate that black carbon particles can form around or aggregate with dust and other mineral particulates, and aggregates can develop thin (<5 nm) insoluble coatings of nitrogen and oxygen.

An important potential future development includes the possibility of quantification of particle sizes and types through systematic grid surveys of samples prepared from specific ice core depths. This type of survey could provide a statistically significant analysis of black carbon morphologies and chemical compositions in Antarctic ice, which could potentially reveal changes in black carbon over time.

Acknowledgements

This work was supported by Australian Antarctic Sciences Grant 4144. The authors acknowledge the use of Curtin University's Microscopy & Microanalysis Facility, whose instrumentation has been partially funded by the University, State and Commonwealth Governments. The authors acknowledge the facilities, and the scientific and technical assistance of the Australian Microscopy & Microanalysis Research Facility at the Centre for Microscopy, Characterisation & Analysis, The University of Western Australia, a facility funded by the University, State, and Commonwealth Governments.

References

- Benner, R., Biddanda, B., Black, B., and McCarthy, M.: Abundance, size distribution, and stable carbon and nitrogen isotopic compositions of marine organic matter isolated by tangential-flow ultrafiltration, *Marine Chemistry*, 57, 243-263, 1997.
- Bisiaux, M. M., Edwards, R., McConnell, J. R., Curran, M. A. J., Van Ommen, T. D., Smith, A. M., Neumann, T. A., Pasteris, D. R., Penner, J. E., and Taylor, K.: Changes in black carbon deposition to Antarctica from two high-resolution ice core records, 1850–2000 AD, *Atmos. Chem. Phys.*, 12, 4107-4115, 2012.
- Bond, T. C., Doherty, S. J., Fahey, D., Forster, P., Berntsen, T., DeAngelo, B., Flanner, M., Ghan, S., Kärcher, B., and Koch, D.: Bounding the role of black carbon in the climate system: A scientific assessment, *Journal of Geophysical Research: Atmospheres*, 118, 5380-5552, 2013.
- Brydson, R.: *Electron Energy Loss Spectroscopy*, Oxford: Bios in association with the Royal Microscopical Society, 2001.
- Burn, L. J., Rosman, K. J. R., Candelone, J.-P., Vallelonga, P., Burton, G. R., Smith, A. M., Morgan, V. I., Barbante, C., Hong, S., and Boutron, C. F.: An ultra-clean technique for accurately analysing Pb isotopes and heavy metals at high spatial resolution in ice cores with sub-pg g(-1) Pb concentrations, *Analytica Chimica Acta*, 634, 228-236, 2009.
- Burn-Nunes, L. J., Vallelonga, P., Loss, R. D., Burton, G. R., Moy, A., Curran, M., Hong, S., Smith, A. M., Edwards, R., Morgan, V. I., and Rosman, K. J. R.: Seasonal variability in the input of lead, barium and indium to Law Dome, Antarctica, *Geochimica et Cosmochimica Acta*, 75, 1-20, 2011.
- Buseck, P. R. and Adachi, K.: Nanoparticles in the Atmosphere, *Elements*, 4, 389-394, 2008.
- Candelone, J.-P., Hong, S., and F. Boutron, C.: An improved method for decontaminating polar snow or ice cores for heavy metal analysis, *Analytica Chimica Acta*, 299, 9-16, 1994.
- Chakrabarty, R. K., Beres, N. D., Moosmuller, H., China, S., Mazzoleni, C., Dubey, M. K., Liu, L., and Mishchenko, M. I.: Soot superaggregates from flaming wildfires and their direct radiative forcing, *Sci. Rep.*, 4, 2014.
- Clarke, A. D., Shinozuka, Y., Kapustin, V. N., Howell, S., Huebert, B., Doherty, S., Anderson, T., Covert, D., Anderson, J., Hua, X., Moore, K. G., McNaughton, C., Carmichael, G., and Weber, R.: Size distributions and mixtures of dust and black carbon aerosol in Asian outflow: Physiochemistry and optical properties, *Journal of Geophysical Research: Atmospheres*, 109, D15S09, 2004.
- Curran, M. A., Van Ommen, T. D., and Morgan, V.: Seasonal characteristics of the major ions in the high-accumulation Dome Summit South ice core, Law Dome, Antarctica, *Annals of Glaciology*, 27, 385-390, 1998.
- Dalwadi, G., Benson, H. E., and Chen, Y.: Comparison of Diafiltration and Tangential Flow Filtration for Purification of Nanoparticle Suspensions, *Pharm Res*, 22, 2152-2162, 2005.

Edwards, R., Sedwick, P., Morgan, V., and Boutron, C.: Iron in ice cores from Law Dome: A record of atmospheric iron deposition for maritime East Antarctica during the Holocene and Last Glacial Maximum, *Geochemistry, Geophysics, Geosystems*, 7, 2006.

Etheridge, D., Steele, L., Langenfelds, R., Francey, R., Barnola, J. M., and Morgan, V.: Natural and anthropogenic changes in atmospheric CO₂ over the last 1000 years from air in Antarctic ice and firn, *Journal of Geophysical Research: Atmospheres* (1984–2012), 101, 4115-4128, 1996.

Flanner, M. G., Zender, C. S., Randerson, J. T., and Rasch, P. J.: Present-day climate forcing and response from black carbon in snow, *Journal of Geophysical Research: Atmospheres* (1984–2012), 112, 2007.

Giovannoni, S., DeLong, E., Schmidt, T., and Pace, N.: Tangential flow filtration and preliminary phylogenetic analysis of marine picoplankton, *Applied and environmental microbiology*, 56, 2572-2575, 1990.

Hansen, J. and Nazarenko, L.: Soot climate forcing via snow and ice albedos, *Proceedings of the National Academy of Sciences of the United States of America*, 101, 423-428, 2004.

Hegg, D. A., Warren, S. G., Grenfell, T. C., Doherty, S. J., Larson, T. V., and Clarke, A. D.: Source Attribution of Black Carbon in Arctic Snow, *Environmental Science & Technology*, 43, 4016-4021, 2009.

Hodnebrog, Ø., Myhre, G., and Samset, B. H.: How shorter black carbon lifetime alters its climate effect, *Nat Commun*, 5, 2014.

Holland, G. J.: Interannual Variability of the Australian Summer Monsoon at Darwin: 1952–82, *Monthly Weather Review*, 114, 594-604, 1986.

Jacobson, M. Z.: Strong radiative heating due to the mixing state of black carbon in atmospheric aerosols, *Nature*, 409, 695-697, 2001.

Johnson, B., Shine, K., and Forster, P.: The semi-direct aerosol effect: Impact of absorbing aerosols on marine stratocumulus, *Quarterly Journal of the Royal Meteorological Society*, 130, 1407-1422, 2004.

Johnson, D. W., Kilsby, C. G., McKenna, D. S., Saunders, R. W., Jenkins, G. J., Smith, F. B., and Foot, J. S.: Airborne observations of the physical and chemical characteristics of the Kuwait oil smoke plume, *Nature*, 353, 617-621, 1991.

Kaars, S. v. d., Wang, X., Kershaw, P., Guichard, F., and Setiabudi, D. A.: A Late Quaternary palaeoecological record from the Banda Sea, Indonesia: patterns of vegetation, climate and biomass burning in Indonesia and northern Australia, *Palaeogeography, Palaeoclimatology, Palaeoecology*, 155, 135-153, 2000.

Koch, D., Schulz, M., Kinne, S., McNaughton, C., Spackman, J. R., Balkanski, Y., Bauer, S., Berntsen, T., Bond, T. C., Boucher, O., Chin, M., Clarke, A., De Luca, N., Dentener, F., Diehl, T., Dubovik, O., Easter, R., Fahey, D. W., Feichter, J., Fillmore, D., Freitag, S., Ghan, S., Ginoux, P., Gong, S., Horowitz, L., Iversen, T., Kirkev, aring, g, A., Klimont, Z., Kondo, Y., Krol, M., Liu, X., Miller, R., Montanaro, V., Moteki, N., Myhre, G., Penner, J. E., Perlwitz, J., Pitari, G., Reddy, S., Sahu, L., Sakamoto, H., Schuster, G., Schwarz, J. P.,

Seland, Ø., Stier, P., Takegawa, N., Takemura, T., Textor, C., van Aardenne, J. A., and Zhao, Y.: Evaluation of black carbon estimations in global aerosol models, *Atmos. Chem. Phys.*, 9, 9001-9026, 2009.

Li, J., Pósfai, M., Hobbs, P. V., and Buseck, P. R.: Individual aerosol particles from biomass burning in southern Africa: 2, Compositions and aging of inorganic particles, *Journal of Geophysical Research: Atmospheres*, 108, 2003.

Martins, J. V., Artaxo, P., Liousse, C., Reid, J. S., Hobbs, P. V., and Kaufman, Y. J.: Effects of black carbon content, particle size, and mixing on light absorption by aerosols from biomass burning in Brazil, *Journal of Geophysical Research: Atmospheres*, 103, 32041-32050, 1998.

McConnell, J. R., Edwards, R., Kok, G. L., Flanner, M. G., Zender, C. S., Saltzman, E. S., Banta, J. R., Pasteris, D. R., Carter, M. M., and Kahl, J. D. W.: 20th-century industrial black carbon emissions altered arctic climate forcing, *Science*, 317, 1381-1384, 2007.

Moffet, R. C. and Prather, K. A.: In-situ measurements of the mixing state and optical properties of soot with implications for radiative forcing estimates, *Proceedings of the National Academy of Sciences*, 106, 11872-11877, 2009.

Murr, L. E., Esquivel, E. V., Bang, J. J., de la Rosa, G., and Gardea-Torresdey, J. L.: Chemistry and nanoparticulate compositions of a 10,000 year-old ice core melt water, *Water Research*, 38, 4282-4296, 2004.

Ohata, S., Moteki, N., and Kondo, Y.: Evaluation of a Method for Measurement of the Concentration and Size Distribution of Black Carbon Particles Suspended in Rainwater, *Aerosol Science and Technology*, 45, 1326-1336, 2011.

Palmer, A. S., van Ommen, T. D., Curran, M. A., Morgan, V., Souney, J. M., and Mayewski, P. A.: High-precision dating of volcanic events (AD 1301–1995) using ice cores from Law Dome, Antarctica, *Journal of Geophysical Research*, 106, 28089–28095, 2001.

Pedro, J. B., McConnell, J. R., van Ommen, T. D., Fink, D., Curran, M. A. J., Smith, A. M., Simon, K. J., Moy, A. D., and Das, S. B.: Solar and climate influences on ice core ^{10}Be records from Antarctica and Greenland during the neutron monitor era, *Earth and Planetary Science Letters*, 355, 174-186, 2012.

Plummer, C. T., Curran, M. A. J., van Ommen, T. D., Rasmussen, S. O., Moy, A. D., Vance, T. R., Clausen, H. B., Vinther, B. M., and Mayewski, P. A.: An independently dated 2000-yr volcanic record from Law Dome, East Antarctica, including a new perspective on the dating of the 1450s CE eruption of Kuwae, Vanuatu, *Clim. Past*, 8, 1929-1940, 2012.

Pósfai, M., Anderson, J. R., Buseck, P. R., and Sievering, H.: Soot and sulfate aerosol particles in the remote marine troposphere, *Journal of Geophysical Research: Atmospheres* (1984–2012), 104, 21685-21693, 1999.

Rothenbacher, S., Messerer, A., and Kasper, G.: Fragmentation and bond strength of airborne diesel soot agglomerates, *Particle and fibre toxicology*, 5, 2008.

- Scarnato, B. V., China, S., Nielsen, K., and Mazzoleni, C.: Perturbations of the optical properties of mineral dust particles by mixing with black carbon: a numerical simulation study, *Atmos. Chem. Phys.*, 15, 6913-6928, 2015.
- Schwarz, J., Gao, R., Fahey, D., Thomson, D., Watts, L., Wilson, J., Reeves, J., Darbeheshti, M., Baumgardner, D., and Kok, G.: Single-particle measurements of midlatitude black carbon and light-scattering aerosols from the boundary layer to the lower stratosphere, *Journal of Geophysical Research: Atmospheres*, 111, 2006.
- Schwarz, J. P., Gao, R. S., Perring, A. E., Spackman, J. R., and Fahey, D. W.: Black carbon aerosol size in snow, *Sci. Rep.*, 3, 2013.
- Schwarz, J. P., Spackman, J. R., Gao, R. S., Watts, L. A., Stier, P., Schulz, M., Davis, S. M., Wofsy, S. C., and Fahey, D. W.: Global-scale black carbon profiles observed in the remote atmosphere and compared to models, *Geophysical Research Letters*, 37, 2010.
- Slowik, J. G., Cross, E. S., Han, J.-H., Davidovits, P., Onasch, T. B., Jayne, J. T., Williams, L. R., Canagaratna, M. R., Worsnop, D. R., and Chakrabarty, R. K.: An inter-comparison of instruments measuring black carbon content of soot particles, *Aerosol Science and Technology*, 41, 295-314, 2007.
- Stier, P., Seinfeld, J. H., Kinne, S., Feichter, J., and Boucher, O.: Impact of nonabsorbing anthropogenic aerosols on clear-sky atmospheric absorption, *Journal of Geophysical Research: Atmospheres*, 111, 2006.
- Stohl, A. and Sodemann, H.: Characteristics of atmospheric transport into the Antarctic troposphere, *Journal of Geophysical Research-Atmospheres*, 115, 2010.
- Torres, A., Bond, T. C., Lehmann, C. M. B., Subramanian, R., and Hadley, O. L.: Measuring Organic Carbon and Black Carbon in Rainwater: Evaluation of Methods, *Aerosol Science and Technology*, 48, 239-250, 2013.
- Utsunomiya, S. and Ewing, R. C.: Application of High-Angle Annular Dark Field Scanning Transmission Electron Microscopy, Scanning Transmission Electron Microscopy-Energy Dispersive X-ray Spectrometry, and Energy-Filtered Transmission Electron Microscopy to the Characterization of Nanoparticles in the Environment, *Environmental Science & Technology*, 37, 786-791, 2003.
- Vallelonga, P., Van de Velde, K., Candelone, J.-P., Morgan, V., Boutron, C., and Rosman, K.: The lead pollution history of Law Dome, Antarctica, from isotopic measurements on ice cores: 1500 AD to 1989 AD, *Earth and Planetary Science Letters*, 204, 291-306, 2002.
- van Ommen, T. D. and Morgan, V.: Peroxide concentrations in the Dome summit south ice core, Law Dome, Antarctica, *Journal of Geophysical Research: Atmospheres* (1984–2012), 101, 15147-15152, 1996.
- van Ommen, T. D. and Morgan, V.: Snowfall increase in coastal East Antarctica linked with southwest Western Australian drought, *Nature Geosci.*, 3, 267-272, 2010.
- Warren, S. G. and Clarke, A. D.: Soot in the atmosphere and snow surface of Antarctica, *Journal of Geophysical Research: Atmospheres*, 95, 1811-1816, 1990.

Supplementary Information

Unsuccessful concentration methods

Drop by drop evaporation without preconcentration

Murr et al. (2004) used a drop-by-drop method to deposit Greenland ice core melt water on a TEM grid, $\sim 3 \mu\text{L}$ at a time. The drop-by-drop method might work on higher concentration samples (i.e. temperate ice cores or snow samples), but due to low concentrations of BC in Antarctic ice cores, characterization of the particles necessitates concentrating the melted ice core prior to depositing it on a TEM grid. To preserve the largest amount of particles, the sample should be processed as quickly as possible. The longer the sample sits melted, the greater chance of losing black carbon to aggregation or diffusion to the walls of the sample container. Depending on concentration of BC in sample, the drop-by-drop method would require a significant amount of sample deposition to grid before there are sufficient particles to image ($\sim 1 \text{ L}$, deposited $3 \mu\text{L}$ at a time), potentially losing particles in the sample as each drop dries on the grid.

Vacuum ablating ice

We attempted to vacuum ablate ice, to avoid putting the BC into solution where it might lose soluble portions of the structure. This was tested on a Christ Alpha 1-2 LD Freeze Dryer. It took approximately six hours for a 5 cm^3 piece of blank ice to halve in size. A substantially larger ice core sample is required to obtain sufficient particles for characterization in low-concentration Antarctic ice.

Anopore filtration followed by back flushing

Preconcentration was attempted using a 200 nm pore-size Anopore polycarbonate filter. An ice core sample was melted and filtered using the peristaltic pump and an Anopore filter in a Teflon filter holder. The filter was then backflushed with $\sim 5 \text{ mL}$ of Milli-q water using a syringe.

SEM imaging of TEM grids made from the backflushed sample solution indicates only a small fraction of particles were recovered from the filter. Further SEM imaging of the filter itself showed large amounts of particulates remained stuck to the filter surface and were not removed through backflushing (Figure S3.1). Ultrasonication was not used to dislodge

particles due to the possible separation of aerosol aggregates, compromising the characterization results of BC aggregates. This could be a useful method for a lower-magnification scanning electron microscopy (SEM) study of larger aerosols, but large pore size and complicated filter structure makes locating smaller BC aggregates difficult.

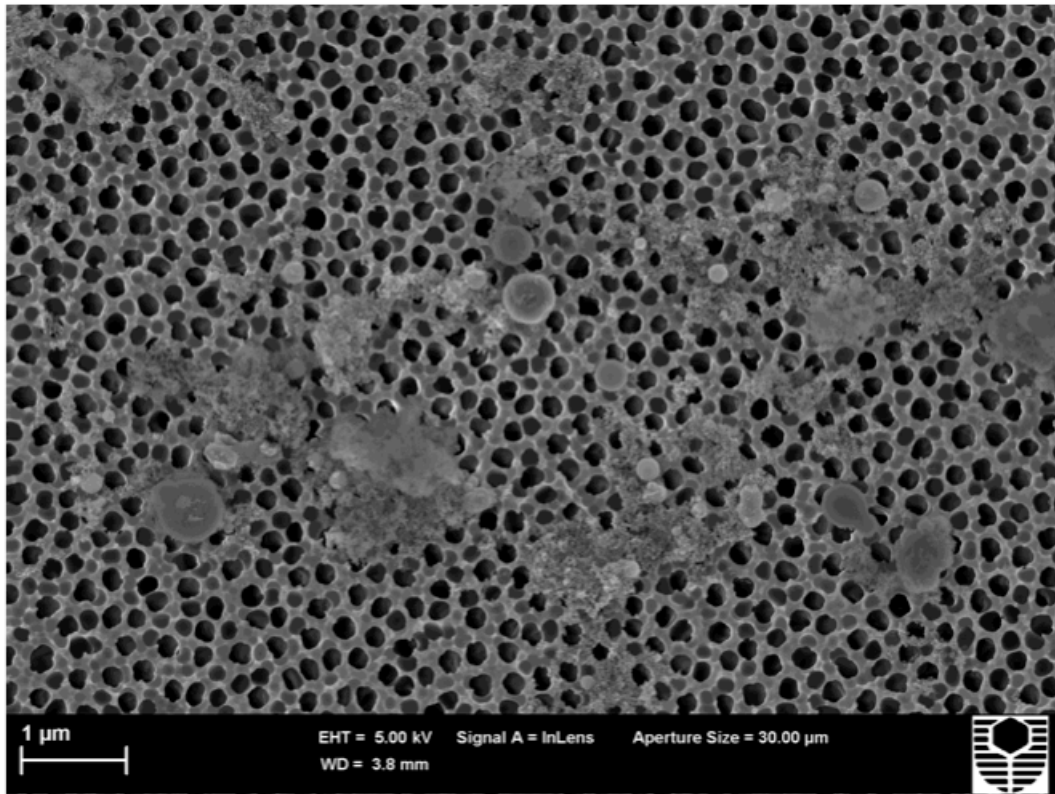


Figure S3.1: SEM image of Anopore filter after filtering 1 L of ice core melt water, and backflushing the filter to remove filtered particles.

Chapter 4. Individual particle morphology, coatings, and impurities of black carbon aerosols in Antarctic ice and tropical rainfall

This chapter been published in *Geophysical Research Letters*. Co-author contributions can be found in Appendix A2.

This article is published as:

Ellis, A., Edwards, R., Saunders, M., Chakrabarty, R. K., Subramanian, R., Timms, N. E., van Riessen, A., Smith, A. M., Lambrinidis, D., Nunes, L. J., Vallelonga, P., Goodwin, I. D., Moy, A. D., Curran, M. A. J., and van Ommen, T. D. (2016), Individual particle morphology, coatings, and impurities of black carbon aerosols in Antarctic ice and tropical rainfall, *Geophys. Res. Lett.*, 43, doi:10.1002/2016GL071042.

Abstract

Black carbon (BC) aerosols are a large source of climate warming, impact atmospheric chemistry, and are implicated in large-scale changes in atmospheric circulation. Inventories of BC emissions suggest significant changes in the global BC aerosol distribution due to human activity. However, little is known regarding BC's atmospheric distribution or aged particle characteristics before the twentieth century. Here we investigate the prevalence and structural properties of BC particles in Antarctic ice cores from 1759, 1838, and 1930 Common Era (CE) using transmission electron microscopy and energy-dispersive X-ray spectroscopy. The study revealed an unexpected diversity in particle morphology, insoluble coatings, and association with metals. In addition to conventionally occurring BC aggregates, we observed single BC monomers, complex aggregates with internally, and externally mixed metal and mineral impurities, tar balls, and organonitrogen coatings. The results of the study show BC particles in the remote Antarctic atmosphere exhibit complexity that is unaccounted for in atmospheric models of BC.

4.1 Introduction

Black carbon aerosols (BC) are primary particles emitted by fossil fuel combustion and biomass burning. They have a multitude of effects on the global atmosphere and Earth's surface, which result in the second largest contribution to climate change after carbon dioxide (CO₂) (Bond et al., 2013). Unlike CO₂ and methane gas (CH₄), BC's atmospheric residence time is relatively short (weeks as opposed to decades) and its atmospheric concentration is highly variable (Kaufman et al., 2002). BC emissions may have already contributed to large-scale changes in atmospheric circulation, with models suggesting that the Northern Hemisphere tropics expand linearly with increasing radiative forcing from BC emissions (Kovilakam and Mahajan, 2015). The physical, chemical, and optical properties of BC are dynamic and evolve during atmospheric transport (Browne et al., 2015; Shen et al., 2014; Wang et al., 2014). Estimates of BC climate sensitivity are complicated by hemispheric differences in both emission sources (fossil fuels or biomass burning) and co-emitted chemical species, which coat and react with BC in the atmosphere. Indeed, BC from East Asian fossil fuel may be removed from the atmosphere faster than expected due to co-emitted sulfate (Shen et al., 2014).

Morphologically, BC particles are semi-fractal aggregates composed of small, ~30 nm semi-graphitic carbon nanospheres (Andreae and Gelencsér, 2006). Graphitic carbon consists of randomly oriented graphite crystallites with a mean inter-crystallite distance of 2.5 nm, embedded in a matrix of amorphous carbon (Franklin, 1950, 1951). After emission, BC rapidly ages in the atmosphere. The fractal dimensions of BC aggregates increase and their surfaces become coated and partially oxidized, affecting both their optical properties and their interaction with water (McFiggans et al., 2006; Oshima et al., 2009). The evolution of the BC surface from hydrophobic to hydrophilic has a major influence on its aerodynamic size, its removal from the atmosphere by wet deposition, and its subsequent transport and residence time in the atmosphere (Shen et al., 2014). Other insoluble particles may become externally and internally mixed with BC, thereby changing its optical properties (Scarnato et al., 2015). While there have been many characterization studies of freshly emitted BC aggregates (Chakrabarty et al., 2006a; Chakrabarty et al., 2006b; Pósfai et al., 2003; Zhu et al., 2013), few studies have investigated the morphology and characteristics of aged BC aggregates in the remote Southern Hemisphere (Pósfai et al., 1999). Consequently, the full range of properties of BC and their climate forcing effects remain uncertain. Furthermore,

little is known with regards to historic records of atmospheric BC before the last few decades. Polar ice-cores preserve an extensive history of atmospherically transported and aged BC particles and provide an opportunity to study changes in the physical and chemical properties of long-distance transported BC during and before the industrial revolution. Building upon the development of a method to concentrate BC particles in water (Ellis et al., 2015), we investigated individual particles in an Antarctic ice core using electron microscopy.

Previous studies of BC in Antarctica have included bulk aerosol measurements, mass concentrations, and optical properties of Antarctic snow and ice (Bisiaux et al., 2012; Warren and Clarke, 1990; Weller et al., 2013; Wolff and Cachier, 1998). These studies identified large seasonal variations in coastal East and West Antarctic BC aerosol concentrations with a primary peak in October that is associated with dry-season biomass burning on nearby continents. A smaller secondary peak in BC concentration is observed during austral summer fire season (Weller et al., 2013) with minimum concentrations in March – April. High-temporal resolution ice core studies found similar seasonality in West and East Antarctic ice concentrations during the past 200 years (Bisiaux et al., 2012). The seasonality and atmospheric circulation associated with BC in the Antarctic atmosphere (Bisiaux et al., 2012; Stohl and Sodemann, 2010) suggests that long-range transported SH biomass burning emissions are the primary source of BC to Antarctica.

Although ultra-trace BC concentrations ($0.08 \mu\text{g kg}^{-1}$) have been determined in Antarctic ice and snow, little is known with regards to individual particle morphology, coatings, and impurities. These characteristics impact the particles' optical and radiative properties, residence time in the atmosphere, and climatic impacts. Here we present results from the detailed analysis of individual particles found in an East Antarctic ice core and modern tropical rain samples from northern Australia. Three samples were prepared from ice core samples from the Law Dome ice cap, East Antarctica dated from 1759, 1838 and 1930 Common Era (CE), predating and postdating global industrialization and western colonization of Australia. Tropical rain samples were collected in northern Australia to provide a complementary modern comparison to Antarctic ice, as wet-deposited BC close to potential source emissions. All samples were analyzed using High-Resolution Transmission Electron Microscope Imaging (HR-TEM) and Scanning Transmission Electron Microscope Energy-Dispersive x-ray Spectroscopy (STEM-EDS, hereafter EDS).

4.2 Materials and Methods

4.2.1 Ice core samples

Antarctic ice core samples consisted of ice sections sub-sampled from the Dome Summit South site (DSS0506, 66°46' S, 112°48' E, 1,370 m elevation) drilled on Law Dome, East Antarctica during the 2005-2006 austral summer. The site has been described and studied in detail (Curran et al., 1998; Edwards et al., 2006; Etheridge et al., 1996; van Ommen and Morgan, 1996). The depth/age scale of the ice core was constructed by matching dissolved ion chemistry and water stable isotope records ($\delta^{18}\text{O}$) to the main DSS ice core record, which was dated using annual layer counting and validated by well-characterized volcanic horizons (Plummer et al., 2012).

4.2.2 Rain samples

Tropical rain samples were collected in Darwin, Northern Territory, Australia, to compare modern BC in wet deposition, close to BC sources. Two rain samples of ~1 L each were collected in April 2014, a period of significant monsoonal rainfall in the Northern Territory. Boundary layer atmospheric circulation to the sampling site during April 2014 was predominately East-West, passing over northern Queensland and the Gulf of Carpentaria before arriving in the Northern Territory.

Samples were collected in low-density polyethylene (LDPE) bottles, rinsed with ultra-pure (UP) water ($\rho > 18.2 \text{ M}\Omega\text{cm}$). A full account of sample collection and handling is described in Ellis et al. (2015).

4.2.3 Ice core decontamination and liquid preconcentration

Mass concentrations of BC in Antarctic snow and ice are typically found in the parts-per-trillion (ppt) level and require preconcentration before analysis by Transmission Electron Microscopy (TEM). While Antarctic snow BC concentrations are low, the concentrations of other species, such as sea salts, may be present at the high parts-per-billion (ppb) level, depending on the location. The presence of relatively high concentrations of dissolved salts species complicates sample preconcentration and obscures BC particles loaded on TEM grids. To concentrate BC particles from ice core samples and rain without concentrating dissolved salts, we used the Tangential Flow Filtration (TFF) preconcentration method (Ellis

et al., 2015). Melt water from 1 m x 5 cm x 5 cm ice core sections, representing approximately two years of deposition to the site, were concentrated by approximately a factor of 1000 using hollow fiber filters (10 nm pore size, Spectrum Labs, USA). The TFF concentrate from each sample was transferred to a TEM grid (SPI 300-mesh gold grids with a continuous SiO/SiO₂ support film) and evaporated down within an ISO 10 clean hood. Tropical rainwater samples were processed identically to the ice core melt-water.

4.2.4 TEM characterization

Characterization (imaging of external morphology and internal structure, size, and composition) of the insoluble particles and their coatings was completed on an FEI Titan G2 80-200 TEM/STEM with ChemiSTEM Technology at The University of Western Australia, operating at 80 kV to minimize the risk of structural damage to the carbon spheres. High-Angle Annular Dark Field Scanning Transmission Electron Microscopy (HAADF-STEM) imaging and element mapping were also carried out at 80 kV on the same instrument. The element maps were obtained by energy dispersive X-ray spectroscopy using the Super-X detector on the Titan with a sub-nm probe size, a probe current of ~0.25 nA, a dwell time of 15 microseconds, and total acquisition time of 20 to 30 minutes. Statistical evaluation of the proportions and size distribution of the various BC morphologies was inhibited because the TEM grids were not surveyed systematically – irregular deposition of particles on the grids and the limited field of view (< 10 μm) resulting from the high magnification of the instrument makes location and characterization of BC particles time intensive, and acquisition of significant BC morphotype population statistics difficult. Therefore, the images selected for this paper represent common BC morphologies and characteristics seen while imaging the TEM grid. Images of additional particle types can be found in the supporting information.

4.3 Results

In all samples, abundant single BC nanospheres (Figure 4.1) in addition to conventional multi-spherule aggregates were observed. The nanoparticles were identified by their ~30 nm diameter, concentric ‘onion’ carbon layering with short-range order, and the K α carbon peak in the EDS spectra. Single BC nanospheres are not thought to exist individually in the atmosphere (Andreae and Gelencsér, 2006) and to our knowledge have not previously been

observed in ice or snow. However, their presence in Antarctic ice suggests that they must be ubiquitous in the global atmosphere. Because of their small size and the confounding presence of larger BC aggregates and other dust particles, the single spheres are difficult to discern without the use of STEM-EDS mapping. They have too little mass to be quantified by real-time single BC particle analysis instruments used in other studies (Slowik et al., 2007). It would be difficult to distinguish the single nanospheres in the presence of concentrated salts or sulfates. The preconcentration method used in this study removes dissolved salts and other water-soluble species, retaining insoluble particles. Our method is also extremely gentle (mechanically), and unlikely to provide enough mechanical force to separate the aggregates (Rothenbacher et al., 2008). Further investigation has revealed many examples of doublet and triplet BC nanospheres of various primary particle sizes (Figure 4.1b-d). Single BC nanospheres were found in all ice core samples (dated to 1759, 1838, and 1930 CE) via HR-TEM. The rain samples also contained all of the nanosphere varieties that were seen in the ice cores, indicating their possible global presence.

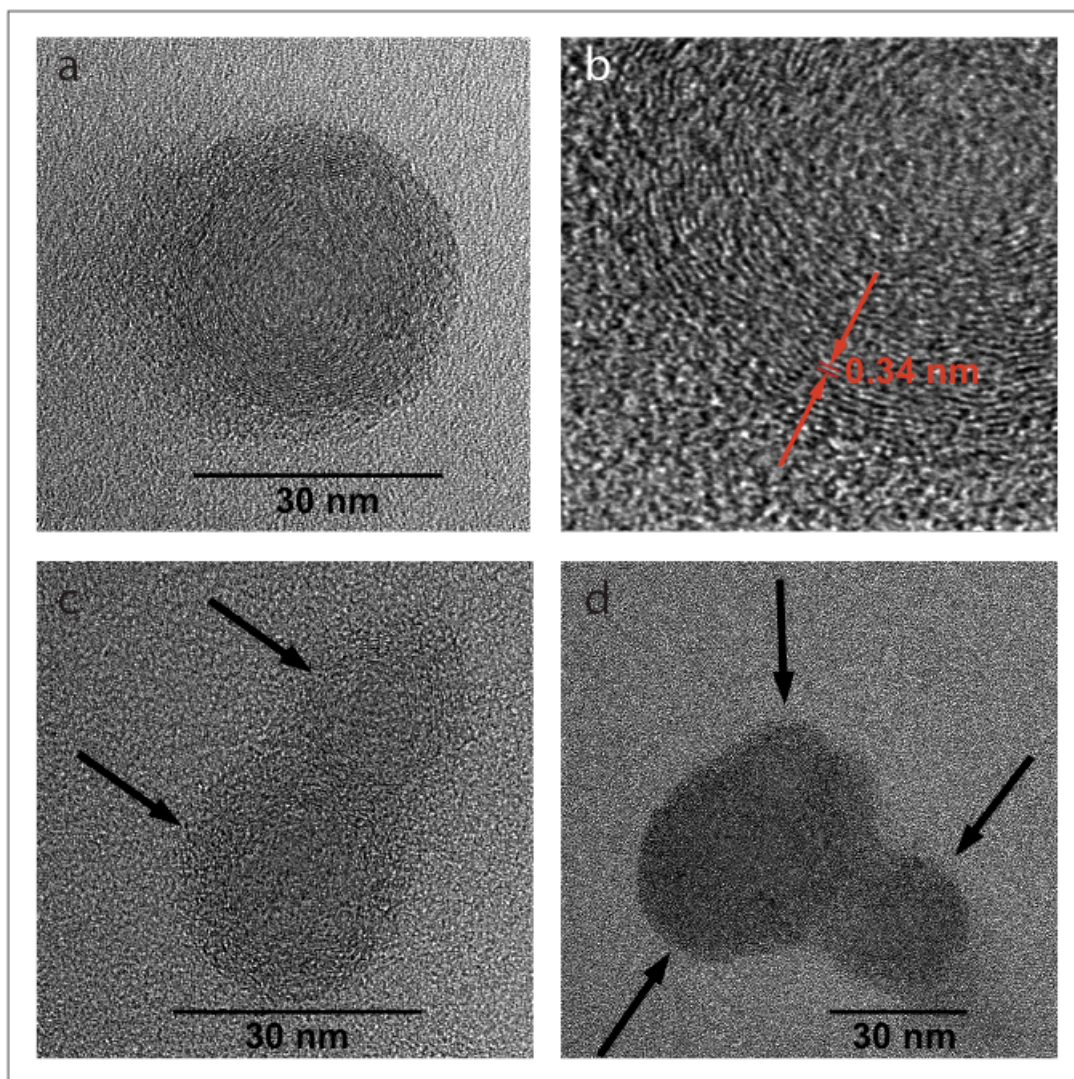


Figure 4.1: Black carbon nanospheres in Antarctic ice dated to 1838 CE: a) single BC nanosphere showing concentric ring structure with short-range internal structure, b) enlarged section of a), showing the concentric layers with 0.34 nm spacing between layers, c) BC particle with two spherules, arrows indicating spheres, and d) BC particle with three spherules, arrows indicating spheres. Additional examples of single spheres from 1759 CE and 1930 CE are included in the supporting information.

Although quantification is difficult for irregularly distributed nanoparticles on TEM grids, a preliminary estimate of the prevalence of single BC nanospheres can be obtained using a single particle soot photometer (SP2, Droplet Measurement Technologies). Indeed, BC size distribution data in 20th century ice from the same location in East Antarctica indicates a substantial fraction of BC particles exist below 0.7 fg (90 nm mass-equivalent diameter assuming a BC density of 1.8 g cm^{-3}), the lower mass limit where the SP2 begins to detect less than 100% of BC aerosols, supporting the existence of these individual nanospheres in

great numbers – primary nanospheres may outnumber the larger BC aggregates that have previously been reported.

This observation raises significant questions about the prevalence of single BC nanospheres, as well as the undescribed effects of single nanospheres on the environment. Modern scattering calculations for BC suggest that variations in size distribution, composition, or shape could have substantial effects on common spherical and Rayleigh-Debye-Gans (RDG) simplifications (Smith and Grainger, 2014). Though the individual nanospheres are likely to be too small to function as cloud condensation nuclei (CCN), aerosol chamber experiments have shown 30 nm metallic nanoparticles (Saunders et al., 2010) as well as conventional BC aggregates (DeMott et al., 1999) acting as ice nuclei in the atmosphere. This suggests the possibility that individual 30 nm BC nanospheres may contribute to the formation of ice particles in the atmosphere, thereby having an as yet unmeasured climate affect.

In addition to the single spherules, many other distinct BC characteristics were observed in the ice cores. We found a continuum of BC aggregate sizes ranging from doublet and triplet BC spherules (Figures 4.1c, d) up to many hundred nanometers (Figures 4.2 and 4.3). While the fractal dimension of the aggregates was not determined, they appeared to be relatively compact as would be expected of BC that has been substantially aged in the atmosphere and suspended in liquid water during the concentration procedure. All BC aggregates exhibited some form of thin insoluble coating (~5 nm) that connected the individual spherules, similar to the thin ‘film’ of carbon found on remote BC aerosols by Pósfai et al. (1999). EDS analysis revealed that the coatings appear to be composed predominately of amorphous carbon combined with varying amounts of nitrogen and oxygen-rich materials.

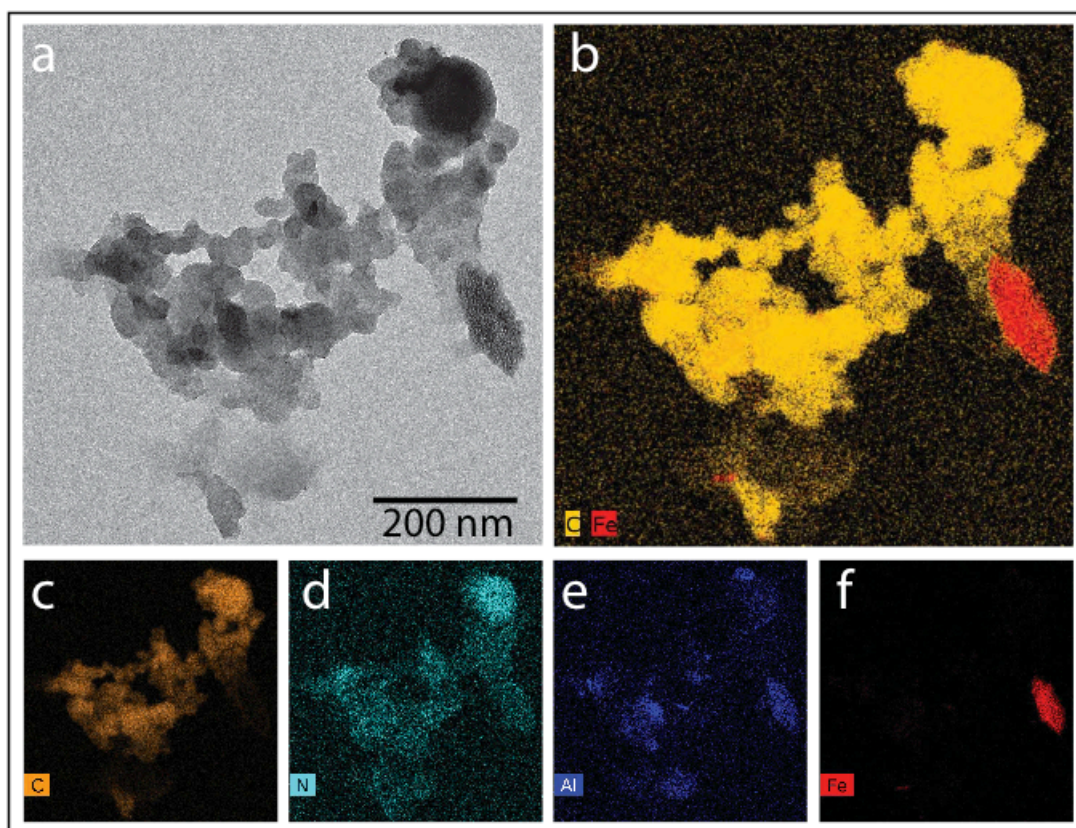


Figure 4.2: TEM images and STEM-EDS maps to show compositional complexity of a black carbon aggregate, from ice dated to 1838 CE, with EDS maps taken from the same field of view as a). a) TEM image of BC aggregate, with tar ball incorporated into the aggregate, b) STEM-EDS map overlay of carbon and iron, to highlight the iron particle connected with a carbon coating, c) carbon map, d) nitrogen map, e) various aluminum-rich inclusions within the BC aggregate, f) iron map.

These coatings appeared to be unaffected by high vacuum (10^{-5} Pa) or an 80 kV electron beam. While we have no definitive way of ascertaining when the coatings formed, it is likely that coatings are part of the atmospheric aging process and may have formed through aqueous cloud chemistry (Lee et al., 2013). The presence of oxygen in the coatings suggests that they are hydrophilic. The presence of a thin hydrophilic coating influences the BC particles' interaction with atmospheric water, its atmospheric residence time, and optical properties.

Coated BC aggregates were routinely found in association with mineral dust particles composed of aluminum-rich silicates and iron. Magnesium, potassium, and zinc were also present in some attached minerals (Figure S4.6, Supplementary Information). Many of the dust particles were found to be connected to the outside of BC aggregates by thin films of carbon, nitrogen, and oxygen (Figure 4.2b, 4.4), as well as being incorporated within the BC

aggregate structure (Figure 4.3b). The external connections of the BC to the dust particles suggest that they are ice residual nuclei, as expected of wet deposited BC in ice cores. Mineral dusts are common ice nuclei (DeMott et al., 2003), and ice crystal scavenging of BC could explain the external connection (Baumgardner et al., 2008).

Small iron particles (~10 nm in diameter) were often found adhered to the surface of BC aggregates (Figures 4.3, 4.5). These attachments can be difficult to distinguish without the use of EDS or HAADF-STEM, in which heavier element inclusions stand out brightly.

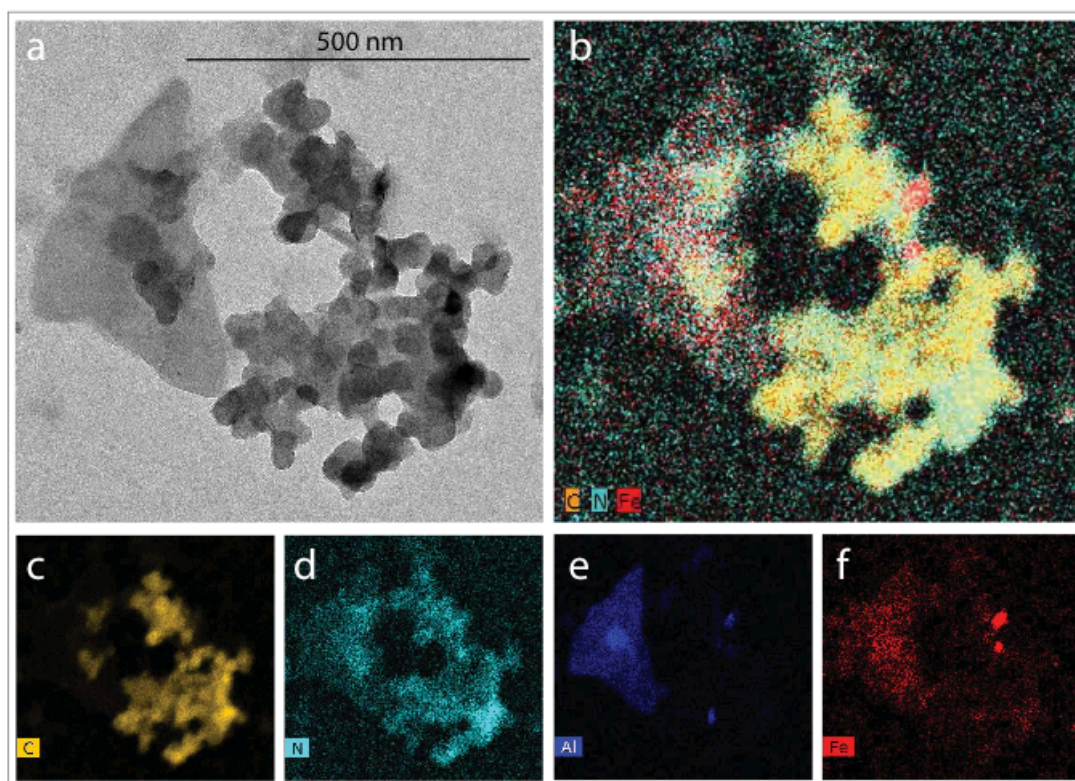


Figure 4.3: Dust particle and BC aggregate dated to 1838 CE, with aluminum and iron dust particles incorporated within the BC aggregate, and EDS maps taken from the same field of view as a). a) TEM image, b) carbon, nitrogen, and iron STEM-EDS maps, overlaid to show the connection of the iron particles to the BC aggregate with a nitrogen-rich coating, c-f) carbon, nitrogen, aluminum, and iron STEM-EDS maps, respectively.

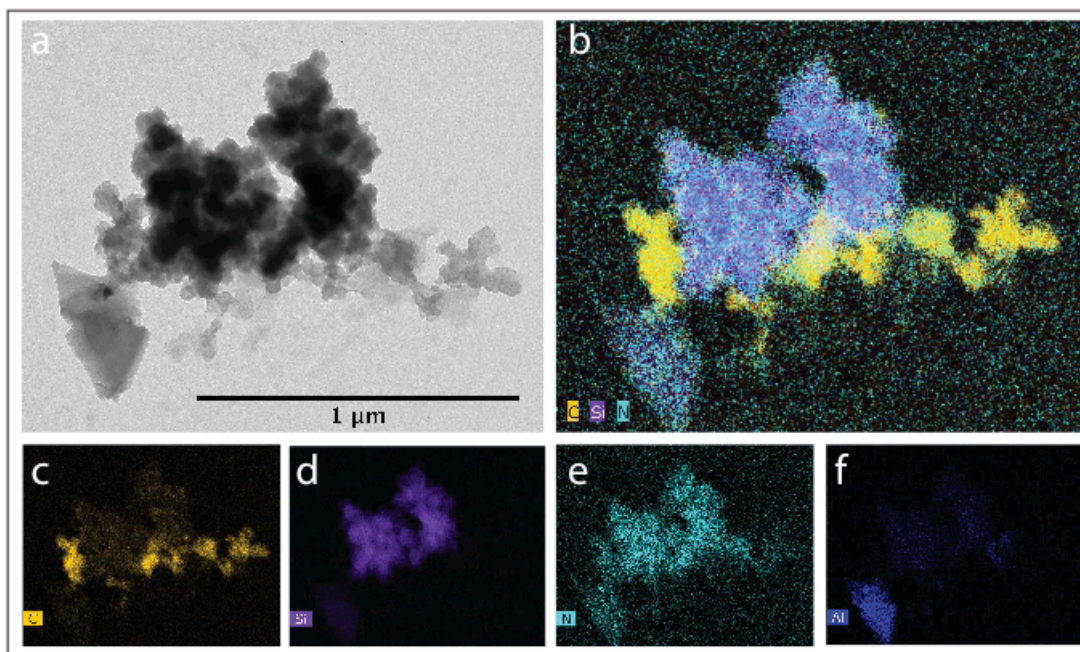


Figure 4.4: Large silica-rich dust particle from ice dated to 1838 CE, with BC attached and mixed into the silica structure, with all components connected with thin (<5 nm), amorphous carbon and nitrogen rich coating, with EDS maps taken from the same field of view as a). a) TEM image, b) carbon, silicon, and nitrogen STEM-EDS maps overlaid to show connection of silicon and BC aggregates, with nitrogen-rich coating, c-f) carbon, silicon, nitrogen, and aluminum STEM-EDS maps, respectively.

BC has previously been imaged with larger dust particles in East Asian outflows (Clarke et al., 2004) and African biomass burning plumes (Li et al., 2003), and the results of our study show that external BC and dust can be connected by insoluble coatings and can be transported long distances without disaggregating. These organic coatings and dust inclusions may have significant effects on BC's optical properties as well as functioning as cloud and ice nuclei in the atmosphere (Lohmann and Diehl, 2006).

The iron attached to the BC is of particular interest with respect to the biogeochemistry of iron in surface waters of the SH and potentially for the formation of water insoluble organic coatings through catalytic polymerization of organic species in biomass burning plumes (Slikboer et al., 2015).

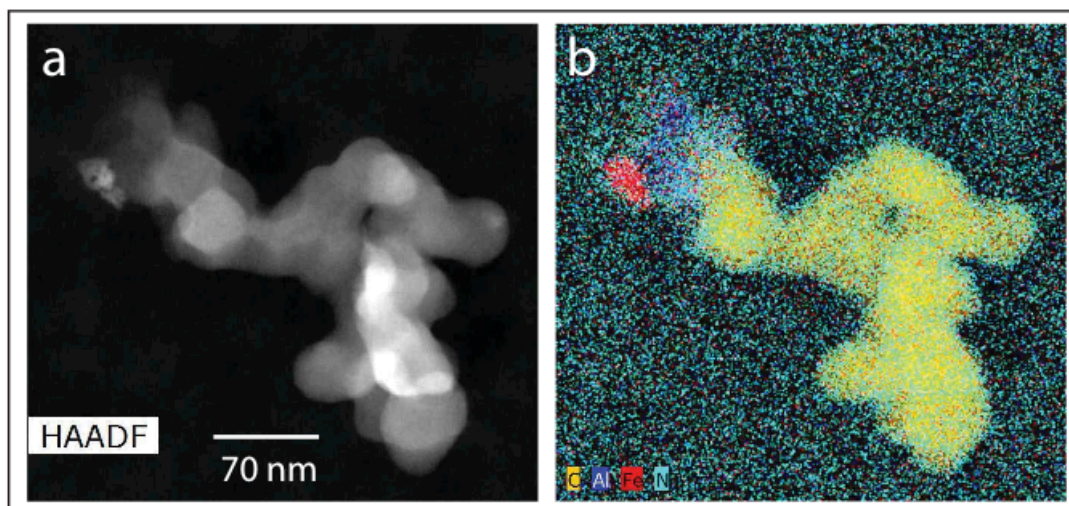


Figure 4.5: BC aggregate from ice dated to 1930 CE attached to aluminosilicate and iron particles with nitrogen-rich coating, with EDS map taken from the same field of view as a). a) High-angle annular dark-field (HAADF) image of the particle, b) energy-dispersive x-ray spectroscopy (EDS) maps of C, Al, Fe, and N, indicating the aluminosilicate and iron particles are attached to the black carbon aggregate with a nitrogen-rich coating.

Tar balls, amorphous, carbon-rich spheres emitted from smoldering fires, also accompanied the BC aggregates, both attached to the outside (Figure 4.6) and incorporated within the BC aggregates (Figure 4.2). Chakrabarty et al. (2006b) noted the existence of tar balls in laboratory combustion tests of biomass fuels, supporting their formation at the emission source. The presence of tar balls in Antarctic ice suggests that the particles were emitted by smoldering biomass burning (Adachi and Buseck, 2011; Chakrabarty et al., 2010). To the best of our knowledge, this is the first determination of tar balls in Antarctica. They represent a previously unaccounted-for component of light absorbing aerosols deposited to the Antarctic ice sheet. If tar balls are present in Antarctic ice they are likely present in air masses over the Southern Ocean and, presumably, the global troposphere. Further evidence of coatings, dust and metals, and single BC nanospheres in all samples are provided in the supporting information, as well as all additional STEM-EDS element maps for the particles described above.

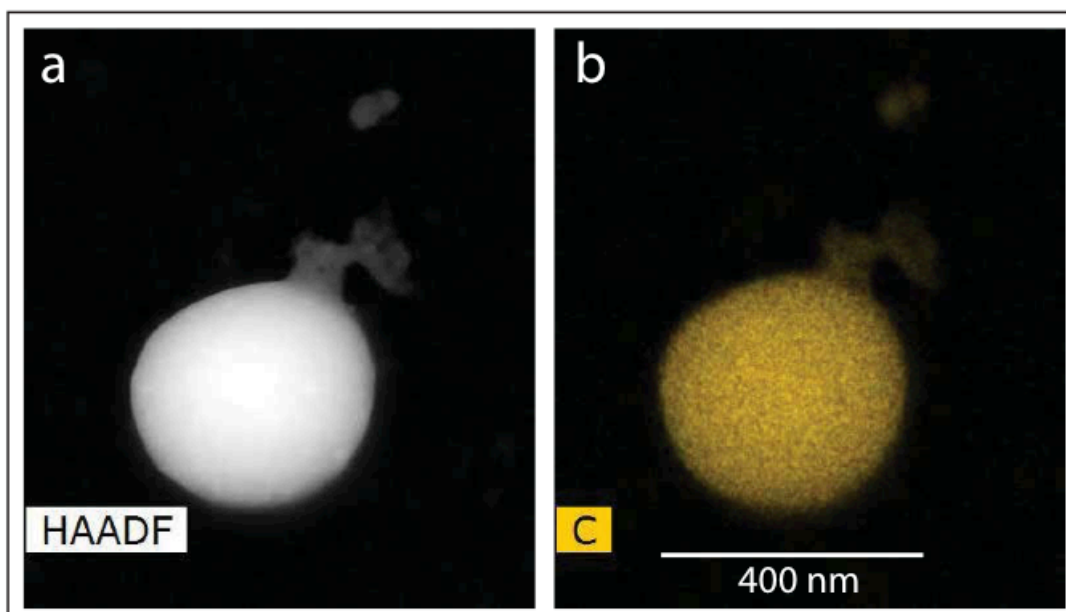


Figure 4.6: a) High-angle annular dark-field (HAADF) image of a tar ball from ice dated to 1838 CE with BC aggregate attached, b) EDS map of carbon from the same field of view as a). Additional EDS maps are included in the supporting information.

4.4 Conclusions

In this study, we found evidence for the deposition of single black carbon (BC) nanospheres over East Antarctica and northern Australia. By extrapolation, we would expect to find these particles throughout the Southern Hemisphere, if not globally. The presence of single BC nanospheres in Antarctic ice dated to 1759 CE, prior to industrialization, suggests the source is likely grass or bush fires. We also found tar balls and BC with nitrogen and oxygen rich insoluble coatings and associated with mineral particles and iron. The coatings appear to cover and connect the BC and many of the mineral particles. This suggests that the coatings and dust inclusions could form in a number of ways: rapidly close to the fire source, due to aqueous chemistry, and physical and chemical ice formation processes. These mixed particles also undergo long-range transport without disaggregating. The impact of the coatings and the external and internal mixing of the mineral particles may impact BC's optical properties and residence time in the atmosphere.

Knowledge of the long-range evolution of BC aerosol characteristics is critical for predicting the associated climate forcing. Mineral inclusions, metal impurities, and insoluble, nitrogen-rich coatings suggest a complex evolution in BC optical properties during transport. The

diversity of particle properties observed in this study demonstrates the complexity of BC in the environment that is as yet unaccounted for in atmospheric chemistry and climate models.

The BC particles analyzed by the study did not display discernible differences between the different time periods, which may reflect the biomass burning-dominated emissions from the Southern Hemisphere. However, the small sample number and limited time span precludes conclusions regarding any systematic changes to BC morphology from the preindustrial period through the 20th Century. Northern Hemisphere shifts from natural biomass burning to anthropogenic industrial emissions during the industrial revolution could be recorded in BC characteristics, suggesting Arctic ice core investigations as an important future application of this study.

Acknowledgments, Samples, and Data

The data used will be available online at the Australian Antarctic Data Centre repository at <https://data.aad.gov.au/>.

This work was supported by Australian Antarctic Sciences grant 4144, Curtin University grant RES-SE-DAP-AW-47679-1, and ARC LIEF grant LE130100029. The authors acknowledge the use of Curtin University's Microscopy & Microanalysis Facility, whose instrumentation has been partially funded by the University, State and Commonwealth Governments. The authors acknowledge the facilities, and the scientific and technical assistance of the Australian Microscopy & Microanalysis Research Facility at the Centre for Microscopy, Characterisation & Analysis, The University of Western Australia, a facility funded by the University, State, and Commonwealth Governments.

References

- Adachi, K., and P. R. Buseck (2011), Atmospheric tar balls from biomass burning in Mexico, *J. Geophys. Res. Atmos.*, 116(D5), D05204, doi:10.1029/2010JD015102.
- Andreae, M. O., and A. Gelencsér (2006), Black carbon or brown carbon? The nature of light-absorbing carbonaceous aerosols, *Atmos. Chem. Phys.*, 6(10), 3131-3148, doi:10.5194/acp-6-3131-2006.
- Baumgardner, D., R. Subramanian, C. Twohy, J. Stith, and G. Kok (2008), Scavenging of black carbon by ice crystals over the northern Pacific, *Geophys. Res. Lett.*, 35(22), L22815, doi:10.1029/2008GL035764.
- Bisiaux, M. M., R. Edwards, J. R. McConnell, M. A. J. Curran, T. D. Van Ommen, A. M. Smith, T. A. Neumann, D. R. Pasteris, J. E. Penner, and K. Taylor (2012), Changes in black carbon deposition to Antarctica from two high-resolution ice core records, 1850–2000 AD, *Atmos. Chem. Phys.*, 12(9), 4107-4115, doi:10.5194/acp-12-4107-2012.
- Bond, T. C., S. J. Doherty, D. Fahey, P. Forster, T. Berntsen, B. DeAngelo, M. Flanner, S. Ghan, B. Kärcher, and D. Koch (2013), Bounding the role of black carbon in the climate system: A scientific assessment, *J. Geophys. Res. Atmos.*, 118(11), 5380-5552, doi:10.1002/jgrd.50171.
- Browne, E. C., J. P. Franklin, M. R. Canagaratna, P. Massoli, T. W. Kirchstetter, D. R. Worsnop, K. R. Wilson, and J. H. Kroll (2015), Changes to the Chemical Composition of Soot from Heterogeneous Oxidation Reactions, *J. Phys. Chem. A*, 119(7), 1154-1163, doi:10.1021/jp511507d.
- Chakrabarty, R., H. Moosmüller, L.-W. Chen, K. Lewis, W. Arnott, C. Mazzoleni, M. Dubey, C. Wold, W. Hao, and S. Kreidenweis (2010), Brown carbon in tar balls from smoldering biomass combustion, *Atmos. Chem. Phys.*, 10(13), 6363-6370, doi:10.5194/acp-10-6363-2010.
- Chakrabarty, R. K., H. Moosmüller, W. P. Arnott, M. A. Garro, and J. Walker (2006a), Structural and fractal properties of particles emitted from spark ignition engines, *Environ. Sci. Technol.*, 40(21), 6647-6654, doi:10.1021/Es060537y.
- Chakrabarty, R. K., H. Moosmüller, M. A. Garro, W. P. Arnott, J. Walker, R. A. Susott, R. E. Babbitt, C. E. Wold, E. N. Lincoln, and W. M. Hao (2006b), Emissions from the laboratory combustion of wildland fuels: Particle morphology and size, *J. Geophys. Res. Atmos.*, 111(D7), D07204, doi:10.1029/2005JD006659.
- Clarke, A. D., et al. (2004), Size distributions and mixtures of dust and black carbon aerosol in Asian outflow: Physiochemistry and optical properties, *J. Geophys. Res. Atmos.*, 109(D15), D15S09, doi:10.1029/2003JD004378.
- Curran, M. A., T. D. Van Ommen, and V. Morgan (1998), Seasonal characteristics of the major ions in the high-accumulation Dome Summit South ice core, Law Dome, Antarctica, *Ann. Glaciol.*, 27, 385-390, doi:10.3198/1998AoG27-1-385-390.

DeMott, P. J., Y. Chen, S. M. Kreidenweis, D. C. Rogers, and D. E. Sherman (1999), Ice formation by black carbon particles, *Geophys. Res. Lett.*, 26(16), 2429-2432, doi:10.1029/1999GL900580.

DeMott, P. J., D. J. Cziczo, A. J. Prenni, D. M. Murphy, S. M. Kreidenweis, D. S. Thomson, R. Borys, and D. C. Rogers (2003), Measurements of the concentration and composition of nuclei for cirrus formation, *Proc. Natl. Acad. Sci. USA*, 100(25), 14655-14660, doi:10.1073/pnas.2532677100.

Edwards, R., P. Sedwick, V. Morgan, and C. Boutron (2006), Iron in ice cores from Law Dome: A record of atmospheric iron deposition for maritime East Antarctica during the Holocene and Last Glacial Maximum, *Geochem. Geophys.*, 7(12), 3907-3910, doi:10.1029/2006GC001307.

Ellis, A., Edwards, R., Saunders, M., Chakrabarty, R. K., Subramanian, R., van Riessen, A., Smith, A. M., Lambrinidis, D., Nunes, L. J., Vallelonga, P., Goodwin, I. D., Moy, A. D., Curran, M. A. J. and van Ommen, T. D. (2015), Characterizing black carbon in rain and ice cores using coupled tangential flow filtration and transmission electron microscopy, *Atmos. Meas. Tech.*, 8(9), 3959-3969, doi:10.5194/amt-8-3959-2015.

Etheridge, D., L. Steele, R. Langenfelds, R. Francey, J. M. Barnola, and V. Morgan (1996), Natural and anthropogenic changes in atmospheric CO₂ over the last 1000 years from air in Antarctic ice and firn, *J. Geophys. Res. Atmos.*, 101(D2), 4115-4128, doi:10.1029/95JD03410.

Franklin, R. E. (1950), On the structure of carbon. *J. chim. Phys. Phys.-Chim. Biol.*, 47, 573-575.

Franklin, R. E. (1951), The structure of graphitic carbons. *Acta Crystallogr.*, 4(3), 253-261.

Kaufman, Y. J., D. Tanre, and O. Boucher (2002), A satellite view of aerosols in the climate system, *Nature*, 419(6903), 215-223, doi:10.1038/nature01091.

Kovilakam, M., and S. Mahajan (2015), Black carbon aerosol-induced Northern Hemisphere tropical expansion, *Geophys. Res. Lett.*, 42(12), 4964-4972, doi:10.1002/2015GL064559.

Lee, A. K. Y., R. Zhao, R. Li, J. Liggio, S.-M. Li, and J. P. D. Abbatt (2013), Formation of Light Absorbing Organo-Nitrogen Species from Evaporation of Droplets Containing Glyoxal and Ammonium Sulfate, *Environ. Sci. Technol.*, 47(22), 12819-12826, doi:10.1021/es402687w.

Li, J., M. Pósfai, P. V. Hobbs, and P. R. Buseck (2003), Individual aerosol particles from biomass burning in southern Africa: 2, Compositions and aging of inorganic particles, *J. Geophys. Res. Atmos.*, 108(D13), 8484, doi:10.1029/2002JD002310.

Lohmann, U., and K. Diehl (2006), Sensitivity Studies of the Importance of Dust Ice Nuclei for the Indirect Aerosol Effect on Stratiform Mixed-Phase Clouds, *J. Atmos. Sci.*, 63(3), 968-982, doi:10.1175/JAS3662.1.

McFiggans, G., et al. (2006), The effect of physical and chemical aerosol properties on warm cloud droplet activation, *Atmos. Chem. Phys.*, 6(9), 2593-2649, doi:10.5194/acp-6-2593-2006.

- Oshima, N., M. Koike, Y. Zhang, and Y. Kondo (2009), Aging of black carbon in outflow from anthropogenic sources using a mixing state resolved model: 2. Aerosol optical properties and cloud condensation nuclei activities, *J. Geophys. Res. Atmos.*, 114(D18), 2156-2202, doi:10.1029/2008JD011681.
- Plummer, C. T., M. A. J. Curran, T. D. van Ommen, S. O. Rasmussen, A. D. Moy, T. R. Vance, H. B. Clausen, B. M. Vinther, and P. A. Mayewski (2012), An independently dated 2000-yr volcanic record from Law Dome, East Antarctica, including a new perspective on the dating of the 1450s CE eruption of Kuwae, Vanuatu, *Clim. Past*, 8(6), 1929-1940, doi:10.5194/cp-8-1929-2012.
- Pósfai, M., J. R. Anderson, P. R. Buseck, and H. Sievering (1999), Soot and sulfate aerosol particles in the remote marine troposphere, *J. Geophys. Res. Atmos.*, 104(D17), 21685-21693, doi:10.1029/1999JD900208.
- Pósfai, M., R. Simonics, J. Li, P. V. Hobbs, and P. R. Buseck (2003), Individual aerosol particles from biomass burning in southern Africa: 1. Compositions and size distributions of carbonaceous particles, *J. Geophys. Res. Atmos.*, 108(D13), 8483, doi:10.1029/2002JD002291.
- Rothenbacher, S., A. Messerer, and G. Kasper (2008), Fragmentation and bond strength of airborne diesel soot agglomerates, *Part. Fib. Toxicol.*, 5(9), 1, doi:10.1186/1743-8977-5-9.
- Saunders, R. W., et al. (2010), An aerosol chamber investigation of the heterogeneous ice nucleating potential of refractory nanoparticles, *Atmos. Chem. Phys.*, 10(3), 1227-1247, doi:10.5194/acp-10-1227-2010.
- Scarnato, B. V., S. China, K. Nielsen, and C. Mazzoleni (2015), Perturbations of the optical properties of mineral dust particles by mixing with black carbon: a numerical simulation study, *Atmos. Chem. Phys.*, 15(12), 6913-6928, doi:10.5194/acp-15-6913-2015.
- Shen, Z., J. Liu, L. Horowitz, D. Henze, S. Fan, D. Mauzerall, J.-T. Lin, and S. Tao (2014), Analysis of transpacific transport of black carbon during HIPPO-3: implications for black carbon aging, *Atmos. Chem. Phys.*, 14(12), 6315-6327, doi:10.5194/acp-14-6315-2014.
- Slikboer, S., L. Grandy, S. L. Blair, S. A. Nizkorodov, R. W. Smith, and H. A. Al-Abadleh (2015), Formation of Light Absorbing Soluble Secondary Organics and Insoluble Polymeric Particles from the Dark Reaction of Catechol and Guaiacol with Fe(III), *Environ. Sci. Technol.*, 49(13), 7793-7801, doi:10.1021/acs.est.5b01032.
- Slowik, J. G., et al. (2007), An inter-comparison of instruments measuring black carbon content of soot particles, *Aerosol Sci. Technol.*, 41(3), 295-314, doi:10.1080/02786820701197078.
- Smith, A. J. A., and R. G. Grainger (2014), Simplifying the calculation of light scattering properties for black carbon fractal aggregates, *Atmos. Chem. Phys.*, 14(15), 7825-7836, doi:10.5194/acp-14-7825-2014.
- Stohl, A., and H. Sodemann (2010), Characteristics of atmospheric transport into the Antarctic troposphere, *J. Geophys. Res. Atmos.*, 115, D02305, doi:10.1029/2009jd012536.

van Ommen, T. D., and V. Morgan (1996), Peroxide concentrations in the Dome summit south ice core, Law Dome, Antarctica, *J. Geophys. Res. Atmos.*, 101(D10), 15147-15152, doi:10.1029/96JD00838.

Wang, X., C. L. Heald, D. A. Ridley, J. P. Schwarz, J. R. Spackman, A. E. Perring, H. Coe, D. Liu, and A. D. Clarke (2014), Exploiting simultaneous observational constraints on mass and absorption to estimate the global direct radiative forcing of black carbon and brown carbon, *Atmos. Chem. Phys.*, 14(20), 10989-11010, doi:10.5194/acp-14-10989-2014.

Warren, S. G., and A. D. Clarke (1990), Soot in the atmosphere and snow surface of Antarctica, *J. Geophys. Res. Atmos.*, 95(D2), 1811-1816, doi:10.1029/JD095iD02p01811.

Weller, R., A. Minikin, A. Petzold, D. Wagenbach, and G. König-Langlo (2013), Characterization of long-term and seasonal variations of black carbon (BC) concentrations at Neumayer, Antarctica, *Atmos. Chem. Phys.*, 13(3), 1579-1590, doi:10.5194/acp-13-1579-2013.

Wolff, E. W., and H. Cachier (1998), Concentrations and seasonal cycle of black carbon in aerosol at a coastal Antarctic station, *J. of Geophys. Res.*, 103(D9), 11033-11041, doi:10.1029/97JD01363.

Zhu, J., P. A. Crozier, and J. R. Anderson (2013), Characterization of light-absorbing carbon particles at three altitudes in East Asian outflow by transmission electron microscopy, *Atmos. Chem. Phys.*, 13(13), 6359-6371, doi:10.5194/acp-13-6359-2013.

Supplementary Information

This supplementary addendum contains additional electron microscopy images, energy dispersive x-ray spectroscopy (EDS) information, and high-angle annular dark-field images (HAADF) to support the data in the corresponding paper. It also contains HYSPLIT (Hybrid Single Particle Lagrangian Integrated Trajectory Model) trajectories for air mass transport to the rain sampling site in Darwin, Northern Territory, Australia.

Electron microscopy images were processed using ImageJ software. The particles described in this paper are meant to be qualitative, as detailed statistical analysis of particle composition and morphology was not conducted. Due to the small field of view ($<1 \mu\text{m}$) relative to the full sample size (3 mm), statistical analysis of particles would take significant instrument time.

Rain samples were collected in an open field, free from overhead obstructions. Sample bottles and funnel were all triple-rinsed in ultra-pure (UP) water ($\rho > 18.2 \text{ M}\Omega \cdot \text{cm}$).

HYSPLIT back-trajectories for the rain samples were calculated for heights of 500 m, 1000 m, and 2000 m to account for different cloud heights originating the sampled rain. For all days, the particle trajectories did not differ dramatically for each of the possible heights.

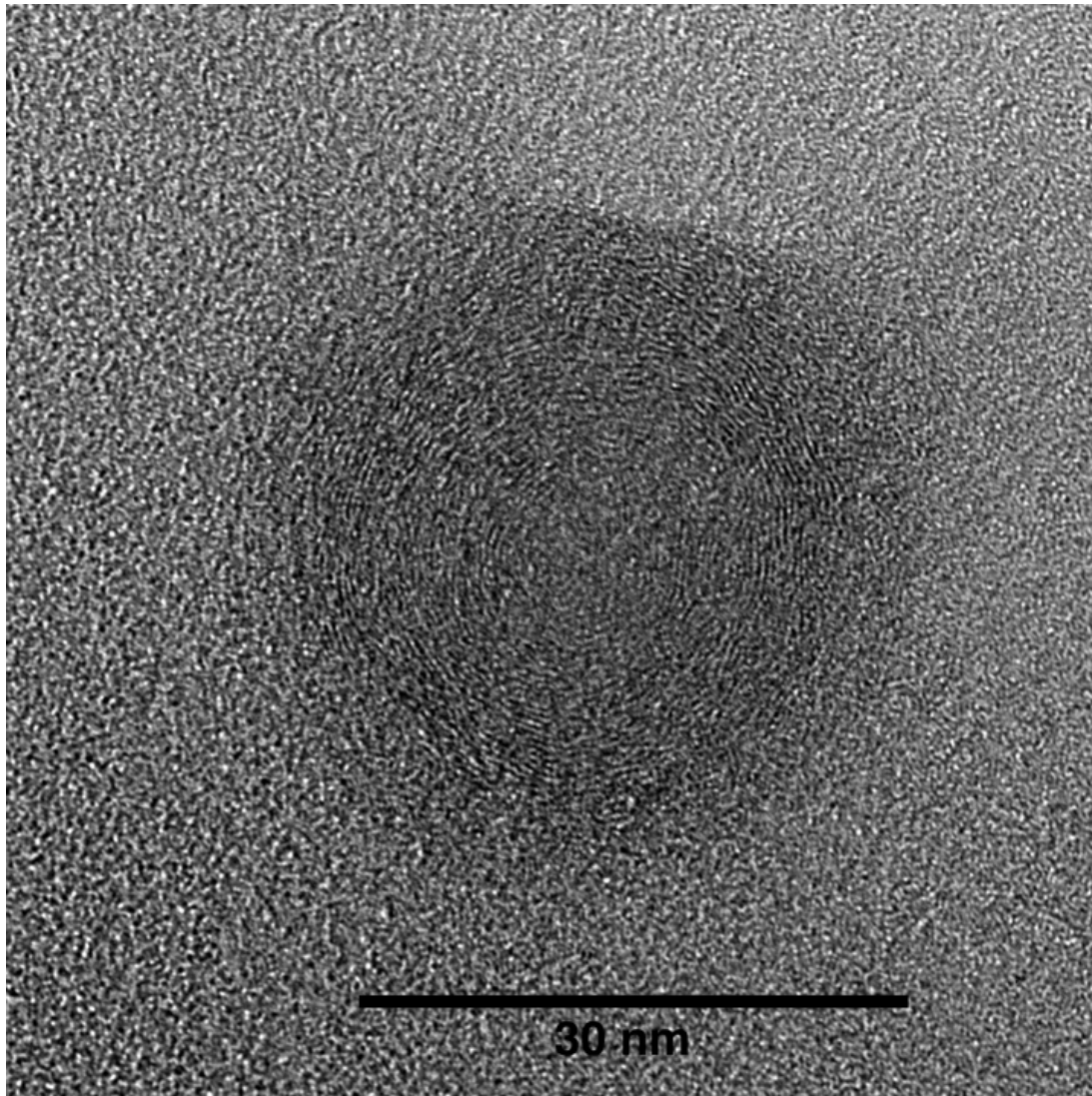


Figure S4.1: Additional image of a single BC spheres found in an ice core dated to 1759 CE

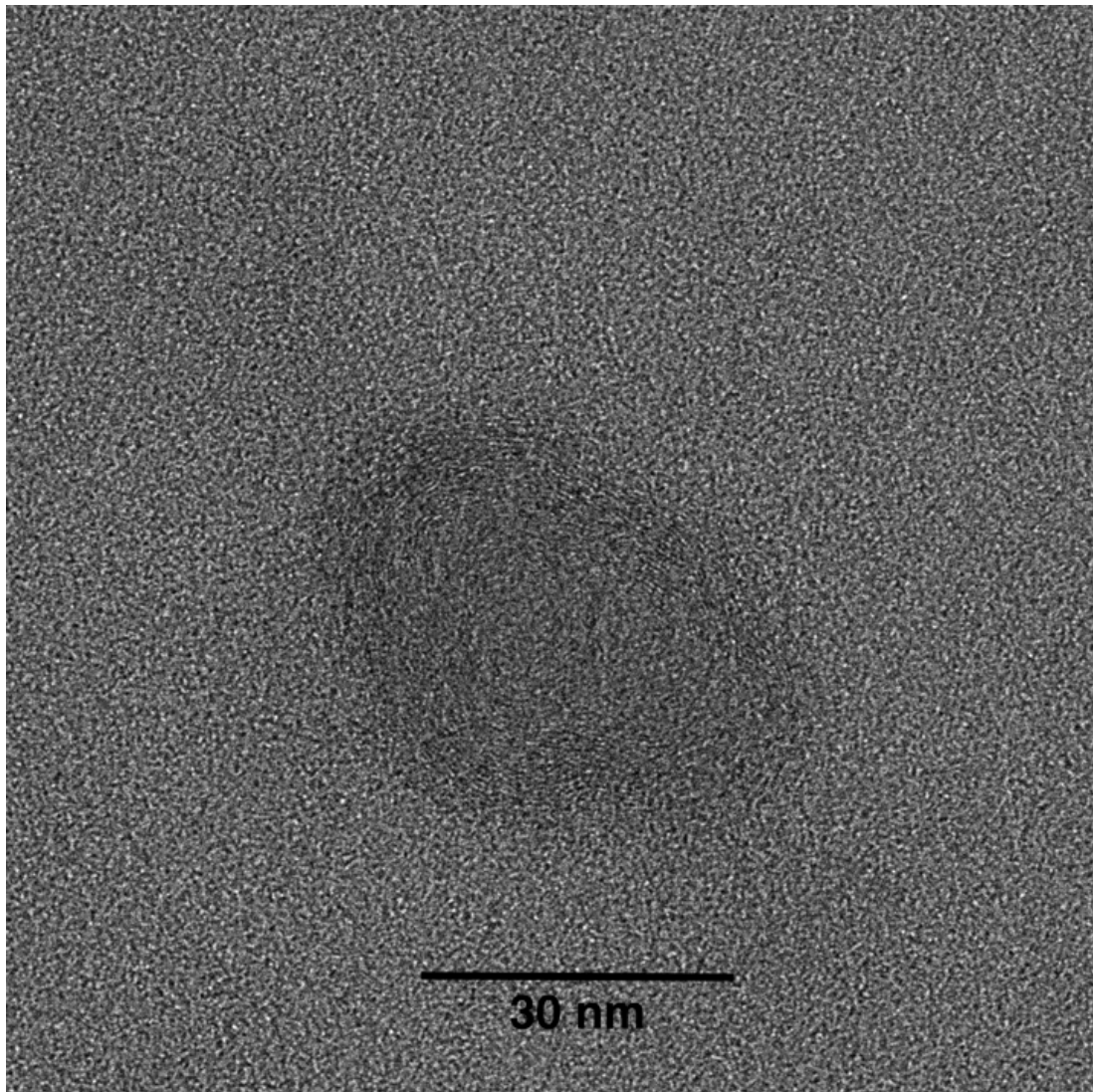


Figure S4.2: Additional image of a single BC sphere found in a rain sample collected in Darwin, Northern Territory, Australia on April 11, 2014.

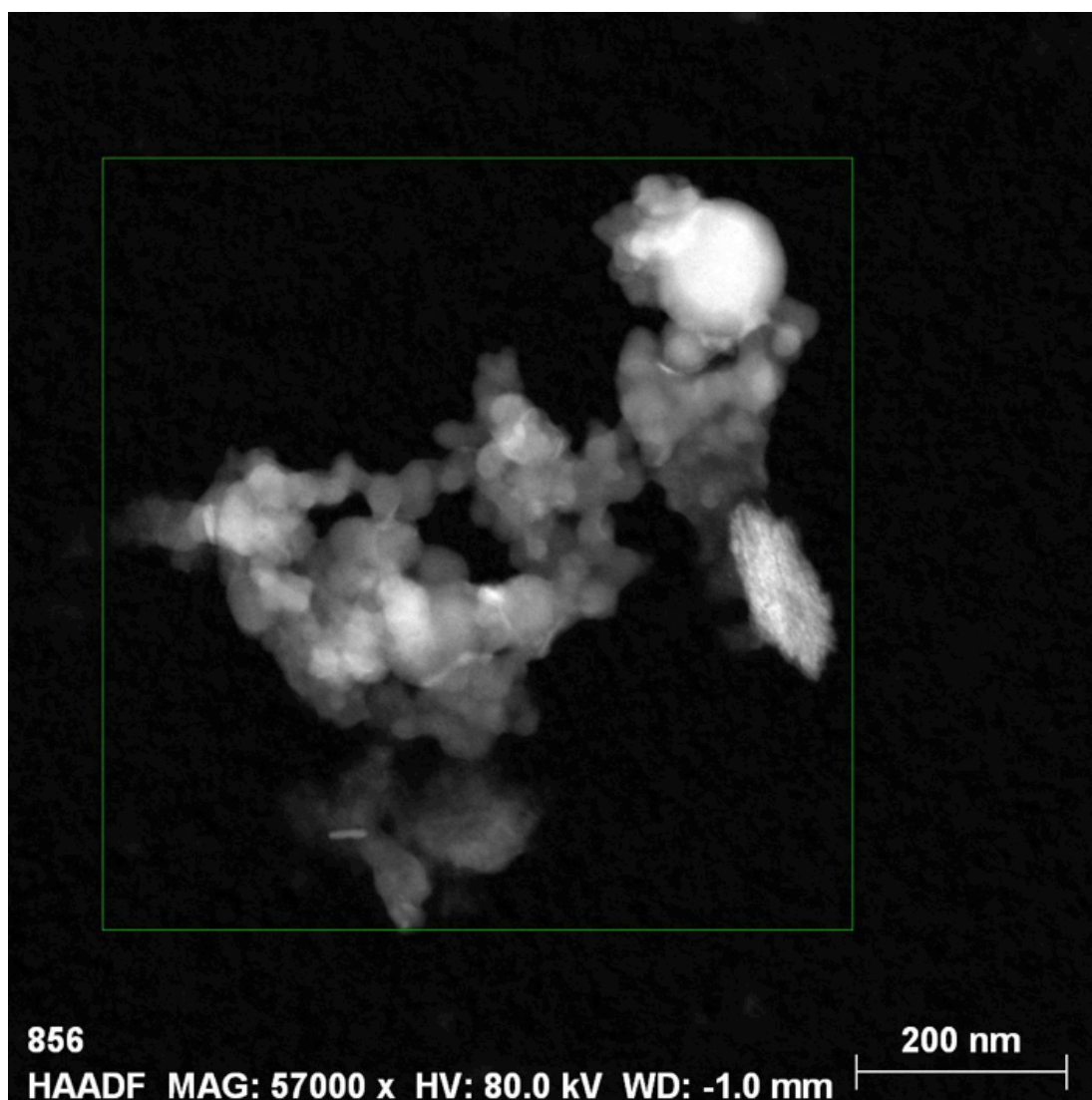


Figure S4.3: Additional HAADF image for Figure 4.2.

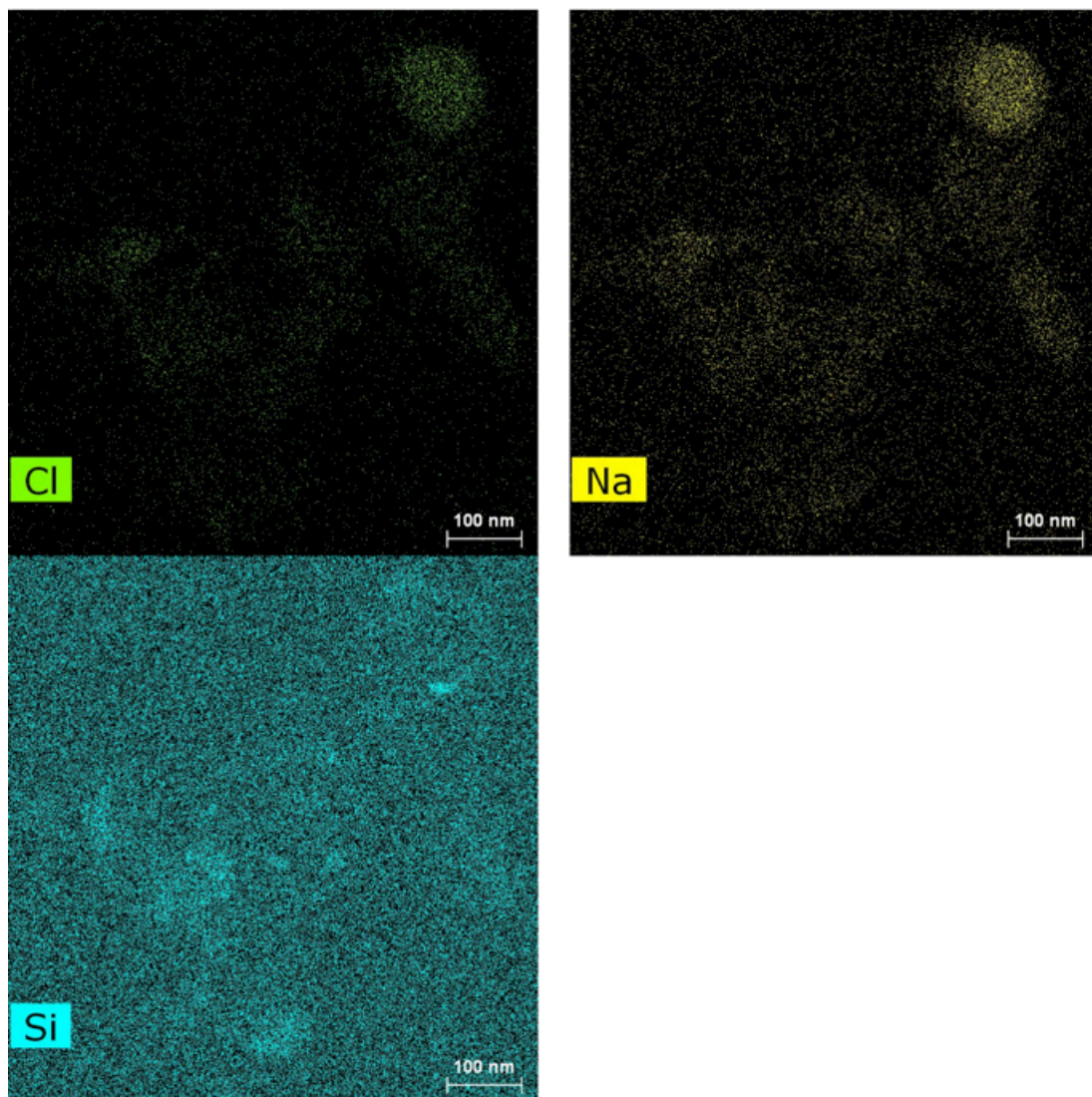


Figure S4.4: Additional STEM-EDS maps for Figure 4.2.

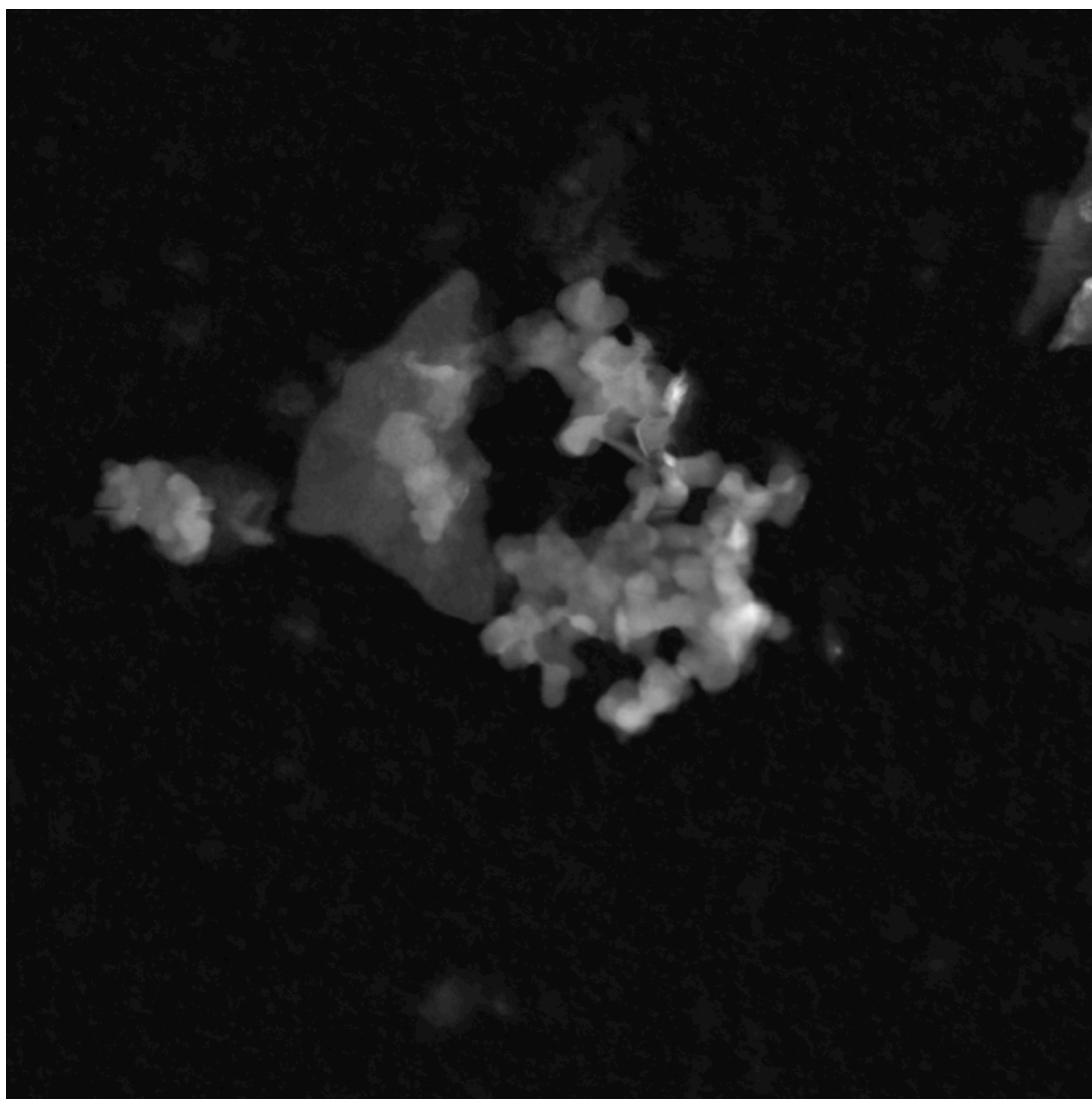


Figure S4.5: Additional HAADF image for Figure 4.3.

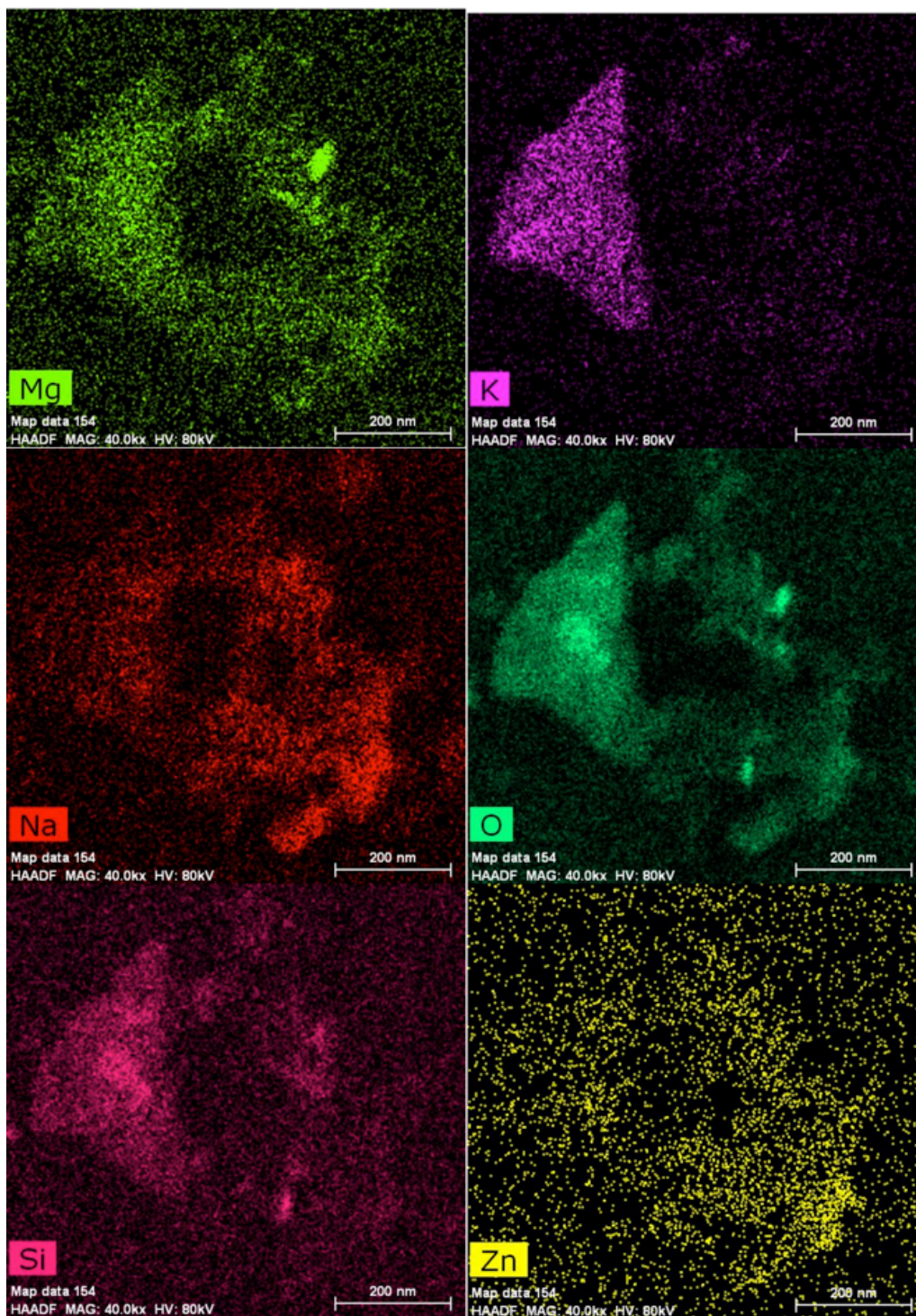


Figure S4.6: Additional STEM-EDS maps for Figure 4.3.

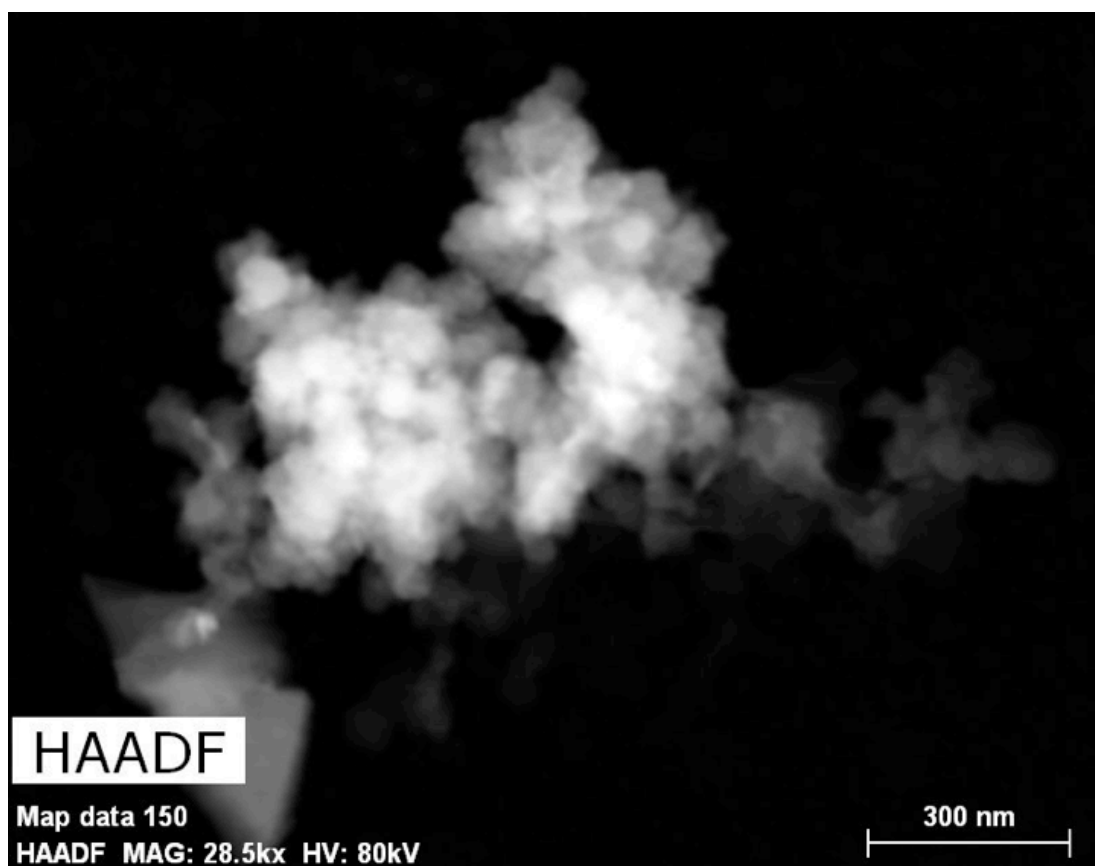


Figure S4.7: Additional HAADF image for Figure 4.4.

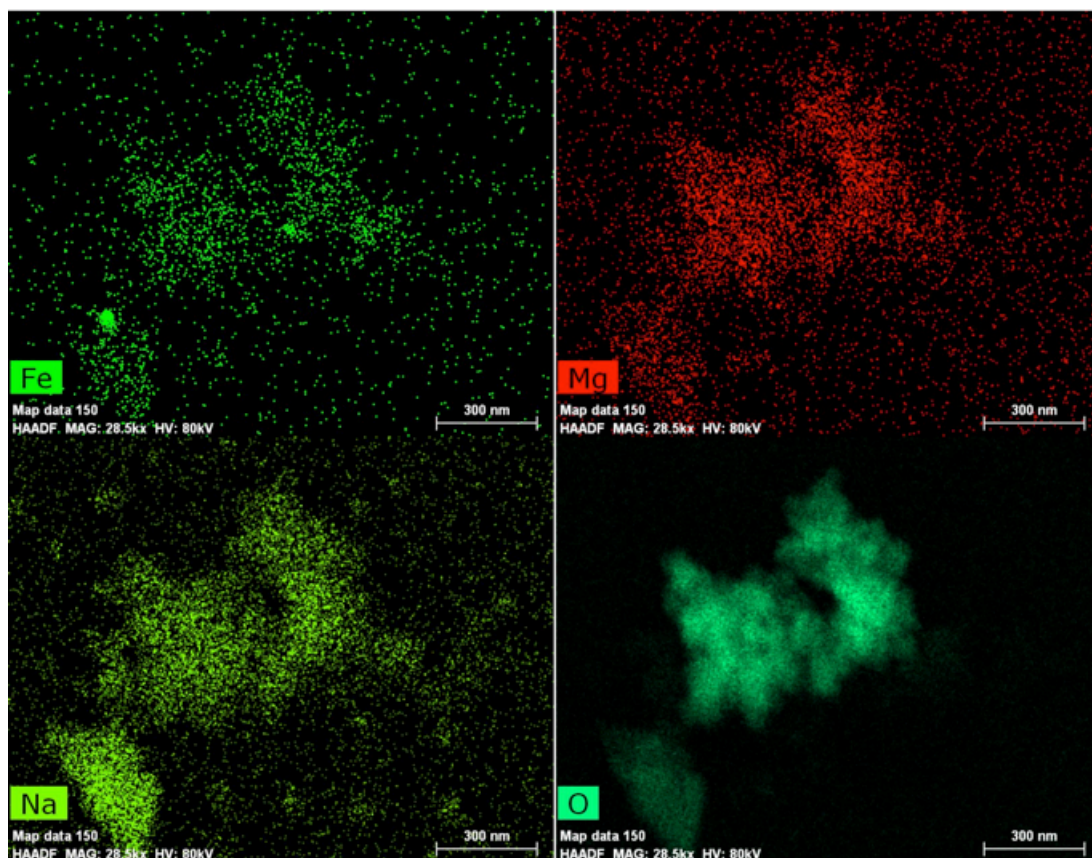


Figure S4.8. Additional STEM-EDS maps for Figure 4.4.

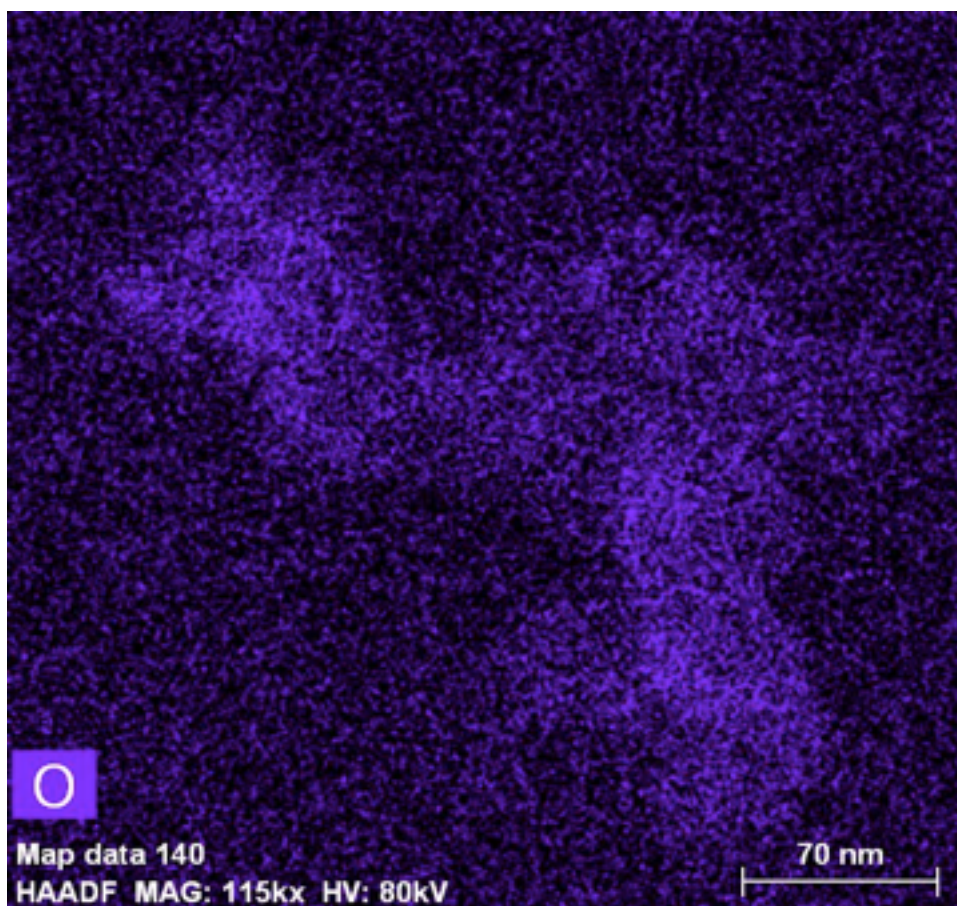


Figure S4.9: Additional STEM-EDS map for Figure 4.5.

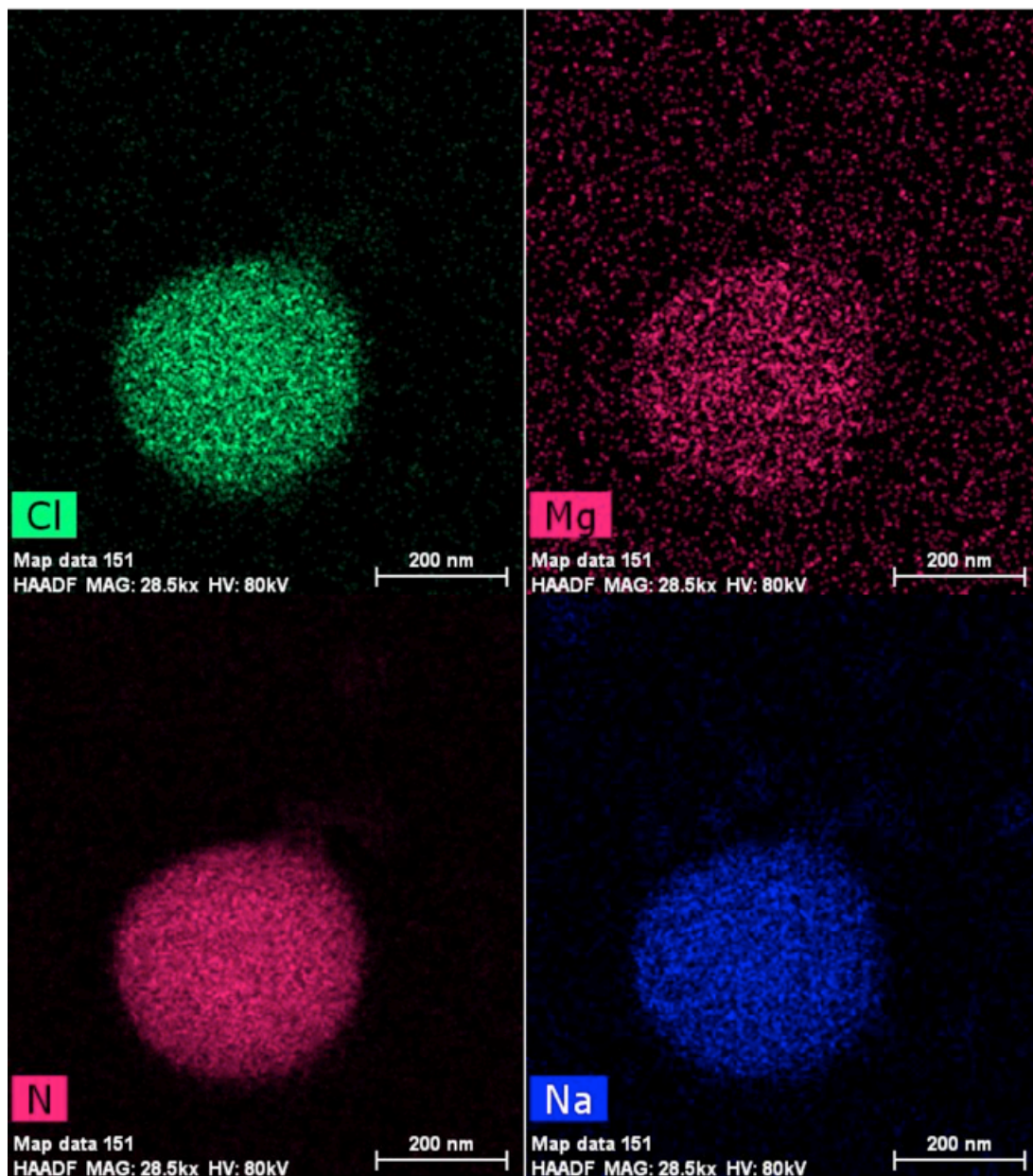


Figure S4.10: Additional STEM-EDS maps for Figure 4.6.

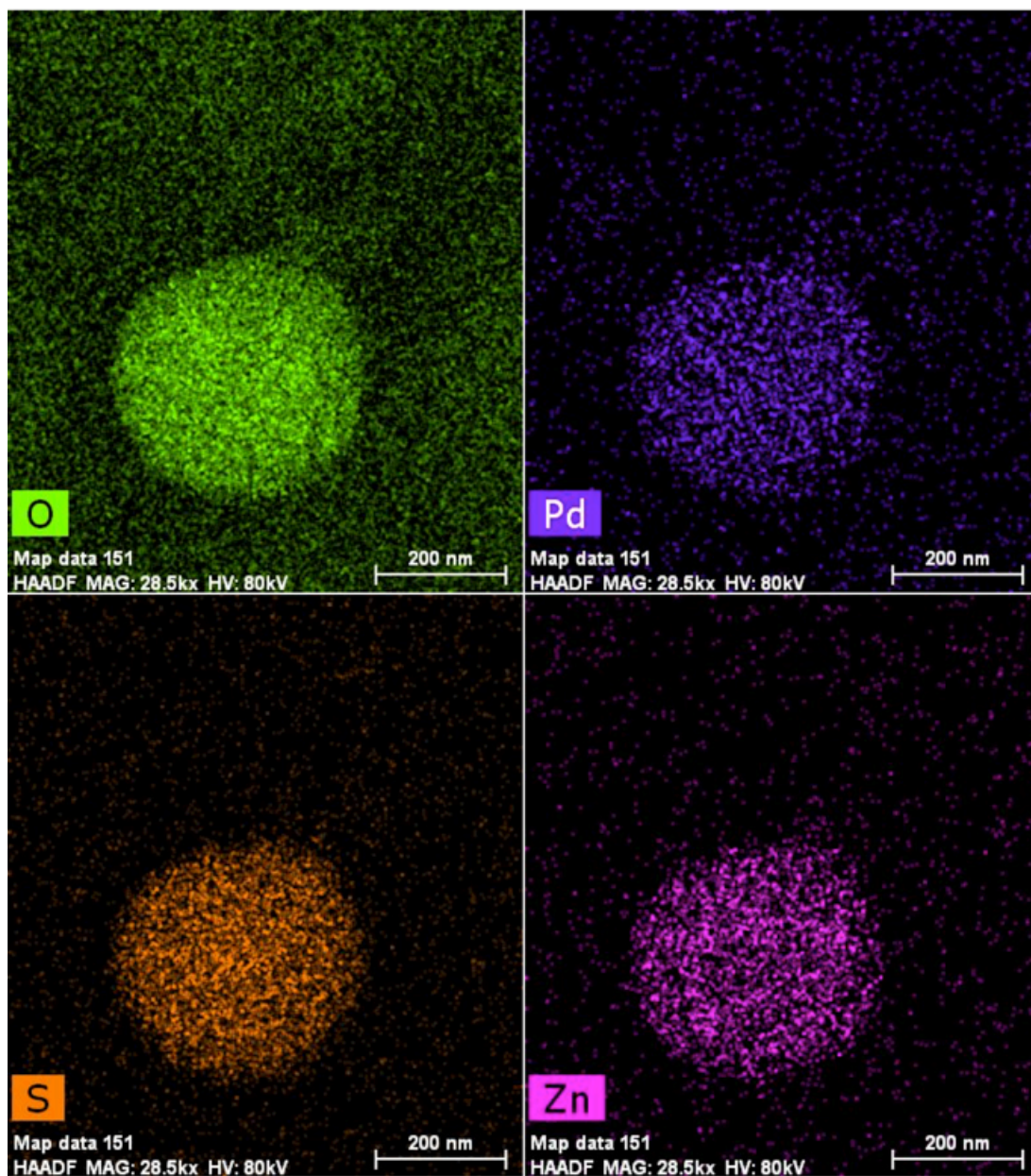


Figure S4.11: Additional STEM-EDS maps for Figure 4.6.

NOAA HYSPLIT MODEL
Backward trajectories ending at 1200 UTC 04 Apr 14
GDAS Meteorological Data

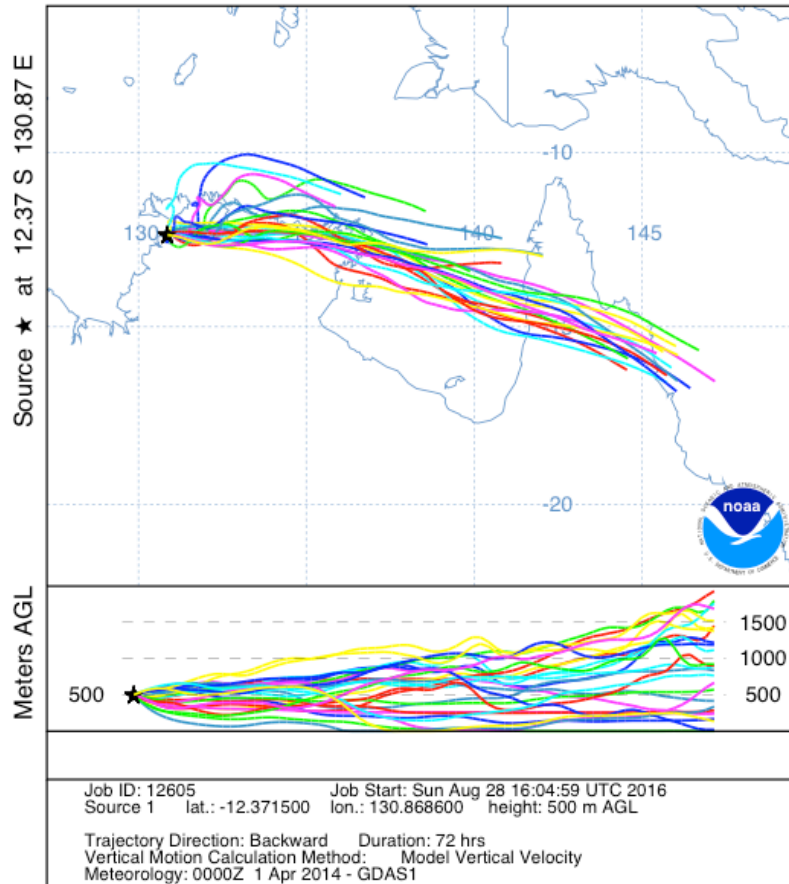


Figure S4.12: HYSPLIT back-trajectories of air-mass transport to Darwin, Northern Territories, Australia for April 4, 2014 for a final atmospheric height of 500 m above ground level.

NOAA HYSPLIT MODEL
 Backward trajectories ending at 1200 UTC 04 Apr 14
 GDAS Meteorological Data

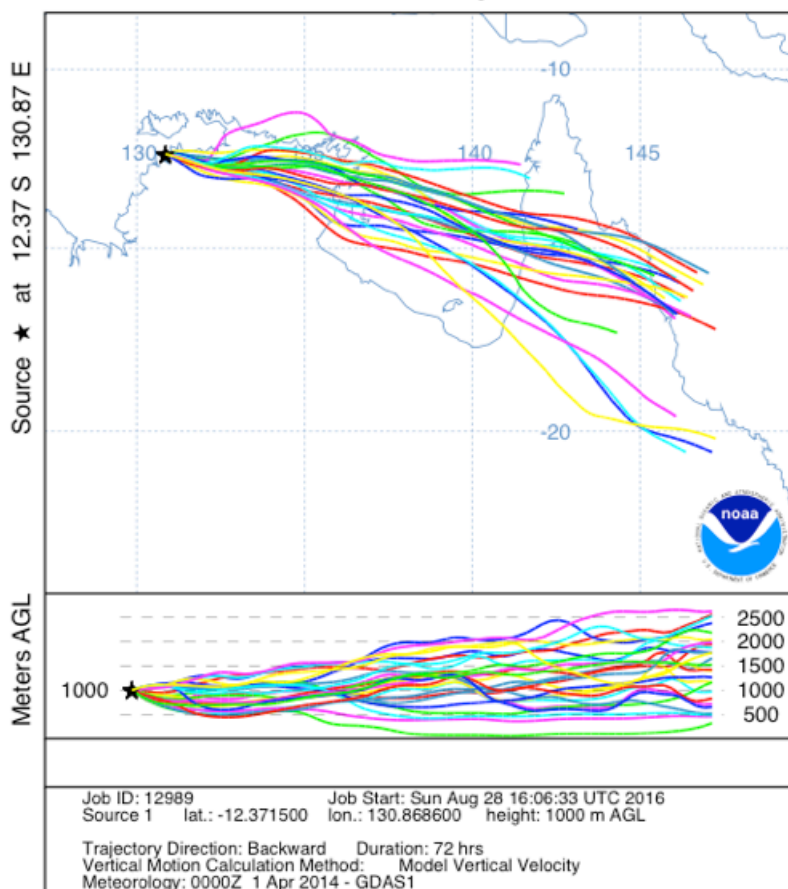


Figure S4.13: HYSPLIT back-trajectories of air-mass transport to Darwin, Northern Territories, Australia for April 4, 2014 for a final atmospheric height of 1000 m above ground level.

NOAA HYSPLIT MODEL
 Backward trajectories ending at 1200 UTC 04 Apr 14
 GDAS Meteorological Data

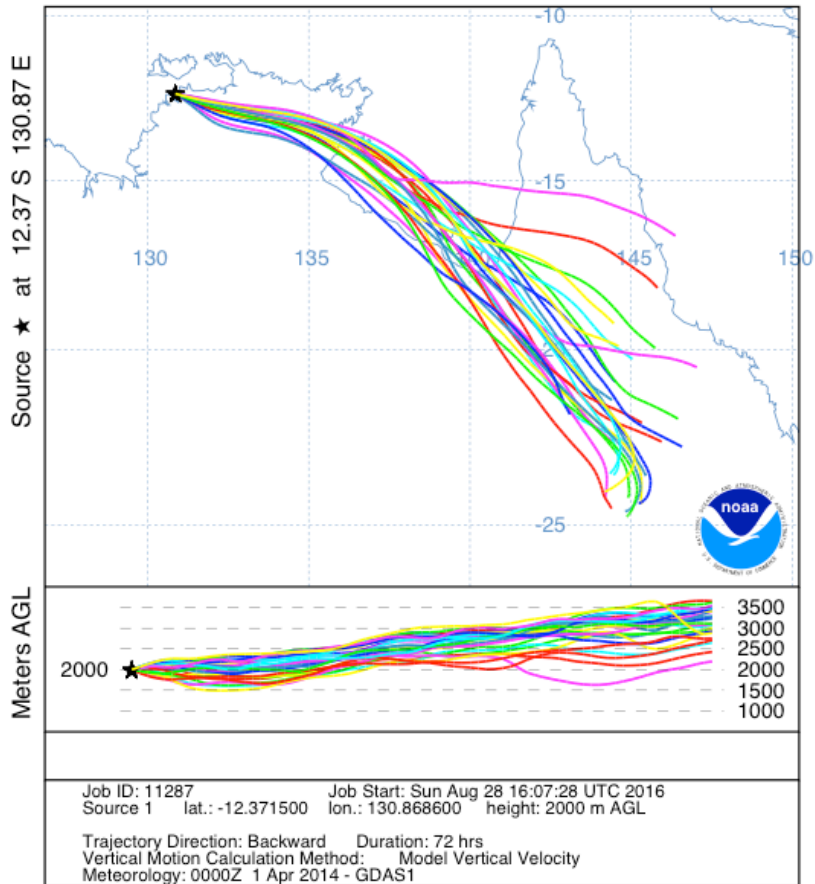


Figure S4.14: HYSPLIT back-trajectories of air-mass transport to Darwin, Northern Territories, Australia for April 4, 2014 for a final atmospheric height of 2000 m above ground level.

NOAA HYSPLIT MODEL
 Backward trajectories ending at 1200 UTC 08 Apr 14
 GDAS Meteorological Data

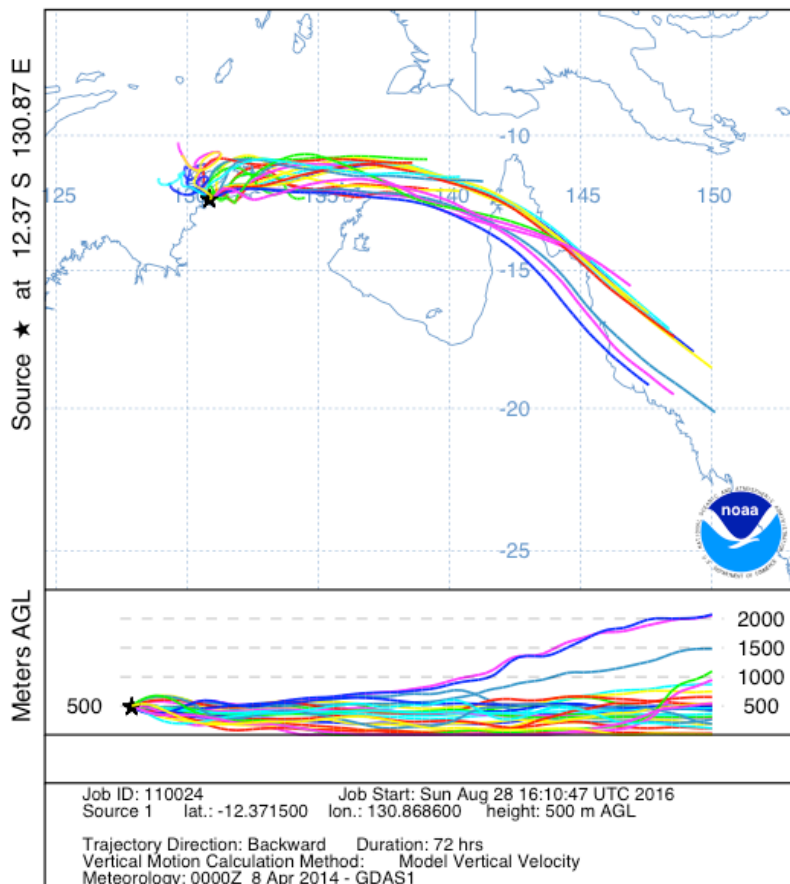


Figure S4.15: HYSPLIT back-trajectories of air-mass transport to Darwin, Northern Territories, Australia for April 8, 2014 for a final atmospheric height of 500 m above ground level.

NOAA HYSPLIT MODEL
Backward trajectories ending at 1200 UTC 08 Apr 14
GDAS Meteorological Data

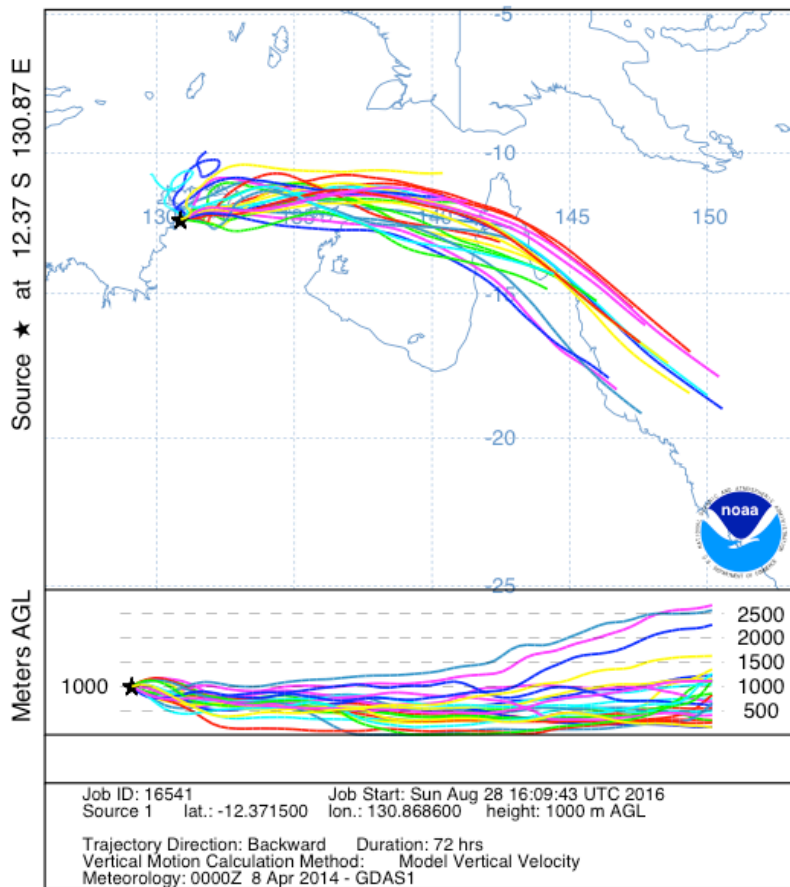


Figure S4.16: HYSPLIT back-trajectories of air-mass transport to Darwin, Northern Territories, Australia for April 8, 2014 for a final atmospheric height of 1000 m above ground level.

NOAA HYSPLIT MODEL
 Backward trajectories ending at 1200 UTC 08 Apr 14
 GDAS Meteorological Data

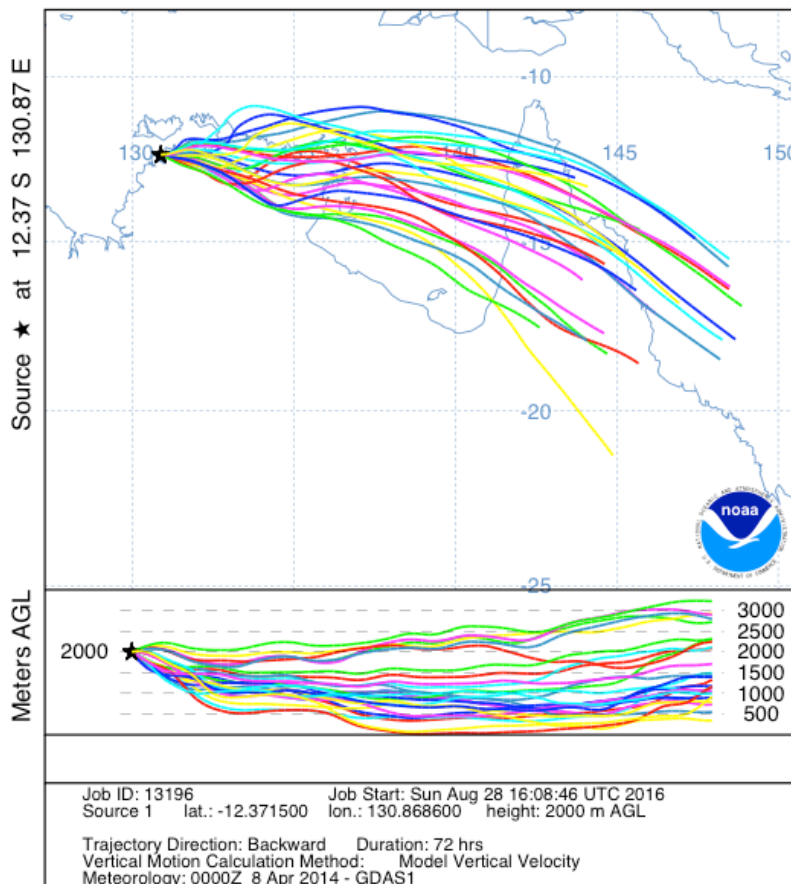


Figure S4.17: HYSPLIT back-trajectories of air-mass transport to Darwin, Northern Territories, Australia for April 8, 2014 for a final atmospheric height of 2000 m above ground level.

NOAA HYSPLIT MODEL
Backward trajectories ending at 1200 UTC 11 Apr 14
GDAS Meteorological Data

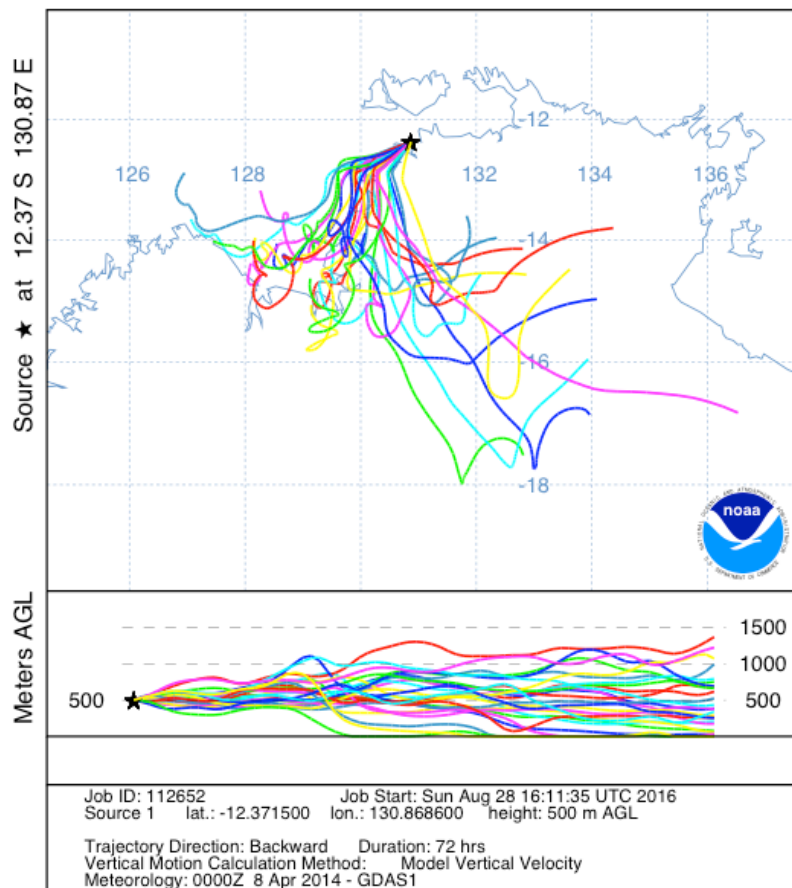


Figure S4.18: HYSPLIT back-trajectories of air-mass transport to Darwin, Northern Territories, Australia for April 11, 2014 for a final atmospheric height of 500 m above ground level.

NOAA HYSPLIT MODEL
Backward trajectories ending at 1200 UTC 11 Apr 14
GDAS Meteorological Data

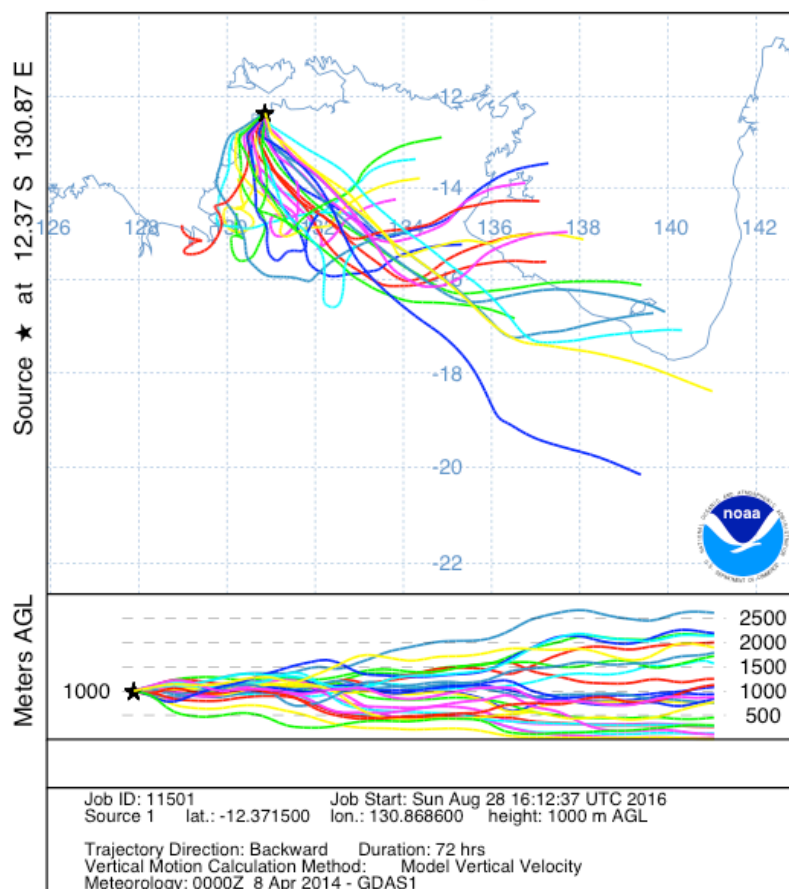


Figure S4.19: HYSPLIT back-trajectories of air-mass transport to Darwin, Northern Territories, Australia for April 11, 2014 for a final atmospheric height of 1000 m above ground level.

NOAA HYSPLIT MODEL
 Backward trajectories ending at 1200 UTC 11 Apr 14
 GDAS Meteorological Data

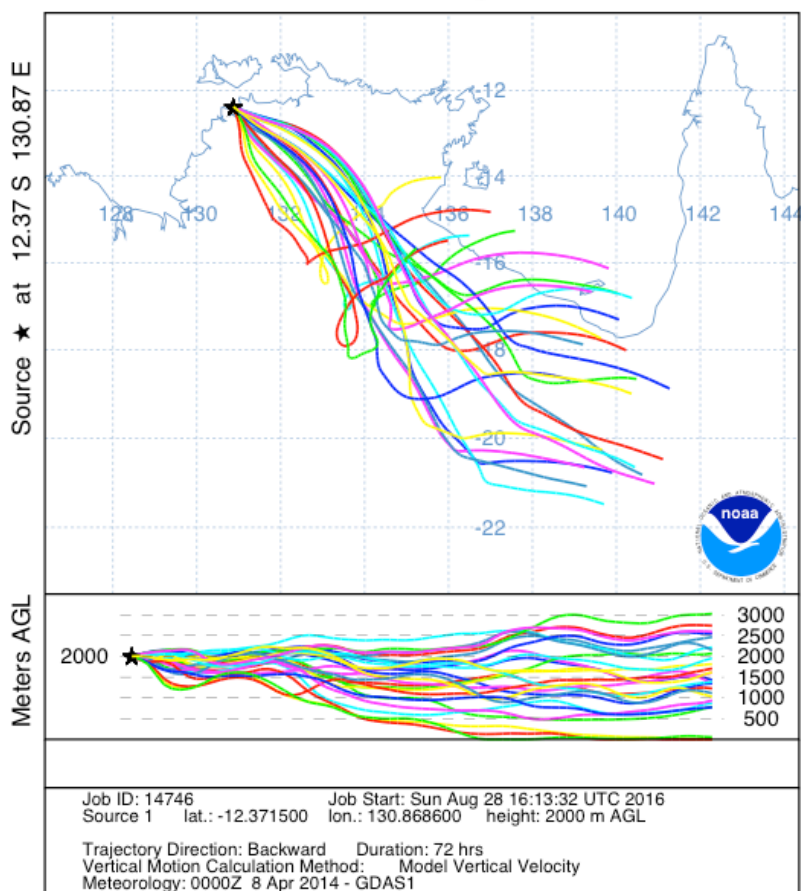


Figure S4.20: HYSPLIT back-trajectories of air-mass transport to Darwin, Northern Territories, Australia for April 4, April 8, and April 22, 2014 for final atmospheric heights of 500 m, 1000 m, and 2000 m above ground level.

Chapter 5. Roosevelt Island Climate Evolution Project: Black carbon deposition to Roosevelt Island, West Antarctica approaches Arctic levels

This chapter is in preparation for submission to *Journal of Geophysical Research: Atmospheres*.

Abstract

Refractory black carbon (rBC) aerosols convert solar radiation to thermal energy contributing to climate change. Unlike the major greenhouse gasses such as CO₂, rBC aerosols exhibit significant spatial and temporal variability, complicating efforts to constrain aerosol climate forcing. Paleorecords of rBC at remote sites are needed to investigate past feedbacks between the global atmosphere, climate, and rBC emissions. As part of the Roosevelt Island Climate Evolution Project (RICE), we have developed snow pit and ice core rBC records from West Antarctica spanning 1890 to 2013 CE. Annual rBC deposition to the region was relatively stable from 1890 to 1998 CE. After 1998, the annual rBC deposition rate increased dramatically with peak snow rBC concentrations and annual deposition rate in late 2011 similar to present-day Greenland ($\sim 1 \text{ ng g}^{-1}$, $96 \mu\text{g m}^{-2} \text{ yr}^{-1}$). The maximum annual rBC deposition in 2011 was ~ 7 times that of the 1887-1987 geometric mean. Satellite observations of biomass burning emissions and atmospheric transport models suggest Southern Hemisphere biomass burning from Australia, Southern Africa and South America to be the primary source of rBC to the region. While, mixing in the atmosphere prevents definitive source apportionment, the increase in annual rBC deposition occurred during a period of increased biomass burning in central and eastern Australia and southern Africa coinciding with southerly atmospheric transport towards West Antarctica from Australia. If the trend in rBC deposition continues, regional snow albedo will be impacted altering surface snow properties and the radiation budget.

5.1 Introduction

Refractory black carbon aerosols (rBC) are the dominant light-absorbing particle in the atmosphere and are emitted by the combustion of biomass and fossil fuels. Light absorbed by rBC is transformed into thermal energy, warming the surrounding air, altering the global radiation budget, and affecting atmospheric dynamics (Moosmuller et al., 2009). The global mean radiative forcing attributed to rBC is uncertain (IPCC, 2013), but recent studies suggest that it represents the second largest anthropogenic contribution to climate change after carbon dioxide (CO₂, Bond et al., 2013). Unlike greenhouse gases, the distribution of rBC in the atmosphere is highly variable, and regional forcing can be significantly higher than the global mean (Ramanathan & Carmichael, 2008). The particulate nature of rBC results in both direct (light absorption) and indirect effects (changes in snowpack albedo and cloud microphysics). High concentrations of rBC in surface snowpacks ($>20 \text{ ng g}^{-1}$) due to high snowfall rBC levels, dry deposition or post-deposition preconcentration darken snow packs resulting in a significant indirect forcing (Flanner et al., 2007; Hansen & Nazarenko, 2004; Ramanathan & Carmichael, 2008). Conversely, climate change can influence the generation of rBC from biomass burning and affect its atmospheric distribution (Flannigan et al., 2000). For example, recent biomass burning reconstructions suggest that anthropogenic climate change has already resulted in an increase in global biomass burning (Marlon et al., 2008). Decadal rBC emission estimates from 1850 to 2000 C.E suggest an increase in both biomass burning and fossil fuel emissions (Lamarque et al., 2010) with emissions from 2000 to 2010 approximately five times that of 1850 to 1860. However, historical rBC emission reconstructions remain highly uncertain.

To investigate the historical climate impact of rBC, over the past 150 years, estimates of both global emissions and the global atmospheric rBC deposition are required. Global historical emission estimates (Bond et al., 2007; Junker & Lioussé, 2008; Lamarque et al., 2010) have been reconstructed based on time-varying emission factors for different anthropogenic sources. For the recent past, global uncontained biomass burning emission estimates such as Global Fire Emissions Database (GFED; Giglio et al., 2013; van der Werf et al., 2010) and Fire Inventory from NCAR (FINN; Wiedinmyer et al., 2011) have been developed from biomass emission factors applied to satellite observations of burnt areas. Longer paleo-records of global biomass burning have come from ensembles of sedimentary charcoal records (Marlon et al., 2008) and tree-ring burn scars (Marlon et al., 2012). In contrast to

paleo-emission records, ice core and snow pit rBC records provide a history of rBC deposition from the atmosphere. Recently, high-temporal resolution (sub-annual) ice core records have been developed for locations in Greenland and Antarctica (Bisiaux et al., 2012; McConnell et al., 2007). rBC deposition to these sites occurs from a combination of so-called wet and dry deposition processes. In the absence of melt or other ablation processes, polar ice cores preserve a record of rBC deposition from annual to glacial time scales. These records have the potential to connect paleo-emission estimates to the global atmospheric distribution and deposition using general circulation models (GCMs) and may provide information on the physical characteristics of individual rBC particles after long-range transport (Ellis et al., 2016; Ellis et al., 2015).

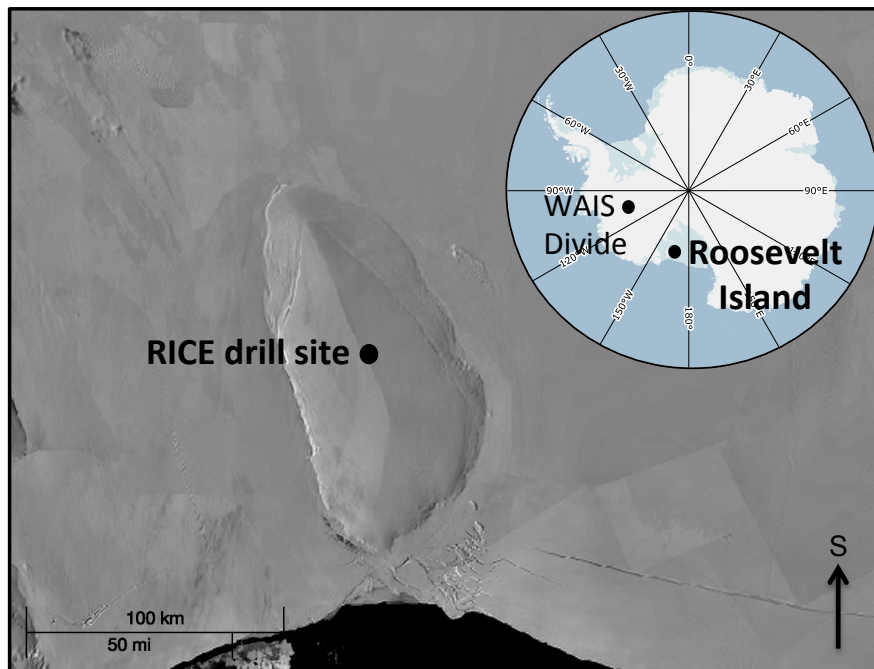


Figure 5.1 Map of Antarctica, with location of Roosevelt Island noted on the Ross Ice Shelf, West Antarctica. Another prominent ice core location, WAIS Divide on the West Antarctic Ice Sheet, is also noted for comparison.

As part of the Roosevelt Island Climate Evolution (RICE) project (<http://www.rice.aq/>), we have reconstructed ice core and snow pit records of rBC deposition to the Roosevelt Island ice cap (Figure 5.1) in the Eastern Ross Ice Shelf, West Antarctica (Conway et al., 1999). The RICE project is an international, multi-institution collaboration to reconstruct the climate and glacial history of the Roosevelt Island ice cap, and by inference, the Ross Ice Shelf and the

West Antarctic ice sheet. During the austral summers of 2011/2012 and 2012/2013, the project drilled a deep ice core (748 m depth), several shallow ice cores and snow pits from near the ice cap divide. A major aim of the RICE rBC study was to investigate the local spatial variability in rBC deposition to assess the uncertainty in the deep ice core record. Here we show the results of the rBC study with respect to deposition variability over the past ~150 years.

5.2 Methods

5.2.1 Ice core and snow pit samples

Roosevelt Island is a coastal ice dome located in the Eastern Ross Ice Shelf, West Antarctica, adjacent to the Ross Sea. The dome is 130 km long (running NW to SE) and 65 km wide with a maximum ice thickness of ~763 m. The ice dome has a maximum elevation of ~550 m and a base ~200 m below sea-level. Roosevelt Island is a high-accumulation site, with annual snow accumulation of ~0.25 m water equivalent (WEQ, Tuohy et al., 2015). The Ross Sea region experiences significant synoptic-scale weather systems from the Southern Ocean (Sinclair et al., 2010), as well as significant periods of fog and rime ice formation in the summer, and potentially throughout the year (Tuohy et al., 2015).

Two RICE ice cores were used in the study. These included upper sections (top 38 m) of the RICE deep core (RICE 11/12A, -79.36286N, -161.70059W, 550 m above sea level) and a shallow ice core (RICE 12/13B, -79.36211N, -161.69839W) drilled during the 2012-2013 field season ~90 m to the South East of the RICE11/12A core site. Ice core sections used by the study were drilled without the use of drilling fluid. These sections were cut into 1 m intervals in the field and transported to GNS Science, in Lower Hutt, New Zealand, where each meter was cut length-wise into multiple replicated sub-samples.

Two snow pits were sampled during the 2012-2013 field season. These were located ~300 m (Ellis pit) and ~500 m (Winton pit) to the south of the RICE 11/12A site. The Winton pit has been described by Winton et al. (2016). These snow pits provide both a known depth horizon to calibrate the ice core data and an assessment of localized spatial reproducibility. The Ellis pit (-79.364930N, -161.70073W) was sampled in January 2013, while the Winton pit (-79.36645N, -161.70053W) was sampled in November 2012. Both snow pits were upwind

from the field camp (-79.36086N, -161.64600W). A map of site and orientation of sampling areas is provided in the supplementary information (Figure S5.1). Samples from the Ellis Pit were collected using ultra-clean protocols at 1 cm resolution from the bottom of the snow pit up to the surface, with the sampling face removed in 50 cm intervals to allow for a clean surface immediately prior to sampling. Winton pit snow samples were collected at 3 cm resolution. Both snow pits were sampled wearing full-coverage clean suits and nitrile gloves. Snow was collected with acid-cleaned plastic trays and ceramic knives and stored in Whirlpak™ bags, unsealed immediately before use. Procedural field blanks were collected for the sampling bags, by opening and resealing bags in the manner used for sampling.

5.2.2 Sample analysis

Ice core rBC concentrations were determined continuously as a component of RICE continuous flow ice core analysis (CFA) campaigns conducted at GNS Science, in Lower Hutt, New Zealand. Analysis of the top 48 m of the RICE 11/12 core took place in 2012 using a CFA system based on that of Osterberg et al., 2006. However, significant problems were found with the ice core meter head, and the rBC data from the 2012 CFA analysis was found to be unreliable. Subsequent CFA campaigns in 2013, and 2014 were based on the University of Copenhagen Centre for Ice and Climate CFA system described in detail by Bigler et al., 2011. Analysis of a duplicate piece of the upper RICE 11/12 core (8 – 48 m) and the RICE 12/13B shallow ice core occurred in 2014. The rBC analytical component of the CFA system was similar to that described by McConnell et al. (2007), Bisiaux et al. (2011), and Bisiaux et al. (2012) with the exception that bubbles were introduced into the sample line close to the melter head to produce segmented flow. The segmented flow bubbles were added to reduce dispersion and were removed close to the rBC analysis system. The rBC analysis system consisted of a Single Particle Soot Photometer (SP2, Droplet Measurement Technologies) coupled with an ultrasonic desolvation system (CETAC UT5000) to nebulize melt water and aerosolize the rBC for analysis by single particle intracavity laser induced incandescence. Ice core data depth resolution using the CFA system was ~1 cm. Snow samples were analyzed in the Trace Research Advanced Clean Air Environment (TRACE) at Curtin University, Perth, Australia using the rBC analysis system. Concentrations of rBC measured by the SP2 for both the ice and snow samples were calibrated using rBC standards based on a commercial 100% carbon ink Ebony-6 ink (MIS Associates). Laboratory ultrapure water (UP water, $\rho > 18.2 \text{ m}\Omega$) blanks and rBC standards were analyzed at regular intervals

during the melting campaign to assess contamination and to monitor for potential instrumental drift. The sensitivity of the SP2, high quality blanks and standards, and laboratory procedure permitted detection of rBC at ultra-trace levels in the samples (e.g. $>0.01 \text{ ng g}^{-1}$ in Antarctic ice) with rBC particle volume equivalent diameters from 100 to 650 nm (Schwarz et al., 2010). Concentrations of rBC determined by the method were comparable to those reported by Bisiaux et al. (2011) for Antarctic ice cores.

5.2.3 Ice core and snow pit timescales

The RICE ice core depth-age relationship spanning the past 2000 years are described in detail by Winstrup et al., 2017 (in prep.). Briefly, the chronology was constructed by annual-layer counting in multiple ice-core impurity records, including black carbon. Both manual and automatic layer counting methods (Winstrup et al., 2012, Winstrup 2016) were employed, with the automated layer-counting routine, StratiCounter, also providing confidence intervals for the resulting age scale.

High levels of sulfate (SO_4) in Roosevelt Island snow from local biogenic and volcanic emissions complicated the designation of ice-core sulfate horizons from large tropical volcanic eruptions. This precluded the use of traditional methods for synchronizing RICE to other Antarctic ice cores. A sparse set of volcanic horizons detected in the RICE pH record was used for validation of the timescale, along with synchronization of high-resolution RICE methane (CH_4) measurements to a similar record from the well-dated WAIS Divide ice core.

Age scales for the two snow pits were constructed and aligned using annual layers in rBC and non-sea-salt-sulfur (nssS) profiles (Winton et al., 2016).

5.2.4 Flux calculations

Snow pit net-annual snow accumulation was calculated using snow density measurements and annual layer counting from the Winton snow pit. Based on the snow pit record and depth-age scale, the estimated net annual accumulation rate for 2011 was $\sim 0.33 \text{ m yr}^{-1}$ WEQ from January 2011 to January 2012. An independent net annual accumulation estimate for the calendar year 2011 from the ice core ($\sim 250 \text{ m}$ to the south) depth-age scale (RICE_2KA) and ice core density was 0.32 m yr^{-1} WEQ for 2011. Black carbon net atmospheric fluxes (here after flux) for the snow pits and the ice core records were estimated from monthly rBC mass

concentration data assuming linear intra-annual depth-age and constant snow accumulation at the sites.

5.3 Results and Discussion

5.3.1 Correlation of rBC concentrations across snow pits and ice cores

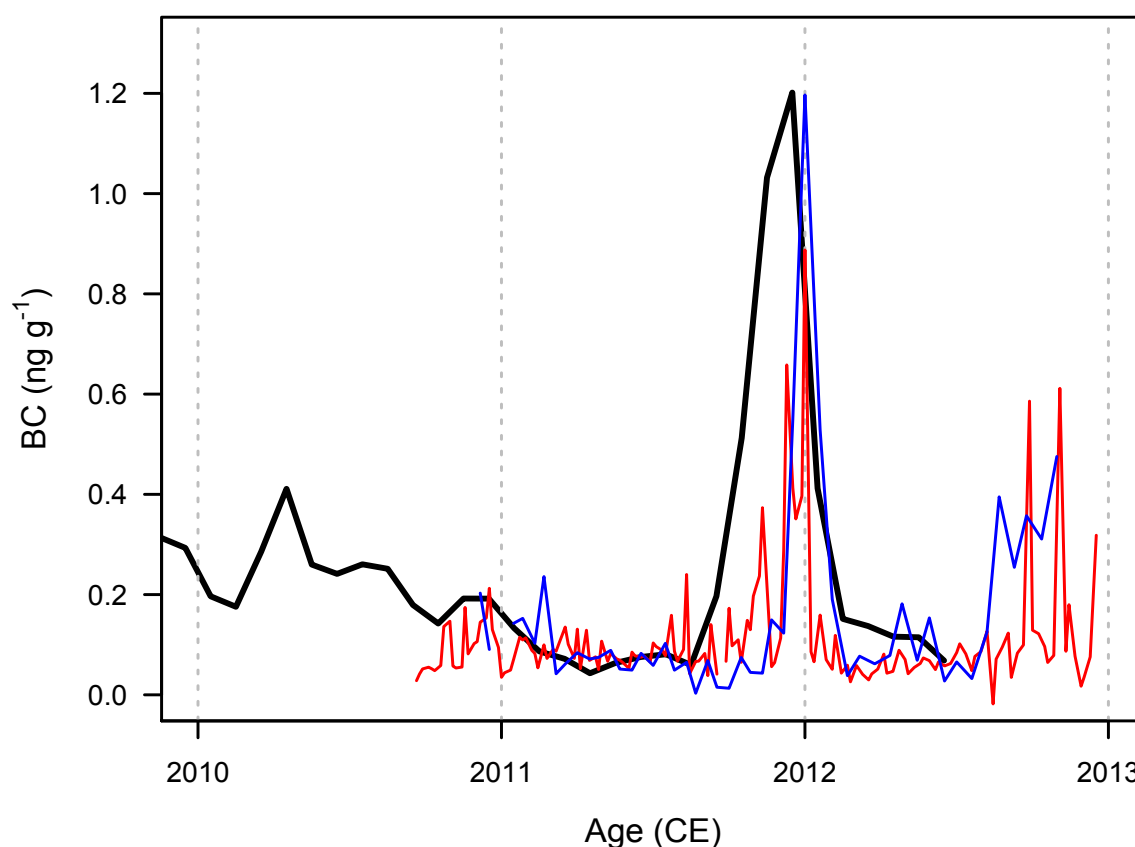


Figure 5.2 RICE rBC concentration records RICE ice core (black) and snow pit records (Winton snow pit blue and Ellis snow pit red). RICE ice core has been resampled to monthly resolution. Snow pit records have not been resampled.

The snow pit rBC records spanned approximately 2.5 years and show significant seasonality in rBC concentration and deposition (Figure 5.2). A large peak in rBC concentration ($>1 \text{ ng g}^{-1}$) was found in both the snow pits and the ice core record (RICE 12/13) corresponding to the late spring austral summer of 2011/2012. This 2012 peak has also been measured at a site in Eastern Wilkes Land, East Antarctica, suggesting significant spatial

extent to the rBC deposition (Caiazza et al., 2017). The measurement of this peak in Eastern Antarctica also suggests that the rBC measured at Roosevelt Island was not due to contamination from camp activities. Peak rBC concentrations varied between 0.8 ng g^{-1} in the Ellis snow pit and $\sim 1.2 \text{ ng g}^{-1}$ in both the Winton snow pit and the ice core record. The peak rBC concentrations are ~ 7 to 15 times higher than mean rBC concentrations at Law Dome or WAIS in Antarctica (Bisiaux et al., 2012) and are similar to concentrations found in present-day Greenland snow (McConnell et al., 2007). No signs of surface melt were found in the snow pit or ice core record to suggest that post-deposition preconcentration or ablation had occurred (Doherty et al., 2013). The increase in rBC deposition also occurred before the beginning of the RICE field seasons, ruling out contamination from camp activity and logistics. The Ellis snow pit rBC record was mapped to the Winton snow pit depth-age relationship (Winton et al., 2016) using both black carbon and sulfur data (Winton et al., 2016) and has a similar peak width to the Winton snow pit due to the mapping. The snow pit depth-age relationship places the peak in rBC to \sim January 2012 based on the pits non-sea-salt sulfur record and constant accumulation. However, the RICE ice core depth-age record suggests that the peak dates to November-December 2011, again assuming constant snow accumulation at the site. It is highly likely that these exceptional peaks in rBC are the same event and that the temporal difference in both the peak height and peak width reflects uncertainty in the intra-annual dating of both the snow pits and ice core. The records show that rBC deposition to RICE was relatively uniform at the 100 m scale.

5.3.2 Comparison of snow pits and ice core records with GFED 4.1 fire emission estimates

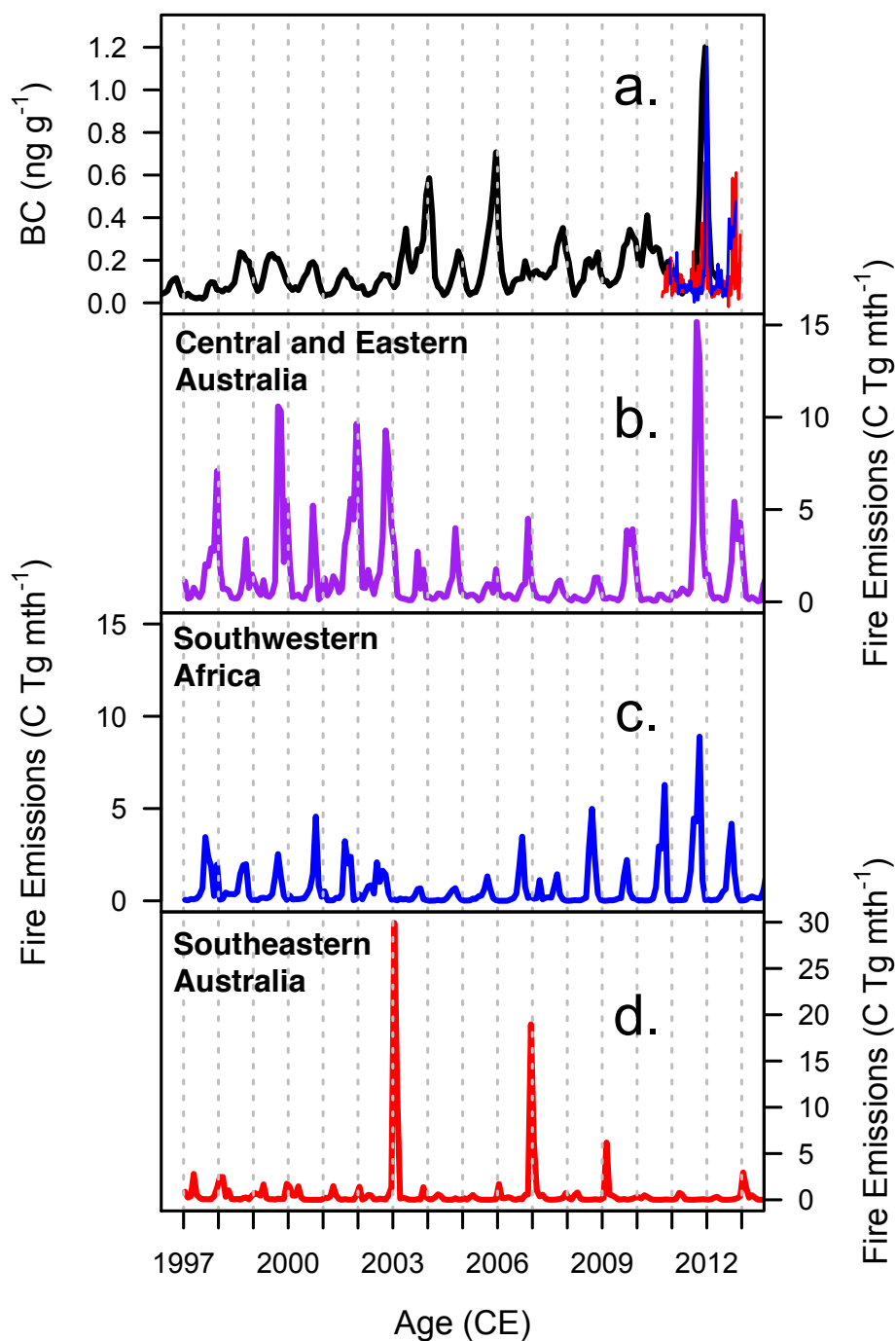


Figure 5.3. RICE ice core and snow pit rBC records and GFED 4.1 fire emissions. (a) RICE ice core (black) and snow pit reconstructed rBC concentrations (Winton pit red and Ellis pit blue); (b) Central and eastern Australia GFED fire emissions as Tg carbon; (c) Southwestern Africa GFED fire emissions; and (d) Southeastern Australia GFED fire emissions.

Assuming that the large peak in rBC was deposited in late 2011, it may be associated with large-scale fires in the interior of Australia and Southern Africa that occurred from September to November of 2011. From 2010 to 2011, Central Australia and arid regions of Southern Africa (Namibia, Botswana, and South Africa) experienced historic rainfall due to a strong La Niña Modokai phase (Boening et al., 2012). Terrestrial primary productivity and biomass build up in these arid and semi-arid regions is limited by water (Ma et al., 2016). Therefore, the increased rainfall resulted in a greening of central Australia (and presumably Southern Africa; (Ma et al., 2016). At the end of the wet period in 2011, large-scale fires occurred in central and Eastern Australia and Southwestern Africa.

Figure 5.3 shows the temporal variability of the ice core and snow pit rBC concentration records with respect to GFED 4.1 fire emissions in Tg of carbon (<http://www.globalfiredata.org/>, Giglio et al., 2013). The central and eastern Australia emission data (Figure 5.3b, calculated from region encompassed by bounding box corner coordinates 131.00E, -21.00N and 155.00E, -35.00N) and Southwestern Africa emissions data (Figure 5.3c, calculated from bounding box corner coordinates 12.00E, -19.00N and 28.00E, -19.00N) show large fire emissions from August to November 2011. The central and eastern Australian GFED emissions peaked in September 2011, while the Southwestern African emissions peaked in October. The broad duration of the 2011 fire emissions may have contributed to the record large RICE rBC peak by spanning multiple meridional atmospheric transport events. Fire emission data from Southeastern Australia (Figure 5.3d, bounding box corners 131.00E, -35.00N and 153.50E, -45.00N) show large forest fire emissions in January 2003 and December 2006 (Figure 5.3d). Peaks associated with these fires were not found in the record. As the uncertainty in the ice core record for 2006 is ± 1 year, it is possible that the January peak in rBC from December 2005 reflects rBC from the December 2006 fires.

5.3.3 RICE Ice core 20th Century trend.

The RICE ice core rBC concentration and annual flux records spanning the 20th Century (1887 to 2012 CE) are shown in Figure 5.4. The rBC concentration record (Figure 5.4a) is composed of highly seasonal events superimposed on decadal scale variations (Figure 5.4c). The annual rBC flux displayed similar decadal variability to the rBC concentration record. Underlying trends in both the annual rBC flux and the monthly rBC concentration were nearly identical, which suggests that variability in the snow accumulation is a smaller

contribution to flux than the variability in inter-annual rBC concentration (Figure S5.3, Supplementary Information).

Both records are characterized by decadal scale oscillations in rBC concentration before a rapid rise from ~1995 to 2012. The rBC concentration trend maximum (0.224 ng g^{-1}) represents an increase of ~ 3 times the 1887 to 1995 trend mean (0.078 ng g^{-1}). The flux trend also increased by a factor of 3 with an 1887 to 1995 trend mean of $17 \mu\text{g m}^2 \text{ yr}^{-1}$ and a maximum flux of $54 \mu\text{g m}^2 \text{ yr}^{-1}$. The maximum rBC flux in 2011 ($96 \mu\text{g m}^2 \text{ yr}^{-1}$) was ~6 times the 1887 to 1995 mean ($17 \mu\text{g m}^2 \text{ yr}^{-1}$). While the hydrological event that impacted Australia in 2010 – 2011 was extreme, other events (Letnic & Dickman, 2006; Verdon-Kidd & Kiem, 2009; Yates et al., 2009) have occurred during the period covered by the record, but do not have a significant impact on the rBC record. Because of the remoteness of the ice core site and the relatively short residence time of rBC in the atmosphere, atmospheric transport and deposition of rBC from the atmosphere are significant sources of variability. The large increase in rBC deposition found in the ice core record likely reflects both changes in emissions and meridional transport.

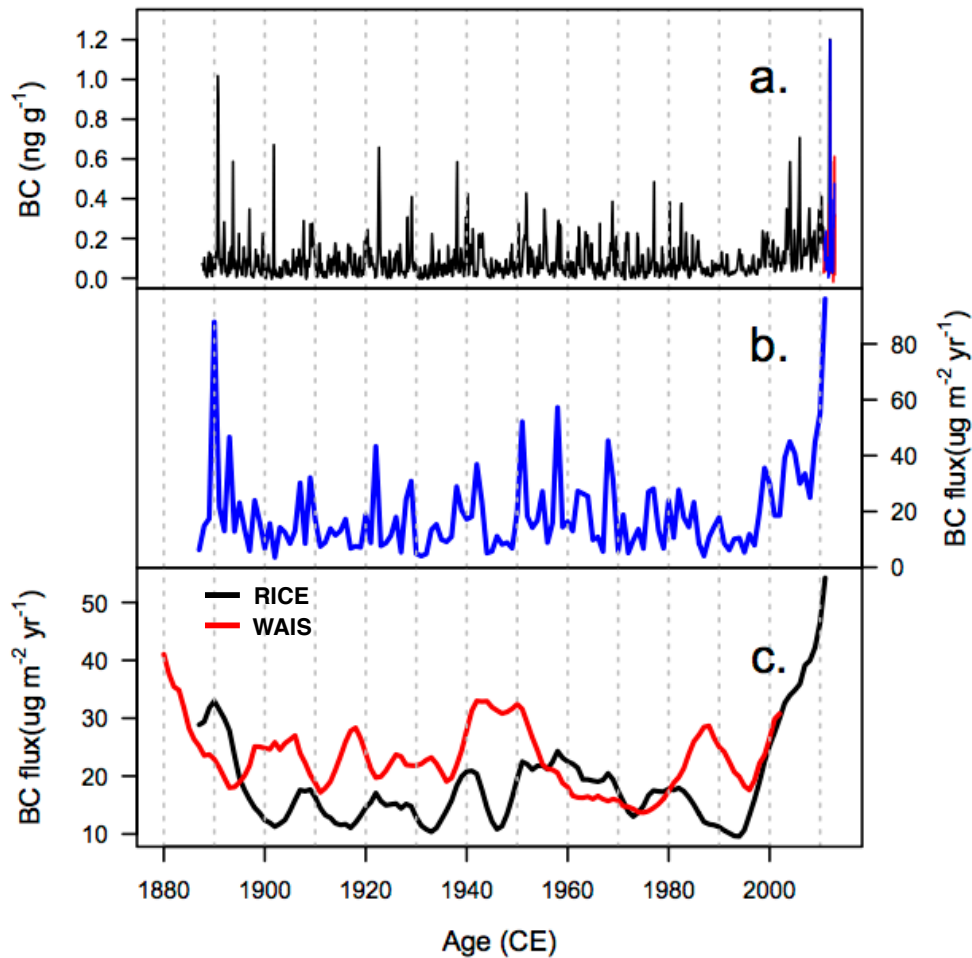


Figure 5.4. RICE ice core and snow pit rBC concentration and atmospheric flux. (a) RICE ice core (black) and snow pit rBC concentration records (Winton snow pit red and Ellis snow pit blue); (b) RICE ice core annual rBC atmospheric flux; and (c) RICE rBC atmospheric flux trend (black) and WAIS ice core rBC atmospheric flux trend (red) determined through single spectrum analysis.

The last 50 years of the WAIS Divide ice core rBC record (Figure 5.4c) hints at a potential increase matching the Roosevelt Island record (Bisiaux et al., 2012), but the record ends before the largest increase from 1998 CE onward. Recent snow pits and shallow cores from WAIS Divide are necessary to demonstrate the spatial extent of the increase in rBC deposition.

5.3.4 Potential causes of increase in rBC deposition to Roosevelt Island

There are a number of potential mechanisms for this increase, summarized below.

1. Increase in emissions from a source region.

Fire emissions peak in November in Australia (Edwards et al., 2006), significantly later in the year than other southern hemisphere sources. Coupled with modeled aerosol trajectories to Roosevelt Island (Neff & Bertler, 2015), seasonal summer burning in Australia's higher latitudes are a possible source. Biomass burning in the Australian continent, a likely emissions source for Roosevelt Island, is sensitive to climate variations. Historical peaks in the charcoal record are closely associated with climate variability, such as maximum El Niño and La Niña frequency (Lynch et al., 2007). Variability associated with the El Niño Southern Oscillation (ENSO) may also drive a 'boom and bust' cycle in Australia, characterized by heavy rainfall during La Niña years causing significant fuel loading, followed by dry conditions where the new growth is subject to severe bushfires (Letnic & Dickman, 2006).

Climate change may amplify drought conditions in Australia (Nicholls, 2004), and models suggest an increasing risk for extreme bushfires in Australia with rising temperatures and lower relative humidity (Pitman et al., 2007). Recent studies have shown a likely increase in frequency of La Niña events, coupled with an increase in frequency of El Niño events, and more rapid oscillation between the two (Cai et al., 2014; Cai et al., 2015). Additionally, Southeast Australia has been affected by persistent drought from 1997 to 2010 known as the 'Big Dry' (Verdon-Kidd & Kiem, 2009), potentially influenced by the positive phase of the southern annular mode (SAM) and subsequent amplification of ENSO events. Southeast and Southwest Australia were the most affected regions by this drought.

2. Shift in transport conditions in the Southern Hemisphere

While emissions may be a factor in the increase, the stronger variable in rBC deposition to Antarctica is transport. rBC removal from the atmosphere happens non-linearly; therefore, a shortening of the trip to Antarctica might significantly increase the concentration of rBC in the airmass that arrives (Bauer et al., 2013). There are several large-scale atmospheric processes that could modulate transport of rBC emissions to Antarctica, and there are some processes that have had significant changes in the last 10-15 years (in conjunction with the increase of rBC at Roosevelt Island):

- The formation of a strong Amundsen Sea low-pressure system and a corresponding "blocking" high-pressure system near New Zealand is a major force in meridional transport, forcing airmasses from Australia south to Antarctica (Neff & Bertler, 2015). This is typical feature of the La Niña phase of ENSO (De Deckker et al., 2010).

- The formation of the Antarctic ozone hole in the late 1970s has had a pronounced effect on SAM, particularly influencing the summertime amplitude of SAM (Thompson et al., 2011). The Australian SAM signature includes variability in precipitation and prevailing winds, though a transport pathway to Antarctica remains unclear.

3. Less precipitation = less removal?

Many of the atmospheric processes above modulate hydroclimate in the SH. Variability in SAM is considered as strong influencer of rainfall over Australia (Hendon et al., 2007). There was a decade-long drought in Australia from 2000 to 2010, a period corresponding to the elevated rBC concentrations at Roosevelt Island. This drought has been linked to climate change-induced variability in the Indian Ocean Dipole (IOD), SAM, and ENSO (Cai et al., 2014). Considering rBC is predominately removed from the atmosphere through wet deposition, a decrease in rainfall in the SH could potentially increase the mass loading of rBC in the atmosphere.

5.4 Conclusions

Ice core and snow pit records from Roosevelt Island, West Antarctica show annual seasonality on BC deposition that is dominated by biomass burning in the southern hemisphere. The results are reproducible across two snow pits and a shallow ice core, suggesting significant spatial correlation. There has been a tripling of BC deposition flux to the site from 1998 CE onward, likely due to a change in BC emissions combined with changes in atmospheric circulation.

There are several potential mechanisms for this increase, including an increase in biomass burning emissions in source regions, a shift in transport conditions promoting meridional transport, or a decrease in precipitation over the Southern Ocean thereby affecting removal rates of rBC and concentrations in the air mass. Many extreme hydroclimate and fire events of the last ~100 years are not recorded in the RICE rBC record, suggesting transport conditions are the dominant contribution to the increase. Utilization of a global atmospheric transport model may constrain the transport mechanism. Comparison of the RICE rBC record with previously published rBC data from the West Antarctic Ice Sheet Divide (WAIS) ice core

revealed that decadal variability in concentration and deposition to the two sites is inversely correlated. This inverse correlation signifies distinct transport conditions to the two sites, potentially due to decadal shifts in the location and intensity of the Amundsen Sea Low in response to the El Niño-Southern Oscillation.

Measurements in austral summer 2011-2012 indicate rBC concentrations reached 1.2 ng g^{-1} , approaching concentrations seen in Greenland. Summer deposition of rBC on the Ross Ice Shelf is of particular importance, as 24-hour daylight could amplify the albedo effect. Studies have suggested that rBC snow concentrations as low as 10 ppb are enough to decrease snow albedo by 1%, accelerating melting (Flanner et al., 2007; Hadley & Kirchstetter, 2012; Hansen & Nazarenko, 2004). Given that rBC can be concentrated in snow melt (Sterle et al., 2013), coupled with increasing temperatures in West Antarctica (Steig et al., 2009), suggest that 10 ppb concentrations are a possibility for surface snow on the Ross Ice Shelf. If the increasing trend of deposition continues, rBC has the potential to affect snow albedo on the Ross Ice Shelf, a major drainage pathway of the West Antarctic Ice Sheet.

Acknowledgements

This work is a contribution to the Roosevelt Island Climate Evolution (RICE) Program, funded by national contributions from New Zealand, Australia, Denmark, Germany, Italy, The People's Republic of China, Sweden, UK, and USA. The main logistic support was provided by Antarctica New Zealand (K049) and the US Antarctic Program.

References

- Bauer, S. E., Bausch, A., Nazarenko, L., Tsigaridis, K., Xu, B., Edwards, R., Bisiaux, M., & McConnell, J. (2013). Historical and future black carbon deposition on the three ice caps: Ice core measurements and model simulations from 1850 to 2100. *Journal of Geophysical Research: Atmospheres*, *118*(14), 7948-7961.
- Bigler, M., Svensson, A., Kettner, E., Vallelonga, P., Nielsen, M. E., & Steffensen, J. P. (2011). Optimization of High-Resolution Continuous Flow Analysis for Transient Climate Signals in Ice Cores. *Environmental Science & Technology*, *45*(10), 4483-4489.
- Bisiaux, M. M., Edwards, R., Heyvaert, A. C., Thomas, J. M., Fitzgerald, B., Susfalk, R. B., Schladow, S. G., & Thaw, M. (2011). Stormwater and Fire as Sources of Black Carbon Nanoparticles to Lake Tahoe. *Environmental Science & Technology*, *45*(6), 2065-2071.
- Bisiaux, M. M., Edwards, R., McConnell, J. R., Curran, M. A. J., Van Ommen, T. D., Smith, A. M., Neumann, T. A., Pasteris, D. R., Penner, J. E., & Taylor, K. (2012). Changes in black carbon deposition to Antarctica from two high-resolution ice core records, 1850–2000 AD. *Atmos. Chem. Phys.*, *12*(9), 4107-4115.
- Boening, C., Willis, J. K., Landerer, F. W., Nerem, R. S., & Fasullo, J. (2012). The 2011 La Niña: So strong, the oceans fell. *Geophysical Research Letters*, *39*(19).
- Bond, T. C., Bhardwaj, E., Dong, R., Jogani, R., Jung, S., Roden, C., Streets, D. G., & Trautmann, N. M. (2007). Historical emissions of black and organic carbon aerosol from energy-related combustion, 1850–2000. *Global Biogeochemical Cycles*, *21*(2).
- Bond, T. C., Doherty, S. J., Fahey, D. W., Forster, P. M., Berntsen, T., DeAngelo, B. J., Flanner, M. G., Ghan, S., Kärcher, B., Koch, D., Kinne, S., Kondo, Y., Quinn, P. K., Sarofim, M. C., Schultz, M. G., Schulz, M., Venkataraman, C., Zhang, H., Zhang, S., Bellouin, N., Guttikunda, S. K., Hopke, P. K., Jacobson, M. Z., Kaiser, J. W., Klimont, Z., Lohmann, U., Schwarz, J. P., Shindell, D., Storelvmo, T., Warren, S. G., & Zender, C. S. (2013). Bounding the role of black carbon in the climate system: A scientific assessment. *Journal of Geophysical Research: Atmospheres*, *118*(11), 5380-5552.
- Cai, W., Borlace, S., Lengaigne, M., van Rensch, P., Collins, M., Vecchi, G., Timmermann, A., Santoso, A., McPhaden, M. J., Wu, L., England, M. H., Wang, G., Guilyardi, E., & Jin, F.-F. (2014). Increasing frequency of extreme El Nino events due to greenhouse warming. *Nature Clim. Change*, *4*(2), 111-116.
- Cai, W., Wang, G., Santoso, A., McPhaden, M. J., Wu, L., Jin, F.-F., Timmermann, A., Collins, M., Vecchi, G., Lengaigne, M., England, M. H., Dommenges, D., Takahashi, K., & Guilyardi, E. (2015). Increased frequency of extreme La Nina events under greenhouse warming. *Nature Clim. Change*, *5*(2), 132-137.
- Conway, H., Hall, B. L., Denton, G. H., Gades, A. M., & Waddington, E. D. (1999). Past and Future Grounding-Line Retreat of the West Antarctic Ice Sheet. *Science*, *286*(5438), 280-283.
- De Deckker, P., Norman, M., Goodwin, I. D., Wain, A., & Gingele, F. X. (2010). Lead isotopic evidence for an Australian source of aeolian dust to Antarctica at times over the last 170,000 years. *Palaeogeography, Palaeoclimatology, Palaeoecology*, *285*(3), 205-223.

- Doherty, S. J., Grenfell, T. C., Forsström, S., Hegg, D. L., Brandt, R. E., & Warren, S. G. (2013). Observed vertical redistribution of black carbon and other insoluble light-absorbing particles in melting snow. *Journal of Geophysical Research: Atmospheres*, *118*(11), 5553-5569.
- Edwards, D. P., Emmons, L. K., Gille, J. C., Chu, A., Attié, J. L., Giglio, L., Wood, S. W., Haywood, J., Deeter, M. N., Massie, S. T., Ziskin, D. C., & Drummond, J. R. (2006). Satellite-observed pollution from Southern Hemisphere biomass burning. *Journal of Geophysical Research: Atmospheres*, *111*(D14)
- Ellis, A., Edwards, R., Saunders, M., Chakrabarty, R. K., Subramanian, R., Timms, N. E., van Riessen, A., Smith, A. M., Lambrinidis, D., Nunes, L. J., Vallelonga, P., Goodwin, I. D., Moy, A. D., Curran, M. A. J., & van Ommen, T. D. (2016). Individual particle morphology, coatings, and impurities of black carbon aerosols in Antarctic ice and tropical rainfall. *Geophysical Research Letters*, *43*(22), 11,875-811,883.
- Ellis, A., Edwards, R., Saunders, M., Chakrabarty, R. K., Subramanian, R., van Riessen, A., Smith, A. M., Lambrinidis, D., Nunes, L. J., Vallelonga, P., Goodwin, I. D., Moy, A. D., Curran, M. A. J., & van Ommen, T. D. (2015). Characterizing black carbon in rain and ice cores using coupled tangential flow filtration and transmission electron microscopy. *Atmos. Meas. Tech.*, *8*(9), 3959-3969.
- Flanner, M. G., Zender, C. S., Randerson, J. T., & Rasch, P. J. (2007). Present-day climate forcing and response from black carbon in snow. *Journal of Geophysical Research: Atmospheres*, *112*(D11)
- Flannigan, M. D., Stocks, B. J., & Wotton, B. M. (2000). Climate change and forest fires. *Science of The Total Environment*, *262*(3), 221-229.
- Giglio, L., Randerson, J. T., & van der Werf, G. R. (2013). Analysis of daily, monthly, and annual burned area using the fourth-generation global fire emissions database (GFED4). *Journal of Geophysical Research: Biogeosciences*, *118*(1), 317-328.
- Hadley, O. L., & Kirchstetter, T. W. (2012). Black-carbon reduction of snow albedo. *Nature Clim. Change*, *2*(6), 437-440.
- Hansen, J., & Nazarenko, L. (2004). Soot climate forcing via snow and ice albedos. *Proceedings of the National Academy of Sciences of the United States of America*, *101*(2), 423-428.
- Hendon, H. H., Thompson, D. W. J., & Wheeler, M. C. (2007). Australian Rainfall and Surface Temperature Variations Associated with the Southern Hemisphere Annular Mode. *Journal of Climate*, *20*(11), 2452-2467.
- IPCC. (2013). *Climate Change 2013: the physical science basis, in: Contribution of Working Group I to the Fifth Assessment Report of the Intergovernmental Panel on Climate Change*. Cambridge, United Kingdom and New York, NY, USA: Cambridge University Press.
- Junker, C., & Lioussé, C. (2008). A global emission inventory of carbonaceous aerosol from historic records of fossil fuel and biofuel consumption for the period 1860–1997. *Atmos. Chem. Phys.*, *8*(5), 1195-1207.

- Lamarque, J. F., Bond, T. C., Eyring, V., Granier, C., Heil, A., Klimont, Z., Lee, D., Liousse, C., Mieville, A., Owen, B., Schultz, M. G., Shindell, D., Smith, S. J., Stehfest, E., Van Aardenne, J., Cooper, O. R., Kainuma, M., Mahowald, N., McConnell, J. R., Naik, V., Riahi, K., & van Vuuren, D. P. (2010). Historical (1850–2000) gridded anthropogenic and biomass burning emissions of reactive gases and aerosols: methodology and application. *Atmos. Chem. Phys.*, *10*(15), 7017-7039.
- Letnic, M., & Dickman, C. (2006). Boom means bust: interactions between the El Niño/Southern Oscillation (ENSO), rainfall and the processes threatening mammal species in arid Australia. *Biodiversity & Conservation*, *15*(12), 3847-3880.
- Lynch, A. H., Beringer, J., Kershaw, P., Marshall, A., Mooney, S., Tapper, N., Turney, C., & Kaars, S. V. D. (2007). Using the Paleorecord to Evaluate Climate and Fire Interactions in Australia. *Annual Review of Earth and Planetary Sciences*, *35*(1), 215-239.
- Ma, X., Huete, A., Cleverly, J., Eamus, D., Chevallier, F., Joiner, J., Poulter, B., Zhang, Y., Guanter, L., Meyer, W., Xie, Z., & Ponce-Campos, G. (2016). Drought rapidly diminishes the large net CO₂ uptake in 2011 over semi-arid Australia. *Scientific Reports*, *6*, 37747.
- Marlon, J. R., Bartlein, P. J., Carcaillet, C., Gavin, D. G., Harrison, S. P., Higuera, P. E., Joos, F., Power, M. J., & Prentice, I. C. (2008). Climate and human influences on global biomass burning over the past two millennia. *Nature Geoscience*, *1*(10), 697-702.
- Marlon, J. R., Bartlein, P. J., Gavin, D. G., Long, C. J., Anderson, R. S., Briles, C. E., Brown, K. J., Colombaroli, D., Hallett, D. J., Power, M. J., Scharf, E. A., & Walsh, M. K. (2012). Long-term perspective on wildfires in the western USA. *Proceedings of the National Academy of Sciences*, *109*(9), E535-E543.
- McConnell, J. R., Edwards, R., Kok, G. L., Flanner, M. G., Zender, C. S., Saltzman, E. S., Banta, J. R., Pasteris, D. R., Carter, M. M., & Kahl, J. D. W. (2007). 20th-century industrial black carbon emissions altered arctic climate forcing. *Science*, *317*(5843), 1381-1384.
- Moosmuller, H., Chakrabarty, R. K., & Arnott, W. P. (2009). Aerosol light absorption and its measurement: A review. *Journal of Quantitative Spectroscopy & Radiative Transfer*, *110*(11), 844-878.
- Neff, P. D., & Bertler, N. A. N. (2015). Trajectory modeling of modern dust transport to the Southern Ocean and Antarctica. *Journal of Geophysical Research: Atmospheres*.
- Nicholls, N. (2004). The Changing Nature of Australian Droughts. *Climatic Change*, *63*(3), 323-336.
- Osterberg, E. C., Handley, M. J., Sneed, S. B., Mayewski, P. A., & Kreutz, K. J. (2006). Continuous ice core melter system with discrete sampling for major ion, trace element, and stable isotope analyses. *Environmental science & technology*, *40*(10), 3355-3361.
- Pitman, A. J., Narisma, G. T., & McAneney, J. (2007). The impact of climate change on the risk of forest and grassland fires in Australia. *Climatic Change*, *84*(3-4), 383-401.
- Ramanathan, V., & Carmichael, G. (2008). Global and regional climate changes due to black carbon. *Nature Geoscience*, *1*(4), 221-227.

Schwarz, J. P., Spackman, J. R., Gao, R. S., Perring, A. E., Cross, E., Onasch, T. B., Ahern, A., Wrobel, W., Davidovits, P., Olfert, J., Dubey, M. K., Mazzoleni, C., & Fahey, D. W. (2010). The Detection Efficiency of the Single Particle Soot Photometer. *Aerosol Science and Technology*, 44(8), 612-628.

Sinclair, K. E., Bertler, N. A. N., & Trompetter, W. J. (2010). Synoptic controls on precipitation pathways and snow delivery to high-accumulation ice core sites in the Ross Sea region, Antarctica. *Journal of Geophysical Research: Atmospheres*, 115(D22), D22112.

Steig, E. J., Schneider, D. P., Rutherford, S. D., Mann, M. E., Comiso, J. C., & Shindell, D. T. (2009). Warming of the Antarctic ice-sheet surface since the 1957 International Geophysical Year. *Nature*, 457(7228), 459-462.

Sterle, K. M., McConnell, J. R., Dozier, J., Edwards, R., & Flanner, M. G. (2013). Retention and radiative forcing of black carbon in eastern Sierra Nevada snow. *The Cryosphere*, 7(1), 365-374.

Thompson, D. W. J., Solomon, S., Kushner, P. J., England, M. H., Grise, K. M., & Karoly, D. J. (2011). Signatures of the Antarctic ozone hole in Southern Hemisphere surface climate change. *Nature Geosci*, 4(11), 741-749.

Tuohy, A., Bertler, N., Neff, P., Edwards, R., Emanuelsson, D., Beers, T., & Mayewski, P. (2015). Transport and deposition of heavy metals in the Ross Sea Region, Antarctica. *Journal of Geophysical Research: Atmospheres*, 120(20), 10,996-911,011.

van der Werf, G. R., Randerson, J. T., Giglio, L., Collatz, G. J., Mu, M., Kasibhatla, P. S., Morton, D. C., DeFries, R. S., Jin, Y., & van Leeuwen, T. T. (2010). Global fire emissions and the contribution of deforestation, savanna, forest, agricultural, and peat fires (1997–2009). *Atmos. Chem. Phys.*, 10(23), 11707-11735.

Verdon-Kidd, D. C., & Kiem, A. S. (2009). Nature and causes of protracted droughts in southeast Australia: Comparison between the Federation, WWII, and Big Dry droughts. *Geophysical Research Letters*, 36(22)

Wiedinmyer, C., Akagi, S. K., Yokelson, R. J., Emmons, L. K., Al-Saadi, J. A., Orlando, J. J., & Soja, A. J. (2011). The Fire INventory from NCAR (FINN): a high resolution global model to estimate the emissions from open burning. *Geosci. Model Dev.*, 4(3), 625-641.

Winstrup, M., Vallelonga, P., Kjær, H. A., Fudge, T. J., Lee, J., Riis, M. H., Edwards, R., Bertler, N. A. N., Blunier, T., Brook, E., Buizert, C., Ciobanu, G., Conway, H., Dahl-Jensen, D., Ellis, A., Emanuelsson, D., Kurbatov, A., Mayewski, P., Neff, P., Pyne, R., Simonsen, M. F., Svensson, A., Tuohy, A., & Waddington, E. (2017). A 2000-year timescale and accumulation reconstruction for Roosevelt Island, West Antarctica. *In prep.*

Winstrup, M., Svensson, A. M., Rasmussen, S. O., Winther, O., Steig, E. J., & Axelrod, A. E. (2012). An automated approach for annual layer counting in ice cores. *Clim. Past*, 8(6), 1881-1895.

Winstrup, M. (2016). A Hidden Markov Model Approach to Infer Timescales for High-Resolution Climate Archives. Paper presented at the AAAL.

Winton, V. H. L., Edwards, R., Delmonte, B., Ellis, A., Andersson, P. S., Bowie, A., Bertler, N. A. N., Neff, P., & Tuohy, A. (2016). Multiple sources of soluble atmospheric iron to Antarctic waters. *Global Biogeochemical Cycles*, 30(3), 421-437.

Yates, C. P., Edwards, A. C., & Russell-Smith, J. (2009). Big fires and their ecological impacts in Australian savannas: size and frequency matters. *International Journal of Wildland Fire*, 17(6), 768-781.

Supplementary Information

Supplementary figures for Chapter 5 are included below.

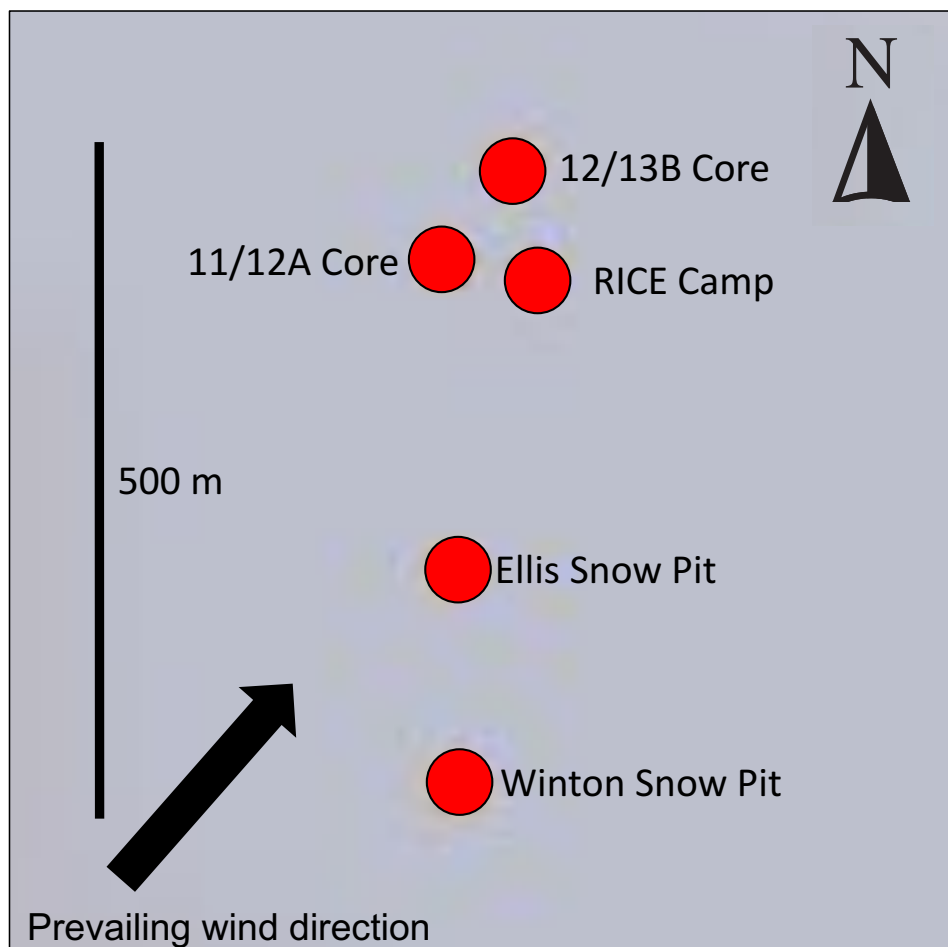


Figure S5.1 Configuration of RICE field camp (with generator), drill site for the main ice core (11/12A), the shallow core (12/13B) and two snow pits.

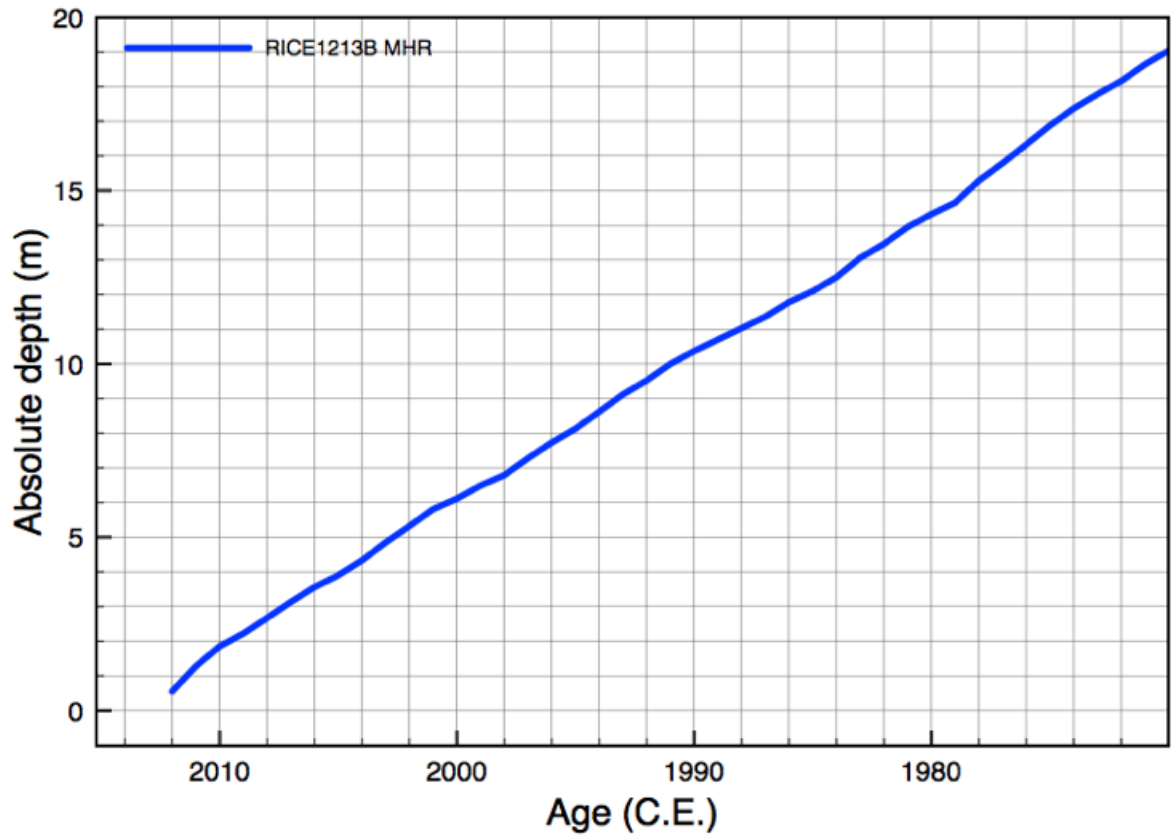


Figure S5.2 Depth-age scale for the shallow core 12/13B, from Ross Edwards (personal communication).

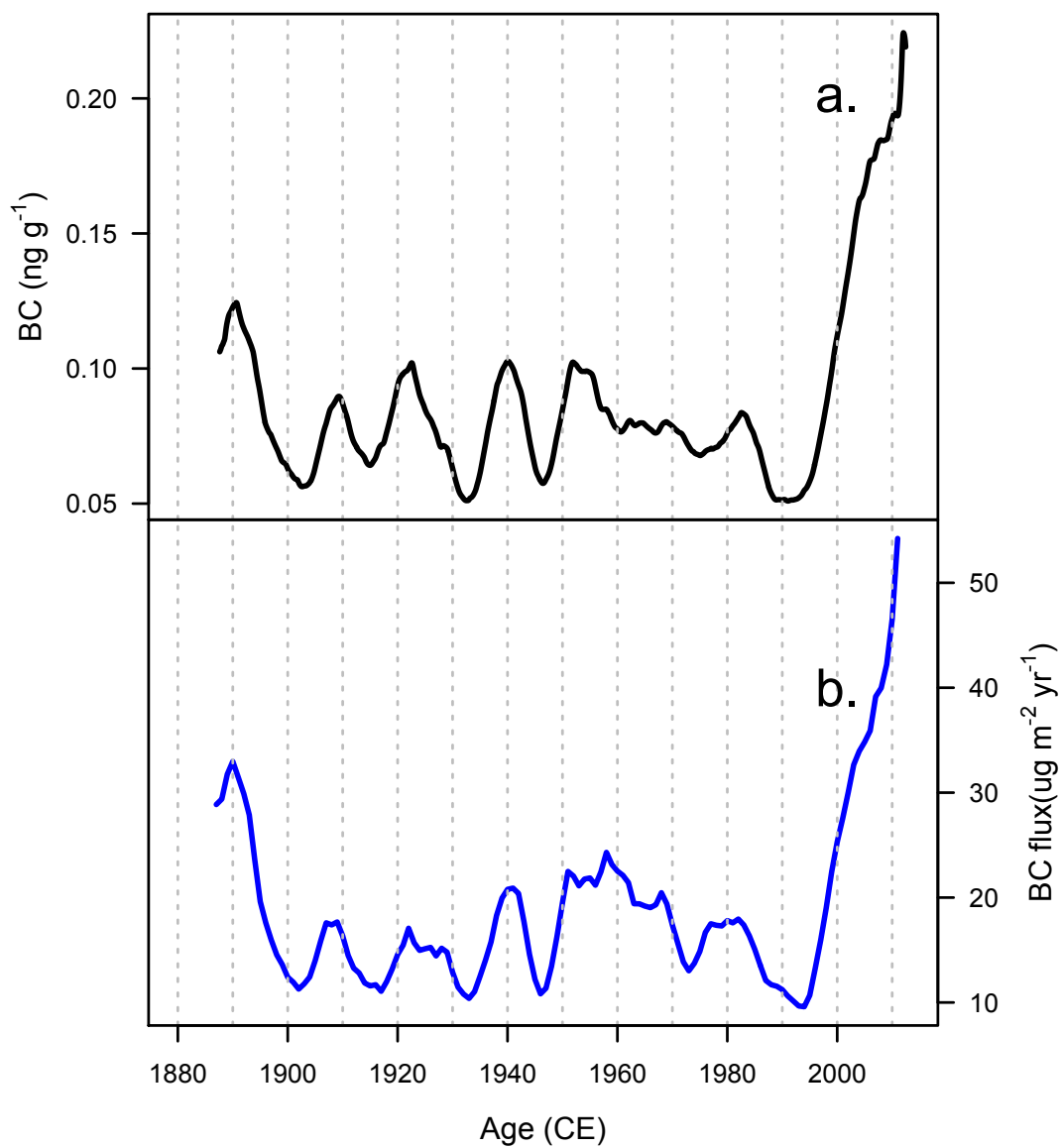


Figure S5.3 A comparison of monthly rBC concentration (a) and annual rBC flux (b) from the ice core record at Roosevelt Island. Underlying trends in both the rBC flux and the monthly rBC concentration are nearly identical, suggesting that annual snow accumulation variability is less of a contribution to flux than the rBC concentration inter-annual variability.

Chapter 6. Black carbon in rain: case studies from northern and western Australia

This chapter is in preparation for submission to *Journal of Geophysical Research: Atmospheres*.

Abstract

Black carbon aerosols (BC) are emitted by combustion and affect radiative and chemical properties of the atmosphere. There are significant uncertainties regarding the lifetime of black carbon in the atmosphere due to the aging of the aerosols and its subsequent interaction and removal from the atmosphere by water. Measurements of BC in rainfall are needed to develop geospatial estimates of BC deposition. Here, we describe a case study of refractory black carbon (rBC) wet deposition measured at two different sites in Australia by single particle laser-induced incandescent photometry. To our knowledge this is the first study of rBC in Australian rainfall. Rain samples were collected from Perth, Western Australia and Darwin in the Northern Territory. Perth samples were collected as the remnants of tropical cyclone Owlyn passed through the region in March, 2015. Darwin samples were collected during the Northern Territory monsoon season from November 2014 through February 2015. Concentrations of rBC in the rainfall varied from $\sim 0.5 - 6 \mu\text{g L}^{-1}$ for Perth and $\sim 1 - 22 \mu\text{g L}^{-1}$ for Darwin, with 24-hour wet depositional flux ranging from $\sim 0.8 - 41 \mu\text{g m}^{-2}$ and $\sim 1 - 314 \mu\text{g m}^{-2}$, respectively. Perth rBC deposition rates decreased as continental winds from the north east shifted to south west winds from off the southern Indian Ocean. Higher rBC concentrations and deposition from Darwin may reflect biomass burning emissions from Indonesia and northern Australia.

6.1 Introduction

Black carbon aerosols are emitted into the atmosphere during the combustion of biomass and fossil fuels. In the atmosphere, they have direct and indirect effects on the climate through radiative absorption and changes in cloud formation (Johnson et al., 2004). BC has a large impact on net climate forcing estimates due to a positive climate forcing comparable to the greenhouse gases (Bond et al., 2013). However, it is relatively short-lived in the atmosphere, with a lifetime of days to a few weeks (Rodhe et al., 1972). The large-scale distribution of BC in the atmosphere is a product of emissions and deposition during atmospheric transport. Initially hydrophobic, BC particles age in the atmosphere and eventually become hydrophilic acting as cloud and ice nuclei (Koehler et al., 2009). Dry deposition of BC occurs immediately after emission; however, wet deposition is thought to exceed dry deposition by an order of magnitude (Bond et al., 2013; Jacobson, 2012). Wet deposition is therefore a major factor determining the longevity of BC in the atmosphere. A growing number of modeling studies address the atmospheric transport, aging and deposition of BC, but the studies are constrained by limited field measurements of wet deposition. Additionally, modeling of the BC aging timescales using available observations (Schwarz et al. (2010) suggests that different source regions have significantly different lifetimes in the atmosphere, partly due to the prevalence and composition of co-emitted species (Zhang et al., 2015). The removal of BC from the atmosphere by wet deposition is crucial to understanding BC residence times in the atmosphere, and consequently global climate forcing models (Bond et al., 2013).

Previous studies have used a number of techniques to measure insoluble carbon in rainwater, including thermal-optical analysis (TOA), single-particle soot photometry (SP2), ultraviolet–visible spectrophotometry, and total organic carbon (TOC) analysis (Torres et al., 2013). Early studies calculated the removal rate of elemental carbon (EC, similar to BC) from the atmosphere through wet deposition at urban sites in Seattle and rural sites in Sweden using quartz-fiber filtration and TOA (Ogren et al., 1984), but the studies were limited by low BC concentrations and required large rain sample volumes for filtration. TOA of organic carbon (OC) and EC in rain at mountainous background sites across a European transect measured EC concentrations ranging from $2.8 \pm 4.3 \mu\text{g C L}^{-1}$ to $28 \pm 38 \mu\text{g C L}^{-1}$ (Cerqueira et al., 2010).

The single particle soot photometer (SP2) uses particle incandescence to measure the mass and particle size of the refractory black carbon (rBC) component of aerosol samples (SP2, Droplet Measurement Technologies, Boulder, Colorado). A real-time analysis system consisting of an ultrasonic nebulizer coupled to the SP2 has been used in the past to measure rBC particles in rain, snow, and ice samples (McConnell et al., 2007; Ohata et al., 2011; Schwarz et al., 2012; Torres et al., 2013). There is evidence that the effectiveness of the rBC measurement using this method drops substantially with larger particle size (>500 nm) through size-dependent nebulization efficiency, and is associated with significant uncertainty due to differences in particle size in snow samples compared to atmospheric measurements (Ohata et al., 2011; Schwarz et al., 2012). Consequently, these studies suggest that SP2 methods to measure rBC in rainwater consistently underestimate rBC mass, but systematic loss can be controlled for through the use of rBC standards. Though TOC analyzer measurements are more accurate at higher concentrations (200 – 5000 $\mu\text{g L}^{-1}$, detection limit 40 $\mu\text{g L}^{-1}$), the SP2 is required for measurements of low rBC concentrations (Torres et al., 2013). The SP2 has been used to measure rBC concentrations in the atmosphere and rainwater in outflows from China, with significant seasonal variability (Mori et al., 2014). Urban rain rBC measurements were also made in Tokyo using the SP2 (Ohata et al., 2011). Ducret and Cachier (1992) measured air and rain organic and black carbon concentrations at multiple locations in Europe and noticed significant regional variability, suggesting that removal rates varied due to changes in hygroscopicity of the particles.

BC emissions in the Southern Hemisphere are dominated by biomass burning, whereas industrial emissions dominate in the Northern Hemisphere. The vast majority of BC rain studies have been conducted in the Northern Hemisphere, often downwind from major urban emissions. Mixing state and co-emitted species substantially affect BC behavior in the atmosphere, including cloud and ice formation, and therefore affect BC lifetime in the atmosphere (Stier et al., 2006). Wet deposition rates in the Southern Hemisphere are necessary in order to constrain global models of atmospheric BC lifetime.

Australian rain samples from Perth, Western Australia and Darwin, Northern Territory were collected and analyzed for rBC concentration using an SP2. Predominant air mass transport to Perth is from the Indian Ocean to the west. Bushfires in Africa and South America are likely sources of long-range transported aerosols over the Indian and Southern Oceans. Black

carbon deposited in Darwin is likely sourced from biomass and industrial emissions in Indonesian and northern Queensland, with significantly shorter BC atmospheric lifetime.

6.2 Methods

6.2.1 Sample collection and handling

Rain samples were collected in Darwin, Northern Territory, and Perth, Western Australia (Figure 6.1). Perth is the largest city in Western Australia with a population of 2 million and predominant wind patterns are from the Indian Ocean. Darwin is the largest city in Northern Territory with a smaller population of 142,000. Darwin is located close to Indonesia and Papua New Guinea, and experiences seasonal monsoon rainfall. The Northern portion of Australia experiences a dry season in winter, May through November, and a monsoonal wet season in the summer months, December through March (Holland, 1986; Kaars et al., 2000). This site was selected as large volumes of rain could be collected in short periods of time.



Figure 6.1 A map of Australia, with sampling locations marked in Perth, Western Australia, and Darwin, Northern Territory. Perth is located on the Indian Ocean with predominant winds from the West. Darwin is in close proximity to seasonal biomass burning in northern Australia and Indonesia.

The Perth and Darwin rain samples were collected using a low-density polyethylene (LDPE) funnel with a 1 L cleaned LDPE (Nalgene) bottle attached via a threaded cap. All sampling equipment was cleaned with ultra-pure (UP, $\rho >18.2 \text{ m}\Omega$) water. In Darwin, the funnel was placed on a bucket in an open field, with no overhead obstructions. In Perth, the sampling occurred on the roof of a building, similarly with no obstructions.

Darwin rain samples were collected at (-12.370541, 130.867107). The Darwin rain samples were initially collected for nanoparticle separation, and were not weighed for total sample volume. Rain samples were therefore compared to the automatic weather station (AWS) data recorded at the Darwin International Airport (-12.4239, 130.8925), the closest weather station to the sampling site with rainfall measurements and 6.52 km from the AWS location. Weather station data was recorded every minute, with 0.2 mm rainfall resolution (where 1 mm of rainfall = 1 L m⁻²). AWS rainfall data was aggregated for the sampling period, to provide an approximation of rainfall in the absence of direct measurements at the rain sampling site.

There are several limitations with this approach, namely the assumption that the rainfall in the two locations is comparable. Research on storm cells in Darwin suggests that the mode in storm cell diameter is ~5 km (May & Ballinger, 2007), and a number of the collected samples did not have corresponding rain measurements at the AWS site, indicating that only some of the storm cells covered both the rain sampling site and the AWS. Therefore, any flux estimates come with significant uncertainties.

Perth rain samples were collected at (-32.007513, 115.895350), on a building rooftop on the Curtin University campus. Perth rain samples were collected in the aftermath of Cyclone Olwyn, which decreased in intensity prior to passing over Perth, and caused rapid variations in atmospheric transport conditions. Perth rain samples were weighed after collection for sample volume. Twenty-four-hour total rainfall measurements were made at the Perth Airport AWS (-31.93, 115.98). Total rainfall during the sampling period was calculated from AWS data in Darwin and measured from collected sample volume in Perth. All weather station data can be found at the Australian Bureau of Meteorology website (www.bom.gov.au).

Hybrid Single-Particle Lagrangian Integrated Trajectory (HYSPLIT) 72-hour back-trajectories (Rolph, 2016; Stein et al., 2015) were calculated at each sampling location and for each sample collection time. Trajectories were also calculated at 500 m, 1000 m, and

2000 m for the Perth samples to account for potential air mass sources for precipitation, as BC wet removal can occur through both nucleation and scavenging during rainfall.

6.2.2 TEM imaging

Rain samples were processed according to the method detailed in Ellis et al. (2015). Briefly, after rBC measurement using the SP2, rain samples were filtered and concentrated using Tangential Flow Filtration (TFF). This technique retains insoluble particles, while removing water and soluble species. The resulting concentrated solution was deposited on a gold Si/SiO₂-coated TEM grid and imaged using a Titan G2 80-200 TEM/STEM with ChemiSTEM Technology. This instrument incorporates scanning transmission electron microscopy (STEM) and ~1 nm resolution EDS mapping for elemental composition.

6.2.3 SP2 analysis

Rain samples were refrigerated immediately after collection to slow particle aggregation or loss to the walls of the sample bottle. Rain samples collected in Darwin were shipped in a cooler with ice packs to Perth. There is likely a small fraction of particle loss due to the shipment time between sample collection in Darwin and rBC analysis in Perth, therefore rBC concentrations reported here should be treated as a minimum value for the sample.

Rainwater samples were analyzed using a single-particle soot photometer (SP2) located at Curtin University, in Perth, Australia. Samples were pumped into an ultrasonic nebulizer and desolvator (Cetac) and subsequently into the SP2 (Sterle et al., 2013). Relative SP2 rBC concentrations for the rain samples were calibrated using a standard suite of set concentrations made of Ebony-6 ink, and run before and after sample analysis to account for possible SP2 drift.

6.2.4 Uncertainty

Perth rain samples were weighed after collection for total sample volume. The funnel used for collection was not measured directly, and instead estimated at ~30 cm in diameter. Rain deposition in units of kg m⁻² was calculated using this estimated diameter. This value was given an uncertainty of ± 50% to account for the potential large variation in collected rainfall with changes in funnel diameter, to avoid suggesting high precision in calculated rBC deposition rates. It should be noted that variability in the diameter of the funnel could

substantially alter the rBC deposition rates calculated in this paper, but as the Perth samples were all collected using the same equipment, the relative deposition rates will be unchanged.

Several duplicate sub-samples were taken in Darwin and Perth to test uncertainty in the sample handling and SP2 analysis. This method does not account for uncertainties in sample collection, as duplicates were taken from a single rain collection sample. Though limited in number, these duplicates were used to calculate standard deviation, which was applied to the additional samples. The duplicated samples include Darwin_9, Darwin_10, Perth_1, Perth_2, and Perth_3. The uncertainties in rBC deposition rates are dominated by the error in estimated rainfall measurements. For calculations, uncertainties in individual measurements were combined using the standard formulas for propagation of uncertainties.

Weather station rain measurement uncertainty was estimated as the instrument resolution, 0.2 kg m^{-2} , as provided by the Australian Bureau of Meteorology.

6.3 Results and Discussion

6.3.1 Black carbon wet deposition in Darwin, Northern Territory and Perth, Western Australia

rBC deposition rates were calculated for individual events (Table 6.1) and extrapolated for 24-hour periods (Table 6.2). Darwin showed variability in rBC concentrations, ranging from $0.8 \pm 0.3 \mu\text{g L}^{-1}$ to $21.8 \pm 0.3 \mu\text{g L}^{-1}$. This range is substantially lower than rBC measurements in Rain from Asian outflows, which ranged from $8.0 \pm 4.1 \mu\text{g L}^{-1}$ to $92 \pm 76 \mu\text{g L}^{-1}$ (Mori et al., 2014).

Concentrations in Perth were lower on average (Table 6.1), with concentration at the beginning of the storm system (Figure 6.3) reaching $5.74 \pm 0.01 \mu\text{g L}^{-1}$ and decreasing to $0.57 \pm 0.03 \mu\text{g L}^{-1}$ when the storm system had dissipated and transport was from offshore (Figure 6.4). On two days where multiple rain samples were collected during a single weather event, rBC depositional flux decreased over the course of the event for both Perth and Darwin rainwater. This is consistent with the trend from the sub-event flux measurements made in Tokyo rainwater in Ohata et al. (2011).

While acknowledging that the wet deposition data set is small, the extrapolated 24-hour wet depositional fluxes for Darwin and Perth were comparable to global, latitudinally averaged BC wet deposition rates described by Jurado et al. (2008). This study used a simple washout ratio of $2 \cdot 10^5$, derived from Jurado et al. (2005), to calculate a wet deposition rates. It should be noted that estimated washout ratios in the literature vary by over an order of magnitude, in part due to the uncertainty associated with wet scavenging of particles. Jurado et al. (2008) predicted BC wet deposition flux of $180 \mu\text{g m}^{-2} \text{d}^{-1}$ for $0\text{--}30^\circ\text{N}$, $70 \mu\text{g m}^{-2} \text{d}^{-1}$ for $0\text{--}30^\circ\text{S}$, and $20 \mu\text{g m}^{-2} \text{d}^{-1}$ for $60^\circ\text{S}\text{--}30^\circ\text{S}$. rBC wet deposition flux in Darwin (12°S) ranged from $1\text{--}314 \mu\text{g m}^{-2} \text{d}^{-1}$, with the highest rBC concentrations occurring in November, close to biomass burning season in Indonesia. rBC flux in Perth (32°S) ranged from $0.8\text{--}41 \mu\text{g m}^{-2} \text{d}^{-1}$, comparable to predicted daily flux values for the latitude.

Table 6.1 rBC concentrations and deposition rates from individual rain events collected in Darwin, Northern Territory and Perth, Western Australia.

Sample ID	Location	Sampling Start Date	Sampling End Date	Sampling Period	BC Concentration ($\mu\text{g L}^{-1}$)	Estimated rainfall during sample period (kg m^{-2})	Event total wet deposition ($\mu\text{g m}^{-2}$)	Event mean wet deposition rate ($\text{ng m}^{-2}\text{s}^{-1}$)	Weather conditions
Darwin_1	Darwin	25/11/2014	25/11/2014	15:30-16:00	21.8 ± 0.3	N/A	-	-	-
Darwin_2	Darwin	26/11/2014	26/11/2014	13:00-13:45	11.4 ± 0.3	4.6 ± 0.2	52 ± 4	19 ± 1	-
Darwin_3	Darwin	26/11/2014	26/11/2014	13:45-14:00	12.1 ± 0.3	N/A	-	-	-
Darwin_4	Darwin	07/01/2015	07/01/2015	16:00-16:30	5.5 ± 0.3	5.0 ± 0.2	28 ± 3	15 ± 1	-
Darwin_5	Darwin	14/01/2015	14/01/2015	12:30-13:30	5.1 ± 0.3	0.4 ± 0.2	2 ± 1	0.6 ± 0.4	-
Darwin_6	Darwin	15/01/2015	15/01/2015	13:30-14:30	1.2 ± 0.3	0.6 ± 0.2	0.7 ± 0.4	0.2 ± 0.2	-
Darwin_7	Darwin	30/01/2015	30/01/2015	12:30-13:00	1.3 ± 0.3	N/A	-	-	Seasonal thunderstorms
Darwin_8	Darwin	03/02/2015	03/02/2015	13:50-14:30	1.1 ± 0.3	0.4 ± 0.2	0.4 ± 0.3	0.2 ± 0.1	-
Darwin_9	Darwin	20/02/2015	20/02/2015	08:30-09:10	2.9 ± 0.3	N/A	-	-	-
Darwin_10	Darwin	20/02/2015	20/02/2015	10:30-11:30	2.3 ± 0.3	3.2 ± 0.2	8 ± 2	2.2 ± 0.6	-
Darwin_11	Darwin	20/02/2015	20/02/2015	13:00-14:00	0.8 ± 0.3	2.6 ± 0.2	2 ± 1	0.5 ± 0.4	-
Darwin_12	Darwin	23/02/2015	23/02/2015	11:00-12:00	11.7 ± 0.3	0.4 ± 0.2	5 ± 3	2.2 ± 0.9	-
Darwin_13	Darwin	24/02/2015	24/02/2015	15:00-16:00	6.6 ± 0.3	N/A	-	-	-
Perth_1	Perth	13/03/2015	14/03/2015	16:27-06:22	5.74 ± 0.01	9.8 ± 4.9	56 ± 28	1.1 ± 0.6	Rain from tail-end of category 3 cyclone, travelling South along the Western Australia coastline
Perth_2	Perth	14/03/2015	15/03/2015	13:41-07:39	3.05 ± 0.04	4.3 ± 2.1	13 ± 7	0.2 ± 0.1	-
Perth_3	Perth	15/03/2015	16/03/2015	07:39-10:00	0.57 ± 0.03	2.3 ± 1.1	1.4 ± 0.8	0.01 ± 0.02	-

Table 6.2 rBC concentrations from individual rain events and extrapolated deposition rates calculated from 24-hour rainfall measurements in Darwin, Northern Territory and Perth, Western Australia.

Sample ID	Location	Sampling Start Date	Sampling End Date	Sampling Time Period	BC Concentration ($\mu\text{g L}^{-1}$)	24-hour AWS rain accumulation (kg m^{-2})	Extrapolated 24-hour wet deposition ($\mu\text{g m}^{-2}$)	24-hour mean wet deposition rate ($\text{ng m}^{-2}\text{s}^{-1}$)	Weather conditions
Darwin_1	Darwin	25/11/2014	25/11/2014	15:30-16:00	21.8 ± 0.3	14.4 ± 0.2	314 ± 9	3.6 ± 0.1	-
Darwin_2	Darwin	26/11/2014	26/11/2014	13:00-13:45	11.4 ± 0.3	4.6 ± 0.2	54 ± 4	0.63 ± 0.05	-
Darwin_3	Darwin	26/11/2014	26/11/2014	13:45-14:00	12.1 ± 0.3	-	-	-	-
Darwin_4	Darwin	07/01/2015	07/01/2015	16:00-16:30	5.5 ± 0.3	6.0 ± 0.2	33 ± 3	0.38 ± 0.03	-
Darwin_5	Darwin	14/01/2015	14/01/2015	12:30-13:30	5.1 ± 0.3	23.2 ± 0.2	119 ± 8	1.38 ± 0.9	-
Darwin_6	Darwin	15/01/2015	15/01/2015	13:30-14:30	1.2 ± 0.3	3.4 ± 0.2	4 ± 1	0.05 ± 0.01	-
Darwin_7	Darwin	30/01/2015	30/01/2015	12:30-13:00	1.3 ± 0.3	11.8 ± 0.2	15 ± 4	0.2 ± 0.05	Seasonal thunderstorms
Darwin_8	Darwin	03/02/2015	03/02/2015	13:50-14:30	1.1 ± 0.3	1.0 ± 0.2	1.0 ± 0.5	0.01 ± 0.01	-
Darwin_9	Darwin	20/02/2015	20/02/2015	08:30-09:10	2.9 ± 0.3	91.2 ± 0.2	188 ± 20	2.2 ± 0.2	-
Darwin_10	Darwin	20/02/2015	20/02/2015	10:30-11:30	2.3 ± 0.3	-	-	-	-
Darwin_11	Darwin	20/02/2015	20/02/2015	13:00-14:00	0.8 ± 0.3	-	-	-	-
Darwin_12	Darwin	23/02/2015	23/02/2015	11:00-12:00	11.7 ± 0.3	0.6 ± 0.2	7 ± 3	0.08 ± 0.03	-
Darwin_13	Darwin	24/02/2015	24/02/2015	15:00-16:00	6.6 ± 0.3	10.6 ± 0.2	70 ± 4	0.8 ± 0.05	-
Perth_1	Perth	13/03/2015	14/03/2015	16:27-06:22	5.74 ± 0.01	7.2 ± 0.2	41 ± 1	0.47 ± 0.01	Rain from tail-end of category 3 cyclone, travelling South along the Western Australia coastline
Perth_2	Perth	14/03/2015	15/03/2015	13:41-07:39	3.05 ± 0.04	4.6 ± 0.2	14 ± 1	0.16 ± 0.01	-
Perth_3	Perth	15/03/2015	16/03/2015	07:39-10:00	0.57 ± 0.03	1.4 ± 0.2	0.8 ± 0.2	0.01 ± 0.00	-

NOAA HYSPLIT MODEL
 Backward trajectories ending at 0800 UTC 20 Feb 15
 GDAS Meteorological Data

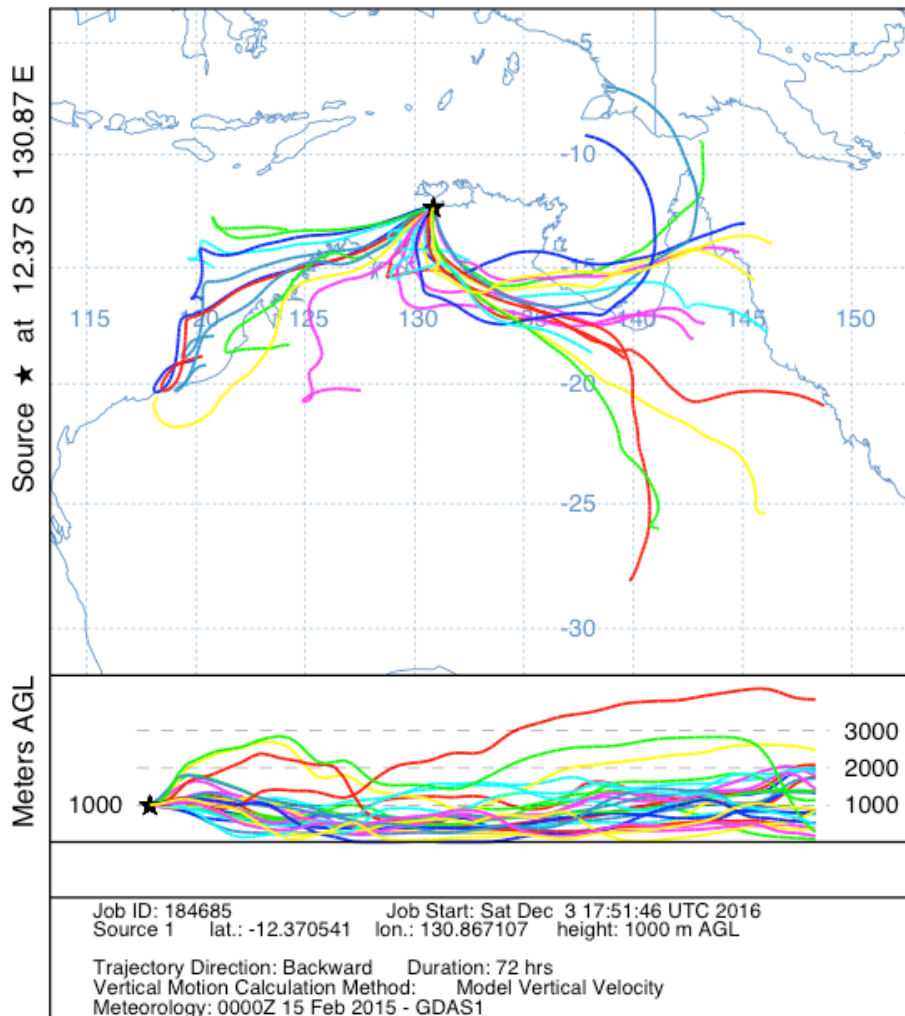


Figure 6.2 HYSPLIT back trajectory for the Darwin sampling site for the samples collected on 20 Feb 2015. Airmass transport was predominately over the Northern Territory, Queensland, and Western Australia before deposition in Darwin. Additional trajectories for a starting airmass height of 500 m and 2000 m are included in the Supplementary Information.

NOAA HYSPLIT MODEL
 Backward trajectories ending at 0000 UTC 14 Mar 15
 GDAS Meteorological Data

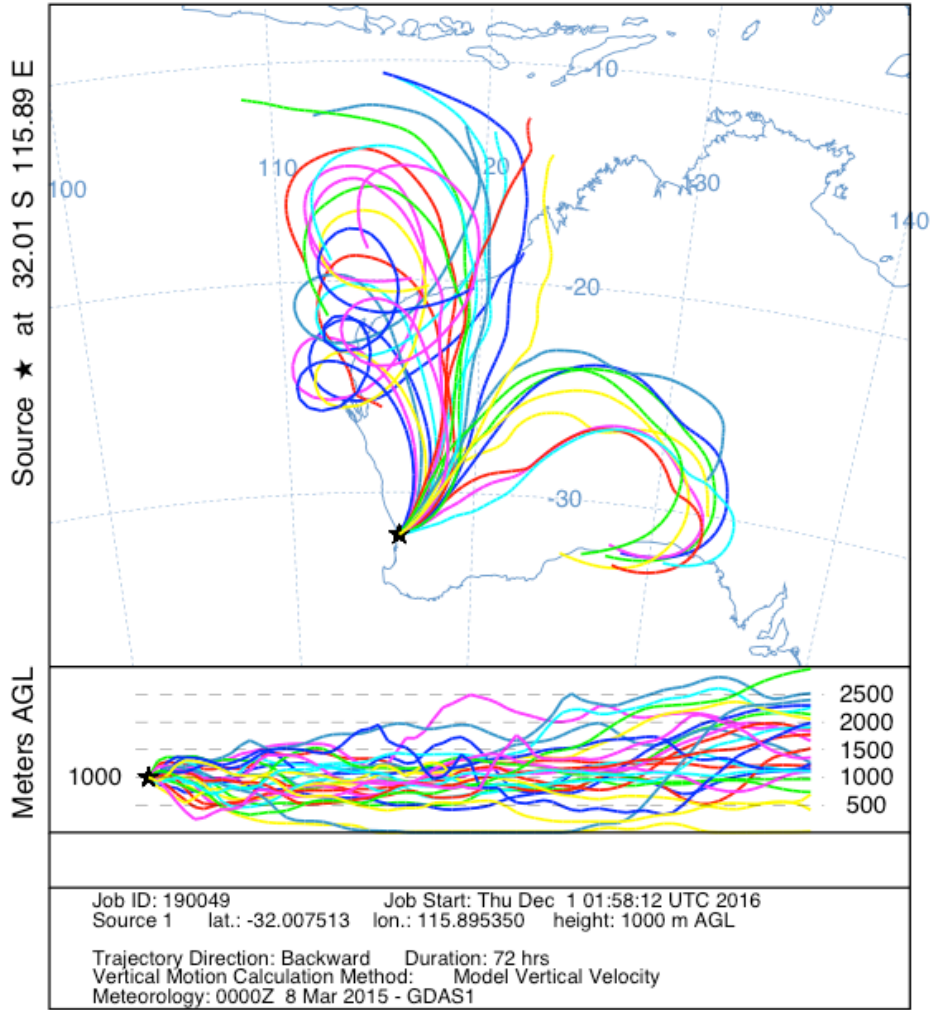


Figure 6.3 HYSPLIT back trajectory for 14 March 2015, for the Perth sampling site, demonstrating transport from Western Australia mobilized by Cyclone Olwyn which passed southward along the west coast on the continent. Additional trajectories for a starting air mass height of 500 m and 2000 m are included in the Supplementary Information.

NOAA HYSPLIT MODEL
 Backward trajectories ending at 0000 UTC 16 Mar 15
 GDAS Meteorological Data

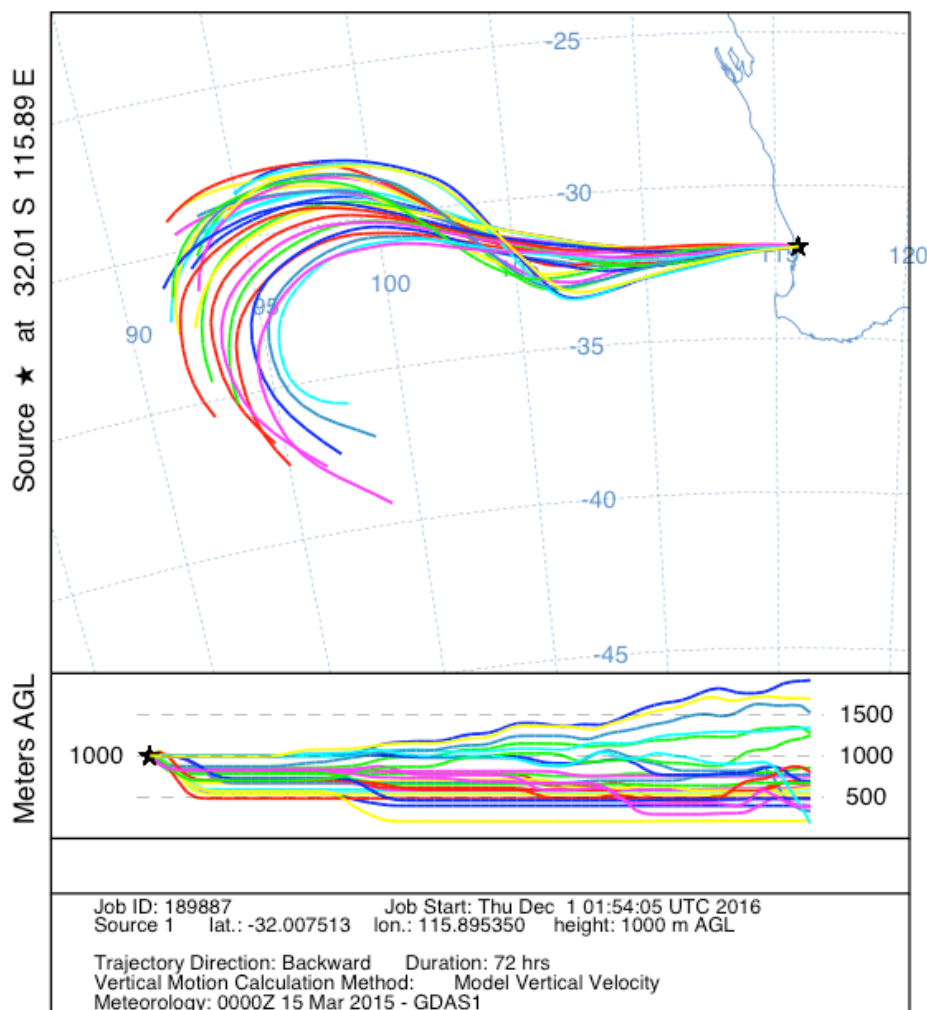


Figure 6.4 HYSPLIT back trajectory for 16 March 2015, for the Perth sampling site, demonstrating long-range remote transport from the Indian Ocean, a common weather pattern in Perth. Additional trajectories for a starting air mass height of 500 m and 2000 m are included in the Supplementary Information.

6.3.2 Particle characterization using electron microscopy

Many uncommon particle morphologies and compositions were found in the Darwin rain samples, detailed in Ellis et al. (2015) and Ellis et al. (2016). A number of morphologies and compositions are relevant to this study, and are therefore included. Numerous BC superaggregates were found in Darwin samples, which are unlikely to be detected by the SP2 system (Figure 6.3). This is due both to the instrument particle size detection range and to the size-limited transport efficiency of the ultrasonic nebulizer, as there is lower nebulization

efficiency for particles greater than 600 nm (Schwarz et al., 2012). These particles may constitute a disproportionate amount of BC mass in the sample.

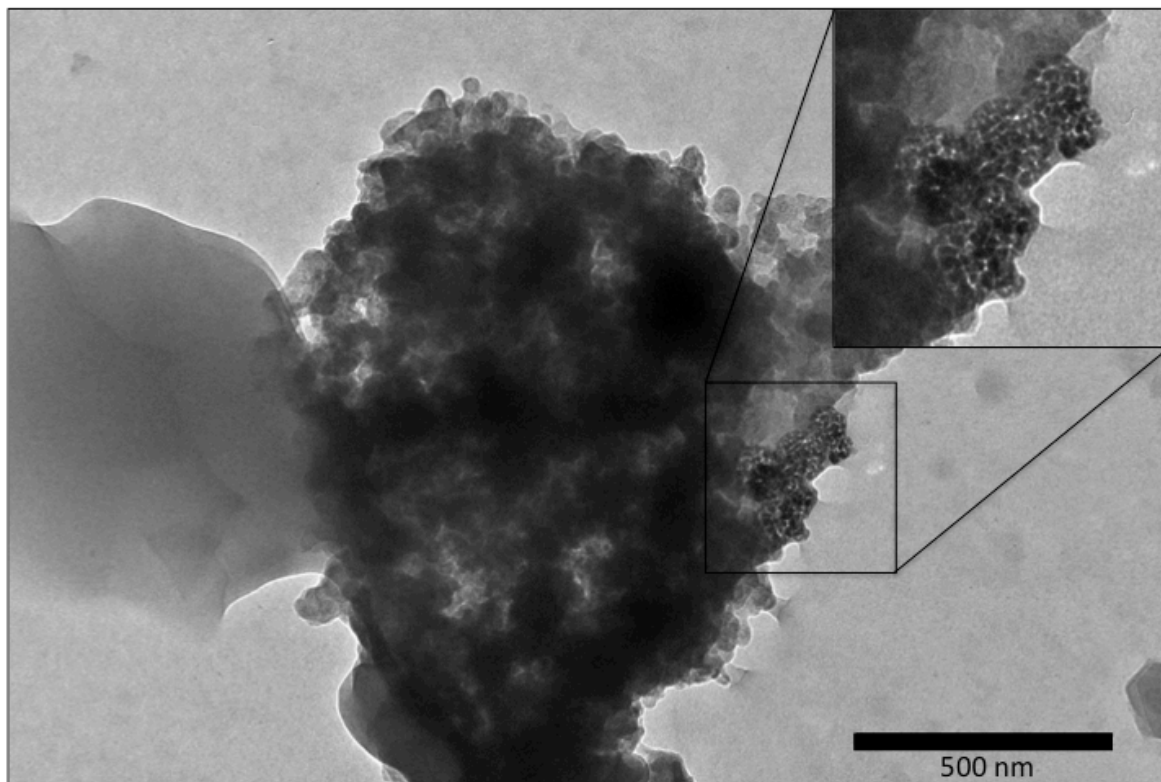


Figure 6.5 Black carbon superaggregates were found in Darwin rain, many of which are larger than the SP2 detection size range. This superaggregate was also attached to a large aluminosilicate dust particle, and contained iron spherules incorporated into the carbon aggregate (inset).

Many particles contained iron spherules and aluminum-rich silicate dust particles incorporated into the BC aggregates, which likely formed shortly after emission and suggest a biomass burning origin (Figure 6.5 inset, Figures 6.6 and 6.7). BC scavenged through rainfall is a likely source of soluble iron in the Southern Ocean, which could have significant implications for iron-limited algae growth (Winton et al., 2016).

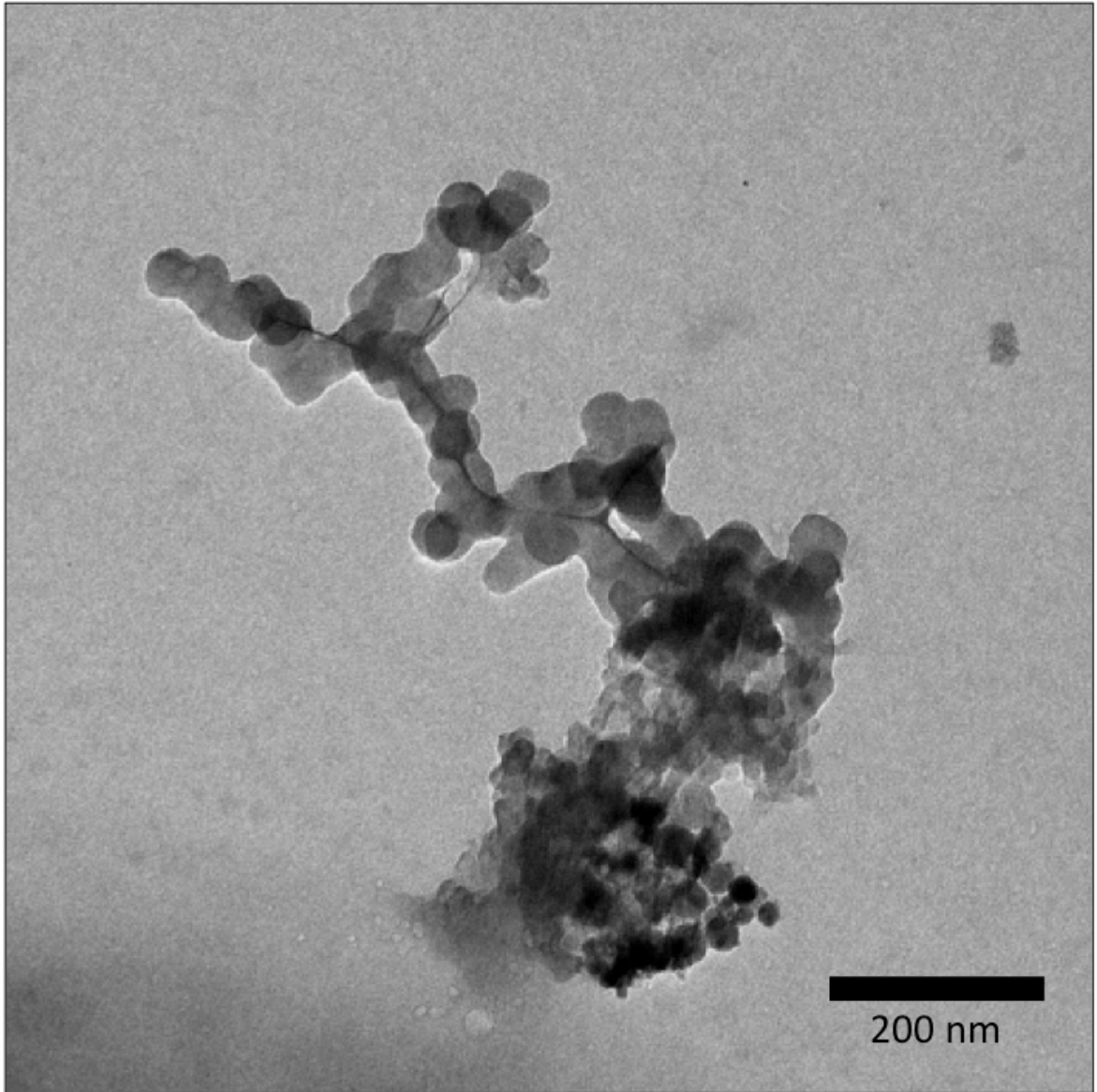


Figure 6.6 A black carbon aggregate from Darwin rain with multiple distinct carbon morphologies present and iron spherules attached to the carbon aggregate (bottom-right).

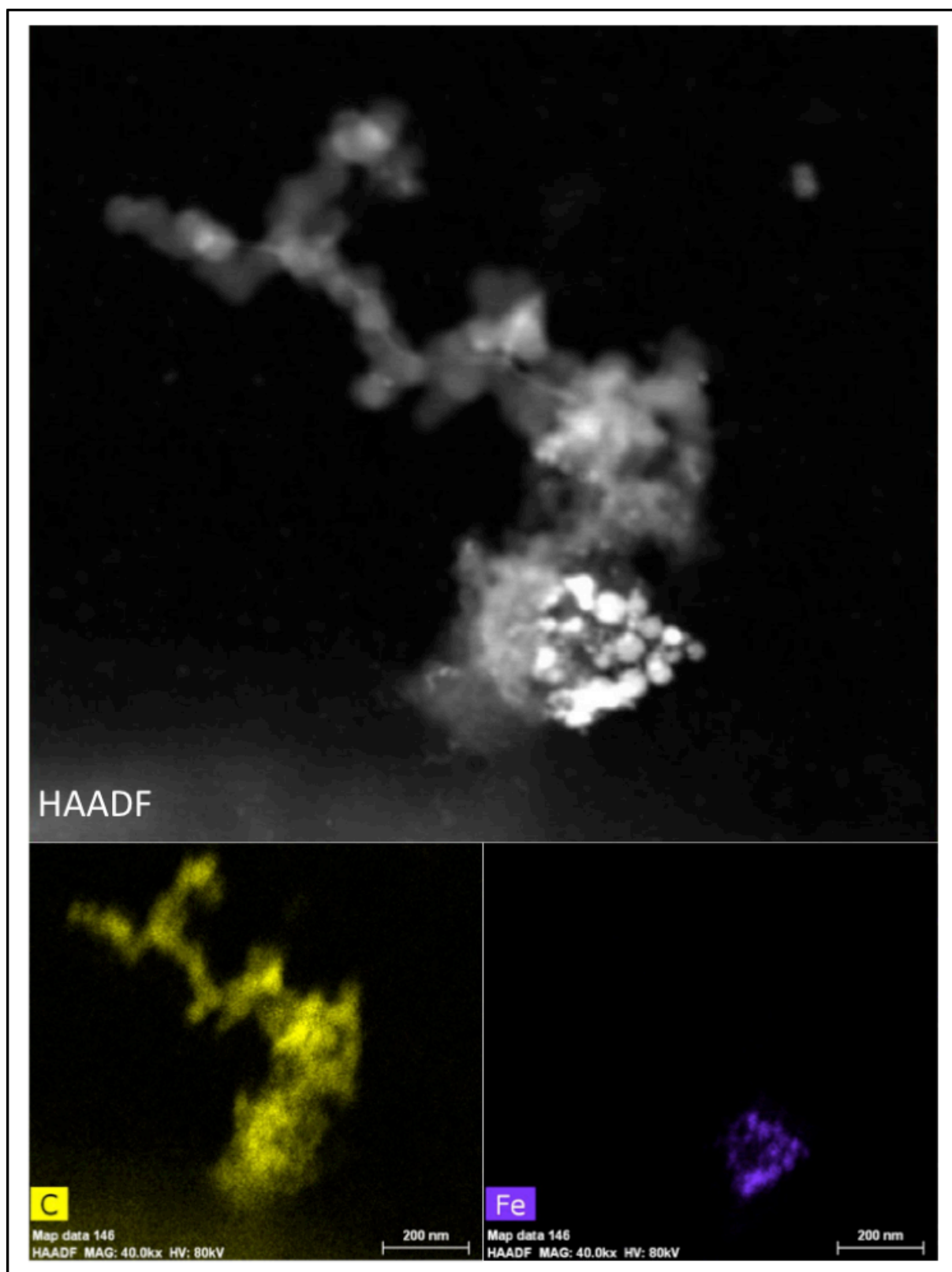


Figure 6.7 HAADF image of the black carbon aggregate in Figure 6.5 (top), along with STEM-EDS spectra maps of carbon (bottom-left) and iron (bottom-right).

6.4 Conclusions

The rain samples from this study were initially collected for method development and electron microscopy characterization; therefore, there are several significant contributions to uncertainty in the study. Never-the-less, there are a number of interesting findings from these case studies:

- A wide range of concentrations ranging from $0.8 \pm 0.3 \mu\text{g L}^{-1}$ to $21.8 \pm 0.3 \mu\text{g L}^{-1}$ were found in rBC deposition in Darwin, but substantially lower concentrations overall than measured in East Asian outflows and rainwater in Tokyo;
- There was a significant drop in rBC concentration from $5.74 \pm 0.01 \mu\text{g L}^{-1}$ to $0.57 \pm 0.03 \mu\text{g L}^{-1}$ in Perth as air mass transport shifted from primarily over land to over the Southern and Indian Oceans.
- BC superaggregates are found in Australian rain samples, and due to measurement inefficiencies by the coupled ultrasonic-nebulizer and SP2 system, measurements likely underestimate total BC mass concentration in the rainwater.

rBC wet deposition flux in Darwin (12°S) ranged from $1 - 314 \mu\text{g m}^{-2} \text{d}^{-1}$, whereas rBC flux in Perth (32°S) ranged from $0.8 - 41 \mu\text{g m}^{-2} \text{d}^{-1}$. While limited in scope, extrapolated 24-hour rBC wet depositional fluxes for Darwin and Perth were comparable to global model predictions. All rBC concentrations measured in the study were substantially lower than SP2 measurements done with rain in the Northern Hemisphere, as expected from BC emission inventories and modelled wet deposition rates. Biomass burning emissions and rainfall in Darwin are out of phase, with monsoonal rainfall in the summer months (wet season) and seasonal bushfires in the winter months (dry season). Therefore, the months with the largest BC emissions have the least amount of rain for wet removal processes.

These rain samples were limited in scope both temporally and spatially, but this study supports the suggestion that global wet deposition is highly variable, and more measurements are needed to accurately constrain BC lifetime in global models. Future studies in the Southern Hemisphere should incorporate measurements for multiple seasons, to help account for the potentially strong effects of rain and biomass burning seasonality on BC wet deposition rates.

Acknowledgements

The authors acknowledge the facilities, and the scientific and technical assistance of the Australian Microscopy & Microanalysis Research Facility at the Centre for Microscopy, Characterisation & Analysis, The University of Western Australia, a facility funded by the University, State, and Commonwealth Governments.

References

- Bond, T. C., Doherty, S. J., Fahey, D. W., Forster, P. M., Berntsen, T., DeAngelo, B. J., Flanner, M. G., Ghan, S., Kärcher, B., Koch, D., Kinne, S., Kondo, Y., Quinn, P. K., Sarofim, M. C., Schultz, M. G., Schulz, M., Venkataraman, C., Zhang, H., Zhang, S., Bellouin, N., Guttikunda, S. K., Hopke, P. K., Jacobson, M. Z., Kaiser, J. W., Klimont, Z., Lohmann, U., Schwarz, J. P., Shindell, D., Storelvmo, T., Warren, S. G., & Zender, C. S. (2013). Bounding the role of black carbon in the climate system: A scientific assessment. *Journal of Geophysical Research: Atmospheres*, *118*(11), 5380-5552.
- Cerqueira, M., Pio, C., Legrand, M., Puxbaum, H., Kasper-Giebl, A., Afonso, J., Preunkert, S., Gelencsér, A., & Fialho, P. (2010). Particulate carbon in precipitation at European background sites. *Journal of Aerosol Science*, *41*(1), 51-61.
- Ducret, J., & Cachier, H. (1992). Particulate carbon content in rain at various temperate and tropical locations. *Journal of Atmospheric Chemistry*, *15*(1), 55-67.
- Ellis, A., Edwards, R., Saunders, M., Chakrabarty, R. K., Subramanian, R., Timms, N. E., van Riessen, A., Smith, A. M., Lambrinidis, D., Nunes, L. J., Vallelonga, P., Goodwin, I. D., Moy, A. D., Curran, M. A. J., & van Ommen, T. D. (2016). Individual particle morphology, coatings, and impurities of black carbon aerosols in Antarctic ice and tropical rainfall. *Geophysical Research Letters*, *43*(22), 11,875-811,883.
- Ellis, A., Edwards, R., Saunders, M., Chakrabarty, R. K., Subramanian, R., van Riessen, A., Smith, A. M., Lambrinidis, D., Nunes, L. J., Vallelonga, P., Goodwin, I. D., Moy, A. D., Curran, M. A. J., & van Ommen, T. D. (2015). Characterizing black carbon in rain and ice cores using coupled tangential flow filtration and transmission electron microscopy. *Atmos. Meas. Tech.*, *8*(9), 3959-3969.
- Holland, G. J. (1986). Interannual Variability of the Australian Summer Monsoon at Darwin: 1952–82. *Monthly Weather Review*, *114*(3), 594-604.
- Jacobson, M. Z. (2012). Investigating cloud absorption effects: Global absorption properties of black carbon, tar balls, and soil dust in clouds and aerosols. *Journal of Geophysical Research: Atmospheres*, *117*(D6)
- Johnson, B., Shine, K., & Forster, P. (2004). The semi-direct aerosol effect: Impact of absorbing aerosols on marine stratocumulus. *Quarterly Journal of the Royal Meteorological Society*, *130*(599), 1407-1422.
- Jurado, E., Dachs, J., Duarte, C. M., & Simó, R. (2008). Atmospheric deposition of organic and black carbon to the global oceans. *Atmospheric Environment*, *42*(34), 7931-7939.
- Jurado, E., Jaward, F., Lohmann, R., Jones, K. C., Simó, R., & Dachs, J. (2005). Wet Deposition of Persistent Organic Pollutants to the Global Oceans. *Environmental Science & Technology*, *39*(8), 2426-2435.
- Kaars, S. v. d., Wang, X., Kershaw, P., Guichard, F., & Setiabudi, D. A. (2000). A Late Quaternary palaeoecological record from the Banda Sea, Indonesia: patterns of vegetation, climate and biomass burning in Indonesia and northern Australia. *Palaeogeography, Palaeoclimatology, Palaeoecology*, *155*(1–2), 135-153.

- Koehler, K. A., DeMott, P. J., Kreidenweis, S. M., Popovicheva, O. B., Petters, M. D., Carrico, C. M., Kireeva, E. D., Khokhlova, T. D., & Shonija, N. K. (2009). Cloud condensation nuclei and ice nucleation activity of hydrophobic and hydrophilic soot particles. *Physical Chemistry Chemical Physics*, *11*(36), 7906-7920.
- May, P. T., & Ballinger, A. (2007). The Statistical Characteristics of Convective Cells in a Monsoon Regime (Darwin, Northern Australia). *Monthly Weather Review*, *135*(1), 82-92.
- McConnell, J. R., Edwards, R., Kok, G. L., Flanner, M. G., Zender, C. S., Saltzman, E. S., Banta, J. R., Pasteris, D. R., Carter, M. M., & Kahl, J. D. W. (2007). 20th-century industrial black carbon emissions altered arctic climate forcing. *Science*, *317*(5843), 1381-1384.
- Mori, T., Kondo, Y., Ohata, S., Moteki, N., Matsui, H., Oshima, N., & Iwasaki, A. (2014). Wet deposition of black carbon at a remote site in the East China Sea. *Journal of Geophysical Research: Atmospheres*, *119*(17), 10485-10498.
- Ogren, J. A., Groblicki, P. J., & Charlson, R. J. (1984). Measurement of the removal rate of elemental carbon from the atmosphere. *Science of The Total Environment*, *36*, 329-338.
- Ohata, S., Moteki, N., & Kondo, Y. (2011). Evaluation of a Method for Measurement of the Concentration and Size Distribution of Black Carbon Particles Suspended in Rainwater. *Aerosol Science and Technology*, *45*(11), 1326-1336.
- Rodhe, H., Persson, C., & Åkesson, O. (1972). An investigation into regional transport of soot and sulfate aerosols. *Atmospheric Environment (1967)*, *6*(9), 675-693.
- Rolph, G. D. (2016). *Real-time Environmental Applications and Display sYstem (READY) Website (<http://ready.arl.noaa.gov>)*. Silver Spring, MD: NOAA Air Resources Laboratory.
- Schwarz, J. P., Doherty, S. J., Li, F., Ruggiero, S. T., Tanner, C. E., Perring, A. E., Gao, R. S., & Fahey, D. W. (2012). Assessing Single Particle Soot Photometer and Integrating Sphere/Integrating Sandwich Spectrophotometer measurement techniques for quantifying black carbon concentration in snow. *Atmos. Meas. Tech.*, *5*(11), 2581-2592.
- Schwarz, J. P., Spackman, J. R., Gao, R. S., Watts, L. A., Stier, P., Schulz, M., Davis, S. M., Wofsy, S. C., & Fahey, D. W. (2010). Global-scale black carbon profiles observed in the remote atmosphere and compared to models. *Geophysical Research Letters*, *37*(18)
- Stein, A. F., Draxler, R. R., Rolph, G. D., Stunder, B. J. B., Cohen, M. D., & Ngan, F. (2015). NOAA's HYSPLIT Atmospheric Transport and Dispersion Modeling System. *Bulletin of the American Meteorological Society*, *96*(12), 2059-2077.
- Sterle, K. M., McConnell, J. R., Dozier, J., Edwards, R., & Flanner, M. G. (2013). Retention and radiative forcing of black carbon in eastern Sierra Nevada snow. *The Cryosphere*, *7*(1), 365-374.
- Stier, P., Seinfeld, J. H., Kinne, S., Feichter, J., & Boucher, O. (2006). Impact of nonabsorbing anthropogenic aerosols on clear-sky atmospheric absorption. *Journal of Geophysical Research: Atmospheres*, *111*(D18)

Torres, A., Bond, T. C., Lehmann, C. M. B., Subramanian, R., & Hadley, O. L. (2013). Measuring Organic Carbon and Black Carbon in Rainwater: Evaluation of Methods. *Aerosol Science and Technology*, 48(3), 239-250.

Winton, V. H. L., Edwards, R., Delmonte, B., Ellis, A., Andersson, P. S., Bowie, A., Bertler, N. A. N., Neff, P., & Tuohy, A. (2016). Multiple sources of soluble atmospheric iron to Antarctic waters. *Global Biogeochemical Cycles*, 30(3), 421-437.

Zhang, J., Liu, J., Tao, S., & Ban-Weiss, G. A. (2015). Long-range transport of black carbon to the Pacific Ocean and its dependence on aging timescale. *Atmos. Chem. Phys.*, 15(20), 11521-11535.

Supplementary Information

Additional HYSPLIT trajectories for the rain samples are included below.

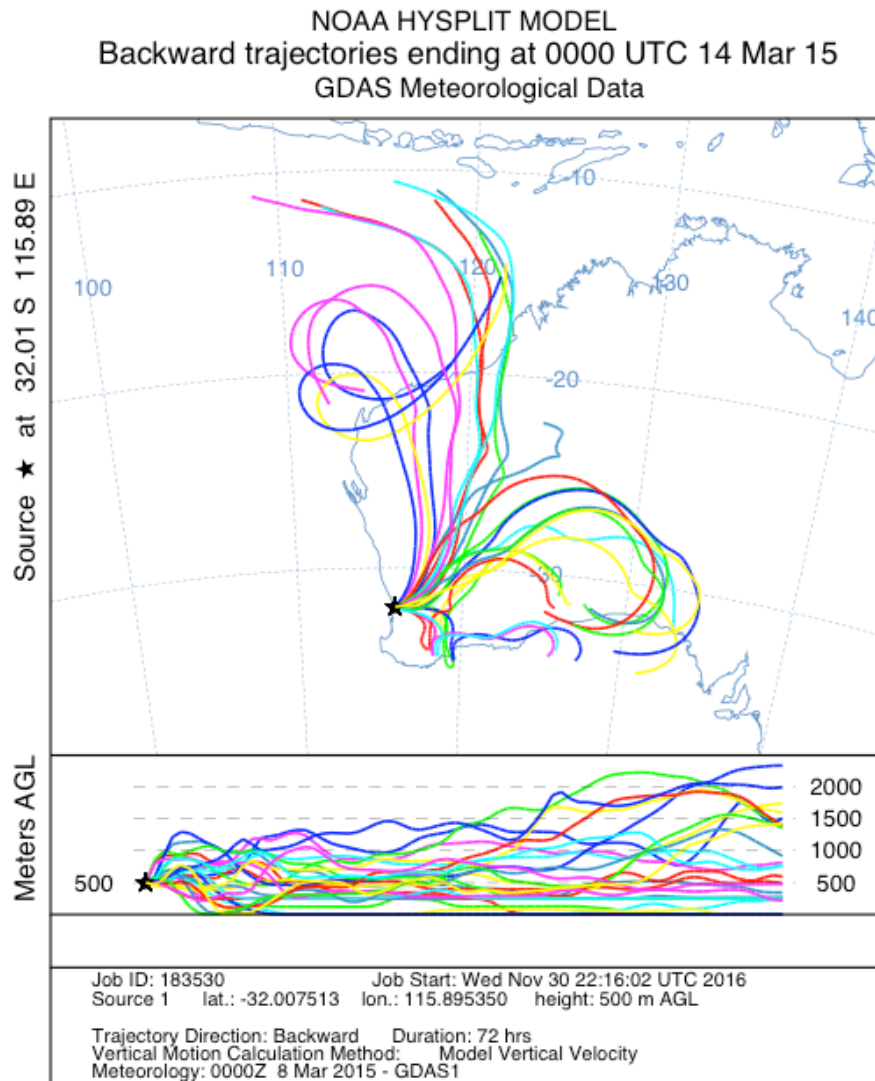


Figure S6.1 HYSPLIT back trajectory for Perth, 14 March 2015 with starting height of 500 m.

NOAA HYSPLIT MODEL
Backward trajectories ending at 0000 UTC 14 Mar 15
GDAS Meteorological Data

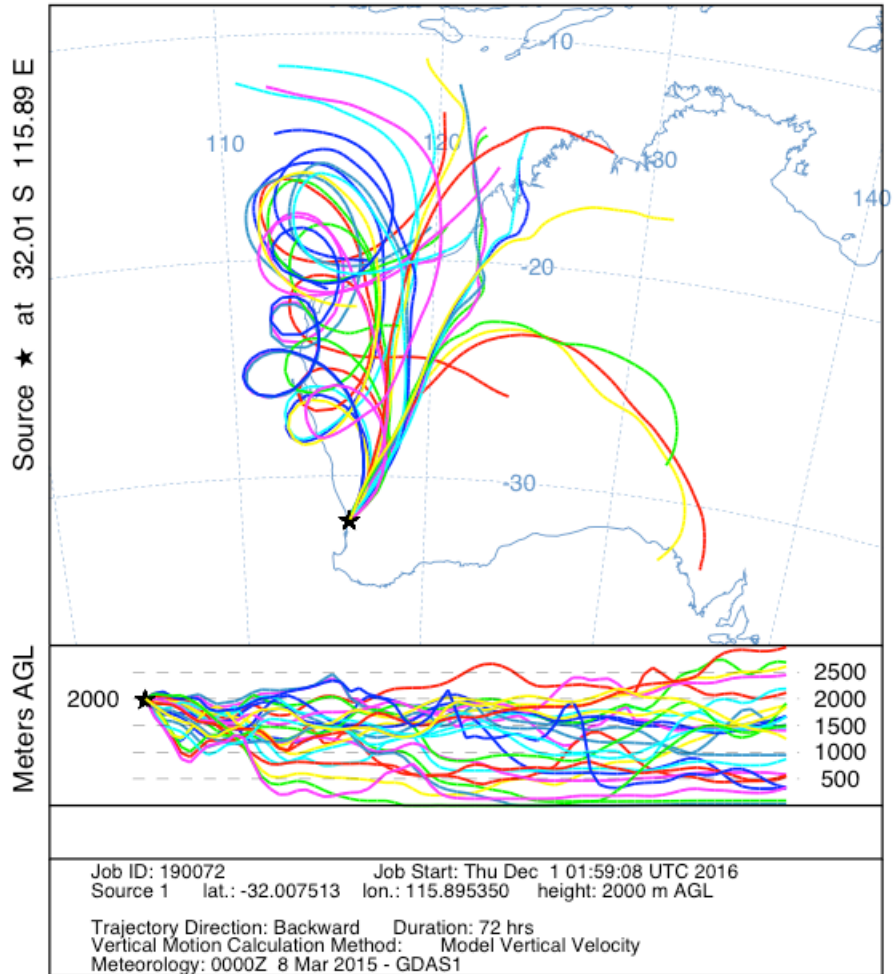


Figure S6.2 HYSPLIT back trajectory for Perth, 14 March 2015 with starting height of 2000 m.

NOAA HYSPLIT MODEL
Backward trajectories ending at 0000 UTC 15 Mar 15
GDAS Meteorological Data

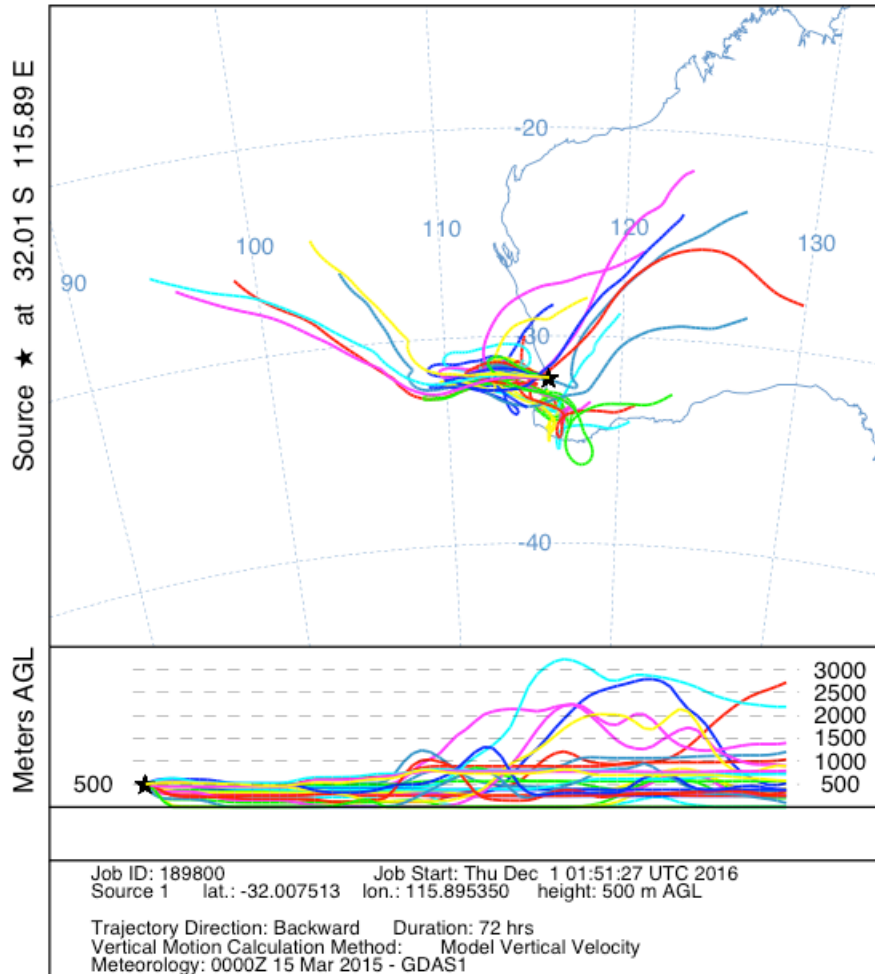


Figure S6.3 HYSPLIT back trajectory for Perth, 15 March 2015 with starting height of 500 m.

NOAA HYSPLIT MODEL
Backward trajectories ending at 0000 UTC 15 Mar 15
GDAS Meteorological Data

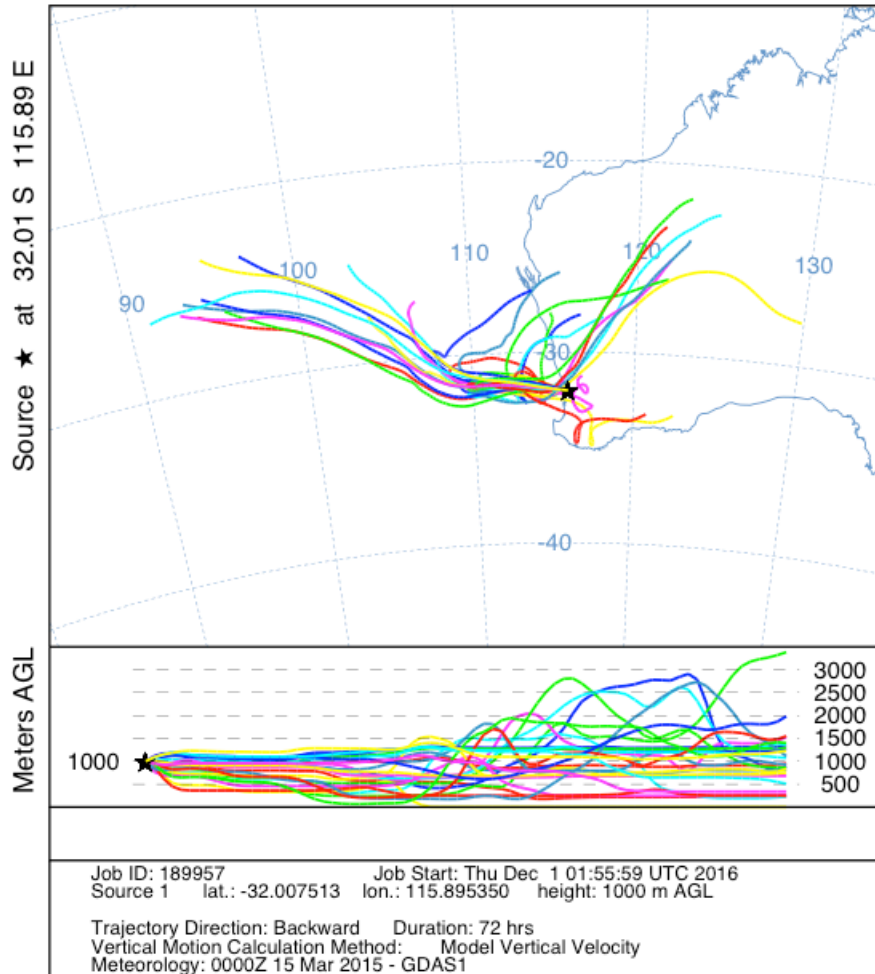


Figure S6.4 HYSPLIT back trajectory for Perth, 15 March 2015 with starting height of 1000 m.

NOAA HYSPLIT MODEL
 Backward trajectories ending at 0000 UTC 15 Mar 15
 GDAS Meteorological Data

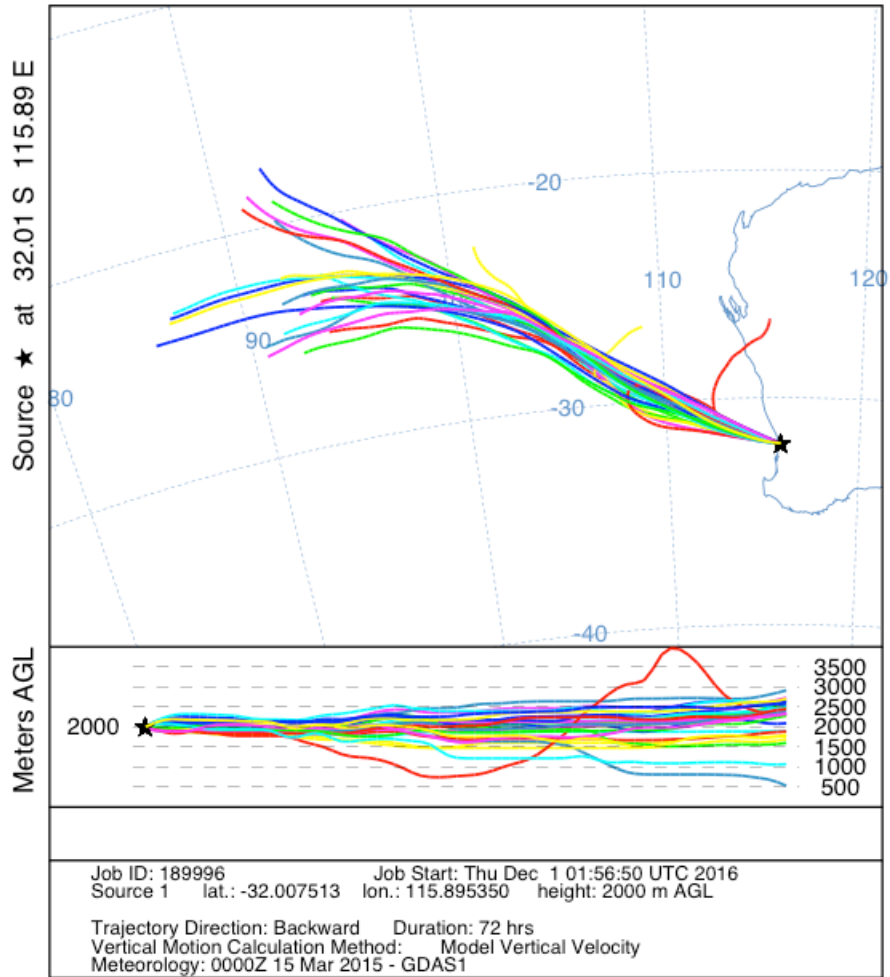


Figure S6.5 HYSPLIT back trajectory for Perth, 15 March 2015 with starting height of 2000 m.

NOAA HYSPLIT MODEL
 Backward trajectories ending at 0000 UTC 16 Mar 15
 GDAS Meteorological Data

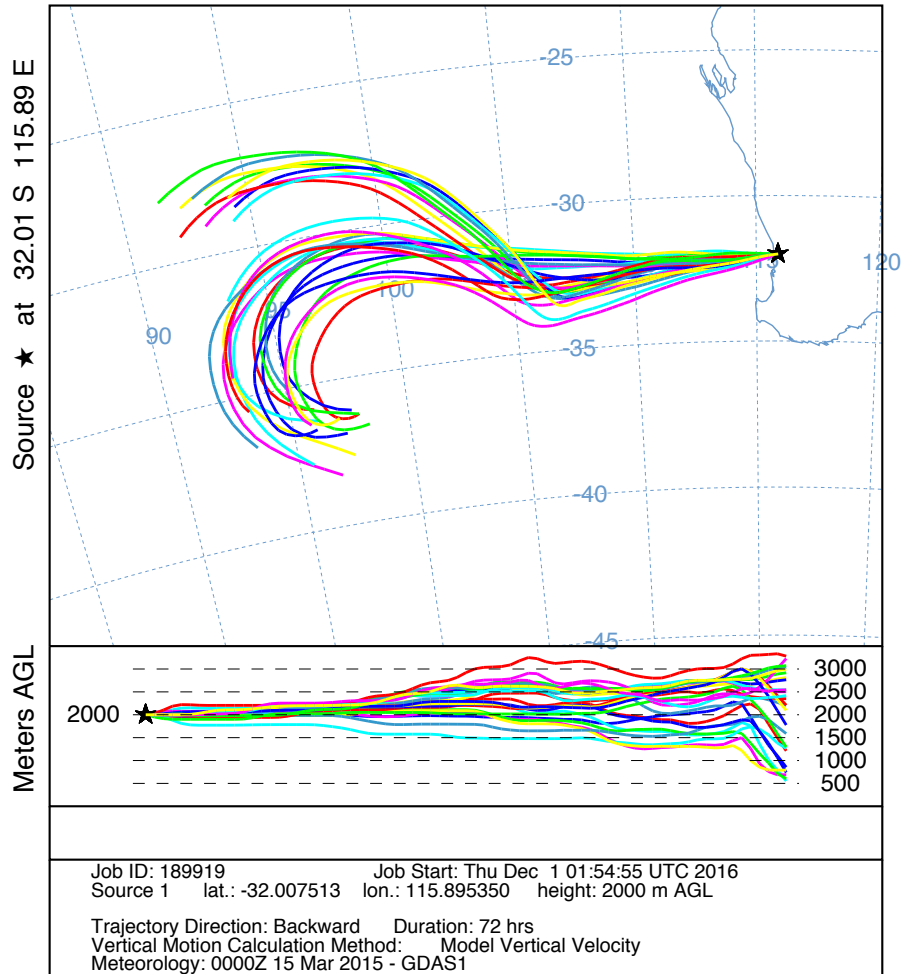


Figure S6.6 HYSPLIT back trajectory for Perth, 16 March 2015 with starting height of 2000 m.

NOAA HYSPLIT MODEL
 Backward trajectories ending at 1500 UTC 25 Nov 14
 GDAS Meteorological Data

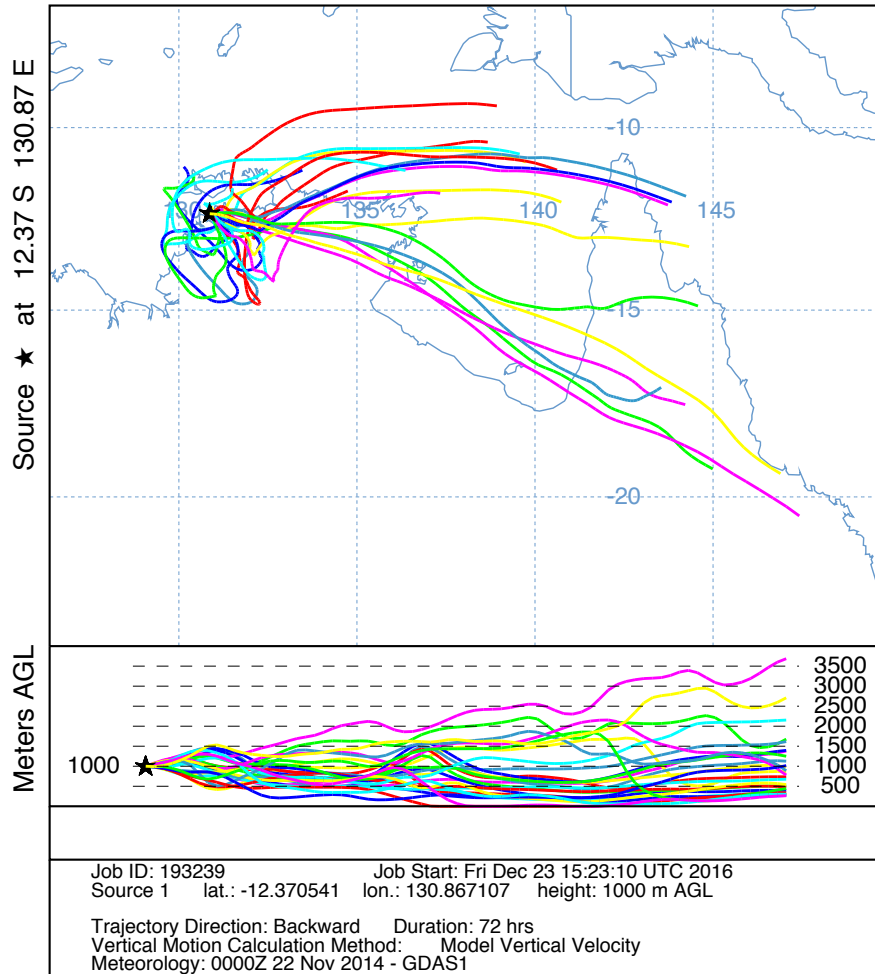


Figure S6.7 HYSPLIT back trajectory for Darwin, 25 November 2014 with starting height of 1000 m.

NOAA HYSPLIT MODEL
 Backward trajectories ending at 1300 UTC 26 Nov 14
 GDAS Meteorological Data

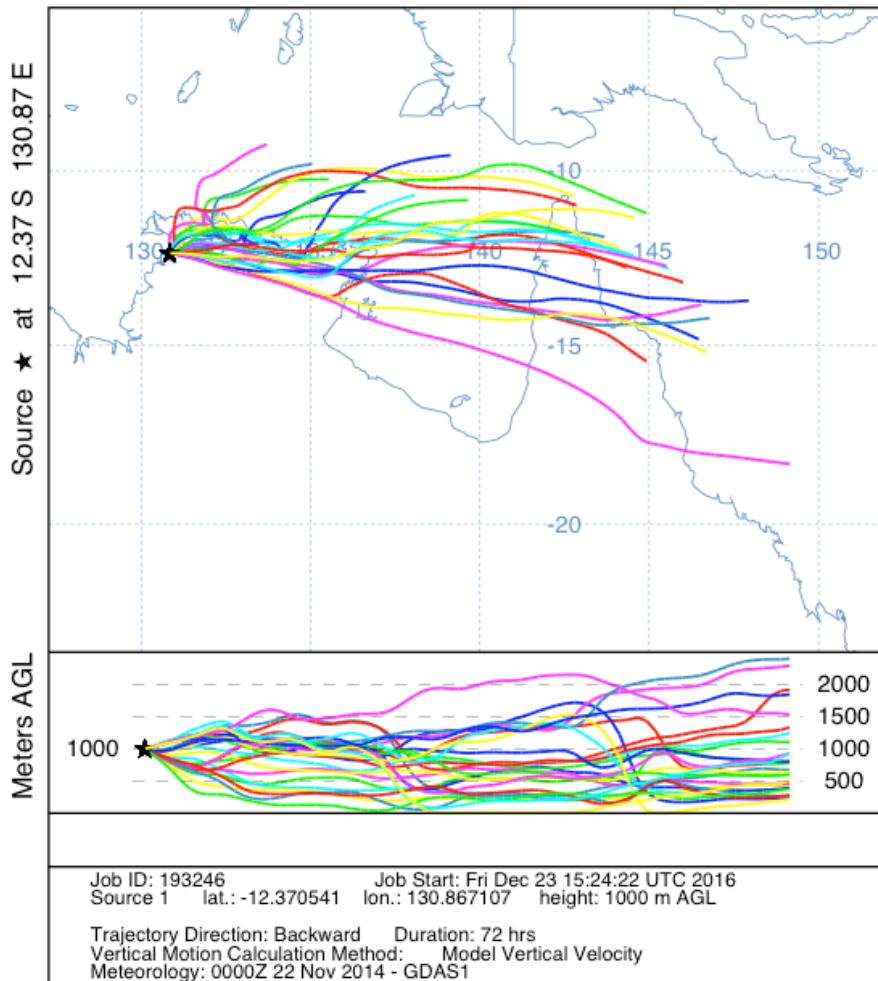


Figure S6.8 HYSPLIT back trajectory for Darwin, 23 November 2014 with starting height of 1000 m.

NOAA HYSPLIT MODEL
Backward trajectories ending at 1200 UTC 30 Jan 15
GDAS Meteorological Data

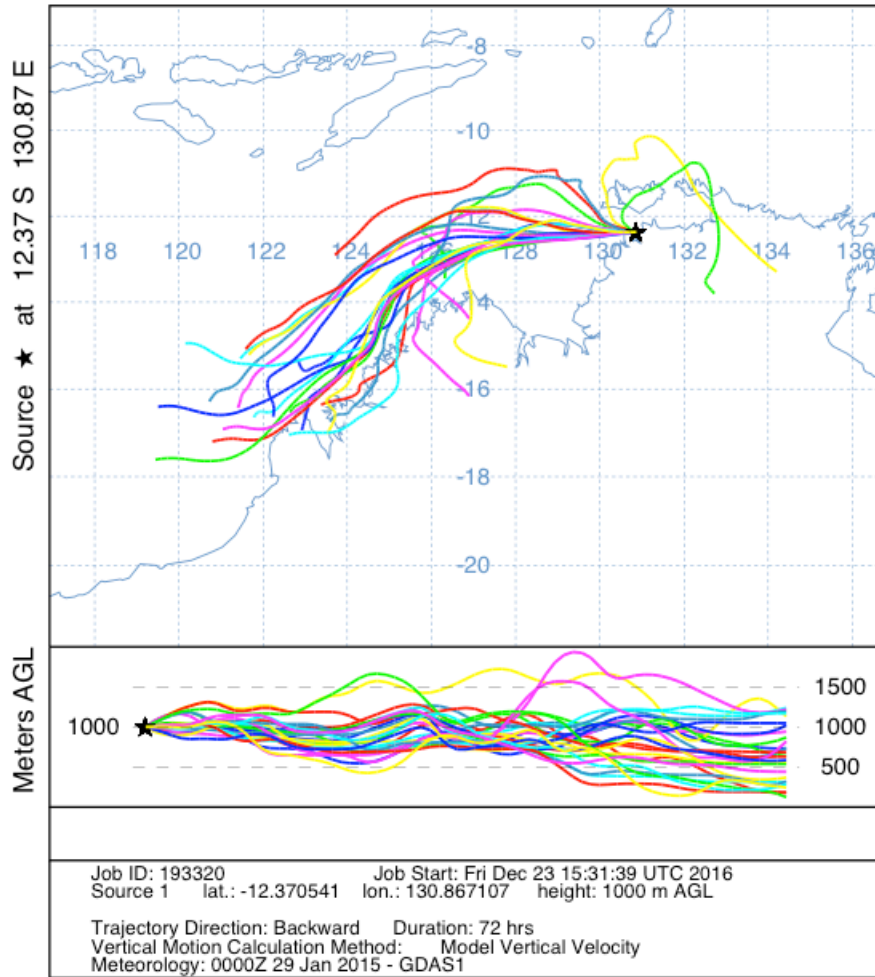


Figure S6.9 HYSPLIT back trajectory for Darwin, 30 January 2015 with starting height of 1000 m.

NOAA HYSPLIT MODEL
Backward trajectories ending at 1100 UTC 23 Feb 15
GDAS Meteorological Data

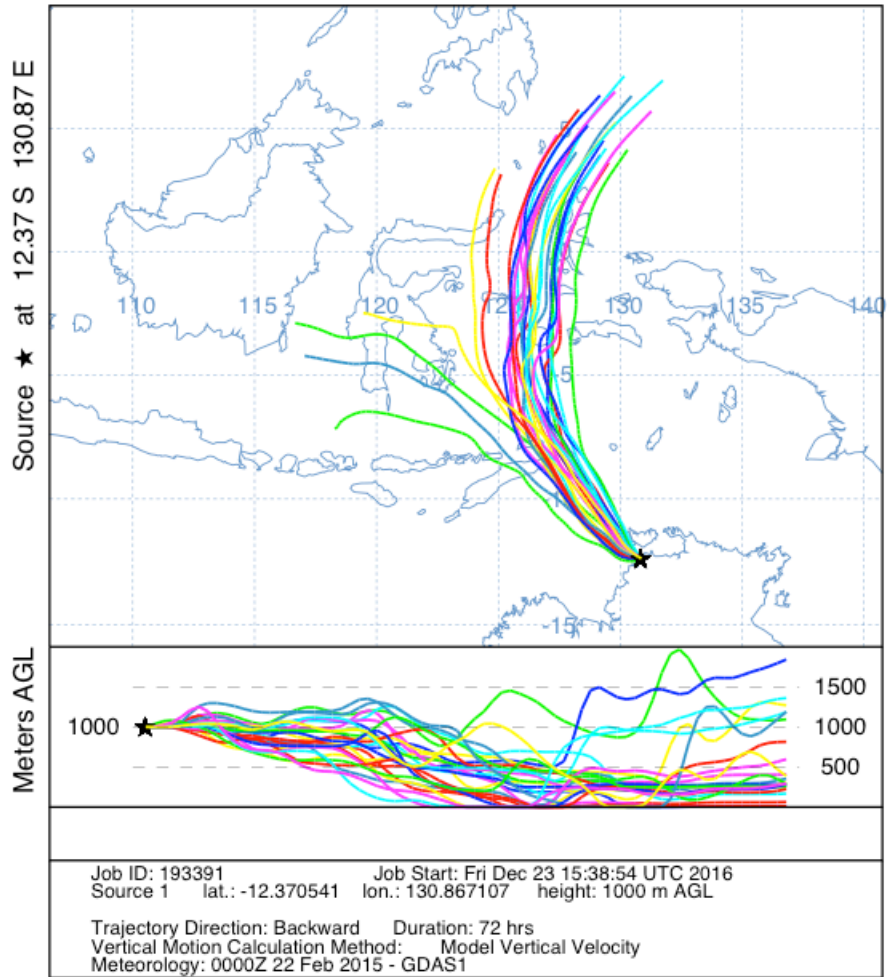


Figure S6.10 HYSPLIT back trajectory for Darwin, 23 February 2015 with starting height of 1000 m.

NOAA HYSPLIT MODEL
 Backward trajectories ending at 1500 UTC 24 Feb 15
 GDAS Meteorological Data

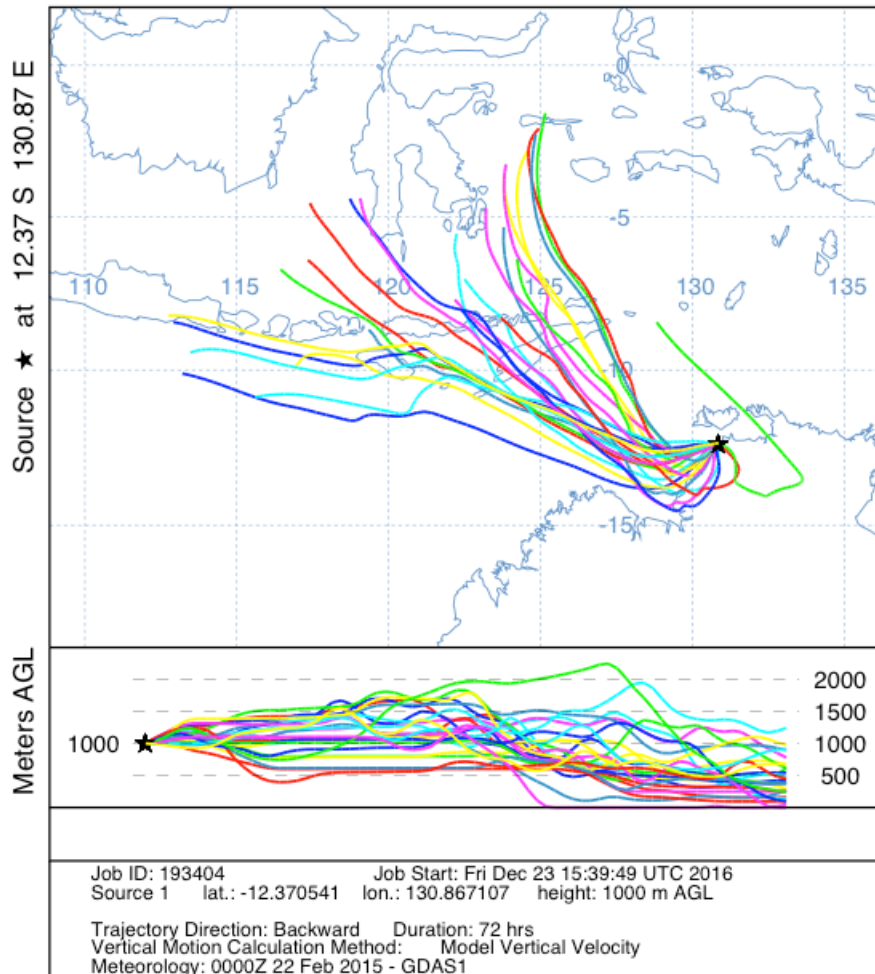


Figure S6.11 HYSPLIT back trajectory for Darwin, 24 February 2015 with starting height of 1000 m.

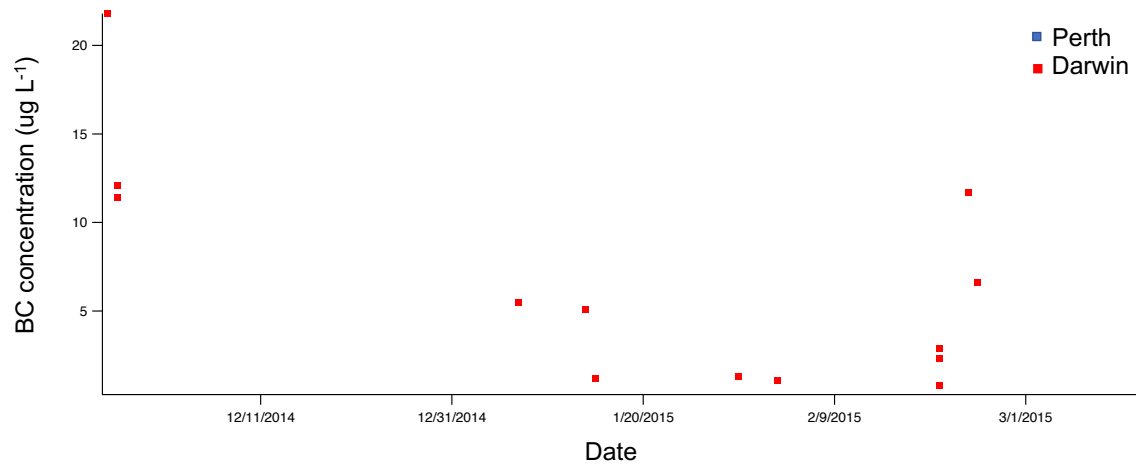


Figure S6.12 Plot of BC concentration vs date of sample collection for Darwin (red) and Perth (blue).

Chapter 7. Thesis summary and conclusions

7.1 Summary and significance

The overarching goal of this project is to constrain the characteristics and concentrations of BC particles in Southern Hemisphere rain, snow, and ice during the Anthropocene, a period of significant human influence on atmospheric composition and climate. This thesis provides a compilation of research regarding the recent history of BC in the atmosphere as well as wet removal processes. As detailed conclusions are included in each individual chapter, this chapter seeks to summarize and connect the results of the research.

We characterized the morphology and composition of individual BC particles in modern Australian rainwater and Antarctic ice dated to pre- to post-industrialization of the Southern Hemisphere. There is limited data on characteristics and wet removal rates of BC in the Southern Hemisphere, where BC emissions are dominated by grass and forest fires in South America, Africa, and Australia. This is partly because BC particles exist in low concentrations in precipitation, including snow, ice, and rainwater. To image these particles, they must first be removed from solution, which necessitated the development of a new tangential flow filtration (TFF) technique to isolate the trace concentrations of insoluble particles. This filtration method was then coupled with particle characterization by various transmission electron microscopy (TEM) techniques, a method also used to characterize individual BC aerosols. The TFF technique is recommended for use in future studies of insoluble aerosols in rainwater and ice core samples, and for potential studies of insoluble particulates in sea-water as the technique can remove soluble salt species while retaining insoluble particles.

TEM imaging and spectroscopy revealed new information on BC particles in ice cores from East Antarctica and rainwater from northern Australia. Using sections of an archived ice core that had been previously analyzed and age constrained, black carbon particles were imaged from historic ice core samples dated to 1759, 1838, and 1930 CE from Law Dome in East Antarctica. Rain samples from Darwin, Australia, provided modern BC particles as a comparison with the historical particles preserved in ice. High resolution TEM spectroscopy revealed ~5 nm nitrogen-rich coatings, often including amorphous carbon. These coatings

connected BC aggregates with dust and iron particles. Significantly, previously unreported single black carbon nanospheres were detected in both ice and rainwater samples. These ~30 nm particles are below the limit of detection for instruments that are used to quantify black carbon, and may be unaccounted for in atmospheric and ice core studies. One significant difference between ice core and rainwater samples was the existence of BC superaggregates in Australian rain. This result has important implications for the measurement of BC in rain using an SP2/ultrasonic nebulizer system, as transport efficiency of the nebulizer drops substantially for particles over ~500 nm, thereby leading to an underestimation of total BC mass in a sample.

Wet deposition was studied through particle morphology and flux in rainwater collected in Perth, Western Australia, and Darwin, Northern Territories. Rain samples in Darwin were collected during the monsoonal rain season with regular rainfall, whereas Perth samples were collected during a cyclone period, where meteorological conditions shifted rapidly from moving over the Australian continent to long-range transport across the Indian and Southern Oceans. The locally-sourced rainfall in Perth and Darwin contained BC likely sourced from biomass and industrial emissions in Indonesian and northern Australia. As expected, the rainwater from terrestrially-sourced airmasses contained significantly higher concentrations of BC than rainfall from the Indian and Southern Oceans. Additionally, BC aggregates in Darwin rain were substantially larger in size than particles in Antarctic ice, potentially due to closer proximity to source regions and/or tropical nucleation scavenging efficiency.

To better understand history of BC deposition in Antarctica, snow pits were sampled and ice cores were extracted from Roosevelt Island, West Antarctica, as part of the Roosevelt Island Climate Evolution (RICE) project. This chapter presents a high temporal resolution reconstruction of the record of black carbon concentrations from 1890 to 2013 CE. Periodicity in black carbon preservation reflects biomass burning patterns in the southern hemisphere on seasonal and decadal timescales. Significantly, the record shows that black carbon deposition has increased dramatically from 1995 CE to 2013 CE paralleling global temperature rise, suggesting a combination of increasing emissions and/or faster transport from biomass burning in the Southern Hemisphere, though the individual contribution of either factor has yet to be determined. The most recent (austral summer 2012) peak at Roosevelt Island has BC concentrations that approach Greenland levels.

7.2 Future work

The results from this research are both significant and timely, given the increasing awareness of the role of BC in the climate system. The following are suggestions for future avenues of research that would provide additional and important insight into the questions raised in this thesis.

The small sample number and limited time span limits conclusions regarding any systematic changes to BC morphology from the preindustrial period through the 20th Century. The Northern Hemisphere paleo record indicates a stronger shift from natural biomass burning to anthropogenic industrial emissions during the industrial revolution, suggesting that Arctic ice cores should be studied for possible variations in BC particle characteristics over time using the techniques developed in our research.

With regards to the Antarctic ice core BC record, periodic follow-up snow pits at Roosevelt Island are needed to determine if the trend of increased deposition is continuing. A follow-up snow pit and shallow core at WAIS Divide and other nearby ice core sites are important to determine spatial extent of the black carbon deposition, as regional extent has significant implications on atmospheric transport conditions as well as potential albedo effects. The increase in BC deposition to Roosevelt island is likely driven by changing atmospheric transport conditions, but there are several potential contributing factors for this increase that need to be accounted for. These include a possible increase in biomass burning emissions and changes in precipitation over the Southern Ocean thereby affecting BC removal rates and atmospheric loading. Utilization of a global atmospheric transport model may help constrain this uncertainty.

Finally, the rain case studies reported in Chapter 6 provide interesting isolated observations of BC wet deposition rates, but to better inform global climate models, a comprehensive study needs to be conducted. Consistent rain sample collection at established weather stations over the course of a year could account for potential seasonal variability in BC wet deposition flux. As Africa is the dominant emitter of biomass burning BC, measurements of BC flux in rain from African outflows would be beneficial for constraining BC removal rates in the Southern Hemisphere.

Chapter 8. Bibliography

- Abram, N. J., Mulvaney, R., Vimeux, F., Phipps, S. J., Turner, J., & England, M. H. (2014). Evolution of the Southern Annular Mode during the past millennium. *Nature Clim. Change*, 4(7), 564-569.
- Adachi, K., & Buseck, P. R. (2011). Atmospheric tar balls from biomass burning in Mexico. *Journal of Geophysical Research: Atmospheres*, 116(D5), D05204.
- Adachi, K., Chung, S. H., & Buseck, P. R. (2010). Shapes of soot aerosol particles and implications for their effects on climate. *Journal of Geophysical Research: Atmospheres*, 115
- Allen, R. J., Sherwood, S. C., Norris, J. R., & Zender, C. S. (2012). Recent Northern Hemisphere tropical expansion primarily driven by black carbon and tropospheric ozone. *Nature*, 485(7398), 350-354.
- Andreae, M. O., & Gelencsér, A. (2006). Black carbon or brown carbon? The nature of light-absorbing carbonaceous aerosols. *Atmos. Chem. Phys.*, 6(10), 3131-3148.
- Ban-Weiss, G. A., Cao, L., Bala, G., & Caldeira, K. (2012). Dependence of climate forcing and response on the altitude of black carbon aerosols. *Climate Dynamics*, 38(5), 897-911.
- Bauer, S. E., Bausch, A., Nazarenko, L., Tsigaridis, K., Xu, B., Edwards, R., Bisiaux, M., & McConnell, J. (2013). Historical and future black carbon deposition on the three ice caps: Ice core measurements and model simulations from 1850 to 2100. *Journal of Geophysical Research: Atmospheres*, 118(14), 7948-7961.
- Baumgardner, D., Kok, G., & Raga, G. (2004). Warming of the Arctic lower stratosphere by light absorbing particles. *Geophysical Research Letters*, 31(6), L06117.
- Baumgardner, D., Subramanian, R., Twohy, C., Stith, J., & Kok, G. (2008). Scavenging of black carbon by ice crystals over the northern Pacific. *Geophysical Research Letters*, 35(22), L22815.
- Benner, R., Biddanda, B., Black, B., & McCarthy, M. (1997). Abundance, size distribution, and stable carbon and nitrogen isotopic compositions of marine organic matter isolated by tangential-flow ultrafiltration. *Marine Chemistry*, 57(3-4), 243-263.
- Bigler, M., Svensson, A., Kettner, E., Vallelonga, P., Nielsen, M. E., & Steffensen, J. P. (2011). Optimization of High-Resolution Continuous Flow Analysis for Transient Climate Signals in Ice Cores. *Environmental Science & Technology*, 45(10), 4483-4489.
- Birch, M. E., & Cary, R. A. (1996). Elemental Carbon-Based Method for Monitoring Occupational Exposures to Particulate Diesel Exhaust. *Aerosol Science and Technology*, 25(3), 221-241.
- Bisiaux, M. M., Edwards, R., Heyvaert, A. C., Thomas, J. M., Fitzgerald, B., Susfalk, R. B., Schladow, S. G., & Thaw, M. (2011). Stormwater and Fire as Sources of Black Carbon Nanoparticles to Lake Tahoe. *Environmental Science & Technology*, 45(6), 2065-2071.

- Bisiaux, M. M., Edwards, R., McConnell, J. R., Curran, M. A. J., Van Ommen, T. D., Smith, A. M., Neumann, T. A., Pasteris, D. R., Penner, J. E., & Taylor, K. (2012). Changes in black carbon deposition to Antarctica from two high-resolution ice core records, 1850–2000 AD. *Atmos. Chem. Phys.*, *12*(9), 4107-4115.
- Boening, C., Willis, J. K., Landerer, F. W., Nerem, R. S., & Fasullo, J. (2012). The 2011 La Niña: So strong, the oceans fell. *Geophysical Research Letters*, *39*(19), L19602.
- Bond, T. C., & Bergstrom, R. W. (2006). Light absorption by carbonaceous particles: An investigative review. *Aerosol Science and Technology*, *40*(1), 27-67.
- Bond, T. C., Bhardwaj, E., Dong, R., Jogani, R., Jung, S., Roden, C., Streets, D. G., & Trautmann, N. M. (2007). Historical emissions of black and organic carbon aerosol from energy-related combustion, 1850–2000. *Global Biogeochemical Cycles*, *21*(2), GB2018.
- Bond, T. C., Doherty, S. J., Fahey, D. W., Forster, P. M., Berntsen, T., DeAngelo, B. J., Flanner, M. G., Ghan, S., Kärcher, B., Koch, D., Kinne, S., Kondo, Y., Quinn, P. K., Sarofim, M. C., Schultz, M. G., Schulz, M., Venkataraman, C., Zhang, H., Zhang, S., Bellouin, N., Guttikunda, S. K., Hopke, P. K., Jacobson, M. Z., Kaiser, J. W., Klimont, Z., Lohmann, U., Schwarz, J. P., Shindell, D., Storelvmo, T., Warren, S. G., & Zender, C. S. (2013). Bounding the role of black carbon in the climate system: A scientific assessment. *Journal of Geophysical Research: Atmospheres*, *118*(11), 5380-5552.
- Bond, T. C., Streets, D. G., Yarber, K. F., Nelson, S. M., Woo, J.-H., & Klimont, Z. (2004). A technology-based global inventory of black and organic carbon emissions from combustion. *Journal of Geophysical Research: Atmospheres*, *109*(D14)
- Browne, E. C., Franklin, J. P., Canagaratna, M. R., Massoli, P., Kirchstetter, T. W., Worsnop, D. R., Wilson, K. R., & Kroll, J. H. (2015). Changes to the Chemical Composition of Soot from Heterogeneous Oxidation Reactions. *The Journal of Physical Chemistry A*, *119*(7), 1154-1163.
- Brydson, R. (2001). *Electron Energy Loss Spectroscopy*: Oxford: Bios in association with the Royal Microscopical Society.
- Burn, L. J., Rosman, K. J. R., Candelone, J.-P., Vallelonga, P., Burton, G. R., Smith, A. M., Morgan, V. I., Barbante, C., Hong, S., & Boutron, C. F. (2009). An ultra-clean technique for accurately analysing Pb isotopes and heavy metals at high spatial resolution in ice cores with sub-pg g(-1) Pb concentrations. *Analytica Chimica Acta*, *634*(2), 228-236.
- Burn-Nunes, L. J., Vallelonga, P., Loss, R. D., Burton, G. R., Moy, A., Curran, M., Hong, S., Smith, A. M., Edwards, R., Morgan, V. I., & Rosman, K. J. R. (2011). Seasonal variability in the input of lead, barium and indium to Law Dome, Antarctica. *Geochimica et Cosmochimica Acta*, *75*(1), 1-20.
- Buseck, P. R., & Adachi, K. (2008). Nanoparticles in the Atmosphere. *Elements*, *4*(6), 389-394.
- Cai, W., Borlace, S., Lengaigne, M., van Rensch, P., Collins, M., Vecchi, G., Timmermann, A., Santoso, A., McPhaden, M. J., Wu, L., England, M. H., Wang, G., Guilyardi, E., & Jin, F.-F. (2014). Increasing frequency of extreme El Niño events due to greenhouse warming. *Nature Clim. Change*, *4*(2), 111-116.

Cai, W., Wang, G., Santoso, A., McPhaden, M. J., Wu, L., Jin, F.-F., Timmermann, A., Collins, M., Vecchi, G., Lengaigne, M., England, M. H., Dommenges, D., Takahashi, K., & Guilyardi, E. (2015). Increased frequency of extreme La Nina events under greenhouse warming. *Nature Clim. Change*, 5(2), 132-137.

Caiazza, L., Baccolo, G., Barbante, C., Becagli, S., Bertò, M., Ciardini, V., Crotti, I., Delmonte, B., Dreossi, G., Frezzotti, M., Gabrieli, J., Giardi, F., Han, Y., Hong, S. B., Hur, S. D., Hwang, H., Kang, J. H., Narcisi, B., Proposito, M., Scarchilli, C., Selmo, E., Severi, M., Spolaor, A., Stenni, B., Traversi, R., & Udisti, R. (2017). Prominent features in isotopic, chemical and dust stratigraphies from coastal East Antarctic ice sheet (Eastern Wilkes Land). *Chemosphere*, 176, 273-287.

Candelone, J.-P., Hong, S., & F. Boutron, C. (1994). An improved method for decontaminating polar snow or ice cores for heavy metal analysis. *Analytica Chimica Acta*, 299(1), 9-16.

Cappa, C. D., Onasch, T. B., Massoli, P., Worsnop, D. R., Bates, T. S., Cross, E. S., Davidovits, P., Hakala, J., Hayden, K. L., Jobson, B. T., Kolesar, K. R., Lack, D. A., Lerner, B. M., Li, S.-M., Mellon, D., Nuaaman, I., Olfert, J. S., Petäjä, T., Quinn, P. K., Song, C., Subramanian, R., Williams, E. J., & Zaveri, R. A. (2012). Radiative Absorption Enhancements Due to the Mixing State of Atmospheric Black Carbon. *Science*, 337(6098), 1078-1081.

Cerqueira, M., Pio, C., Legrand, M., Puxbaum, H., Kasper-Giebl, A., Afonso, J., Preunkert, S., Gelencsér, A., & Fialho, P. (2010). Particulate carbon in precipitation at European background sites. *Journal of Aerosol Science*, 41(1), 51-61.

Chakrabarty, R., Moosmüller, H., Chen, L.-W., Lewis, K., Arnott, W., Mazzoleni, C., Dubey, M., Wold, C., Hao, W., & Kreidenweis, S. (2010). Brown carbon in tar balls from smoldering biomass combustion. *Atmospheric Chemistry and Physics*, 10(13), 6363-6370.

Chakrabarty, R. K., Beres, N. D., Moosmüller, H., China, S., Mazzoleni, C., Dubey, M. K., Liu, L., & Mishchenko, M. I. (2014). Soot superaggregates from flaming wildfires and their direct radiative forcing. *Sci. Rep.*, 4(5508)

Chakrabarty, R. K., Moosmüller, H., Arnott, W. P., Garro, M. A., Slowik, J. G., Cross, E. S., Han, J.-H., Davidovits, P., Onasch, T. B., & Worsnop, D. R. (2007). Light scattering and absorption by fractal-like carbonaceous chain aggregates: comparison of theories and experiment. *Applied Optics*, 46(28), 6990-7006.

Chakrabarty, R. K., Moosmüller, H., Arnott, W. P., Garro, M. A., & Walker, J. (2006a). Structural and fractal properties of particles emitted from spark ignition engines. *Environmental Science & Technology*, 40(21), 6647-6654.

Chakrabarty, R. K., Moosmüller, H., Garro, M. A., Arnott, W. P., Walker, J., Susott, R. A., Babbitt, R. E., Wold, C. E., Lincoln, E. N., & Hao, W. M. (2006b). Emissions from the laboratory combustion of wildland fuels: Particle morphology and size. *Journal of Geophysical Research: Atmospheres*, 111(D7)

- Chen, Y., Shah, N., Braun, A., Huggins, F. E., & Huffman, G. P. (2005). Electron Microscopy Investigation of Carbonaceous Particulate Matter Generated by Combustion of Fossil Fuels. *Energy & Fuels*, *19*(4), 1644-1651.
- Chow, J. C., Watson, J. G., Chen, L. W. A., Chang, M. C. O., Robinson, N. F., Trimble, D., & Kohl, S. (2007). The IMPROVE_A Temperature Protocol for Thermal/Optical Carbon Analysis: Maintaining Consistency with a Long-Term Database. *Journal of the Air & Waste Management Association*, *57*(9), 1014-1023.
- Clarke, A. D., Shinozuka, Y., Kapustin, V. N., Howell, S., Huebert, B., Doherty, S., Anderson, T., Covert, D., Anderson, J., Hua, X., Moore, K. G., McNaughton, C., Carmichael, G., & Weber, R. (2004). Size distributions and mixtures of dust and black carbon aerosol in Asian outflow: Physiochemistry and optical properties. *Journal of Geophysical Research: Atmospheres*, *109*(D15), D15S09.
- Collins, W. D., Rasch, P. J., Boville, B. A., Hack, J. J., McCaa, J. R., Williamson, D. L., Kiehl, J. T., Briegleb, B., Bitz, C., & Lin, S. (2004). Description of the NCAR community atmosphere model (CAM 3.0). *NCAR Tech. Note NCAR/TN-464+ STR*, 226
- Conway, H., Hall, B. L., Denton, G. H., Gades, A. M., & Waddington, E. D. (1999). Past and Future Grounding-Line Retreat of the West Antarctic Ice Sheet. *Science*, *286*(5438), 280-283.
- Cook, J., & Highwood, E. J. (2004). Climate response to tropospheric absorbing aerosols in an intermediate general-circulation model. *Quarterly Journal of the Royal Meteorological Society*, *130*(596), 175-191.
- Croft, B., Lohmann, U., & von Salzen, K. (2005). Black carbon ageing in the Canadian Centre for Climate modeling and analysis atmospheric general circulation model. *Atmos. Chem. Phys.*, *5*(7), 1931-1949.
- Crutzen, P. J., & Andreae, M. O. (1990). Biomass Burning in the Tropics - Impact on Atmospheric Chemistry and Biogeochemical Cycles. *Science*, *250*(4988), 1669-1678.
- Curran, M. A., Van Ommen, T. D., & Morgan, V. (1998). Seasonal characteristics of the major ions in the high-accumulation Dome Summit South ice core, Law Dome, Antarctica. *Annals of Glaciology*, *27*, 385-390.
- Dalwadi, G., Benson, H. E., & Chen, Y. (2005). Comparison of Diafiltration and Tangential Flow Filtration for Purification of Nanoparticle Suspensions. *Pharmaceutical Research*, *22*(12), 2152-2162.
- De Deckker, P., Norman, M., Goodwin, I. D., Wain, A., & Gingele, F. X. (2010). Lead isotopic evidence for an Australian source of aeolian dust to Antarctica at times over the last 170,000 years. *Palaeogeography, Palaeoclimatology, Palaeoecology*, *285*(3), 205-223.
- DeMott, P. J., Chen, Y., Kreidenweis, S. M., Rogers, D. C., & Sherman, D. E. (1999). Ice formation by black carbon particles. *Geophysical Research Letters*, *26*(16), 2429-2432.
- DeMott, P. J., Cziczo, D. J., Prenni, A. J., Murphy, D. M., Kreidenweis, S. M., Thomson, D. S., Borys, R., & Rogers, D. C. (2003). Measurements of the concentration and composition of nuclei for cirrus formation. *Proceedings of the National Academy of Sciences*, *100*(25), 14655-14660.

- Doherty, S. J., Grenfell, T. C., Forsström, S., Hegg, D. L., Brandt, R. E., & Warren, S. G. (2013). Observed vertical redistribution of black carbon and other insoluble light-absorbing particles in melting snow. *Journal of Geophysical Research: Atmospheres*, *118*(11), 5553-5569.
- Ducret, J., & Cachier, H. (1992). Particulate carbon content in rain at various temperate and tropical locations. *Journal of Atmospheric Chemistry*, *15*(1), 55-67.
- Dwyer, E., Gregoire, J. M., & Malingreau, J. P. (1998). A global analysis of vegetation fires using satellite images: Spatial and temporal dynamics. *Ambio*, *27*(3), 175-181.
- Edwards, D. P., Emmons, L. K., Gille, J. C., Chu, A., Attié, J. L., Giglio, L., Wood, S. W., Haywood, J., Deeter, M. N., Massie, S. T., Ziskin, D. C., & Drummond, J. R. (2006a). Satellite-observed pollution from Southern Hemisphere biomass burning. *Journal of Geophysical Research: Atmospheres*, *111*(D14)
- Edwards, R., Sedwick, P., Morgan, V., & Boutron, C. (2006b). Iron in ice cores from Law Dome: A record of atmospheric iron deposition for maritime East Antarctica during the Holocene and Last Glacial Maximum. *Geochemistry, Geophysics, Geosystems*, *7*(12)
- Ellis, A., Edwards, R., Saunders, M., Chakrabarty, R. K., Subramanian, R., Timms, N. E., van Riessen, A., Smith, A. M., Lambrinidis, D., Nunes, L. J., Vallelonga, P., Goodwin, I. D., Moy, A. D., Curran, M. A. J., & van Ommen, T. D. (2016). Individual particle morphology, coatings, and impurities of black carbon aerosols in Antarctic ice and tropical rainfall. *Geophysical Research Letters*, *43*(22), 11,875-811,883.
- Ellis, A., Edwards, R., Saunders, M., Chakrabarty, R. K., Subramanian, R., van Riessen, A., Smith, A. M., Lambrinidis, D., Nunes, L. J., Vallelonga, P., Goodwin, I. D., Moy, A. D., Curran, M. A. J., & van Ommen, T. D. (2015). Characterizing black carbon in rain and ice cores using coupled tangential flow filtration and transmission electron microscopy. *Atmos. Meas. Tech.*, *8*(9), 3959-3969.
- EPICA Community Members (2004). Eight glacial cycles from an Antarctic ice core. *Nature*, *429*(6992), 623-628.
- Etheridge, D., Steele, L., Langenfelds, R., Francey, R., Barnola, J. M., & Morgan, V. (1996). Natural and anthropogenic changes in atmospheric CO₂ over the last 1000 years from air in Antarctic ice and firn. *Journal of Geophysical Research: Atmospheres (1984–2012)*, *101*(D2), 4115-4128.
- Fiebig, M., Lunder, C. R., & Stohl, A. (2009). Tracing biomass burning aerosol from South America to Troll Research Station, Antarctica. *Geophysical Research Letters*, *36*
- Fierce, L., Bond, T. C., Bauer, S. E., Mena, F., & Riemer, N. (2016). Black carbon absorption at the global scale is affected by particle-scale diversity in composition. *Nature Communications*, *7*, 12361.
- Flanner, M. G., Zender, C. S., Randerson, J. T., & Rasch, P. J. (2007a). Present-day climate forcing and response from black carbon in snow. *Journal of Geophysical Research: Atmospheres*, *112*(D11)

- Flanner, M. G., Zender, C. S., Randerson, J. T., & Rasch, P. J. (2007b). Present-day climate forcing and response from black carbon in snow. *Journal of Geophysical Research: Atmospheres (1984–2012)*, *112*(D11)
- Flannigan, M. D., Stocks, B. J., & Wotton, B. M. (2000). Climate change and forest fires. *Science of The Total Environment*, *262*(3), 221-229.
- Franklin, R. E. (1950). On the structure of carbon. *The Journal de Chimie Physique et de Physico-Chimie Biologique*, *47*, 573-575.
- Franklin, R. E. (1951). The structure of graphitic carbons. *Acta crystallographica*, *4*(3), 253-261.
- Giglio, L., Randerson, J. T., & van der Werf, G. R. (2013). Analysis of daily, monthly, and annual burned area using the fourth-generation global fire emissions database (GFED4). *Journal of Geophysical Research: Biogeosciences*, *118*(1), 317-328.
- Giovannoni, S., DeLong, E., Schmidt, T., & Pace, N. (1990). Tangential flow filtration and preliminary phylogenetic analysis of marine picoplankton. *Applied and environmental microbiology*, *56*(8), 2572-2575.
- Hadley, O. L., & Kirchstetter, T. W. (2012). Black-carbon reduction of snow albedo. *Nature Clim. Change*, *2*(6), 437-440.
- Hansen, A. D. A., Bodhaine, B. A., Dutton, E. G., & Schnell, R. C. (1988). Aerosol black carbon measurements at the South Pole: Initial results, 1986-1987. *Geophysical Research Letters*, *15*(11), 1193-1196.
- Hansen, J., & Nazarenko, L. (2004). Soot climate forcing via snow and ice albedos. *Proceedings of the National Academy of Sciences of the United States of America*, *101*(2), 423-428.
- Hansen, J., Sato, M., Ruedy, R., Lacis, A., & Oinas, V. (2000). Global warming in the twenty-first century: An alternative scenario. *Proceedings of the National Academy of Sciences*, *97*(18), 9875-9880.
- Hegg, D. A., Warren, S. G., Grenfell, T. C., Doherty, S. J., Larson, T. V., & Clarke, A. D. (2009). Source Attribution of Black Carbon in Arctic Snow. *Environmental Science & Technology*, *43*(11), 4016-4021.
- Hendon, H. H., Thompson, D. W. J., & Wheeler, M. C. (2007). Australian Rainfall and Surface Temperature Variations Associated with the Southern Hemisphere Annular Mode. *Journal of Climate*, *20*(11), 2452-2467.
- Hiscock, W. T., Fischer, H., Bigler, M., Gfeller, G., Leuenberger, D., & Mini, O. (2013). Continuous Flow Analysis of Labile Iron in Ice-Cores. *Environmental Science & Technology*, *47*(9), 4416-4425.
- Hodnebrog, Ø., Myhre, G., & Samset, B. H. (2014). How shorter black carbon lifetime alters its climate effect. *Nat Commun*, *5*(6065)

Hoerling, M., Hurrell, J., Eischeid, J., & Phillips, A. (2006). Detection and Attribution of Twentieth-Century Northern and Southern African Rainfall Change. *Journal of Climate*, 19(16), 3989-4008.

Holland, G. J. (1986). Interannual Variability of the Australian Summer Monsoon at Darwin: 1952–82. *Monthly Weather Review*, 114(3), 594-604.

IPCC. (2013). *Climate Change 2013: the physical science basis, in: Contribution of Working Group I to the Fifth Assessment Report of the Intergovernmental Panel on Climate Change*. Cambridge, United Kingdom and New York, NY, USA: Cambridge University Press.

Jacobson, M. Z. (2000). Physically-based treatment of elemental carbon optics: Implications for global direct forcing of aerosols. *Geophysical Research Letters*, 27(2), 217-220.

Jacobson, M. Z. (2001). Strong radiative heating due to the mixing state of black carbon in atmospheric aerosols. *Nature*, 409(6821), 695-697.

Jacobson, M. Z. (2012). Investigating cloud absorption effects: Global absorption properties of black carbon, tar balls, and soil dust in clouds and aerosols. *Journal of Geophysical Research: Atmospheres*, 117(D6)

Janssen, N. A. H., Hoek, G., Simic-Lawson, M., Fischer, P., van Bree, L., ten Brink, H., Keuken, M., Atkinson, R. W., Anderson, H. R., Brunekreef, B., & Cassee, F. R. (2011). Black Carbon as an Additional Indicator of the Adverse Health Effects of Airborne Particles Compared with PM(10) and PM(2.5). *Environmental Health Perspectives*, 119(12), 1691-1699.

Jeong, C.-H., Hopke, P. K., Kim, E., & Lee, D.-W. (2004). The comparison between thermal-optical transmittance elemental carbon and Aethalometer black carbon measured at multiple monitoring sites. *Atmospheric Environment*, 38(31), 5193-5204.

Johnson, B., Shine, K., & Forster, P. (2004). The semi-direct aerosol effect: Impact of absorbing aerosols on marine stratocumulus. *Quarterly Journal of the Royal Meteorological Society*, 130(599), 1407-1422.

Johnson, D. W., Kilsby, C. G., McKenna, D. S., Saunders, R. W., Jenkins, G. J., Smith, F. B., & Foot, J. S. (1991). Airborne observations of the physical and chemical characteristics of the Kuwait oil smoke plume. *Nature*, 353(6345), 617-621.

Junker, C., & Lioussé, C. (2008). A global emission inventory of carbonaceous aerosol from historic records of fossil fuel and biofuel consumption for the period 1860–1997. *Atmos. Chem. Phys.*, 8(5), 1195-1207.

Jurado, E., Dachs, J., Duarte, C. M., & Simó, R. (2008). Atmospheric deposition of organic and black carbon to the global oceans. *Atmospheric Environment*, 42(34), 7931-7939.

Jurado, E., Jaward, F., Lohmann, R., Jones, K. C., Simó, R., & Dachs, J. (2005). Wet Deposition of Persistent Organic Pollutants to the Global Oceans. *Environmental Science & Technology*, 39(8), 2426-2435.

- Kaars, S. v. d., Wang, X., Kershaw, P., Guichard, F., & Setiabudi, D. A. (2000). A Late Quaternary palaeoecological record from the Banda Sea, Indonesia: patterns of vegetation, climate and biomass burning in Indonesia and northern Australia. *Palaeogeography, Palaeoclimatology, Palaeoecology*, *155*(1–2), 135-153.
- Kahnert, M., & Devasthale, A. (2011). Black carbon fractal morphology and short-wave radiative impact: a modeling study. *Atmospheric Chemistry and Physics*, *11*(22), 11745-11759.
- Kaufman, Y. J., Tanre, D., & Boucher, O. (2002). A satellite view of aerosols in the climate system. *Nature*, *419*(6903), 215-223.
- Knox, A., Evans, G. J., Brook, J. R., Yao, X., Jeong, C. H., Godri, K. J., Sabaliauskas, K., & Slowik, J. G. (2009). Mass Absorption Cross-Section of Ambient Black Carbon Aerosol in Relation to Chemical Age. *Aerosol Science and Technology*, *43*(6), 522-532.
- Koch, D., Bond, T. C., Streets, D., Unger, N., & van der Werf, G. R. (2007). Global impacts of aerosols from particular source regions and sectors. *Journal of Geophysical Research: Atmospheres*, *112*(D2)
- Koch, D., & Hansen, J. (2005). Distant origins of Arctic black carbon: A Goddard Institute for Space Studies ModelE experiment. *Journal of Geophysical Research: Atmospheres*, *110*(D4), D04204.
- Koch, D., Schulz, M., Kinne, S., McNaughton, C., Spackman, J. R., Balkanski, Y., Bauer, S., Berntsen, T., Bond, T. C., Boucher, O., Chin, M., Clarke, A., De Luca, N., Dentener, F., Diehl, T., Dubovik, O., Easter, R., Fahey, D. W., Feichter, J., Fillmore, D., Freitag, S., Ghan, S., Ginoux, P., Gong, S., Horowitz, L., Iversen, T., Kirkev, aring, g, A., Klimont, Z., Kondo, Y., Krol, M., Liu, X., Miller, R., Montanaro, V., Moteki, N., Myhre, G., Penner, J. E., Perlwitz, J., Pitari, G., Reddy, S., Sahu, L., Sakamoto, H., Schuster, G., Schwarz, J. P., Seland, Ø., Stier, P., Takegawa, N., Takemura, T., Textor, C., van Aardenne, J. A., & Zhao, Y. (2009). Evaluation of black carbon estimations in global aerosol models. *Atmos. Chem. Phys.*, *9*(22), 9001-9026.
- Koehler, K. A., DeMott, P. J., Kreidenweis, S. M., Popovicheva, O. B., Petters, M. D., Carrico, C. M., Kireeva, E. D., Khokhlova, T. D., & Shonija, N. K. (2009). Cloud condensation nuclei and ice nucleation activity of hydrophobic and hydrophilic soot particles. *Physical Chemistry Chemical Physics*, *11*(36), 7906-7920.
- Kovilakam, M., & Mahajan, S. (2015). Black carbon aerosol-induced Northern Hemisphere tropical expansion. *Geophysical Research Letters*, *42*(12), 4964-4972.
- Lack, D. A., & Cappa, C. D. (2010). Impact of brown and clear carbon on light absorption enhancement, single scatter albedo and absorption wavelength dependence of black carbon. *Atmos. Chem. Phys.*, *10*(9), 4207-4220.
- Lamarque, J. F., Bond, T. C., Eyring, V., Granier, C., Heil, A., Klimont, Z., Lee, D., Liousse, C., Mieville, A., Owen, B., Schultz, M. G., Shindell, D., Smith, S. J., Stehfest, E., Van Aardenne, J., Cooper, O. R., Kainuma, M., Mahowald, N., McConnell, J. R., Naik, V., Riahi, K., & van Vuuren, D. P. (2010). Historical (1850–2000) gridded anthropogenic and biomass

burning emissions of reactive gases and aerosols: methodology and application. *Atmos. Chem. Phys.*, 10(15), 7017-7039.

Lammel, G., & Novakov, T. (1995). Water nucleation properties of carbon black and diesel soot particles. *Atmospheric Environment*, 29(7), 813-823.

Lee, A. K. Y., Zhao, R., Li, R., Liggio, J., Li, S.-M., & Abbatt, J. P. D. (2013). Formation of Light Absorbing Organo-Nitrogen Species from Evaporation of Droplets Containing Glyoxal and Ammonium Sulfate. *Environmental Science & Technology*, 47(22), 12819-12826.

Legrand, M., & Mayewski, P. (1997). Glaciochemistry of polar ice cores: A review. *Reviews of Geophysics*, 35(3), 219-243.

Letnic, M., & Dickman, C. (2006). Boom means bust: interactions between the El Niño/Southern Oscillation (ENSO), rainfall and the processes threatening mammal species in arid Australia. *Biodiversity & Conservation*, 15(12), 3847-3880.

Li, J., Anderson, J. R., & Buseck, P. R. (2003a). TEM study of aerosol particles from clean and polluted marine boundary layers over the North Atlantic. *Journal of Geophysical Research-Atmospheres*, 108(D6)

Li, J., Pósfai, M., Hobbs, P. V., & Buseck, P. R. (2003b). Individual aerosol particles from biomass burning in southern Africa: 2, Compositions and aging of inorganic particles. *Journal of Geophysical Research: Atmospheres*, 108(D13)

Liou, K. N., Takano, Y., & Yang, P. (2011). Light absorption and scattering by aggregates: Application to black carbon and snow grains. *Journal of Quantitative Spectroscopy & Radiative Transfer*, 112(10), 1581-1594.

Liu, S., Aiken, A. C., Gorkowski, K., Dubey, M. K., Cappa, C. D., Williams, L. R., Herndon, S. C., Massoli, P., Fortner, E. C., Chhabra, P. S., Brooks, W. A., Onasch, T. B., Jayne, J. T., Worsnop, D. R., China, S., Sharma, N., Mazzoleni, C., Xu, L., Ng, N. L., Liu, D., Allan, J. D., Lee, J. D., Fleming, Z. L., Mohr, C., Zotter, P., Szidat, S., & Prévôt, A. S. H. (2015). Enhanced light absorption by mixed source black and brown carbon particles in UK winter. *Nature Communications*, 6, 8435.

Lohmann, U., & Diehl, K. (2006). Sensitivity Studies of the Importance of Dust Ice Nuclei for the Indirect Aerosol Effect on Stratiform Mixed-Phase Clouds. *Journal of the Atmospheric Sciences*, 63(3), 968-982.

Lorius, C., Jouzel, J., Raynaud, D., Hansen, J., & Treut, H. L. (1990). The ice-core record: climate sensitivity and future greenhouse warming. *Nature*, 347(6289), 139-145.

Luthi, D., Le Floch, M., Bereiter, B., Blunier, T., Barnola, J.-M., Siegenthaler, U., Raynaud, D., Jouzel, J., Fischer, H., Kawamura, K., & Stocker, T. F. (2008). High-resolution carbon dioxide concentration record 650,000-800,000 years before present. *Nature*, 453(7193), 379-382.

Lynch, A. H., Beringer, J., Kershaw, P., Marshall, A., Mooney, S., Tapper, N., Turney, C., & Kaars, S. V. D. (2007). Using the Paleorecord to Evaluate Climate and Fire Interactions in Australia. *Annual Review of Earth and Planetary Sciences*, 35(1), 215-239.

- Ma, X., Huete, A., Cleverly, J., Eamus, D., Chevallier, F., Joiner, J., Poulter, B., Zhang, Y., Guanter, L., Meyer, W., Xie, Z., & Ponce-Campos, G. (2016). Drought rapidly diminishes the large net CO₂ uptake in 2011 over semi-arid Australia. *Scientific Reports*, *6*, 37747.
- Marlon, J. R., Bartlein, P. J., Carcaillet, C., Gavin, D. G., Harrison, S. P., Higuera, P. E., Joos, F., Power, M. J., & Prentice, I. C. (2008). Climate and human influences on global biomass burning over the past two millennia. *Nature Geoscience*, *1*(10), 697-702.
- Marlon, J. R., Bartlein, P. J., Gavin, D. G., Long, C. J., Anderson, R. S., Briles, C. E., Brown, K. J., Colombaroli, D., Hallett, D. J., Power, M. J., Scharf, E. A., & Walsh, M. K. (2012). Long-term perspective on wildfires in the western USA. *Proceedings of the National Academy of Sciences*, *109*(9), E535-E543.
- Marshall, G. J. (2003). Trends in the Southern Annular Mode from Observations and Reanalyses. *Journal of Climate*, *16*(24), 4134-4143.
- Martins, J. V., Artaxo, P., Liousse, C., Reid, J. S., Hobbs, P. V., & Kaufman, Y. J. (1998). Effects of black carbon content, particle size, and mixing on light absorption by aerosols from biomass burning in Brazil. *Journal of Geophysical Research: Atmospheres*, *103*(D24), 32041-32050.
- Masson-Delmotte, V., Buiron, D., Ekaykin, A., Frezzotti, M., Gallée, H., Jouzel, J., Krinner, G., Landais, A., Motoyama, H., Oerter, H., Pol, K., Pollard, D., Ritz, C., Schlosser, E., Sime, L. C., Sodemann, H., Stenni, B., Uemura, R., & Vimeux, F. (2011). A comparison of the present and last interglacial periods in six Antarctic ice cores. *Clim. Past*, *7*(2), 397-423.
- May, P. T., & Ballinger, A. (2007). The Statistical Characteristics of Convective Cells in a Monsoon Regime (Darwin, Northern Australia). *Monthly Weather Review*, *135*(1), 82-92.
- McConnell, J. R., Edwards, R., Kok, G. L., Flanner, M. G., Zender, C. S., Saltzman, E. S., Banta, J. R., Pasteris, D. R., Carter, M. M., & Kahl, J. D. W. (2007). 20th-century industrial black carbon emissions altered arctic climate forcing. *Science*, *317*(5843), 1381-1384.
- McConnell, J. R., Lamorey, G. W., Lambert, S. W., & Taylor, K. C. (2002). Continuous Ice-Core Chemical Analyses Using Inductively Coupled Plasma Mass Spectrometry. *Environmental Science & Technology*, *36*(1), 7-11.
- McFiggans, G., Artaxo, P., Baltensperger, U., Coe, H., Facchini, M. C., Feingold, G., Fuzzi, S., Gysel, M., Laaksonen, A., Lohmann, U., Mentel, T. F., Murphy, D. M., O'Dowd, C. D., Snider, J. R., & Weingartner, E. (2006). The effect of physical and chemical aerosol properties on warm cloud droplet activation. *Atmos. Chem. Phys.*, *6*(9), 2593-2649.
- Moffet, R. C., & Prather, K. A. (2009). In-situ measurements of the mixing state and optical properties of soot with implications for radiative forcing estimates. *Proceedings of the National Academy of Sciences*, *106*(29), 11872-11877.
- Moosmuller, H., Chakrabarty, R. K., & Arnott, W. P. (2009). Aerosol light absorption and its measurement: A review. *Journal of Quantitative Spectroscopy & Radiative Transfer*, *110*(11), 844-878.

- Mori, T., Kondo, Y., Ohata, S., Moteki, N., Matsui, H., Oshima, N., & Iwasaki, A. (2014). Wet deposition of black carbon at a remote site in the East China Sea. *Journal of Geophysical Research: Atmospheres*, *119*(17), 10485-10498.
- Moteki, N., Kondo, Y., Miyazaki, Y., Takegawa, N., Komazaki, Y., Kurata, G., Shirai, T., Blake, D. R., Miyakawa, T., & Koike, M. (2007). Evolution of mixing state of black carbon particles: Aircraft measurements over the western Pacific in March 2004. *Geophysical Research Letters*, *34*(11)
- Murr, L. (2008). Microstructures and Nanostructures for Environmental Carbon Nanotubes and Nanoparticulate Soots. *International Journal of Environmental Research and Public Health*, *5*(5), 321.
- Murr, L. E., Esquivel, E. V., Bang, J. J., de la Rosa, G., & Gardea-Torresdey, J. L. (2004). Chemistry and nanoparticulate compositions of a 10,000 year-old ice core melt water. *Water Research*, *38*(19), 4282-4296.
- Neale, R. B., Chen, C.-C., Gettelman, A., Lauritzen, P. H., Park, S., Williamson, D. L., Conley, A. J., Garcia, R., Kinnison, D., & Lamarque, J.-F. (2010). Description of the NCAR community atmosphere model (CAM 5.0). *NCAR Tech. Note NCAR/TN-486+ STR*,
- Neff, P. D., & Bertler, N. A. N. (2015). Trajectory modeling of modern dust transport to the Southern Ocean and Antarctica. *Journal of Geophysical Research: Atmospheres*,
- Nicholls, N. (2004). The Changing Nature of Australian Droughts. *Climatic Change*, *63*(3), 323-336.
- O'Brien, R. E., Wang, B., Laskin, A., Riemer, N., West, M., Zhang, Q., Sun, Y., Yu, X.-Y., Alpert, P., Knopf, D. A., Gilles, M. K., & Moffet, R. C. (2015). Chemical imaging of ambient aerosol particles: Observational constraints on mixing state parameterization. *Journal of Geophysical Research: Atmospheres*, *120*(18), 9591-9605.
- Ogren, J. A., Groblicki, P. J., & Charlson, R. J. (1984). Measurement of the removal rate of elemental carbon from the atmosphere. *Science of The Total Environment*, *36*, 329-338.
- Ohata, S., Moteki, N., & Kondo, Y. (2011). Evaluation of a Method for Measurement of the Concentration and Size Distribution of Black Carbon Particles Suspended in Rainwater. *Aerosol Science and Technology*, *45*(11), 1326-1336.
- Oshima, N., Koike, M., Zhang, Y., & Kondo, Y. (2009). Aging of black carbon in outflow from anthropogenic sources using a mixing state resolved model: 2. Aerosol optical properties and cloud condensation nuclei activities. *Journal of Geophysical Research: Atmospheres*, *114*(D18), D18202.
- Osterberg, E. C., Handley, M. J., Sneed, S. B., Mayewski, P. A., & Kreutz, K. J. (2006). Continuous ice core melter system with discrete sampling for major ion, trace element, and stable isotope analyses. *Environmental science & technology*, *40*(10), 3355-3361.
- Palmer, A. S., van Ommen, T. D., Curran, M. A., Morgan, V., Souney, J. M., & Mayewski, P. A. (2001). High-precision dating of volcanic events (AD 1301–1995) using ice cores from Law Dome, Antarctica. *Journal of Geophysical Research*, *106*(D22), 28089–28095.

- Pedro, J. B., McConnell, J. R., van Ommen, T. D., Fink, D., Curran, M. A. J., Smith, A. M., Simon, K. J., Moy, A. D., & Das, S. B. (2012). Solar and climate influences on ice core ^{10}Be records from Antarctica and Greenland during the neutron monitor era. *Earth and Planetary Science Letters*, 355(0), 174-186.
- Petit, J. R., Jouzel, J., Raynaud, D., Barkov, N. I., Barnola, J. M., Basile, I., Bender, M., Chappellaz, J., Davis, M., Delaygue, G., Delmotte, M., Kotlyakov, V. M., Legrand, M., Lipenkov, V. Y., Lorius, C., Pepin, L., Ritz, C., Saltzman, E., & Stievenard, M. (1999). Climate and atmospheric history of the past 420,000 years from the Vostok ice core, Antarctica. *Nature*, 399(6735), 429-436.
- Pitman, A. J., Narisma, G. T., & McAneney, J. (2007). The impact of climate change on the risk of forest and grassland fires in Australia. *Climatic Change*, 84(3-4), 383-401.
- Plummer, C. T., Curran, M. A. J., van Ommen, T. D., Rasmussen, S. O., Moy, A. D., Vance, T. R., Clausen, H. B., Vinther, B. M., & Mayewski, P. A. (2012). An independently dated 2000-yr volcanic record from Law Dome, East Antarctica, including a new perspective on the dating of the 1450s CE eruption of Kuwae, Vanuatu. *Clim. Past*, 8(6), 1929-1940.
- Pósfai, M., Anderson, J. R., Buseck, P. R., & Sievering, H. (1999). Soot and sulfate aerosol particles in the remote marine troposphere. *Journal of Geophysical Research: Atmospheres*, 104(D17), 21685-21693.
- Pósfai, M., Simonics, R., Li, J., Hobbs, P. V., & Buseck, P. R. (2003). Individual aerosol particles from biomass burning in southern Africa: 1. Compositions and size distributions of carbonaceous particles. *Journal of Geophysical Research: Atmospheres*, 108(D13), 8483.
- Quinn, P. K., Bates, T. S., Baum, E., Doubleday, N., Fiore, A. M., Flanner, M., Fridlind, A., Garrett, T. J., Koch, D., Menon, S., Shindell, D., Stohl, A., & Warren, S. G. (2008). Short-lived pollutants in the Arctic: their climate impact and possible mitigation strategies. *Atmos. Chem. Phys.*, 8(6), 1723-1735.
- Ramanathan, V., & Carmichael, G. (2008). Global and regional climate changes due to black carbon. *Nature Geoscience*, 1(4), 221-227.
- Rasmussen, S. O., Andersen, K. K., Svensson, A. M., Steffensen, J. P., Vinther, B. M., Clausen, H. B., Siggaard-Andersen, M. L., Johnsen, S. J., Larsen, L. B., Dahl-Jensen, D., Bigler, M., Röthlisberger, R., Fischer, H., Goto-Azuma, K., Hansson, M. E., & Ruth, U. (2006). A new Greenland ice core chronology for the last glacial termination. *Journal of Geophysical Research: Atmospheres*, 111(D6), D06102.
- Reddington, C. L., Spracklen, D. V., Artaxo, P., Ridley, D. A., Rizzo, L. V., & Arana, A. (2016). Analysis of particulate emissions from tropical biomass burning using a global aerosol model and long-term surface observations. *Atmos. Chem. Phys.*, 16(17), 11083-11106.
- Reddy, M. S., & Boucher, O. (2007). Climate impact of black carbon emitted from energy consumption in the world's regions. *Geophysical Research Letters*, 34(11)
- Rodhe, H., Persson, C., & Åkesson, O. (1972). An investigation into regional transport of soot and sulfate aerosols. *Atmospheric Environment (1967)*, 6(9), 675-693.

Rolph, G. D. (2016). *Real-time Environmental Applications and Display sYstem (READY) Website* (<http://ready.arl.noaa.gov>). Silver Spring, MD: NOAA Air Resources Laboratory.

Rothenbacher, S., Messerer, A., & Kasper, G. (2008). Fragmentation and bond strength of airborne diesel soot agglomerates. *Particle and Fibre Toxicology*, 5(9)

Röthlisberger, R., Bigler, M., Hutterli, M., Sommer, S., Stauffer, B., Junghans, H. G., & Wagenbach, D. (2000). Technique for Continuous High-Resolution Analysis of Trace Substances in Firm and Ice Cores. *Environmental Science & Technology*, 34(2), 338-342.

Rotstayn, L. D., Cai, W. J., Dix, M. R., Farquhar, G. D., Feng, Y., Ginoux, P., Herzog, M., Ito, A., Penner, J. E., Roderick, M. L., & Wang, M. H. (2007). Have Australian rainfall and cloudiness increased due to the remote effects of Asian anthropogenic aerosols? *Journal of Geophysical Research-Atmospheres*, 112(D9)

Rotstayn, L. D., Keywood, M. D., Forgan, B. W., Gabric, A. J., Galbally, I. E., Gras, J. L., Luhar, A. K., McTainsh, G. H., Mitchell, R. M., & Young, S. A. (2009). Possible impacts of anthropogenic and natural aerosols on Australian climate: a review. *International Journal of Climatology*, 29(4), 461-479.

Sato, M., Hansen, J., Koch, D., Lacis, A., Ruedy, R., Dubovik, O., Holben, B., Chin, M., & Novakov, T. (2003). Global atmospheric black carbon inferred from AERONET. *Proceedings of the National Academy of Sciences*, 100(11), 6319-6324.

Saunders, R. W., Möhler, O., Schnaiter, M., Benz, S., Wagner, R., Saathoff, H., Connolly, P. J., Burgess, R., Murray, B. J., Gallagher, M., Wills, R., & Plane, J. M. C. (2010). An aerosol chamber investigation of the heterogeneous ice nucleating potential of refractory nanoparticles. *Atmos. Chem. Phys.*, 10(3), 1227-1247.

Scarnato, B. V., China, S., Nielsen, K., & Mazzoleni, C. (2015). Perturbations of the optical properties of mineral dust particles by mixing with black carbon: a numerical simulation study. *Atmos. Chem. Phys.*, 15(12), 6913-6928.

Schmidt, M. W. I., & Noack, A. G. (2000). Black carbon in soils and sediments: Analysis, distribution, implications, and current challenges. *Global Biogeochemical Cycles*, 14(3), 777-793.

Schwarz, J., Gao, R., Fahey, D., Thomson, D., Watts, L., Wilson, J., Reeves, J., Darbeheshti, M., Baumgardner, D., & Kok, G. (2006). Single-particle measurements of midlatitude black carbon and light-scattering aerosols from the boundary layer to the lower stratosphere. *Journal of Geophysical Research: Atmospheres*, 111(D16)

Schwarz, J. P., Doherty, S. J., Li, F., Ruggiero, S. T., Tanner, C. E., Perring, A. E., Gao, R. S., & Fahey, D. W. (2012). Assessing Single Particle Soot Photometer and Integrating Sphere/Integrating Sandwich Spectrophotometer measurement techniques for quantifying black carbon concentration in snow. *Atmos. Meas. Tech.*, 5(11), 2581-2592.

Schwarz, J. P., Gao, R. S., Perring, A. E., Spackman, J. R., & Fahey, D. W. (2013). Black carbon aerosol size in snow. *Sci. Rep.*, 3

Schwarz, J. P., Spackman, J. R., Fahey, D. W., Gao, R. S., Lohmann, U., Stier, P., Watts, L. A., Thomson, D. S., Lack, D. A., Pfister, L., Mahoney, M. J., Baumgardner, D., Wilson, J. C.,

& Reeves, J. M. (2008). Coatings and their enhancement of black carbon light absorption in the tropical atmosphere. *Journal of Geophysical Research-Atmospheres*, 113(D3)

Schwarz, J. P., Spackman, J. R., Gao, R. S., Perring, A. E., Cross, E., Onasch, T. B., Ahern, A., Wrobel, W., Davidovits, P., Olfert, J., Dubey, M. K., Mazzoleni, C., & Fahey, D. W. (2010a). The Detection Efficiency of the Single Particle Soot Photometer. *Aerosol Science and Technology*, 44(8), 612-628.

Schwarz, J. P., Spackman, J. R., Gao, R. S., Watts, L. A., Stier, P., Schulz, M., Davis, S. M., Wofsy, S. C., & Fahey, D. W. (2010b). Global-scale black carbon profiles observed in the remote atmosphere and compared to models. *Geophysical Research Letters*, 37(18)

Seinfeld, J. H., & Pandis, S. N. (2016). *Atmospheric chemistry and physics: from air pollution to climate change*: John Wiley & Sons.

Shen, Z., Liu, J., Horowitz, L., Henze, D., Fan, S., Mauzerall, D., Lin, J.-T., & Tao, S. (2014). Analysis of transpacific transport of black carbon during HIPPO-3: implications for black carbon aging. *Atmospheric Chemistry and Physics*, 14(12), 6315-6327.

Shi, G., Cai, W. J., Cowan, T., Ribbe, J., Rotstayn, L., & Dix, M. (2008). Variability and trend of North West Australia rainfall: Observations and coupled climate modeling. *Journal of Climate*, 21(12), 2938-2959.

Sigl, M., Winstrup, M., McConnell, J. R., Welten, K. C., Plunkett, G., Ludlow, F., Buntgen, U., Caffee, M., Chellman, N., Dahl-Jensen, D., Fischer, H., Kipfstuhl, S., Kostick, C., Maselli, O. J., Mekhaldi, F., Mulvaney, R., Muscheler, R., Pasteris, D. R., Pilcher, J. R., Salzer, M., Schupbach, S., Steffensen, J. P., Vinther, B. M., & Woodruff, T. E. (2015). Timing and climate forcing of volcanic eruptions for the past 2,500 years. *Nature*, 523(7562), 543-549.

Sinclair, K. E., Bertler, N. A. N., & Trompeter, W. J. (2010). Synoptic controls on precipitation pathways and snow delivery to high-accumulation ice core sites in the Ross Sea region, Antarctica. *Journal of Geophysical Research: Atmospheres*, 115(D22), D22112.

Slikboer, S., Grandy, L., Blair, S. L., Nizkorodov, S. A., Smith, R. W., & Al-Abadleh, H. A. (2015). Formation of Light Absorbing Soluble Secondary Organics and Insoluble Polymeric Particles from the Dark Reaction of Catechol and Guaiacol with Fe(III). *Environmental Science & Technology*, 49(13), 7793-7801.

Slowik, J. G., Cross, E. S., Han, J.-H., Davidovits, P., Onasch, T. B., Jayne, J. T., Williams, L. R., Canagaratna, M. R., Worsnop, D. R., & Chakrabarty, R. K. (2007a). An inter-comparison of instruments measuring black carbon content of soot particles. *Aerosol Science and Technology*, 41(3), 295-314.

Slowik, J. G., Cross, E. S., Han, J. H., Davidovits, P., Onasch, T. B., Jayne, J. T., Williams, L. R., Canagaratna, M. R., Worsnop, D. R., Chakrabarty, R. K., Moosmuller, H., Arnott, W. P., Schwarz, J. P., Gao, R. S., Fahey, D. W., Kok, G. L., & Petzold, A. (2007b). An inter-comparison of instruments measuring black carbon content of soot particles. *Aerosol Science and Technology*, 41(3), 295-314.

Spahni, R., Chappellaz, J., Stocker, T. F., Loulergue, L., Hausammann, G., Kawamura, K., Flückiger, J., Schwander, J., Raynaud, D., Masson-Delmotte, V., & Jouzel, J. (2005).

Atmospheric Methane and Nitrous Oxide of the Late Pleistocene from Antarctic Ice Cores. *Science*, 310(5752), 1317-1321.

Steig, E. J., Schneider, D. P., Rutherford, S. D., Mann, M. E., Comiso, J. C., & Shindell, D. T. (2009). Warming of the Antarctic ice-sheet surface since the 1957 International Geophysical Year. *Nature*, 457(7228), 459-462.

Stein, A. F., Draxler, R. R., Rolph, G. D., Stunder, B. J. B., Cohen, M. D., & Ngan, F. (2015). NOAA's HYSPLIT Atmospheric Transport and Dispersion Modeling System. *Bulletin of the American Meteorological Society*, 96(12), 2059-2077.

Stephens, M., Turner, N., & Sandberg, J. (2003). Particle identification by laser-induced incandescence in a solid-state laser cavity. *Applied Optics*, 42(19), 3726-3736.

Sterle, K. M., McConnell, J. R., Dozier, J., Edwards, R., & Flanner, M. G. (2013). Retention and radiative forcing of black carbon in eastern Sierra Nevada snow. *The Cryosphere*, 7(1), 365-374.

Stier, P., Seinfeld, J. H., Kinne, S., & Boucher, O. (2007). Aerosol absorption and radiative forcing. *Atmos. Chem. Phys.*, 7(19), 5237-5261.

Stier, P., Seinfeld, J. H., Kinne, S., Feichter, J., & Boucher, O. (2006). Impact of nonabsorbing anthropogenic aerosols on clear-sky atmospheric absorption. *Journal of Geophysical Research: Atmospheres*, 111(D18)

Stohl, A., & Sodemann, H. (2010). Characteristics of atmospheric transport into the Antarctic troposphere. *Journal of Geophysical Research-Atmospheres*, 115

Thompson, D. W. J., Solomon, S., Kushner, P. J., England, M. H., Grise, K. M., & Karoly, D. J. (2011). Signatures of the Antarctic ozone hole in Southern Hemisphere surface climate change. *Nature Geosci*, 4(11), 741-749.

Torres, A., Bond, T. C., Lehmann, C. M. B., Subramanian, R., & Hadley, O. L. (2013). Measuring Organic Carbon and Black Carbon in Rainwater: Evaluation of Methods. *Aerosol Science and Technology*, 48(3), 239-250.

Tsigaridis, K., Krol, M., Dentener, F. J., Balkanski, Y., Lathiere, J., Metzger, S., Hauglustaine, D. A., & Kanakidou, M. (2006). Change in global aerosol composition since preindustrial times. *Atmospheric Chemistry and Physics*, 6, 5143-5162.

Tuohy, A., Bertler, N., Neff, P., Edwards, R., Emanuelsson, D., Beers, T., & Mayewski, P. (2015). Transport and deposition of heavy metals in the Ross Sea Region, Antarctica. *Journal of Geophysical Research: Atmospheres*, 120(20), 10,996-911,011.

Utsunomiya, S., & Ewing, R. C. (2003). Application of High-Angle Annular Dark Field Scanning Transmission Electron Microscopy, Scanning Transmission Electron Microscopy-Energy Dispersive X-ray Spectrometry, and Energy-Filtered Transmission Electron Microscopy to the Characterization of Nanoparticles in the Environment. *Environmental Science & Technology*, 37(4), 786-791.

Vallelonga, P., Van de Velde, K., Candelone, J.-P., Morgan, V., Boutron, C., & Rosman, K. (2002). The lead pollution history of Law Dome, Antarctica, from isotopic measurements on ice cores: 1500 AD to 1989 AD. *Earth and Planetary Science Letters*, *204*(1), 291-306.

van der Werf, G. R., Randerson, J. T., Giglio, L., Collatz, G. J., Mu, M., Kasibhatla, P. S., Morton, D. C., DeFries, R. S., Jin, Y., & van Leeuwen, T. T. (2010). Global fire emissions and the contribution of deforestation, savanna, forest, agricultural, and peat fires (1997–2009). *Atmos. Chem. Phys.*, *10*(23), 11707-11735.

van Ommen, T. D., & Morgan, V. (1996). Peroxide concentrations in the Dome summit south ice core, Law Dome, Antarctica. *Journal of Geophysical Research: Atmospheres* (1984–2012), *101*(D10), 15147-15152.

van Ommen, T. D., & Morgan, V. (2010). Snowfall increase in coastal East Antarctica linked with southwest Western Australian drought. *Nature Geosci*, *3*(4), 267-272.

Verdon-Kidd, D. C., & Kiem, A. S. (2009). Nature and causes of protracted droughts in southeast Australia: Comparison between the Federation, WWII, and Big Dry droughts. *Geophysical Research Letters*, *36*(22)

Vignati, E., Karl, M., Krol, M., Wilson, J., Stier, P., & Cavalli, F. (2010). Sources of uncertainties in modeling black carbon at the global scale. *Atmos. Chem. Phys.*, *10*(6), 2595-2611.

Wang, G., & Cai, W. (2013). Climate-change impact on the 20th-century relationship between the Southern Annular Mode and global mean temperature. *Scientific Reports*, *3*, 2039.

Wang, X., Heald, C. L., Ridley, D. A., Schwarz, J. P., Spackman, J. R., Perring, A. E., Coe, H., Liu, D., & Clarke, A. D. (2014). Exploiting simultaneous observational constraints on mass and absorption to estimate the global direct radiative forcing of black carbon and brown carbon. *Atmos. Chem. Phys.*, *14*(20), 10989-11010.

Warren, S. G., & Clarke, A. D. (1990). Soot in the atmosphere and snow surface of Antarctica. *Journal of Geophysical Research: Atmospheres*, *95*(D2), 1811-1816.

Weller, R., Minikin, A., Petzold, A., Wagenbach, D., & König-Langlo, G. (2013). Characterization of long-term and seasonal variations of black carbon (BC) concentrations at Neumayer, Antarctica. *Atmos. Chem. Phys.*, *13*(3), 1579-1590.

Wiedinmyer, C., Akagi, S. K., Yokelson, R. J., Emmons, L. K., Al-Saadi, J. A., Orlando, J. J., & Soja, A. J. (2011). The Fire INventory from NCAR (FINN): a high resolution global model to estimate the emissions from open burning. *Geosci. Model Dev.*, *4*(3), 625-641.

Winstrup, M., Svensson, A. M., Rasmussen, S. O., Winther, O., Steig, E. J., & Axelrod, A. E. (2012). An automated approach for annual layer counting in ice cores. *Clim. Past*, *8*(6), 1881-1895.

Winstrup, M. (2016). A Hidden Markov Model Approach to Infer Timescales for High-Resolution Climate Archives. Paper presented at the AAAI.

Winstrup, M., Vallenga, P., Kjær, H. A., Fudge, T. J., Lee, J., Riis, M. H., Edwards, R., Bertler, N. A. N., Blunier, T., Brook, E., Buizert, C., Ciobanu, G., Conway, H., Dahl-Jensen, D., Ellis, A., Emanuelsson, D., Kurbatov, A., Mayewski, P., Neff, P., Pyne, R., Simonsen, M. F., Svensson, A., Tuohy, A., & Waddington, E. (2017). A 2000-year timescale and accumulation reconstruction for Roosevelt Island, West Antarctica. *In prep.*

Winton, V. H. L., Edwards, R., Delmonte, B., Ellis, A., Andersson, P. S., Bowie, A., Bertler, N. A. N., Neff, P., & Tuohy, A. (2016). Multiple sources of soluble atmospheric iron to Antarctic waters. *Global Biogeochemical Cycles*, 30(3), 421-437.

Wolff, E. W., & Cachier, H. (1998). Concentrations and seasonal cycle of black carbon in aerosol at a coastal Antarctic station. *Journal of Geophysical Research*, 103(D9), 11033-11041.

Xu, B., Cao, J., Hansen, J., Yao, T., Joswita, D. R., Wang, N., Wu, G., Wang, M., Zhao, H., Yang, W., Liu, X., & He, J. (2009). Black soot and the survival of Tibetan glaciers. *Proceedings of the National Academy of Sciences*, 106(52), 22114-22118.

Yates, C. P., Edwards, A. C., & Russell-Smith, J. (2009). Big fires and their ecological impacts in Australian savannas: size and frequency matters. *International Journal of Wildland Fire*, 17(6), 768-781.

Zhang, J., Liu, J., Tao, S., & Ban-Weiss, G. A. (2015). Long-range transport of black carbon to the Pacific Ocean and its dependence on aging timescale. *Atmos. Chem. Phys.*, 15(20), 11521-11535.

Zhu, J., Crozier, P. A., & Anderson, J. R. (2013). Characterization of light-absorbing carbon particles at three altitudes in East Asian outflow by transmission electron microscopy. *Atmos. Chem. Phys.*, 13(13), 6359-6371.

Every reasonable effort has been made to acknowledge the owners of copyright material. I would be pleased to hear from any copyright owner who has been omitted or incorrectly acknowledged.

Appendix A. Statements of Co-Author Contributions

Appendix A1: Statement of contribution for paper 1

Statement of Authorship

Title of Paper: Characterizing black carbon in rain and ice cores using coupled tangential flow filtration and transmission electron microscopy

Citation details: Ellis, A., Edwards, R., Saunders, M., Chakrabarty, R. K., Subramanian, R., van Riessen, A., Smith, A. M., Lambrinidis, D., Nunes, L. J., Vallelonga, P., Goodwin, I. D., Moy, A. D., Curran, M. A. J., and van Ommen, T. D.: Characterizing black carbon in rain and ice cores using coupled tangential flow filtration and transmission electron microscopy, *Atmos. Meas. Tech.*, 8, 3959-3969, doi:10.5194/amt-8-3959-2015, 2015.


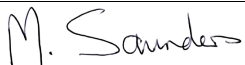
Status: **Published**





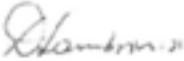






I, Aja Anne Ellis, designed and conducted the experiment, interpreted the results, and authored the above manuscript with support from the co-authors.



08 October 2015

As a Co-Author, I endorse that the level of contribution by the candidate indicated above is appropriate.

Name	Signature	Date
Ross Edwards		October 13, 2015
Martin Saunders		October 12, 2015

Rajan K. Chakrabarty		Oct 9, 2015
R. Subramanian		Oct 9, 2015
Arie van Riessen		12-Oct-15
Andrew M. Smith		12th October 2015
Dionisia Lambrinidis		10th December 2015
Laurie J. Nunes		October 15 2015
Paul Vallelonga		13 th October 2015
Ian D. Goodwin		Oct 11, 2015
Andrew D. Moy		16th Oct, 2015
Mark A. J. Curran	 <small>Digitally signed by Mark A. J. Curran, DN: cn=Mark A. J. Curran, o=Mark A. J. Curran, email=mark.curran@psu.edu, c=US Date: 2015.10.12 16:47:40 -0700</small>	Oct 12, 2015
Tas D. van Ommen	 <small>Digitally signed by Tas van Ommen, DN: cn=Tas van Ommen, o=University of Groningen, email=t.van.ommen@psu.edu, c=US Date: 2015.10.12 16:48:00 -0700</small>	Oct 12, 2015

Appendix A2: Statement of contribution for paper 2

Statement of Authorship

Title of Paper: Individual particle morphology, coatings, and impurities of black carbon aerosols in Antarctic ice

Citation details: Ellis, A., Edwards, R., Saunders, M., Chakrabarty, R. K., Subramanian, N. E. Timms, R., van Riessen, A., Smith, A. M., Lambrinidis, D., Nunes, L. J., Vallelonga, P., Goodwin, I. D., Moy, A. D., Curran, M. A. J., and van Ommen, T. D.: Individual particle morphology, coatings, and impurities of black carbon aerosols in Antarctic ice, *submitted to Geophysical Research Letters*, August 2016.


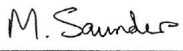
Status: **Submitted**

I, Aja Anne Ellis, designed and conducted the experiment, interpreted the results, and authored the above manuscript with support from the co-authors.



04 September 2016

As a Co-Author, I endorse that the level of contribution by the candidate indicated above is appropriate.

Name	Signature	Date
Ross Edwards		05/09/2016
Martin Saunders		8/9/16

Rajan K. Chelamberty	R Chelamberty	09/08/16
Nicholas E. Timms	NT	09/08/16
R. Subramanian	R Subramanian	
Arie van Kleesen	A van Kleesen	11/9/16.
Andrew M. Smith	A Smith	20/09/16.
Dimitris Lambrinidis	D Lambrinidis	21/09/16
LUIGI J. NUZZO	L Nuzzo	23/09/16
Paul Vellelonge	P Vellelonge	11/11/2016
Ian D. Goodwin	I D Goodwin	11/11/2016
Andrew D. Moy	A D Moy	8/9/2016.
Mark A. J. Curran	M A J Curran	17/10/2016
Tas D. van Oremen	T D van Oremen	8/11/2016

Appendix B. Copyright agreements for published papers

Licence and copyright agreement

The following licence and copyright agreement is valid for any article published by Copernicus Publications on behalf of the European Geosciences Union (EGU) in the journal Atmospheric Measurement Techniques and its discussion forum Atmospheric Measurement Techniques Discussions.

Author's certification

By submitting the manuscript, the authors certify the following:



- They are authorized by their co-authors to enter into these arrangements.
- The work described has not been published before (except in the form of an abstract or proceedings-type publication – including discussion papers – or as part of a published lecture or thesis); it is not under consideration for publication elsewhere; and its publication has been approved by all the author(s) and by the responsible authorities – tacitly or explicitly – of the institutes where the work was carried out.
- They have secured the right to reproduce any material that has already been published or copyrighted elsewhere.
- They agree to the following licence and copyright agreement:

Copyright


- The copyright of any article is retained by the author(s). More information on the transfer of copyright can be found below.
- Authors grant Copernicus Publications a licence to publish the article and identify itself as the original publisher.
- Authors grant Copernicus Publications commercial rights to produce hardcopy volumes of the journal for purchase by libraries and individuals.
- Authors grant any third party the right to use the article freely under the stipulation that the original authors are given credit and the appropriate citation details are mentioned.
- The article is distributed under the [Creative Commons Attribution 3.0](#) License. Unless otherwise stated, associated published material is distributed under the same licence.

Creative Commons Attribution 3.0 License

Anyone is free

-  **to share** — to copy, distribute, and transmit the work
-  **to remix** — to adapt the work

under the following conditions:

-  **Attribution** — The original authors must be given credit.
 - For any reuse or distribution, it must be made clear to others what the licence terms of this work are.
 - Any of these conditions can be waived if the copyright holders give permission.
 - Nothing in this licence impairs or restricts the author's moral rights.

The full [legal code](#) of this licence.

Copyright transfers

Many authors have strict regulations in their employment contract regarding their publications. A transfer of copyright to the institution or company is common as well as the reservation of specific usage rights. In open-access publications in combination with the Creative Commons License, a transfer of the **copyright** to the institution is possible as it belongs to the author anyway.

Any **usage rights** are regulated through the Creative Commons License. As Copernicus Publications uses the Creative Commons Attribution 3.0 License, anyone (the author, his/her institution/company, the publisher, as well as the public) is free to copy, distribute, transmit, and adapt the work as long as the original author is given credit (see above). Therefore, specific usage rights cannot be reserved by the author or his/her institution/company, and the publisher cannot include the statement "all rights reserved" in any published paper.

A copyright transfer from the author to his/her institution/company can be expressed in a special "copyright statement" at the end of the publication. Authors are asked to include the following sentence: "The author's copyright for this publication has been transferred to *institution/company*".

Crown copyright

The licence and copyright agreement of Copernicus Publications respects the Crown copyright. For articles written by authors affiliated with the British Government and its institutions, a copyright statement will be included as indicated in the manuscript preparation guidelines. Authors are asked to use the following statement, which has been approved by the Information Policy department of The National Archives:

The works published in this journal are distributed under the Creative Commons Attribution 3.0 License. This licence does not affect the Crown copyright work, which is reusable under the Open Government Licence (OGL). The Creative Commons Attribution 3.0 License and the OGL are interoperable and do not conflict with, reduce or limit each other.

© Crown copyright YEAR

Reproduction request

All articles published by Copernicus Publications are licensed under the Creative Commons Attribution 3.0 License (see details above) together with an author copyright. Therefore, there is no need from the publisher's side to give permission for the reproduction of articles. We suggest contacting the author to inform him/her about the further usage of

the material. However, as the author decided to publish the scientific results under the CC-BY licence, he/she consented to share the work under the condition that the original authors be given credit.

**JOHN WILEY AND SONS LICENSE
TERMS AND CONDITIONS**

Nov 30, 2016

This Agreement between Aja Ellis ("You") and John Wiley and Sons ("John Wiley and Sons") consists of your license details and the terms and conditions provided by John Wiley and Sons and Copyright Clearance Center.

License Number	3998780303851
License date	Nov 30, 2016
Licensed Content Publisher	John Wiley and Sons
Licensed Content Publication	Geophysical Research Letters
Licensed Content Title	Individual particle morphology, coatings, and impurities of black carbon aerosols in Antarctic ice and tropical rainfall
Licensed Content Author	Aja Ellis,Ross Edwards,Martin Saunders,Rajan K. Chakrabarty,R. Subramanian,Nicholas E. Timms,Arie Riessen,Andrew M. Smith,Dionisia Lambrinidis,Laurie J. Nunes,Paul Vallelonga,Ian D. Goodwin,Andrew D. Moy,Mark A. J. Curran,Tas D. Ommen
Licensed Content Date	Nov 19, 2016
Licensed Content Pages	1
Type of use	Dissertation/Thesis
Requestor type	Author of this Wiley article
Format	Print and electronic
Portion	Full article
Will you be translating?	No
Title of your thesis / dissertation	History and characterization of remote southern hemisphere black carbon aerosols during the Anthropocene
Expected completion date	Nov 2016
Expected size (number of pages)	250
Requestor Location	Aja Ellis 663 Maryland Ave PITTSBURGH, PA 15232 United States Attn: Aja Ellis
Publisher Tax ID	EU826007151
Billing Type	Invoice
Billing Address	Aja Ellis 663 Maryland Ave PITTSBURGH, PA 15232 United States Attn: Aja Ellis
Total	0.00 USD
Terms and Conditions	

TERMS AND CONDITIONS

This copyrighted material is owned by or exclusively licensed to John Wiley & Sons, Inc. or one of its group companies (each a "Wiley Company") or handled on behalf of a society with which a Wiley Company has exclusive publishing rights in relation to a particular work (collectively "WILEY"). By clicking "accept" in connection with completing this licensing transaction, you agree that the following terms and conditions apply to this transaction (along with the billing and payment terms and conditions established by the Copyright Clearance Center Inc., ("CCC's Billing and Payment terms and conditions"), at the time that you opened your RightsLink account (these are available at any time at <http://myaccount.copyright.com>).

Terms and Conditions

- The materials you have requested permission to reproduce or reuse (the "Wiley Materials") are protected by copyright.
- You are hereby granted a personal, non-exclusive, non-sub licensable (on a stand-alone basis), non-transferable, worldwide, limited license to reproduce the Wiley Materials for the purpose specified in the licensing process. This license, **and any CONTENT (PDF or image file) purchased as part of your order**, is for a one-time use only and limited to any maximum distribution number specified in the license. The first instance of republication or reuse granted by this license must be completed within two years of the date of the grant of this license (although copies prepared before the end date may be distributed thereafter). The Wiley Materials shall not be used in any other manner or for any other purpose, beyond what is granted in the license. Permission is granted subject to an appropriate acknowledgement given to the author, title of the material/book/journal and the publisher. You shall also duplicate the copyright notice that appears in the Wiley publication in your use of the Wiley Material. Permission is also granted on the understanding that nowhere in the text is a previously published source acknowledged for all or part of this Wiley Material. Any third party content is expressly excluded from this permission.
- With respect to the Wiley Materials, all rights are reserved. Except as expressly granted by the terms of the license, no part of the Wiley Materials may be copied, modified, adapted (except for minor reformatting required by the new Publication), translated, reproduced, transferred or distributed, in any form or by any means, and no derivative works may be made based on the Wiley Materials without the prior permission of the respective copyright owner. **For STM Signatory Publishers clearing permission under the terms of the [STM Permissions Guidelines](#) only, the terms of the license are extended to include subsequent editions and for editions in other languages, provided such editions are for the work as a whole in situ and does not involve the separate exploitation of the permitted figures or extracts**, You may not alter, remove or suppress in any manner any copyright, trademark or other notices displayed by the Wiley Materials. You may not license, rent, sell, loan, lease, pledge, offer as security, transfer or assign the Wiley Materials on a stand-alone basis, or any of the rights granted to you hereunder to any other person.
- The Wiley Materials and all of the intellectual property rights therein shall at all times remain the exclusive property of John Wiley & Sons Inc, the Wiley Companies, or their respective licensors, and your interest therein is only that of having possession of and the right to reproduce the Wiley Materials pursuant to Section 2 herein during the continuance of this Agreement. You agree that you own no right, title or interest in or to the Wiley Materials or any of the intellectual property rights therein. You shall have no rights hereunder other than the license as provided for above in Section 2. No right,

license or interest to any trademark, trade name, service mark or other branding ("Marks") of WILEY or its licensors is granted hereunder, and you agree that you shall not assert any such right, license or interest with respect thereto

- NEITHER WILEY NOR ITS LICENSORS MAKES ANY WARRANTY OR REPRESENTATION OF ANY KIND TO YOU OR ANY THIRD PARTY, EXPRESS, IMPLIED OR STATUTORY, WITH RESPECT TO THE MATERIALS OR THE ACCURACY OF ANY INFORMATION CONTAINED IN THE MATERIALS, INCLUDING, WITHOUT LIMITATION, ANY IMPLIED WARRANTY OF MERCHANTABILITY, ACCURACY, SATISFACTORY QUALITY, FITNESS FOR A PARTICULAR PURPOSE, USABILITY, INTEGRATION OR NON-INFRINGEMENT AND ALL SUCH WARRANTIES ARE HEREBY EXCLUDED BY WILEY AND ITS LICENSORS AND WAIVED BY YOU.
- WILEY shall have the right to terminate this Agreement immediately upon breach of this Agreement by you.
- You shall indemnify, defend and hold harmless WILEY, its Licensors and their respective directors, officers, agents and employees, from and against any actual or threatened claims, demands, causes of action or proceedings arising from any breach of this Agreement by you.
- IN NO EVENT SHALL WILEY OR ITS LICENSORS BE LIABLE TO YOU OR ANY OTHER PARTY OR ANY OTHER PERSON OR ENTITY FOR ANY SPECIAL, CONSEQUENTIAL, INCIDENTAL, INDIRECT, EXEMPLARY OR PUNITIVE DAMAGES, HOWEVER CAUSED, ARISING OUT OF OR IN CONNECTION WITH THE DOWNLOADING, PROVISIONING, VIEWING OR USE OF THE MATERIALS REGARDLESS OF THE FORM OF ACTION, WHETHER FOR BREACH OF CONTRACT, BREACH OF WARRANTY, TORT, NEGLIGENCE, INFRINGEMENT OR OTHERWISE (INCLUDING, WITHOUT LIMITATION, DAMAGES BASED ON LOSS OF PROFITS, DATA, FILES, USE, BUSINESS OPPORTUNITY OR CLAIMS OF THIRD PARTIES), AND WHETHER OR NOT THE PARTY HAS BEEN ADVISED OF THE POSSIBILITY OF SUCH DAMAGES. THIS LIMITATION SHALL APPLY NOTWITHSTANDING ANY FAILURE OF ESSENTIAL PURPOSE OF ANY LIMITED REMEDY PROVIDED HEREIN.
- Should any provision of this Agreement be held by a court of competent jurisdiction to be illegal, invalid, or unenforceable, that provision shall be deemed amended to achieve as nearly as possible the same economic effect as the original provision, and the legality, validity and enforceability of the remaining provisions of this Agreement shall not be affected or impaired thereby.
- The failure of either party to enforce any term or condition of this Agreement shall not constitute a waiver of either party's right to enforce each and every term and condition of this Agreement. No breach under this agreement shall be deemed waived or excused by either party unless such waiver or consent is in writing signed by the party granting such waiver or consent. The waiver by or consent of a party to a breach of any provision of this Agreement shall not operate or be construed as a waiver of or consent to any other or subsequent breach by such other party.
- This Agreement may not be assigned (including by operation of law or otherwise) by you without WILEY's prior written consent.

- Any fee required for this permission shall be non-refundable after thirty (30) days from receipt by the CCC.
- These terms and conditions together with CCC's Billing and Payment terms and conditions (which are incorporated herein) form the entire agreement between you and WILEY concerning this licensing transaction and (in the absence of fraud) supersedes all prior agreements and representations of the parties, oral or written. This Agreement may not be amended except in writing signed by both parties. This Agreement shall be binding upon and inure to the benefit of the parties' successors, legal representatives, and authorized assigns.
- In the event of any conflict between your obligations established by these terms and conditions and those established by CCC's Billing and Payment terms and conditions, these terms and conditions shall prevail.
- WILEY expressly reserves all rights not specifically granted in the combination of (i) the license details provided by you and accepted in the course of this licensing transaction, (ii) these terms and conditions and (iii) CCC's Billing and Payment terms and conditions.
- This Agreement will be void if the Type of Use, Format, Circulation, or Requestor Type was misrepresented during the licensing process.
- This Agreement shall be governed by and construed in accordance with the laws of the State of New York, USA, without regards to such state's conflict of law rules. Any legal action, suit or proceeding arising out of or relating to these Terms and Conditions or the breach thereof shall be instituted in a court of competent jurisdiction in New York County in the State of New York in the United States of America and each party hereby consents and submits to the personal jurisdiction of such court, waives any objection to venue in such court and consents to service of process by registered or certified mail, return receipt requested, at the last known address of such party.

WILEY OPEN ACCESS TERMS AND CONDITIONS

Wiley Publishes Open Access Articles in fully Open Access Journals and in Subscription journals offering Online Open. Although most of the fully Open Access journals publish open access articles under the terms of the Creative Commons Attribution (CC BY) License only, the subscription journals and a few of the Open Access Journals offer a choice of Creative Commons Licenses. The license type is clearly identified on the article.

The Creative Commons Attribution License

The [Creative Commons Attribution License \(CC-BY\)](#) allows users to copy, distribute and transmit an article, adapt the article and make commercial use of the article. The CC-BY license permits commercial and non-

Creative Commons Attribution Non-Commercial License

The [Creative Commons Attribution Non-Commercial \(CC-BY-NC\) License](#) permits use, distribution and reproduction in any medium, provided the original work is properly cited and is not used for commercial purposes.(see below)

Creative Commons Attribution-Non-Commercial-NoDerivs License

The [Creative Commons Attribution Non-Commercial-NoDerivs License](#) (CC-BY-NC-ND) permits use, distribution and reproduction in any medium, provided the original work is properly cited, is not used for commercial purposes and no modifications or adaptations are made. (see below)

Use by commercial "for-profit" organizations

Use of Wiley Open Access articles for commercial, promotional, or marketing purposes requires further explicit permission from Wiley and will be subject to a fee.

Further details can be found on Wiley Online Library

<http://olabout.wiley.com/WileyCDA/Section/id-410895.html>

Other Terms and Conditions:

v1.10 Last updated September 2015

Questions? customercare@copyright.com or +1-855-239-3415 (toll free in the US) or +1-978-646-2777.

Appendix C. Reprinted published papers



Characterizing black carbon in rain and ice cores using coupled tangential flow filtration and transmission electron microscopy

A. Ellis¹, R. Edwards¹, M. Saunders², R. K. Chakrabarty³, R. Subramanian⁴, A. van Riessen¹, A. M. Smith⁵, D. Lambrinidis⁶, L. J. Nunes¹, P. Vallelonga⁷, I. D. Goodwin⁸, A. D. Moy^{9,10}, M. A. J. Curran^{9,10}, and T. D. van Ommen^{9,10}

¹Physics and Astronomy, Curtin University, Perth, WA, Australia

²Centre for Microscopy, Characterisation, and Analysis, The University of Western Australia, Perth, WA, Australia

³Department of Energy, Environmental & Chemical Engineering, Washington University in St. Louis, St. Louis, MO, USA

⁴Department of Mechanical Engineering, Carnegie Mellon University, Pittsburgh, PA, USA

⁵Australian Nuclear Science and Technology Organisation, Sydney, NSW, Australia

⁶Research Institute for the Environment and Livelihoods, Charles Darwin University, Darwin, NT, Australia

⁷Centre for Ice and Climate, Niels Bohr Institute, University of Copenhagen, Copenhagen, Denmark

⁸Marine Climate Risk Group, Department of Environmental Sciences, Macquarie University, NSW, Australia

⁹Australian Antarctic Division, Channel Highway, Kingston, TAS, Australia

¹⁰Antarctic Climate and Ecosystems Cooperative Research Centre, University of Tasmania, Hobart, TAS, Australia

Correspondence to: A. Ellis (aja.a.ellis@gmail.com)

Received: 7 May 2015 – Published in Atmos. Meas. Tech. Discuss.: 19 June 2015

Revised: 11 September 2015 – Accepted: 14 September 2015 – Published: 29 September 2015

Abstract. Antarctic ice cores have been used to study the history of black carbon (BC), but little is known with regards to the physical and chemical characteristics of these particles in the remote atmosphere. Characterization remains limited by ultra-trace concentrations in ice core samples and the lack of adequate methods to isolate the particles unaltered from the melt water. To investigate the physical and chemical characteristics of these particles, we have developed a tangential flow filtration (TFF) method combined with transmission electron microscopy (TEM). Tests using ultrapure water and polystyrene latex particle standards resulted in excellent blanks and significant particle recovery. This approach has been applied to melt water from Antarctic ice cores as well as tropical rain from Darwin, Australia with successful results: TEM analysis revealed a variety of BC particle morphologies, insoluble coatings, and the attachment of BC to mineral dust particles. The TFF-based concentration of these particles has proven to give excellent results for TEM studies of BC particles in Antarctic ice cores and can be used for future studies of insoluble aerosols in rainwater and ice core samples.

1 Introduction

Carbonaceous aerosols emitted by combustion processes are comprised of black carbon (BC) and organic matter. These aerosols can stay suspended from days to weeks in the troposphere and for over a year in the stratosphere (Buseck and Adachi, 2008; Stohl and Sodemann, 2010). They impact the radiative, physical, and chemical properties of the atmosphere, affecting climate through direct optical effects and indirectly through changes in cloud formation and structure (Johnson et al., 2004). The contribution of BC to radiative forcing is significantly affected by particle shape, size, and mixing state, which is in turn affected by emission source and aging in the atmosphere (Jacobson, 2001; Moffet and Prather, 2009). Understanding the behavior of BC and other carbonaceous aerosols in the remote atmosphere is important for validating aerosol parameterization in general circulation models (Koch et al., 2009). Wet deposition through rain and snow is the primary removal process of BC from the atmosphere (Bond et al., 2013), and has a large impact on BC's atmospheric residence time and distribution (Hodnebrog et al., 2014). Furthermore, when deposited to highly reflective sur-

faces such as snow, the presence of BC can decrease surface albedo and accelerate melting (Flanner et al., 2007; Hansen and Nazarenko, 2004; McConnell et al., 2007). Therefore, studies of BC in modern and historic rain, snow, and ice samples are needed to understand their modern atmospheric distribution and their presence in the paleo-atmosphere, and in turn to study their impact on paleoclimate forcing and future climate change.

Several methods exist for determining BC concentrations in the atmosphere, such as optical absorption methods, thermo-optical analysis, photoacoustic absorption spectroscopy, and aerosol mass spectrometry (Slowik et al., 2007). Single particle mass concentration and particle size can be measured in real-time by single particle intracavity laser-induced incandescence (SP2, Droplet Measurement Technologies, Boulder, CO, USA). Black carbon particles can also be characterized individually using electron microscopy (Pósfai et al., 1999). Many studies have measured BC abundance (as number and mass concentrations) in the atmosphere (Schwarz et al., 2006). Transmission electron microscopy (TEM) coupled with electron energy loss spectrometry (EELS) and energy-dispersive X-ray spectrometry (EDS) have long been used to determine the size, morphological, and elemental characteristics of atmospheric aerosols (Pósfai et al., 1999). Scanning transmission electron microscopy (STEM) coupled with EDS has been used to study aerosol particles (Utsunomiya and Ewing, 2003), with high resolution imaging and STEM EDS mapping revealing nanoscale inclusions in larger aerosols that would go unnoticed with traditional TEM imaging.

Previous studies have investigated BC mass concentrations in rainwater (Ohata et al., 2011; Torres et al., 2013), snow packs (Hegg et al., 2009; Warren and Clarke, 1990), and ice cores (Bisiaux et al., 2012; McConnell et al., 2007), but little data exists regarding the morphology, chemical composition, and insoluble coatings of BC particles in rain and snow. This is particularly true of aged, long-range transported particles that have been deposited at the polar ice caps.

To the best of our knowledge, only one study has previously studied the morphology of carbonaceous aerosols in precipitation. Murr et al. (2004) analyzed particles in ice cores from the Greenland ice cap by melting the ice and depositing 180 mL of sample on a 5 mm TEM grid, a few microliters at a time. As made evident by this process, isolating these particles for characterization is technically challenging, especially in ultra-clean Antarctic ice, where their abundance is often less than $0.1 \mu\text{g kg}^{-1}$ (Bisiaux et al., 2012). As Antarctic ice cores have substantially lower BC concentrations than that observed in Greenland ice, larger sample volumes (> 1 L melt water) are necessary to acquire sufficient particles for characterization, making this drop-by-drop method impractical. Salts and other dissolved species cause additional problems with the drop-by-drop method because they are also deposited on the grid, coating it with large amounts of unwanted material. When concentrated on TEM

grids, these precipitated particles can hinder the detection and analysis of BC simply by obscuring particle morphology, especially when BC is present in ultra-trace concentrations.

An ideal preconcentration method for insoluble BC particles in polar ice should be reasonably quick, concentrate large volumes of ice melt water, remove salts, and keep the particles in motion to limit aggregation. Tangential flow filtration (TFF) is a technique that uses a continuous flow of solution tangentially across a filter membrane to avoid sample build-up on the surface of the membrane (and subsequent sample loss). Hollow fiber filters have been employed to concentrate environmental water samples (Benner et al., 1997; Giovannoni et al., 1990) as well as nanoparticles for pharmaceutical applications (Dalwadi et al., 2005). TFF has a high particle recovery, can concentrate large sample volumes (> 1 L) without membrane fouling, does not cause nanoparticle aggregation, and can preserve fragile aerosol structures (Benner et al., 1997; Dalwadi et al., 2005). An important benefit of TFF to the study of BC particles is that it can concentrate particles whilst removing dissolved salts and other species, depending on the pore size of the filter.

To study individual BC particles and other carbonaceous aerosols in global precipitation, we investigated the use of TFF to concentrate BC prior to analysis by TEM. Particle recovery rates and blanks were investigated using polystyrene latex (PSL) particle standards and ultrapure water. Test samples included tropical rainwater from Darwin, Australia as well as Antarctic ice cores. The rainwater provided an example of equatorial wet deposition of particles, whereas Antarctic ice provides both a modern example of polar deposition as well as a historical record of these particles in the global atmosphere.

2 Methodology

2.1 Clean room laboratory environment

Sample preparation and cleaning of laboratory and field equipment was performed in the Trace Research and Advanced Clean Environment (TRACE) laboratory at Curtin University. The TRACE facility is a 450 m² clean-air laboratory facility described by Burn et al. (2009). The facility includes a large positive pressure clean-air exclusion space (ISO Class 5) housing five smaller clean-air laboratory modules (ISO Class 4) including a cold laboratory module. With the exception of the cold laboratory module, the modules draw clean air from the exclusion space through a series of high-efficiency particle air (HEPA) filters in the module roof. Module air passes through the floor and either recirculates back into the module and the exclusion space or is exhausted through the base of clean air hood. Air inside the cold laboratory module is filtered by a recirculating cryogenic air filtration HEPA system. The BC concentration in the exclusion space air was determined using a single-particle soot photometer (SP2) and found to be less than 1 BC particle m⁻³

for particles with a mass equivalent diameter range of 70 to 700 nm (assuming a constant density of 1.8 g cc^{-1} as in Schwarz et al., 2013).

Mechanical decontamination of ice core samples was conducted in the TRACE cold laboratory module at -12°C . All other sample preparation and TEM grid preparation activities were conducted in a clean-air bench inside a laboratory module.

The modules are fitted with an ultrapure water (UP, $\rho > 18.2 \text{ m}\Omega$) system fed by a laboratory-wide reverse osmosis and deionized water supply. This water was used for cleaning all laboratory benches, fittings, tubing, and plastic ware. Melted samples were kept in Teflon or low-density polyethylene (LDPE) bottles, filled and rinsed multiple times with UP water. All surfaces were cleaned with UP water prior to sample decontamination.

2.2 Reagents and materials

2.2.1 Blanks

The entirety of this concentration method was blank-tested with laboratory-made UP ice. The blank ice was made by freezing UP water in a cleaned 3 L perfluoro alkoxyalkane container (PFA, Savillex). The ice was removed from the container, cut into rectangles on a clean band saw in the cold laboratory module, and bagged in plastic layflat bags. This was to mimic the condition and treatment of the Antarctic ice core samples.

2.2.2 Polystyrene latex particles

200 nm polystyrene latex (PSL) spheres (SPI Supplies, Structure Probe, Inc., West Chester, PA) were used to test the filtration and microscopy method, as they can be suspended in water and are readily identified on TEM grids.

2.2.3 Filters

50 kD pore size modified polyethersulfone (mPES) Hollow Fiber Filters (HFFs, Spectrum Laboratories, California) with 20 cm^2 membrane surface area, gamma irradiated for sterility, were used to concentrate samples. The 50 kD ($\sim 10 \text{ nm}$) pore size was selected to retain as many particles as possible while minimizing filtration time. Any soluble species or particulates smaller than 10 nm are removed from the solution during filtration, including dissolved salts.

2.2.4 Grids

The TEM grids used for the study were SPITM 300-mesh gold grids with a continuous (non-porous) SiO_2/SiO support film. Gold was selected due to its resistance to corrosive UP water. Additionally, the carbon coating on the traditional copper TEM grids had irregularities that made distinguishing the actual carbonaceous sample difficult, and silicon dioxide coat-

ings did not interfere with identification of carbonaceous particles using EDS spectra.

2.3 Instrumentation

A scanning electron microscope (SEM) was used to look at TEM grids prior to TEM analysis, to verify that sufficient particles were present on the grid. Scanning electron microscopy was performed with a Zeiss Neon 40EsB FIBSEM operated at 5 kV, located at Curtin University's Microscopy & Microanalysis Facility.

The transmission electron microscopy was performed on a FEI Titan G2 80-200 TEM/STEM with ChemiSTEM Technology, which incorporates scanning transmission electron microscopy (STEM) with $\sim 1 \text{ nm}$ resolution EDS mapping. Samples were imaged using both TEM and STEM, both operating at 80 kV. This instrument is located at the University of Western Australia. Additional imaging and spectroscopy was performed on a JEOL 2100 TEM operated at 120 kV and equipped with a Gatan Tridiem energy filter for EELS and energy filtered transmission electron microscopy (EFTEM) work.

2.4 Samples

2.4.1 Ice core samples

The DSS0506 ice core samples used in this study were collected in the 2005–2006 austral summer from Law Dome, East Antarctica. The ice core drilling location was at Dome Summit South (DSS), and provides overlapping ice core to the main DSS ice core ($66^\circ 46' 11'' \text{ S}$, $112^\circ 48' 25'' \text{ E}$, 1370 m elevation). Ice and snow from this site have been the subjects of a large number of studies (Burn-Nunes et al., 2011; Curran et al., 1998; Etheridge et al., 1996; Palmer et al., 2001; Pedro et al., 2012; Vallenga et al., 2002; van Ommen and Morgan, 1996, 2010). The flux of BC deposition at the same sampling site in Law Dome, East Antarctica has been quantified using an SP2 (Bisiaux et al., 2012). The ice core used in this study was cut longitudinally into two parallel sections, 1 m long with a 5 cm by 5 cm cross-section. One section was used for measuring trace ion chemicals and stable isotopes, and the matching section was transported to the TRACE facility at Curtin University for BC studies. The ice was dated by matching the dissolved ion chemistry and water stable isotope records ($\delta^{18}\text{O}$) to the main DSS ice core record to produce a depth age scale for DSS0506. The main DSS ice core record was dated using annual layer counting and identification of volcanic horizons (Plummer et al., 2012). The cores used in this study are DSS0506-38U from 70.5 m and dated to 1930 CE, DSS0506-69U from 131.5 m and dated to 1838 CE, and DSS0506-93U from 178.3 m and dated to 1759 CE. Approximately 1 cm of ice was removed from all sides during decontamination, resulting in ~ 1.5 to 2 L of melt water.

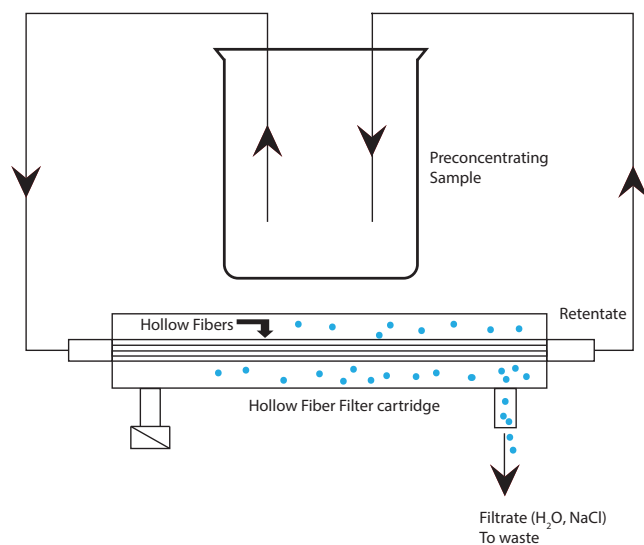


Figure 1. Tangential flow filtration setup for concentration of rain or melted ice core sample H_2O . Water sample recirculates through the hollow fiber filter, with H_2O and dissolved species removed through open side port of filter cartridge.

2.4.2 Rain samples

Monsoon rain samples were collected in Darwin, in tropical northern Australia. The region experiences a dry season (May–November) and a monsoonal wet season in the summer months (December–March) (Holland, 1986; Kaars et al., 2000), and is in close proximity to equatorial Asian biomass burning as well as annually occurring northern Australian bushfires. The samples used to test this method were collected on 8 and 11 April 2014, during the end of the wet period in Darwin when large volumes of rain could be collected in short periods of time. Rain was collected using an UP water cleaned Teflon funnel with a 1 L cleaned low density polyethylene bottle (LDPE, Nalgene) attached via a threaded cap. The funnel was placed on a bucket in an open field, with no overhead obstructions.

2.5 Decontamination and concentration method

The ice core decontamination procedure was adapted from the methods of Burn et al. (2009), Candelone et al. (1994), and Edwards et al. (2006), using materials described in Sect. 2.1 of this paper.

Ice core sections were placed on a cleaned plastic covered surface in the TRACE facility cold laboratory module. The exterior of the ice core was progressively removed and discarded using an acid-cleaned stainless steel chisel. The chisel was cleaned with 2 % nitric acid before use and rinsed with UP water in-between different ice core samples. Approximately 5 mm were removed from all surfaces of the ice using the chisel. After removing the exterior, the ice samples were transferred into an acid-cleaned colander

made from a 3 L fluorinated high-density polyethylene bottle with large holes drilled into the bottom. The colander was cleaned in 10 % nitric acid and rinsed with UP water before use. The ice samples were then rinsed with large amounts of UP water to remove a further ~ 5 mm from all surfaces. Finally the samples were removed from the colander with acid-cleaned polypropylene tongs and transferred into a 3 L perfluoro alkoxyalkane container. Ice pieces were added periodically to the perfluoro alkoxyalkane melt water container over the course of the filtration, as to keep the sample cold while filtering to avoid possible aggregation. Rain samples were filtered directly from the sampling container (1 L LDPE Nalgene bottle).

The TFF setup consisted of a recirculating HFF connected to a multichannel peristaltic pump (Ismatec IPC pump, IDEX Health & Science), detailed in Fig. 1. Samples were pumped through filters with standard PVC two-stop pump tubing and PFA tubing.

During concentration, sample water was recirculated from the bottle using the peristaltic pump, through a HFF, and then back into the sample bottle. One of two side ports on the HFF was left open over a waste container to allow filtrate to be removed with little backpressure, as backpressure on the filtrate removal line would have slowed the filtration rate. The sample bottle was elevated above the filter, and the height difference between filter and sample bottle was used to increase or decrease backpressure on the filter, speeding or slowing filtrate removal as required. Filtrate was removed at 250 mL h^{-1} , resulting in a concentration of 2 L to 1.5 mL in approximately 8 h.

The pump direction was periodically reversed, with the sample moving backwards through the filter, for ~ 5 s to avoid particle build-up on the membrane surface. The filter is also backflushed immediately prior to collecting the final concentrated sample with 1 mL of water (Fig. 2) to remove any additional particles from the membrane. Samples were concentrated to 1.5 mL in the sample bottle, transferred to a cleaned polypropylene centrifuge vial, and gently shaken to avoid particle size separation. Concentrated samples were then deposited on 5 mm TEM grids, $30 \mu\text{L}$ at a time using a clean PP pipette tip. The TEM grid was held elevated off the laboratory bench surface by SPI stainless steel tweezers in the TRACE module clean air hood at room temperature ($\sim 22^\circ\text{C}$) while the sample was evaporating down. Each $30 \mu\text{L}$ drop was left to evaporate fully between drops, depositing particles on the surface of the grid. To avoid particle separation in the solution, the sample vial was shaken immediately before each deposition. The sample vial was stored at 2°C between drops. Approximately 0.18 mL of sample was deposited to each grid.

2.6 Particle characterization using electron microscopy

Insoluble particles were characterized using electron microscopy, initially to check for sample recovery, and eventu-

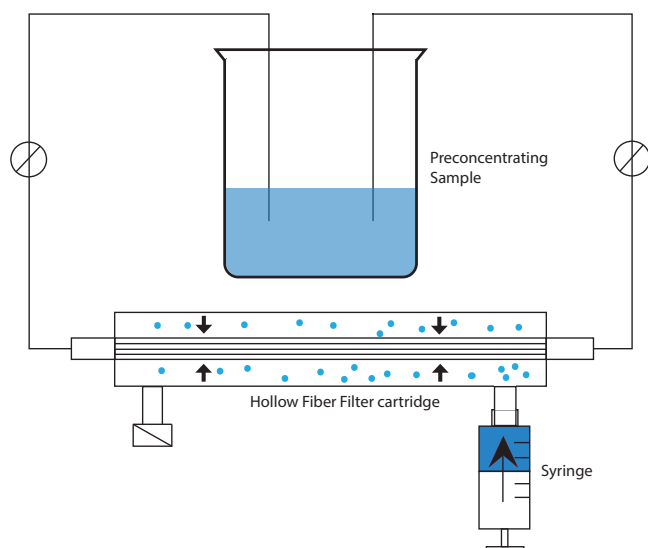


Figure 2. Backflush of hollow fiber filter membrane setup, performed by stopping the peristaltic pump and injecting 1 mL of ultrapure water into the open side port using a syringe.

ally for quantification of particle size, morphology, and composition. During recovery method development, secondary electron imaging in the SEM was used to look for particles remaining on filters as well as for inspecting TEM grids for particles recovered through filtration.

The silicon-coated grid exhibited some charging effects under the electron beam, and damaged squares of film (i.e., holes from handling with tweezers) could collapse completely when imaged in normal TEM mode. Often, spreading the beam out over a large section of grid and waiting a few minutes before imaging at higher magnification could prevent sample jumping. Film squares with large objects, such as bacteria or dust particles $> 10 \mu\text{m}$, were more susceptible to complete collapse from charging.

On the TEM, the entire area of each grid was initially surveyed at $200\text{--}500\times$ magnification to locate particles, which were then imaged at higher magnifications and EELS/EDS spectra were acquired to characterize particle types. Particles were imaged at $\sim 10\,000\times$ magnification for complex, larger aggregates, and $100\,000\text{--}200\,000\times$ magnification for fine structure and individual particle morphology. Seemingly empty portions of the grid were also surveyed at higher magnification, to verify that potential deposits of smaller particles were not overlooked.

BC was identified using various TEM results, including spherule aggregate structure, the presence of carbon peaks in EDS or EELS spectra, size of primary spherules ($\sim 30 \text{ nm}$), and “onion-ring” structure of spherules. STEM imaging and EDS were used to preserve beam-sensitive structures, such as coatings on the particles. EFTEM elemental maps were acquired using the traditional three-window technique using

energy windows adjusted to provide optimum signal-to-noise (Brydson, 2001).

2.7 Testing the cleanliness of the system

As the concentration method will concentrate both sample and contaminants, blanks were tested on each major step of the procedure to exclude the possibility of procedural contamination. Unused TEM grids were scanned prior to use for sampling. To test the cleanliness of the water, blank UP water was concentrated and deposited on TEM grids for imaging. Laboratory-made UP water blank ice was decontaminated and concentrated using the method in Sect. 2.5. The TEM samples were prepared from the concentrated solution.

3 Results and discussion

3.1 Blanks

No BC was found on any of the unused TEM grids or in any of the UP water tests. An UP water blank on the hollow fiber filter after filtering a rain sample was inspected on the TEM, and there was little evidence of cross contamination. Three, $\sim 500 \text{ nm}$ alumina silicate dust particles were found on the entire grid, surveying at $500\times$ magnification.

3.2 Tangential flow filtration

Using TFF, the ice core samples were concentrated from an average initial volume of $\sim 2 \text{ L}$ to a final volume of $1.5 \pm 0.1 \text{ mL}$, a factor of ~ 1300 . The concentration factor varied slightly due to the initial volume of the ice core melt water, which was different for each ice core sample used. This was due to variations in the size of each ice core.

The TFF method was tested with polystyrene latex (PSL) spheres (200 nm diameter). A prepared standard of 1 L of $1 \mu\text{g kg}^{-1}$ (1 ppb) PSL particles was concentrated from 1 L to $\sim 1.5 \text{ mL}$ using the method in Sect. 2.5, resulting in a final concentration of $\sim 670 \mu\text{g kg}^{-1}$. This concentrated standard was then deposited on a SiO_2/SiO coated TEM grid. SEM images of the prepared sample grid showed significant sample recovery for characterization, with areas of the grid completely obscured with spheres (Fig. 3).

Using an average BC concentration of $0.08 \mu\text{g kg}^{-1}$ from the same Law Dome location in Antarctica (Bisiaux et al., 2012) and a concentration ratio of 2 L to 1.5 mL , the final BC concentration of the ice core samples was $\sim 100 \mu\text{g kg}^{-1}$. A number of methods were tested to extract particles from water samples in this study, and these methods are detailed in Appendix A. Comparison of this TFF method with the “failed” methods in Appendix A indicate that particle recovery from TFF is more effective at both concentrating particles and keeping particles suspended in a solution, which can then be deposited on a TEM grid for characterization. Given that the melting of snow samples does not affect the

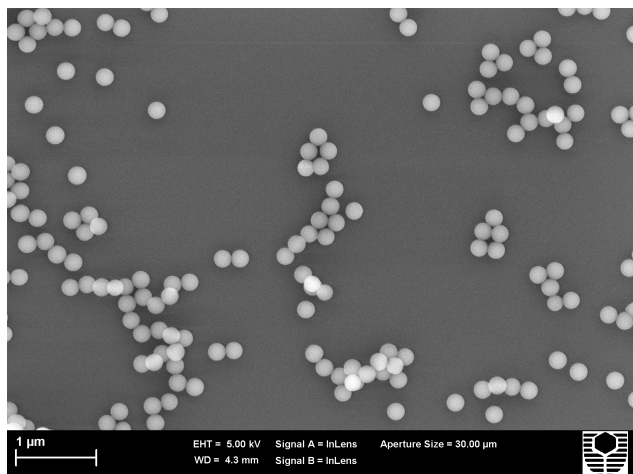


Figure 3. SEM image of PSL spheres from concentration method test on SiO_2/SiO coated grid surface, concentrated from 1 to $\sim 667 \mu\text{g kg}^{-1}$ using TFF.

size distribution of BC aerosols (Schwarz et al., 2013), the only information lost in the melting of the ice core would be any possible soluble constituents of the BC aerosols, such as soluble coatings.

3.3 Transmission electron microscopy

Results presented from this study pertaining to the relative and absolute abundance of different particle types are qualitative only, because a statistically rigorous survey of all particles on the grid was not completed. Nevertheless, the images included in this paper have been chosen to be representative of particles commonly seen while scanning the grid.

Sample charging on the SiO_2/SiO -coated grids caused difficulty with TEM and STEM imaging, as the grid would periodically shift abruptly while collecting an image. The silicon and oxygen provided a useful background when looking for carbon in EDS and EELS spectra, but a carbon-coated grid would be more stable for high-resolution imaging on the nanometer scale.

Black carbon aggregates were readily identified by their onion structure and morphology on TEM grids from both rain samples and ice core samples. In addition, STEM EDS revealed coatings and inclusions in the aggregates that would have otherwise been overlooked. STEM EDS also preserved beam-sensitive sample, including nitrogen and oxygen coatings up to 5 nm thick on the BC aggregates (Fig. 4).

Various mineral dust particles were also successfully identified in both sample suites via imaging coupled with EELS and EDS analysis (Figs. 5 and 6) and EELS and EFTEM analysis helped characterize complex dust particles containing Al, Si, Fe, and C (Fig. 6). The mixing of BC and other particulates shown in Figs. 5–7 is significant, as internal mixing of BC with other particles such as dust can affect their radiative forcing (Clarke et al., 2004; Scarnato et al., 2015).

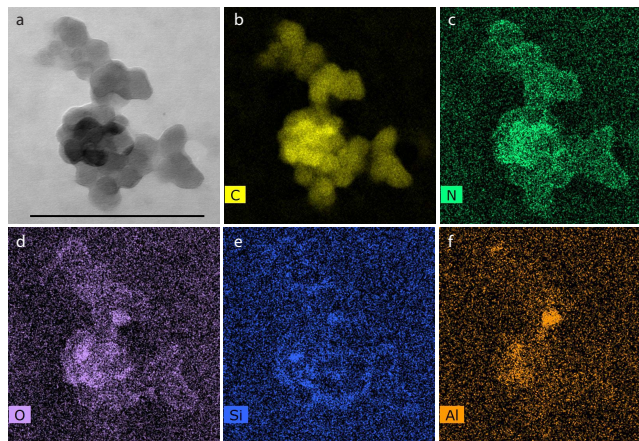


Figure 4. An example of a BC aggregate with nitrogen and oxygen coating and aluminum-rich silicate inclusions from Law Dome, Antarctica ice core dated to 1759 CE. (a) STEM image, scale bar = 300 nm. (b–f) a series of STEM EDS maps for C, N, O, Si and Al, respectively. Element maps shown are from same field of view as image (a).

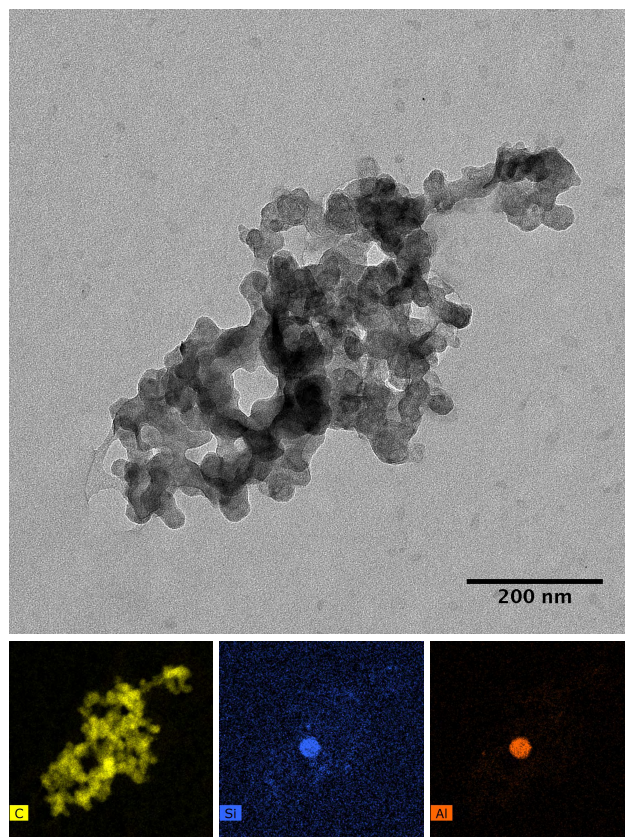


Figure 5. TEM image of a particle from Darwin rain sample collected 11 April 2014, with accompanying STEM EDS maps of carbon, silicon, and aluminum. Element maps are from the same field of view as the TEM image.

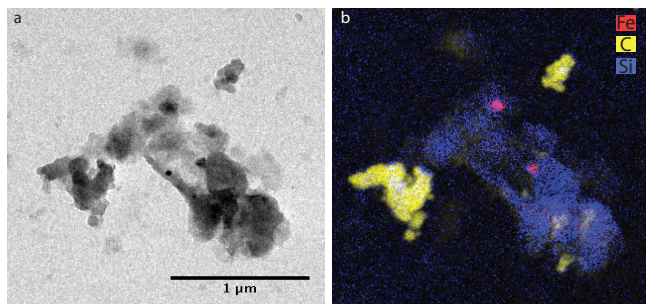


Figure 6. Examples of particles concentrated from a Law Dome, Antarctica ice core dated to 1930 CE. (a) TEM image and (b) EFTEM map of a complex aggregate particle where red is iron, blue is silicon, and yellow is carbon.

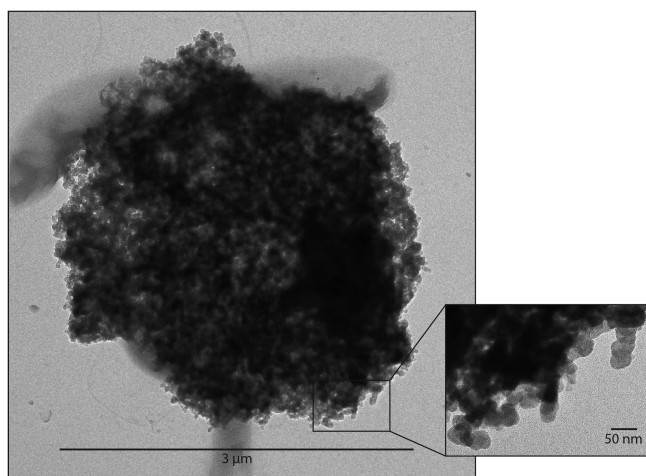


Figure 7. Aged superaggregate from Darwin rain sample collected 8 April 2014. Inset is of an enlarged section of aggregate, showing individual BC sphere structure.

STEM-EDS can distinguish variations in BC composition that may routinely be overlooked.

Both the rain and ice cores had a large quantity of BC particles, with graphitic carbon “onions” of ~ 30 nm in diameter aggregated into larger particles of ~ 80 to > 1000 nm in diameter. These particles often showed association with aluminosilicate dust particles (Fig. 5). Black carbon particles in both the rain and ice cores appeared to be significantly aged in the atmosphere as indicated by the collapsed structure of the carbon spherules (Figs. 4–7).

The surveys in this study permitted qualitative comparisons between samples. For example, in general, the rain samples had many larger BC aggregates (> 200 nm), whereas BC aggregates found in the ice cores were significantly smaller (~ 100 nm) and displayed a much more compact structure. Rain samples also contained numerous superaggregates as described in (Chakrabarty et al., 2014). These superaggregates were $> 1 \mu\text{m}$ in diameter and were absent in the ice cores (Fig. 7). Given the high particle yields from the TFF

concentration method, it is anticipated that more systematic TEM surveys could facilitate more statistically robust data on particle type and size distributions. However, this is beyond the scope of this study.

The tangential flow filtration concentration method has been used to preserve fragile structures of particles and to avoid aggregation of nanoparticles. Nevertheless, disaggregation, aggregation, and aggregate collapse are still possible outcomes of the method. However, we see no obvious evidence that these factor significantly into the results.

Tests of bond strength between carbon spheres in BC show that aggregates are unlikely to fragment into smaller units (Rothenbacher et al., 2008). Hence, disaggregation from this method is unlikely. Additionally, both the rain samples and the ice core melt water samples were processed in an identical way, including the filtration technique to concentrate the samples and the evaporation technique to deposit particles on the TEM grids. Both rain and ice core samples contained significant variations in particle size, including large amounts of smaller BC aggregates (~ 100 nm). This variety suggests that method-induced aggregation did not result in significant changes to the particle population.

The collapsed structure of the black carbon aggregates seen in the ice core samples is supported by reports of BC aging in the atmosphere (Johnson et al., 1991; Li et al., 2003; Martins et al., 1998). The BC contained in Antarctic ice cores has aged significantly from emission to deposition and would therefore likely contain collapsed aggregates. As BC is wet deposited in the rain samples, the particles are likely hydrophilic. The transition from hydrophobic to hydrophilic is a result of atmospheric aging (Stier et al., 2006), suggesting that the BC in rain has also aged significantly before deposition and will contain collapsed aggregates as well.

While post-deposition processes within the glacier cannot be ruled out, volume equivalent diameters of BC particles found in the ice (Bisiaux et al., 2012) are similar to those determined over the remote Southern Ocean by the HIPPO project (Schwarz et al., 2010). Snow densification and ice metamorphosis are more likely to aggregate BC particles into crystal junctions. If this were significant, larger particles would be expected rather than smaller ones. The differences between the BC found in rain and Antarctic ice likely reflect the loss of large aggregates during long-distance transport to Antarctica.

4 Conclusion

The results presented herein clearly show that the combination of tangential flow filtration and transmission electron microscopy methods provides an effective way to characterize both centuries-old atmospheric aerosols preserved in Antarctic ice and modern aerosols in rain water. Using a clean decontamination procedure and tangential flow filtration method, aerosols in rain and Antarctic ice have been concentrated by a factor of ~ 1300 . Tangential flow filtration

method tests with polystyrene latex particle standards have shown sufficient particle recovery for transmission electron microscopy characterization, and blank tests with ultrapure laboratory ice indicate that this process does not introduce any measureable contaminants. The results in this paper indicate that black carbon particles can form around or aggregate with dust and other mineral particulates, and aggregates can develop thin (< 5 nm) insoluble coatings of nitrogen and oxygen.

An important potential future development includes the possibility of quantification of particle sizes and types through systematic grid surveys of samples prepared from specific ice core depths. This type of survey could provide a statistically significant analysis of black carbon morphologies and chemical compositions in Antarctic ice, which could potentially reveal changes in black carbon over time.

Appendix A: Unsuccessful concentration methods

A1 Drop by drop evaporation without preconcentration

Murr et al. (2004) used a drop-by-drop method to deposit Greenland ice core melt water on a TEM grid, $\sim 3 \mu\text{L}$ at a time. The drop-by-drop method might work on higher concentration samples (i.e., temperate ice cores or snow samples), but due to low concentrations of BC in Antarctic ice cores, characterization of the particles necessitates concentrating the melted ice core prior to depositing it on a TEM grid. To preserve the largest amount of particles, the sample should be processed as quickly as possible. The longer the sample sits melted, the greater chance of losing black carbon to aggregation or diffusion to the walls of the sample container. Depending on concentration of BC in sample, the drop-by-drop method would require a significant amount of sample deposition to grid before there are sufficient particles to image ($\sim 1 \text{ L}$, deposited $3 \mu\text{L}$ at a time), potentially losing particles in the sample as each drop dries on the grid.

A2 Vacuum ablating ice

We attempted to vacuum ablate ice, to avoid putting the BC into solution where it might lose soluble portions of the structure. This was tested on a Christ Alpha 1–2 LD Freeze Dryer. It took approximately 6 hours for a 5 cm^3 piece of blank ice to halve in size. A substantially larger ice core sample is required to obtain sufficient particles for characterization in low-concentration Antarctic ice.

A3 Anopore filtration followed by back flushing

Preconcentration was attempted using a 200 nm pore-size Anopore polycarbonate filter. An ice core sample was melted and filtered using the peristaltic pump and an Anopore filter in a Teflon filter holder. The filter was then backflushed with $\sim 5 \text{ mL}$ of Milli-q water using a syringe.

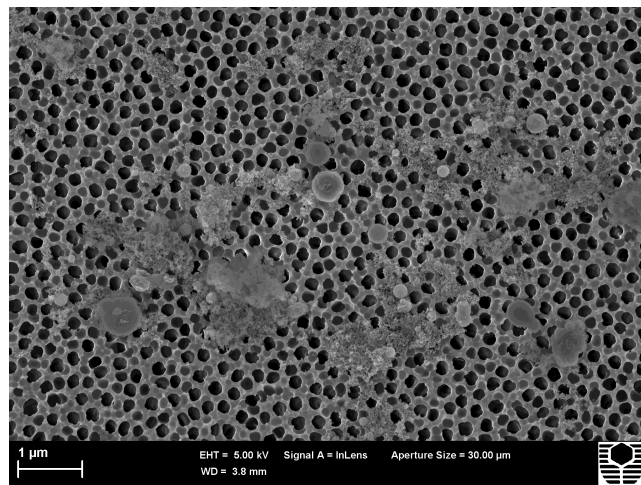


Figure A1. SEM image of Anopore filter after filtering 1 L of ice core melt water, and backflushing the filter to remove filtered particles.

SEM imaging of TEM grids made from the backflushed sample solution indicates only a small fraction of particles were recovered from the filter. Further SEM imaging of the filter itself showed large amounts of particulates remained stuck to the filter surface and were not removed through backflushing (Fig. A1). Ultrasonication was not used to dislodge particles due to the possible separation of aerosol aggregates, compromising the characterization results of BC aggregates. This could be a useful method for a lower-magnification scanning electron microscopy (SEM) study of larger aerosols, but large pore size and complicated filter structure makes locating smaller BC aggregates difficult.

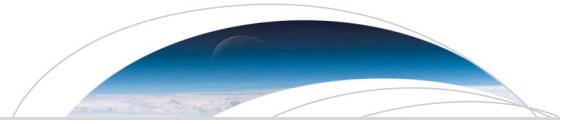
Acknowledgements. This work was supported by Australian Antarctic Sciences Grant 4144. The authors acknowledge the use of Curtin University's Microscopy & Microanalysis Facility, whose instrumentation has been partially funded by the University, State and Commonwealth Governments. The authors acknowledge the facilities, and the scientific and technical assistance of the Australian Microscopy & Microanalysis Research Facility at the Centre for Microscopy, Characterisation & Analysis, The University of Western Australia, a facility funded by the University, State, and Commonwealth Governments.

Edited by: P. Herckes

References

- Benner, R., Biddanda, B., Black, B., and McCarthy, M.: Abundance, size distribution, and stable carbon and nitrogen isotopic compositions of marine organic matter isolated by tangential-flow ultrafiltration, *Mar. Chem.*, 57, 243–263, doi:10.1016/S0304-4203(97)00013-3, 1997.
- Bisiaux, M. M., Edwards, R., McConnell, J. R., Curran, M. A. J., Van Ommen, T. D., Smith, A. M., Neumann, T. A., Pasteris, D. R., Penner, J. E., and Taylor, K.: Changes in black carbon deposition to Antarctica from two high-resolution ice core records, 1850–2000 AD, *Atmos. Chem. Phys.*, 12, 4107–4115, doi:10.5194/acp-12-4107-2012, 2012.
- Bond, T. C., Doherty, S. J., Fahey, D., Forster, P., Berntsen, T., DeAngelo, B., Flanner, M., Ghan, S., Kärcher, B., and Koch, D.: Bounding the role of black carbon in the climate system: a scientific assessment, *J. Geophys. Res.-Atmos.*, 118, 5380–5552, 2013.
- Brydson, R.: *Electron Energy Loss Spectroscopy*, Bios in association with the Royal Microscopical Society, Oxford, 2001.
- Burn, L. J., Rosman, K. J. R., Candelone, J.-P., Vallelonga, P., Burton, G. R., Smith, A. M., Morgan, V. I., Barbante, C., Hong, S., and Boutron, C. F.: An ultra-clean technique for accurately analysing Pb isotopes and heavy metals at high spatial resolution in ice cores with sub-pg g(-1) Pb concentrations, *Anal. Chim. Acta*, 634, 228–236, doi:10.1016/j.aca.2008.11.067, 2009.
- Burn-Nunes, L. J., Vallelonga, P., Loss, R. D., Burton, G. R., Moy, A., Curran, M., Hong, S., Smith, A. M., Edwards, R., Morgan, V. I., and Rosman, K. J. R.: Seasonal variability in the input of lead, barium and indium to Law Dome, Antarctica, *Geochim. Cosmochim. Ac.*, 75, 1–20, doi:10.1016/j.gca.2010.09.037, 2011.
- Buseck, P. R. and Adachi, K.: Nanoparticles in the atmosphere, *Elements*, 4, 389–394, doi:10.2113/Gselements.4.6.389, 2008.
- Candelone, J.-P., Hong, S., and Boutron, C. F.: An improved method for decontaminating polar snow or ice cores for heavy metal analysis, *Anal. Chim. Acta*, 299, 9–16, doi:10.1016/0003-2670(94)00327-0, 1994.
- Chakrabarty, R. K., Beres, N. D., Moosmuller, H., China, S., Mazzoleni, C., Dubey, M. K., Liu, L., and Mishchenko, M. I.: Soot superaggregates from flaming wildfires and their direct radiative forcing, *Sci. Rep.* 4, 5508, doi:10.1038/srep05508, 2014.
- Clarke, A. D., Shinozuka, Y., Kapustin, V. N., Howell, S., Huebert, B., Doherty, S., Anderson, T., Covert, D., Anderson, J., Hua, X., Moore, K. G., McNaughton, C., Carmichael, G., and Weber, R.: Size distributions and mixtures of dust and black carbon aerosol in Asian outflow: Physicochemistry and optical properties, *J. Geophys. Res.-Atmos.*, 109, D15S09, 2004.
- Curran, M. A., Van Ommen, T. D., and Morgan, V.: Seasonal characteristics of the major ions in the high-accumulation Dome Summit South ice core, Law Dome, Antarctica, *Ann. Glaciol.*, 27, 385–390, 1998.
- Dalwadi, G., Benson, H. E., and Chen, Y.: Comparison of diafiltration and tangential flow filtration for purification of nanoparticle suspensions, *Pharm. Res.*, 22, 2152–2162, doi:10.1007/s11095-005-7781-z, 2005.
- Edwards, R., Sedwick, P., Morgan, V., and Boutron, C.: Iron in ice cores from Law Dome: a record of atmospheric iron deposition for maritime East Antarctica during the Holocene and Last Glacial Maximum, *Geochem. Geophys. Geosy.*, 7, Q12Q01, doi:10.1029/2006GC001307, 2006.
- Etheridge, D., Steele, L., Langenfelds, R., Francey, R., Barnola, J. M., and Morgan, V.: Natural and anthropogenic changes in atmospheric CO₂ over the last 1000 years from air in Antarctic ice and firn, *J. Geophys. Res.-Atmos.*, 101, 4115–4128, 1996.
- Flanner, M. G., Zender, C. S., Randerson, J. T., and Rasch, P. J.: Present-day climate forcing and response from black carbon in snow, *J. Geophys. Res.-Atmos.*, 112, D11202, doi:10.1029/2006jd008003, 2007.
- Giovannoni, S., DeLong, E., Schmidt, T., and Pace, N.: Tangential flow filtration and preliminary phylogenetic analysis of marine picoplankton, *Appl. Environ. Microb.*, 56, 2572–2575, 1990.
- Hansen, J. and Nazarenko, L.: Soot climate forcing via snow and ice albedos, *P. Natl. Acad. Sci. USA*, 101, 423–428, doi:10.1073/Pnas.2237157100, 2004.
- Hegg, D. A., Warren, S. G., Grenfell, T. C., Doherty, S. J., Larson, T. V., and Clarke, A. D.: Source attribution of black carbon in Arctic snow, *Environ. Sci. Technol.*, 43, 4016–4021, doi:10.1021/es803623f, 2009.
- Hodnebrog, Ø., Myhre, G., and Samset, B. H.: How shorter black carbon lifetime alters its climate effect, *Nat. Commun.*, 5, 6065, doi:10.1038/ncomms6065, 2014.
- Holland, G. J.: Interannual variability of the Australian summer monsoon at Darwin: 1952–82, *Mon. Weather Rev.*, 114, 594–604, doi:10.1175/1520-0493(1986)114<0594:IVOTAS>2.0.CO;2, 1986.
- Jacobson, M. Z.: Strong radiative heating due to the mixing state of black carbon in atmospheric aerosols, *Nature*, 409, 695–697, 2001.
- Johnson, B., Shine, K., and Forster, P.: The semi-direct aerosol effect: impact of absorbing aerosols on marine stratocumulus, *Q. J. Roy. Meteor. Soc.*, 130, 1407–1422, 2004.
- Johnson, D. W., Kilsby, C. G., McKenna, D. S., Saunders, R. W., Jenkins, G. J., Smith, F. B., and Foot, J. S.: Airborne observations of the physical and chemical characteristics of the Kuwait oil smoke plume, *Nature*, 353, 617–621, 1991.
- Kaars, S. v. d., Wang, X., Kershaw, P., Guichard, F., and Setiabudi, D. A.: A Late Quaternary palaeoecological record from the Banda Sea, Indonesia: patterns of vegetation, climate and biomass burning in Indonesia and northern Australia, *Palaeogeogr. Palaeoclimatol.*, 155, 135–153, doi:10.1016/S0031-0182(99)00098-X, 2000.

- Koch, D., Schulz, M., Kinne, S., McNaughton, C., Spackman, J. R., Balkanski, Y., Bauer, S., Bernsten, T., Bond, T. C., Boucher, O., Chin, M., Clarke, A., De Luca, N., Dentener, F., Diehl, T., Dubovik, O., Easter, R., Fahey, D. W., Feichter, J., Fillmore, D., Freitag, S., Ghan, S., Ginoux, P., Gong, S., Horowitz, L., Iversen, T., Kirkevåg, A., Klimont, Z., Kondo, Y., Krol, M., Liu, X., Miller, R., Montanaro, V., Moteki, N., Myhre, G., Penner, J. E., Perlwitz, J., Pitari, G., Reddy, S., Sahu, L., Sakamoto, H., Schuster, G., Schwarz, J. P., Seland, Ø., Stier, P., Takegawa, N., Takemura, T., Textor, C., van Aardenne, J. A., and Zhao, Y.: Evaluation of black carbon estimations in global aerosol models, *Atmos. Chem. Phys.*, 9, 9001–9026, doi:10.5194/acp-9-9001-2009, 2009.
- Li, J., Pósfai, M., Hobbs, P. V., and Buseck, P. R.: Individual aerosol particles from biomass burning in southern Africa: 2, Compositions and aging of inorganic particles, *J. Geophys. Res.-Atmos.*, 108, 8484, doi:10.1029/2002JD002310, 2003.
- Martins, J. V., Artaxo, P., Liousse, C., Reid, J. S., Hobbs, P. V., and Kaufman, Y. J.: Effects of black carbon content, particle size, and mixing on light absorption by aerosols from biomass burning in Brazil, *J. Geophys. Res.-Atmos.*, 103, 32041–32050, 1998.
- McConnell, J. R., Edwards, R., Kok, G. L., Flanner, M. G., Zender, C. S., Saltzman, E. S., Banta, J. R., Pasteris, D. R., Carter, M. M., and Kahl, J. D. W.: 20th-century industrial black carbon emissions altered arctic climate forcing, *Science*, 317, 1381–1384, doi:10.1126/Science.1144856, 2007.
- Moffet, R. C. and Prather, K. A.: In-situ measurements of the mixing state and optical properties of soot with implications for radiative forcing estimates, *P. Natl. Acad. Sci. USA*, 106, 11872–11877, 2009.
- Murr, L. E., Esquivel, E. V., Bang, J. J., de la Rosa, G., and Gardea-Torresdey, J. L.: Chemistry and nanoparticulate compositions of a 10,000 year-old ice core melt water, *Water Res.*, 38, 4282–4296, doi:10.1016/J.Watres.2004.08.010, 2004.
- Ohata, S., Moteki, N., and Kondo, Y.: Evaluation of a method for measurement of the concentration and size distribution of black carbon particles suspended in rainwater, *Aerosol Sci. Tech.*, 45, 1326–1336, doi:10.1080/02786826.2011.593590, 2011.
- Palmer, A. S., van Ommen, T. D., Curran, M. A., Morgan, V., Souney, J. M., and Mayewski, P. A.: High-precision dating of volcanic events (AD 1301–1995) using ice cores from Law Dome, Antarctica, *J. Geophys. Res.*, 106, 28089, doi:10.1029/2001JD000330, 2001.
- Pedro, J. B., McConnell, J. R., van Ommen, T. D., Fink, D., Curran, M. A. J., Smith, A. M., Simon, K. J., Moy, A. D., and Das, S. B.: Solar and climate influences on ice core ^{10}Be records from Antarctica and Greenland during the neutron monitor era, *Earth Planet. Sc. Lett.*, 355, 174–186, doi:10.1016/j.epsl.2012.08.038, 2012.
- Plummer, C. T., Curran, M. A. J., van Ommen, T. D., Rasmussen, S. O., Moy, A. D., Vance, T. R., Clausen, H. B., Vinther, B. M., and Mayewski, P. A.: An independently dated 2000 yr volcanic record from Law Dome, East Antarctica, including a new perspective on the dating of the 1450s CE eruption of Kuwae, Vanuatu, *Clim. Past*, 8, 1929–1940, doi:10.5194/cp-8-1929-2012, 2012.
- Pósfai, M., Anderson, J. R., Buseck, P. R., and Sievering, H.: Soot and sulfate aerosol particles in the remote marine troposphere, *J. Geophys. Res.-Atmos.*, 104, 21685–21693, 1999.
- Rothenbacher, S., Messerer, A., and Kasper, G.: Fragmentation and bond strength of airborne diesel soot agglomerates, *Particle and fibre toxicology*, 5, 9, doi:10.1186/1743-8977-5-9, 2008.
- Scarnato, B. V., China, S., Nielsen, K., and Mazzoleni, C.: Perturbations of the optical properties of mineral dust particles by mixing with black carbon: a numerical simulation study, *Atmos. Chem. Phys.*, 15, 6913–6928, doi:10.5194/acp-15-6913-2015, 2015.
- Schwarz, J., Gao, R., Fahey, D., Thomson, D., Watts, L., Wilson, J., Reeves, J., Darbeheshti, M., Baumgardner, D., and Kok, G.: Single-particle measurements of midlatitude black carbon and light-scattering aerosols from the boundary layer to the lower stratosphere, *J. Geophys. Res.-Atmos.*, 111, D16207, doi:10.1029/2006JD007076, 2006.
- Schwarz, J. P., Spackman, J. R., Gao, R. S., Watts, L. A., Stier, P., Schulz, M., Davis, S. M., Wofsy, S. C., and Fahey, D. W.: Global-scale black carbon profiles observed in the remote atmosphere and compared to models, *Geophys. Res. Lett.*, 37, L18812, doi:10.1029/2010GL044372, 2010.
- Schwarz, J. P., Gao, R. S., Perring, A. E., Spackman, J. R., and Fahey, D. W.: Black carbon aerosol size in snow, *Sci. Rep.*, 3, 1356, doi:10.1038/srep01356, 2013.
- Slowik, J. G., Cross, E. S., Han, J.-H., Davidovits, P., Onasch, T. B., Jayne, J. T., Williams, L. R., Canagaratna, M. R., Worsnop, D. R., and Chakrabarty, R. K.: An inter-comparison of instruments measuring black carbon content of soot particles, *Aerosol Sci. Tech.*, 41, 295–314, 2007.
- Stier, P., Seinfeld, J. H., Kinne, S., Feichter, J., and Boucher, O.: Impact of nonabsorbing anthropogenic aerosols on clear-sky atmospheric absorption, *J. Geophys. Res.-Atmos.*, 111, D18201, doi:10.1029/2006JD007147, 2006.
- Stohl, A. and Sodemann, H.: Characteristics of atmospheric transport into the Antarctic troposphere, *J. Geophys. Res.-Atmos.*, 115, D02305, doi:10.1029/2009jd012536, 2010.
- Torres, A., Bond, T. C., Lehmann, C. M. B., Subramanian, R., and Hadley, O. L.: Measuring organic carbon and black carbon in rainwater: evaluation of methods, *Aerosol Sci. Tech.*, 48, 239–250, doi:10.1080/02786826.2013.868596, 2013.
- Utsunomiya, S., and Ewing, R. C.: Application of high-angle annular dark field scanning transmission electron microscopy, scanning transmission electron microscopy-energy dispersive X-ray spectrometry, and energy-filtered transmission electron microscopy to the characterization of nanoparticles in the environment, *Environ. Sci. Technol.*, 37, 786–791, doi:10.1021/es026053t, 2003.
- Vallelonga, P., Van de Velde, K., Candelone, J.-P., Morgan, V., Boutron, C., and Rosman, K.: The lead pollution history of Law Dome, Antarctica, from isotopic measurements on ice cores: 1500 AD to 1989 AD, *Earth Planet. Sc. Lett.*, 204, 291–306, 2002.
- van Ommen, T. D. and Morgan, V.: Peroxide concentrations in the Dome summit south ice core, Law Dome, Antarctica, *J. Geophys. Res.-Atmos.*, 101, 15147–15152, 1996.
- van Ommen, T. D. and Morgan, V.: Snowfall increase in coastal East Antarctica linked with southwest Western Australian drought, *Nature Geosci.*, 3, 267–272, 2010.
- Warren, S. G. and Clarke, A. D.: Soot in the atmosphere and snow surface of Antarctica, *J. Geophys. Res.-Atmos.*, 95, 1811–1816, doi:10.1029/JD095iD02p01811, 1990.



RESEARCH LETTER

10.1002/2016GL071042

Key Points:

- Individual black carbon particles extracted from Antarctic ice
- Single spherule black carbon aerosol particles found in modern rain and in ice cores dating both before and after industrialization
- Black carbon particles found with iron inclusions, suggesting a transport pathway for iron deposition in the Southern Ocean

Supporting Information:

- Supporting Information S1

Correspondence to:

R. Edwards,
r.edwards@curtin.edu.au

Citation:

Ellis, A., et al. (2016), Individual particle morphology, coatings, and impurities of black carbon aerosols in Antarctic ice and tropical rainfall, *Geophys. Res. Lett.*, 43, 11,875–11,883, doi:10.1002/2016GL071042.

Received 2 SEP 2016

Accepted 1 NOV 2016

Accepted article online 4 NOV 2016

Published online 19 NOV 2016

Individual particle morphology, coatings, and impurities of black carbon aerosols in Antarctic ice and tropical rainfall

Aja Ellis^{1,2}, Ross Edwards¹, Martin Saunders³, Rajan K. Chakrabarty⁴, R. Subramanian², Nicholas E. Timms⁵, Arie van Riessen¹, Andrew M. Smith⁶, Dionisia Lambrinidis⁷, Laurie J. Nunes¹, Paul Vallelonga⁸, Ian D. Goodwin⁹, Andrew D. Moy^{10,11}, Mark A. J. Curran^{10,11}, and Tas D. van Ommen^{10,11}

¹Physics and Astronomy, Curtin University, Perth, Western Australia, Australia, ²Department of Mechanical Engineering, Carnegie Mellon University, Pittsburgh, Pennsylvania, USA, ³Centre for Microscopy, Characterisation, and Analysis, University of Western Australia, Perth, Western Australia, Australia, ⁴Department of Energy, Environmental & Chemical Engineering, Washington University in St. Louis, St. Louis, Missouri, USA, ⁵Department of Applied Geology, Curtin University, Perth, Western Australia, Australia, ⁶Australian Nuclear Science and Technology Organisation, Sydney, New South Wales, Australia, ⁷Research Institute for the Environment and Livelihoods, Charles Darwin University, Darwin, Northern Territory, Australia, ⁸Centre for Ice and Climate, Niels Bohr Institute, University of Copenhagen, Copenhagen, Denmark, ⁹Marine Climate Risk Group, Department of Environmental Sciences, Macquarie University, Sydney, New South Wales, Australia, ¹⁰Australian Antarctic Division, Kingston, Tasmania, Australia, ¹¹Antarctic Climate and Ecosystems Cooperative Research Centre, University of Tasmania, Hobart, Tasmania, Australia

Abstract Black carbon (BC) aerosols are a large source of climate warming, impact atmospheric chemistry, and are implicated in large-scale changes in atmospheric circulation. Inventories of BC emissions suggest significant changes in the global BC aerosol distribution due to human activity. However, little is known regarding BC's atmospheric distribution or aged particle characteristics before the twentieth century. Here we investigate the prevalence and structural properties of BC particles in Antarctic ice cores from 1759, 1838, and 1930 Common Era (C.E.) using transmission electron microscopy and energy-dispersive X-ray spectroscopy. The study revealed an unexpected diversity in particle morphology, insoluble coatings, and association with metals. In addition to conventionally occurring BC aggregates, we observed single BC monomers, complex aggregates with internally, and externally mixed metal and mineral impurities, tar balls, and organonitrogen coatings. The results of the study show BC particles in the remote Antarctic atmosphere exhibit complexity that is unaccounted for in atmospheric models of BC.

1. Introduction

Black carbon (BC) aerosols are primary particles emitted by fossil fuel combustion and biomass burning. They have a multitude of effects on the global atmosphere and Earth's surface, which result in the second largest contribution to climate change after carbon dioxide (CO₂) [Bond et al., 2013]. Unlike CO₂ and methane gas (CH₄), BC's atmospheric residence time is relatively short (weeks as opposed to decades) and its atmospheric concentration is highly variable [Kaufman et al., 2002]. BC emissions may have already contributed to large-scale changes in atmospheric circulation, with models suggesting that the Northern Hemisphere tropics expand linearly with increasing radiative forcing from BC emissions [Kovilakam and Mahajan, 2015]. The physical, chemical, and optical properties of BC are dynamic and evolve during atmospheric transport [Browne et al., 2015; Shen et al., 2014; Wang et al., 2014]. Estimates of BC climate sensitivity are complicated by hemispheric differences in both emission sources (fossil fuels or biomass burning) and coemitted chemical species, which coat and react with BC in the atmosphere. Indeed, BC from East Asian fossil fuel may be removed from the atmosphere faster than expected due to coemitted sulfate [Shen et al., 2014].

Morphologically, BC particles are semifractal aggregates composed of small, ~30 nm semigraphitic carbon nanospheres [Andreae and Gelencsér, 2006]. Graphitic carbon consists of randomly oriented graphite crystallites with a mean intercrystallite distance of 2.5 nm, embedded in a matrix of amorphous carbon [Franklin, 1950, 1951]. After emission, BC rapidly ages in the atmosphere. The fractal dimensions of BC aggregates increase, and their surfaces become coated and partially oxidized, affecting both their optical

properties and their interaction with water [McFiggans *et al.*, 2006; Oshima *et al.*, 2009]. The evolution of the BC surface from hydrophobic to hydrophilic has a major influence on its aerodynamic size, its removal from the atmosphere by wet deposition, and its subsequent transport and residence time in the atmosphere [Shen *et al.*, 2014]. Other insoluble particles may become externally and internally mixed with BC, thereby changing its optical properties [Scarnato *et al.*, 2015]. While there have been many characterization studies of freshly emitted BC aggregates [Chakrabarty *et al.*, 2006a; Chakrabarty *et al.*, 2006b; Pósfai *et al.*, 2003; Zhu *et al.*, 2013], few studies have investigated the morphology and characteristics of aged BC aggregates in the remote Southern Hemisphere (SH) [Pósfai *et al.*, 1999]. Consequently, the full range of properties of BC and their climate forcing effects remain uncertain. Furthermore, little is known with regard to historic records of atmospheric BC before the last few decades. Polar ice cores preserve an extensive history of atmospherically transported and aged BC particles and provide an opportunity to study changes in the physical and chemical properties of long-distance transported BC during and before the industrial revolution. Building upon the development of a method to concentrate BC particles in water [Ellis *et al.*, 2015], we investigated individual particles in an Antarctic ice core using electron microscopy.

Previous studies of BC in Antarctica have included bulk aerosol measurements, mass concentrations, and optical properties of Antarctic snow and ice [Bisiaux *et al.*, 2012; Warren and Clarke, 1990; Weller *et al.*, 2013; Wolff and Cachier, 1998]. These studies identified large seasonal variations in coastal East and West Antarctic BC aerosol concentrations with a primary peak in October that is associated with dry-season biomass burning on nearby continents. A smaller secondary peak in BC concentration is observed during austral summer fire season [Weller *et al.*, 2013] with minimum concentrations in March–April. High-temporal resolution ice core studies found similar seasonality in West and East Antarctic ice concentrations during the past 200 years [Bisiaux *et al.*, 2012]. The seasonality and atmospheric circulation associated with BC in the Antarctic atmosphere [Bisiaux *et al.*, 2012; Stohl and Sodemann, 2010] suggest that long-range transported SH biomass burning emissions are the primary source of BC to Antarctica.

Although ultratrace BC concentrations ($0.08 \mu\text{g kg}^{-1}$) have been determined in Antarctic ice and snow, little is known with regard to individual particle morphology, coatings, and impurities. These characteristics impact the particles' optical and radiative properties, residence time in the atmosphere, and climatic impacts. Here we present results from the detailed analysis of individual particles found in an East Antarctic ice core and modern tropical rain samples from northern Australia. Three samples were prepared from ice core samples from the Law Dome ice cap, East Antarctica, dated from 1759, 1838, and 1930 Common Era (C.E.), predating and postdating global industrialization and western colonization of Australia. Tropical rain samples were collected in northern Australia to provide a complementary modern comparison to Antarctic ice, as wet-deposited BC close to potential source emissions. All samples were analyzed using high-resolution transmission electron microscope imaging (HR-TEM) and scanning transmission electron microscope energy-dispersive X-ray spectroscopy (STEM-EDS, hereafter EDS).

2. Materials and Methods

2.1. Ice Core Samples

Antarctic ice core samples consisted of ice sections subsampled from the Dome Summit South site (DSS0506, $66^{\circ}46'S$, $112^{\circ}48'E$, 1370 m elevation) drilled on Law Dome, East Antarctica, during the 2005–2006 austral summer. The site has been described and studied in detail [Curran *et al.*, 1998; Edwards *et al.*, 2006; Etheridge *et al.*, 1996; van Ommen and Morgan, 1996]. The depth/age scale of the ice core was constructed by matching dissolved ion chemistry and water stable isotope records ($\delta^{18}\text{O}$) to the main DSS ice core record, which was dated using annual layer counting and validated by well-characterized volcanic horizons [Plummer *et al.*, 2012].

2.2. Rain Samples

Tropical rain samples were collected in Darwin, Northern Territory, Australia, to compare modern BC in wet deposition, close to BC sources. Two rain samples of ~ 1 L each were collected in April 2014, a period of significant monsoonal rainfall in the Northern Territory. Boundary layer atmospheric circulation to the sampling site during April 2014 was predominately east-west, passing over northern Queensland and the Gulf of Carpentaria before arriving in the Northern Territory.

Samples were collected in low-density polyethylene bottles, rinsed with ultrapure (UP) water ($\rho > 18.2 \text{ M}\Omega \text{ cm}$). A full account of sample collection and handling is described in *Ellis et al.* [2015].

2.3. Ice Core Decontamination and Liquid Preconcentration

Mass concentrations of BC in Antarctic snow and ice are typically found in the parts per trillion level and require preconcentration before analysis by transmission electron microscopy (TEM). While Antarctic snow BC concentrations are low, the concentrations of other species, such as sea salts, may be present at the high parts per billion level, depending on the location. The presence of relatively high concentrations of dissolved salts species complicates sample preconcentration and obscures BC particles loaded on TEM grids. To concentrate BC particles from ice core samples and rain without concentrating dissolved salts, we used the tangential flow filtration (TFF) preconcentration method [*Ellis et al.*, 2015]. Meltwater from $1 \text{ m} \times 5 \text{ cm} \times 5 \text{ cm}$ ice core sections, representing approximately 2 years of deposition to the site, was concentrated by approximately a factor of 1000 using hollow fiber filters (10 nm pore size, Spectrum Labs, USA). The TFF concentrate from each sample was transferred to a TEM grid (SPI 300-mesh gold grids with a continuous SiO/SiO_2 support film) and evaporated down within an ISO 10 clean hood. Tropical rainwater samples were processed identically to the ice core meltwater.

2.4. TEM Characterization

Characterization (imaging of external morphology and internal structure, size, and composition) of the insoluble particles and their coatings was completed on an FEI Titan G2 80-200 TEM/STEM with ChemiSTEM Technology at The University of Western Australia, operating at 80 kV to minimize the risk of structural damage to the carbon spheres. High-angle annular dark-field scanning transmission electron microscopy (HAADF-STEM) imaging and element mapping were also carried out at 80 kV on the same instrument. The element maps were obtained by energy-dispersive X-ray spectroscopy using the Super-X detector on the Titan with a subnanometer probe size, a probe current of $\sim 0.25 \text{ nA}$, a dwell time of 15 ms, and total acquisition time of 20 to 30 min. Statistical evaluation of the proportions and size distribution of the various BC morphologies was inhibited because the TEM grids were not surveyed systematically—irregular deposition of particles on the grids and the limited field of view ($< 10 \mu\text{m}$) resulting from the high magnification of the instrument makes location and characterization of BC particles time intensive, and acquisition of significant BC morphotype population statistics difficult. Therefore, the images selected for this paper represent common BC morphologies and characteristics seen while imaging the TEM grid. Images of additional particle types can be found in the supporting information.

3. Results

In all samples, abundant single BC nanospheres (Figure 1) in addition to conventional multispherule aggregates were observed. The nanoparticles were identified by their $\sim 30 \text{ nm}$ diameter, concentric “onion” carbon layering with short-range order, and the $K\alpha$ carbon peak in the EDS spectra. Single BC nanospheres are not thought to exist individually in the atmosphere [*Andreae and Gelencsér*, 2006] and to our knowledge have not previously been observed in ice or snow. However, their presence in Antarctic ice suggests that they must be ubiquitous in the global atmosphere. Because of their small size and the confounding presence of larger BC aggregates and other dust particles, the single spheres are difficult to discern without the use of STEM-EDS mapping. They have too little mass to be quantified by real-time single BC particle analysis instruments used in other studies [*Slowik et al.*, 2007]. It would be difficult to distinguish the single nanospheres in the presence of concentrated salts or sulfates. The preconcentration method used in this study removes dissolved salts and other water-soluble species, retaining insoluble particles. Our method is also extremely gentle (mechanically) and unlikely to provide enough mechanical force to separate the aggregates [*Rothenbacher et al.*, 2008]. Further investigation has revealed many examples of doublet and triplet BC nanospheres of various primary particle sizes (Figures 1b–1d). Single BC nanospheres were found in all ice core samples (dated to 1759, 1838, and 1930 C.E.) via HR-TEM. The rain samples also contained all of the nanosphere varieties that were seen in the ice cores, indicating their possible global presence.

Although quantification is difficult for irregularly distributed nanoparticles on TEM grids, a preliminary estimate of the prevalence of single BC nanospheres can be obtained using a single particle soot

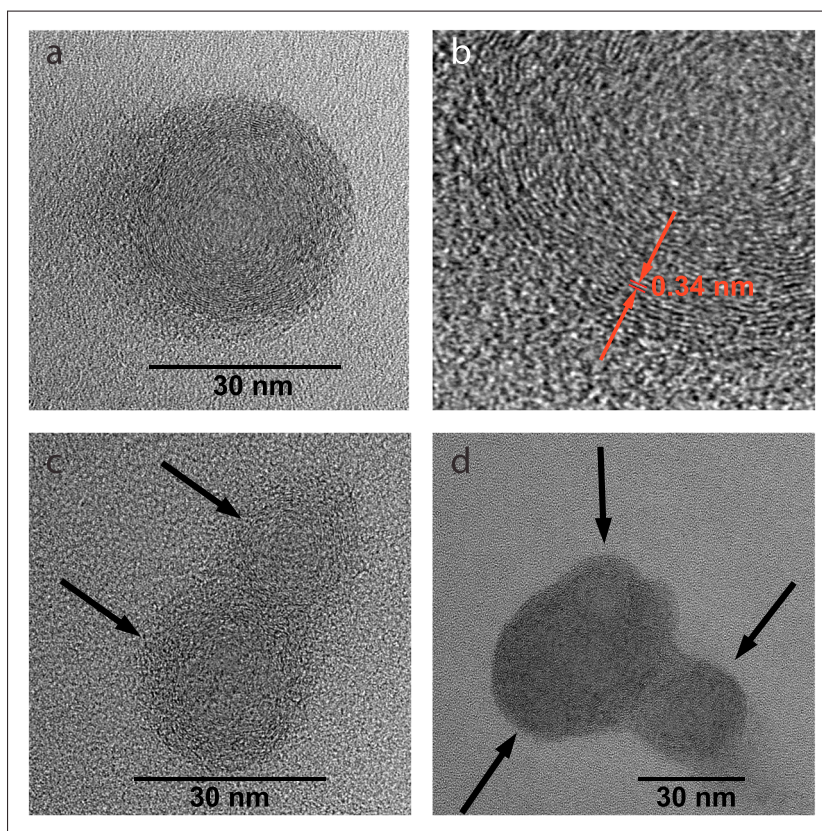


Figure 1. Black carbon nanospheres in Antarctic ice dated to 1838 C.E.: (a) single BC nanosphere showing concentric ring structure with short-range internal structure, (b) enlarged section of Figure 1a, showing the concentric layers with 0.34 nm spacing between layers, (c) BC particle with two spherules, arrows indicating spheres, and (d) BC particle with three spherules, arrows indicating spheres. Additional examples of single spheres from 1759 CE and 1930 CE are included in the supporting information.

photometer (SP2, Droplet Measurement Technologies). Indeed, BC size distribution data in twentieth century ice from the same location in East Antarctica indicate that a substantial fraction of BC particles exists below the below 0.7 fg (90 nm mass-equivalent diameter assuming a BC density of 1.8 g/cm^3), the lower mass limit where the SP2 begins to detect less than 100% of BC aerosols, supporting the existence of these individual nanospheres in great numbers—primary nanospheres may outnumber the larger BC aggregates that have previously been reported.

This observation raises significant questions about the prevalence of single BC nanospheres, as well as the undescribed effects of single nanospheres on the environment. Modern scattering calculations for BC suggest that variations in size distribution, composition, or shape could have substantial effects on common spherical and Rayleigh-Debye-Gans simplifications [Smith and Grainger, 2014]. Though the individual nanospheres are likely to be too small to function as cloud condensation nuclei, aerosol chamber experiments have shown 30 nm metallic nanoparticles [Saunders et al., 2010] as well as conventional BC aggregates [DeMott et al., 1999] acting as ice nuclei in the atmosphere. This suggests the possibility that individual 30 nm BC nanospheres may contribute to the formation of ice particles in the atmosphere, thereby having an as yet unmeasured climate affect.

In addition to the single spherules, many other distinct BC characteristics were observed in the ice cores. We found a continuum of BC aggregate sizes ranging from doublet and triplet BC spherules (Figures 1c and 1d) up to many hundred nanometers (Figures 2 and 3). While the fractal dimension of the aggregates was not determined, they appeared to be relatively compact as would be expected of BC that has been substantially aged in the atmosphere and suspended in liquid water during the concentration procedure. All BC aggregates exhibited some form of thin insoluble coating ($\sim 5 \text{ nm}$) that connected the individual spherules, similar

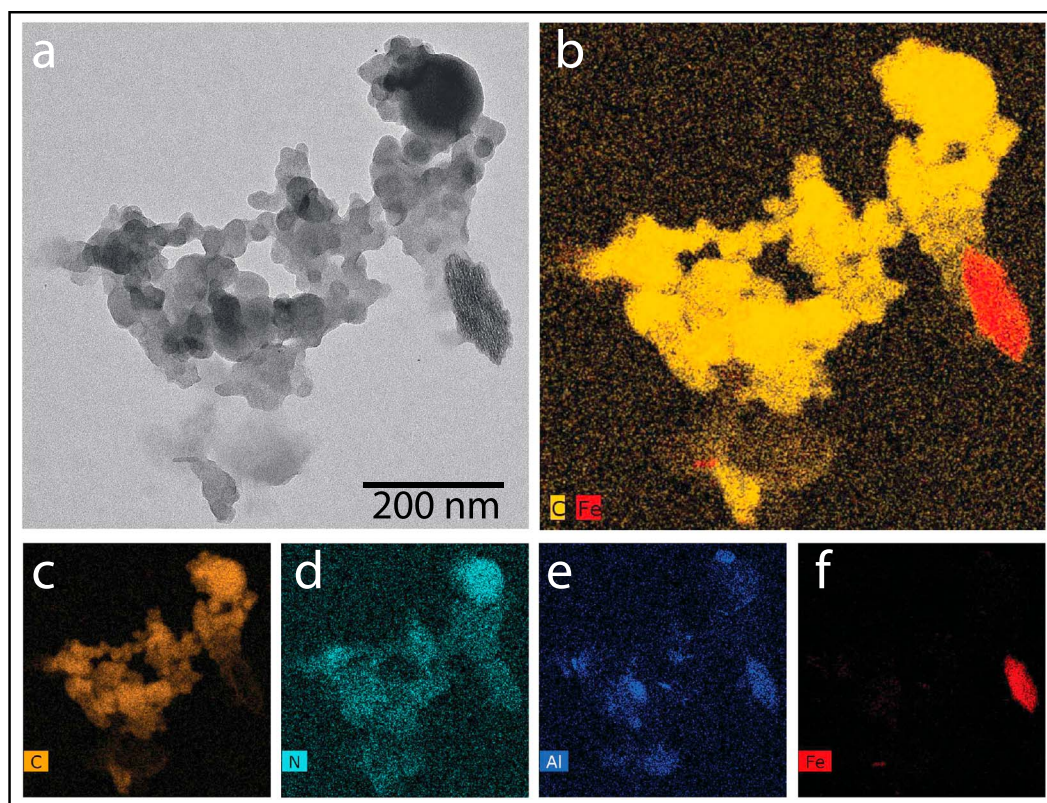


Figure 2. TEM images and STEM-EDS maps to show compositional complexity of a black carbon aggregate, from ice dated to 1838 C.E., with EDS maps taken from the same field of view as Figure 2a. (a) TEM image of BC aggregate, with tar ball incorporated into the aggregate, (b) STEM-EDS map overlay of carbon and iron, to highlight the iron particle connected with a carbon coating, (c) carbon map, (d) nitrogen map, (e) various aluminum-rich inclusions within the BC aggregate, and (f) iron map.

to the thin “film” of carbon found on remote BC aerosols by Pósfai *et al.* [1999]. EDS analysis revealed that the coatings appear to be composed predominately of amorphous carbon combined with varying amounts of nitrogen and oxygen-rich materials. These coatings appeared to be unaffected by high vacuum (10^{-5} Pa) or an 80 kV electron beam. While we have no definitive way of ascertaining when the coatings formed, it is likely that coatings are part of the atmospheric aging process and may have formed through aqueous cloud chemistry [Lee *et al.*, 2013]. The presence of oxygen in the coatings suggests that they are hydrophilic. The presence of a thin hydrophilic coating influences the BC particles’ interaction with atmospheric water, its atmospheric residence time, and optical properties.

Coated BC aggregates were routinely found in association with mineral dust particles composed of aluminum-rich silicates and iron. Magnesium, potassium, and zinc were also present in some attached minerals (Figure S6 in the supporting information). Many of the dust particles were found to be connected to the outside of BC aggregates by thin films of carbon, nitrogen, and oxygen (Figures 2b and 4), as well as being incorporated within the BC aggregate structure (Figure 3b). The external connections of the BC to the dust particles suggest that they are ice residual nuclei, as expected of wet-deposited BC in ice cores. Mineral dusts are common ice nuclei [DeMott *et al.*, 2003], and ice crystal scavenging of BC could explain the external connection [Baumgardner *et al.*, 2008].

Small iron particles (~10 nm in diameter) were often found adhered to the surface of BC aggregates (Figures 3 and 5). These attachments can be difficult to distinguish without the use of EDS or HAADF-STEM, in which heavier element inclusions stand out brightly.

BC has previously been imaged with larger dust particles in East Asian outflows [Clarke *et al.*, 2004] and African biomass burning plumes [Li *et al.*, 2003], and the results of our study show that external BC and dust

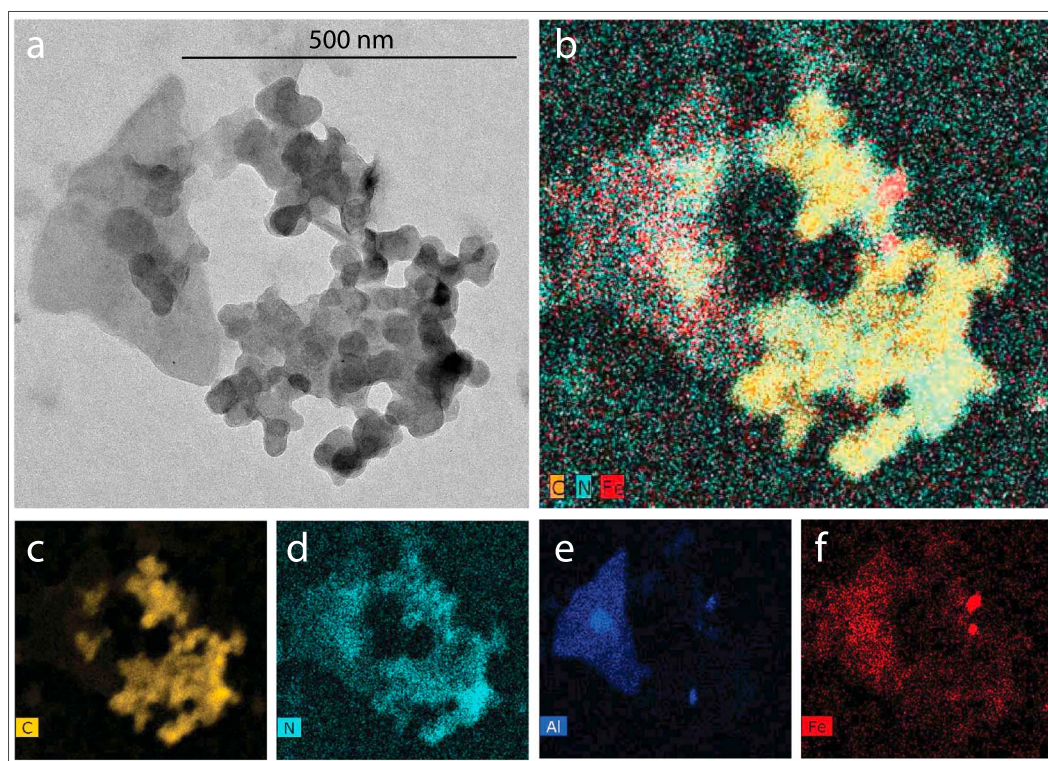


Figure 3. Dust particle and BC aggregate dated to 1838 C.E., with aluminum and iron dust particles incorporated within the BC aggregate, and EDS maps taken from the same field of view as Figure 3a. (a) TEM image, (b) carbon, nitrogen, and iron STEM-EDS maps overlaid to show the connection of the iron particles to the BC aggregate with a nitrogen-rich coating, (c–f) carbon, nitrogen, aluminum, and iron STEM-EDS maps, respectively.

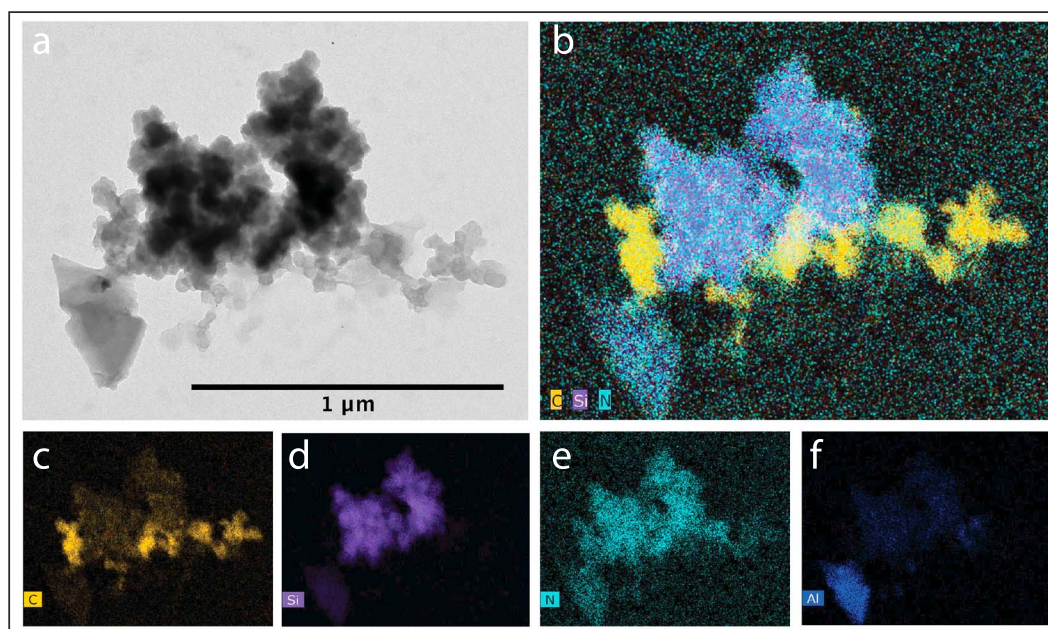


Figure 4. Large silica-rich dust particle from ice dated to 1838 C.E., with BC attached and mixed into the silica structure, with all components connected with thin (<5 nm), amorphous carbon and nitrogen-rich coating, with EDS maps taken from the same field of view as Figure 4a. (a) TEM image, (b) carbon, silicon, and nitrogen STEM-EDS maps overlaid to show connection of silicon and BC aggregates, with nitrogen-rich coating, (c–f) carbon, silicon, nitrogen, and aluminum STEM-EDS maps, respectively.

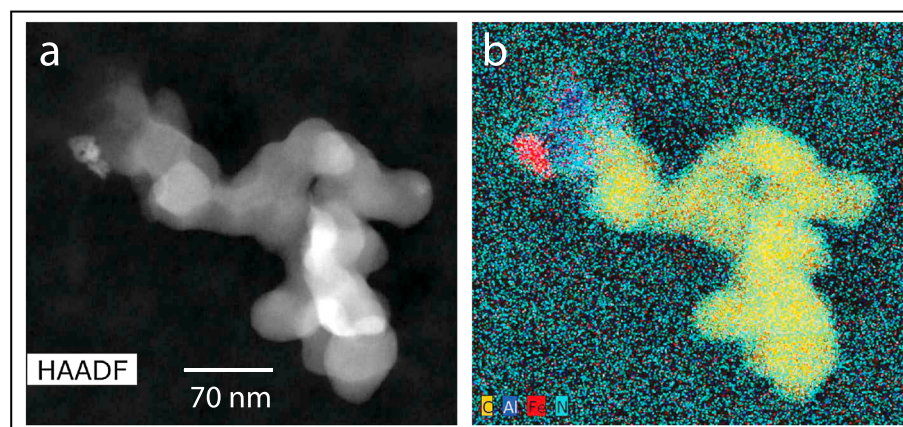


Figure 5. BC aggregate from ice dated to 1930 C.E. attached to aluminosilicate and iron particles with nitrogen-rich coating, with EDS map taken from the same field of view as Figure 5a. (a) High-angle annular dark-field (HAADF) image of the particle, (b) energy-dispersive X-ray spectroscopy (EDS) maps of C, Al, Fe, and N, indicating the aluminosilicate and iron particles are attached to the black carbon aggregate with a nitrogen-rich coating.

can be connected by insoluble coatings and can be transported long distances without disaggregating. These organic coatings and dust inclusions may have significant effects on BC's optical properties as well as functioning as cloud and ice nuclei in the atmosphere [Lohmann and Diehl, 2006].

The iron attached to the BC is of particular interest with respect to the biogeochemistry of iron in surface waters of the SH and potentially for the formation of water insoluble organic coatings through catalytic polymerization of organic species in biomass burning plumes [Slikboer *et al.*, 2015].

Tar balls, amorphous, carbon-rich spheres emitted from smoldering fires, also accompanied the BC aggregates, both attached to the outside (Figure 6) and incorporated within the BC aggregates (Figure 2). Chakrabarty *et al.* [2006b] noted the existence of tar balls in laboratory combustion tests of biomass fuels, supporting their formation at the emission source. The presence of tar balls in Antarctic ice suggests that the particles were emitted by smoldering biomass burning [Adachi and Buseck, 2011; Chakrabarty *et al.*, 2010]. To the best of our knowledge, this is the first determination of tar balls in Antarctica. They represent a previously unaccounted for component of light absorbing aerosols deposited to the Antarctic ice sheet. If tar balls are present in Antarctic ice, then they are likely present in air masses over the Southern Ocean

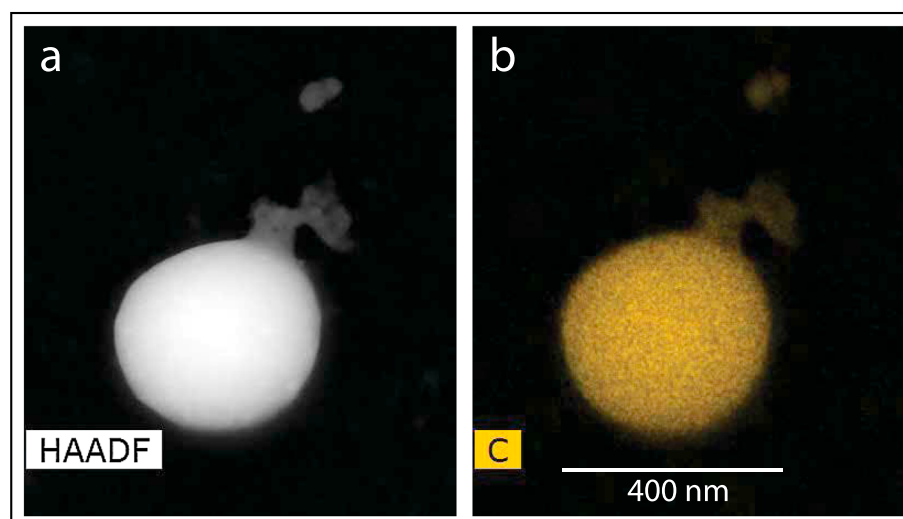


Figure 6. (a) High-angle annular dark-field (HAADF) image of a tar ball from ice dated to 1838 C.E. with BC aggregate attached, (b) EDS map of carbon from the same field of view as Figure 6a. Additional EDS maps are included in the supporting information.

and, presumably, the global troposphere. Further evidence of coatings, dust and metals, and single BC nanospheres in all samples are provided in the supporting information, as well as all additional STEM-EDS element maps for the particles described above.

4. Conclusions

In this study we found evidence for the deposition of single black carbon (BC) nanospheres over East Antarctica and northern Australia. By extrapolation, we would expect to find these particles throughout the Southern Hemisphere, if not globally. The presence of single BC nanospheres in Antarctic ice dated to 1759 C.E., prior to industrialization, suggests that the source is likely grass or bush fires. We also found tar balls and BC with nitrogen and oxygen-rich insoluble coatings and associated with mineral particles and iron. The coatings appear to cover and connect the BC and many of the mineral particles. This suggests that the coatings and dust inclusions could form in a number of ways: rapidly close to the fire source, due to aqueous chemistry, and physical and chemical ice formation processes. These mixed particles also undergo long-range transport without disaggregating. The impact of the coatings and the external and internal mixing of the mineral particles may impact BC's optical properties and residence time in the atmosphere.

Knowledge of the long-range evolution of BC aerosol characteristics is critical for predicting the associated climate forcing. Mineral inclusions, metal impurities, and insoluble, nitrogen-rich coatings suggest a complex evolution in BC optical properties during transport. The diversity of particle properties observed in this study demonstrates the complexity of BC in the environment that is as yet unaccounted for in atmospheric chemistry and climate models.

The BC particles analyzed by the study did not display discernable differences between the different time periods, which may reflect the biomass burning-dominated emissions from the Southern Hemisphere. However, the small sample number and limited time span precludes conclusions regarding any systematic changes to BC morphology from the preindustrial period through the twentieth century. Northern Hemisphere shifts from natural biomass burning to anthropogenic industrial emissions during the industrial revolution could be recorded in BC characteristics, suggesting Arctic ice core investigations as an important future application of this study.

Acknowledgments

The data used will be available online at the Australian Antarctic Data Centre repository at <https://data.aad.gov.au/>. This work was supported by Australian Antarctic Sciences grant 4144, Curtin University grant RES-SE-DAP-AW-47679-1, and ARC LIEF grant LE130100029. The authors acknowledge the use of Curtin University's Microscopy and Microanalysis Facility, whose instrumentation has been partially funded by the University, State, and Commonwealth Governments. The authors acknowledge the facilities and the scientific and technical assistance of the Australian Microscopy and Microanalysis Research Facility at the Centre for Microscopy, Characterisation and Analysis, University of Western Australia, a facility funded by the University, State, and Commonwealth Governments.

References

- Adachi, K., and P. R. Buseck (2011), Atmospheric tar balls from biomass burning in Mexico, *J. Geophys. Res.*, *116*, D05204, doi:10.1029/2010JD015102.
- Andreae, M. O., and A. Gelencsér (2006), Black carbon or brown carbon? The nature of light-absorbing carbonaceous aerosols, *Atmos. Chem. Phys.*, *6*, 3131–3148, doi:10.5194/acp-6-3131-2006.
- Baumgardner, D., R. Subramanian, C. Twohy, J. Stith, and G. Kok (2008), Scavenging of black carbon by ice crystals over the northern Pacific, *Geophys. Res. Lett.*, *35*, L22815, doi:10.1029/2008GL035764.
- Bisiaux, M. M., R. Edwards, J. R. McConnell, M. A. J. Curran, T. D. Van Ommen, A. M. Smith, T. A. Neumann, D. R. Pasteris, J. E. Penner, and K. Taylor (2012), Changes in black carbon deposition to Antarctica from two high-resolution ice core records, 1850–2000 AD, *Atmos. Chem. Phys.*, *12*, 4107–4115, doi:10.5194/acp-12-4107-2012.
- Bond, T. C., S. J. Doherty, D. Fahey, P. Forster, T. Berntsen, B. DeAngelo, M. Flanner, S. Ghan, B. Kärcher, and D. Koch (2013), Bounding the role of black carbon in the climate system: A scientific assessment, *J. Geophys. Res.: Atmos.*, *118*, 5380–5552, doi:10.1002/jgrd.50171.
- Browne, E. C., J. P. Franklin, M. R. Canagaratna, P. Massoli, T. W. Kirchstetter, D. R. Worsnop, K. R. Wilson, and J. H. Kroll (2015), Changes to the chemical composition soot from heterogeneous oxidation reactions, *J. Phys. Chem. A*, *119*, 1154–1163, doi:10.1021/jp511507d.
- Chakrabarty, R., H. Moosmüller, L.-W. Chen, K. Lewis, W. Arnott, C. Mazzoleni, M. Dubey, C. Wold, W. Hao, and S. Kreidenweis (2010), Brown carbon in tar balls from smoldering biomass combustion, *Atmos. Chem. Phys.*, *10*, 6363–6370, doi:10.5194/acp-10-6363-2010.
- Chakrabarty, R. K., H. Moosmüller, W. P. Arnott, M. A. Garro, and J. Walker (2006a), Structural and fractal properties of particles emitted from spark ignition engines, *Environ. Sci. Technol.*, *40*, 6647–6654, doi:10.1021/Es060537y.
- Chakrabarty, R. K., H. Moosmüller, M. A. Garro, W. P. Arnott, J. Walker, R. A. Susott, R. E. Babbitt, C. E. Wold, E. N. Lincoln, and W. M. Hao (2006b), Emissions from the laboratory combustion of wildland fuels: Particle morphology and size, *J. Geophys. Res.*, *111*, D07204, doi:10.1029/2005JD006659.
- Clarke, A. D., et al. (2004), Size distributions and mixtures of dust and black carbon aerosol in Asian outflow: Physicochemistry and optical properties, *J. Geophys. Res.*, *109*, D15509, doi:10.1029/2003JD004378.
- Curran, M. A., T. D. Van Ommen, and V. Morgan (1998), Seasonal characteristics of the major ions in the high-accumulation Dome Summit South ice core, Law Dome, Antarctica, *Ann. Glaciol.*, *27*, 385–390, doi:10.3198/1998AoG27-1-385-390.
- DeMott, P. J., Y. Chen, S. M. Kreidenweis, D. C. Rogers, and D. E. Sherman (1999), Ice formation by black carbon particles, *Geophys. Res. Lett.*, *26*(16), 2429–2432, doi:10.1029/1999GL900580.
- DeMott, P. J., D. J. Cziczo, A. J. Prenni, D. M. Murphy, S. M. Kreidenweis, D. S. Thomson, R. Borys, and D. C. Rogers (2003), Measurements of the concentration and composition of nuclei for cirrus formation, *Proc. Natl. Acad. Sci. U.S.A.*, *100*(25), 14,655–14,660, doi:10.1073/pnas.2532677100.

- Edwards, R., P. Sedwick, V. Morgan, and C. Boutron (2006), Iron in ice cores from Law Dome: A record of atmospheric iron deposition for maritime East Antarctica during the Holocene and Last Glacial Maximum, *Geochem. Geophys.*, *7*(12), 3907–3910, doi:10.1029/2006GC001307.
- Ellis, A., et al. (2015), Characterizing black carbon in rain and ice cores using coupled tangential flow filtration and transmission electron microscopy, *Atmos. Meas. Tech.*, *8*(9), 3959–3969, doi:10.5194/amt-8-3959-2015.
- Etheridge, D., L. Steele, R. Langenfelds, R. Francey, J. M. Barnola, and V. Morgan (1996), Natural and anthropogenic changes in atmospheric CO₂ over the last 1000 years from air in Antarctic ice and firn, *J. Geophys. Res.*, *101*(D2), 4115–4128, doi:10.1029/95JD03410.
- Franklin, R. E. (1950), On the structure of carbon, *J. Chim. Phys. Phys.-Chim. Biol.*, *47*, 573–575.
- Franklin, R. E. (1951), The structure of graphitic carbons, *Acta Crystallogr.*, *4*(3), 253–261.
- Kaufman, Y. J., D. Tanre, and O. Boucher (2002), A satellite view of aerosols in the climate system, *Nature*, *419*(6903), 215–223, doi:10.1038/nature01091.
- Kovilakam, M., and S. Mahajan (2015), Black carbon aerosol-induced Northern Hemisphere tropical expansion, *Geophys. Res. Lett.*, *42*, 4964–4972, doi:10.1002/2015GL064559.
- Lee, A. K. Y., R. Zhao, R. Li, J. Liggio, S.-M. Li, and J. P. D. Abbatt (2013), Formation of light absorbing organo-nitrogen species from evaporation of droplets containing glyoxal and ammonium sulfate, *Environ. Sci. Technol.*, *47*(22), 12,819–12,826, doi:10.1021/es402687w.
- Li, J., M. Pósfai, P. V. Hobbs, and P. R. Buseck (2003), Individual aerosol particles from biomass burning in southern Africa: 2. Compositions and aging of inorganic particles, *J. Geophys. Res.*, *108*(D13), 8484, doi:10.1029/2002JD002310.
- Lohmann, U., and K. Diehl (2006), Sensitivity studies of the importance of dust ice nuclei for the indirect aerosol effect on stratiform mixed-phase clouds, *J. Atmos. Sci.*, *63*(3), 968–982, doi:10.1175/JAS3662.1.
- McFiggans, G., et al. (2006), The effect of physical and chemical aerosol properties on warm cloud droplet activation, *Atmos. Chem. Phys.*, *6*(9), 2593–2649, doi:10.5194/acp-6-2593-2006.
- Oshima, N., M. Koike, Y. Zhang, and Y. Kondo (2009), Aging of black carbon in outflow from anthropogenic sources using a mixing state resolved model: 2. Aerosol optical properties and cloud condensation nuclei activities, *J. Geophys. Res.*, *114*, 2156–2202, doi:10.1029/2008JD011681.
- Plummer, C. T., M. A. J. Curran, T. D. van Ommen, S. O. Rasmussen, A. D. Moy, T. R. Vance, H. B. Clausen, B. M. Vinther, and P. A. Mayewski (2012), An independently dated 2000-yr volcanic record from Law Dome, East Antarctica, including a new perspective on the dating of the 1450s CE eruption of Kuwae, Vanuatu, *Clim. Past*, *8*, 1929–1940, doi:10.5194/cp-8-1929-2012.
- Pósfai, M., J. R. Anderson, P. R. Buseck, and H. Sievering (1999), Soot and sulfate aerosol particles in the remote marine troposphere, *J. Geophys. Res.*, *104*(D17), 21,685–21,693, doi:10.1029/1999JD900208.
- Pósfai, M., R. Simonics, J. Li, P. V. Hobbs, and P. R. Buseck (2003), Individual aerosol particles from biomass burning in southern Africa: 1. Compositions and size distributions of carbonaceous particles, *J. Geophys. Res.*, *108*(D13), 8483, doi:10.1029/2002JD002291.
- Rothembacher, S., A. Messerer, and G. Kasper (2008), Fragmentation and bond strength of airborne diesel soot agglomerates, *Part. Fib. Toxicol.*, *5*(9), 1, doi:10.1186/1743-8977-5-9.
- Saunders, R. W., et al. (2010), An aerosol chamber investigation of the heterogeneous ice nucleating potential of refractory nanoparticles, *Atmos. Chem. Phys.*, *10*(3), 1227–1247, doi:10.5194/acp-10-1227-2010.
- Scarnato, B. V., S. China, K. Nielsen, and C. Mazzoleni (2015), Perturbations of the optical properties of mineral dust particles by mixing with black carbon: A numerical simulation study, *Atmos. Chem. Phys.*, *15*(12), 6913–6928, doi:10.5194/acp-15-6913-2015.
- Shen, Z., J. Liu, L. Horowitz, D. Henze, S. Fan, D. Mauzerall, J.-T. Lin, and S. Tao (2014), Analysis of transpacific transport of black carbon during HIPPO-3: Implications for black carbon aging, *Atmos. Chem. Phys.*, *14*(12), 6315–6327, doi:10.5194/acp-14-6315-2014.
- Slikboer, S., L. Grandy, S. L. Blair, S. A. Nizkorodov, R. W. Smith, and H. A. Al-Abadleh (2015), Formation of light absorbing soluble secondary organics and insoluble polymeric particles from the dark reaction of catechol and guaiacol with Fe(III), *Environ. Sci. Technol.*, *49*, 7793–7801, doi:10.1021/acs.est.5b01032.
- Slowik, J. G., et al. (2007), An inter-comparison of instruments measuring black carbon content of soot particles, *Aerosol Sci. Technol.*, *41*(3), 295–314, doi:10.1080/02786820701197078.
- Smith, A. J. A., and R. G. Grainger (2014), Simplifying the calculation of light scattering properties for black carbon fractal aggregates, *Atmos. Chem. Phys.*, *14*(15), 7825–7836, doi:10.5194/acp-14-7825-2014.
- Stohl, A., and H. Sodemann (2010), Characteristics of atmospheric transport into the Antarctic troposphere, *J. Geophys. Res.*, *115*, D02305, doi:10.1029/2009JD012536.
- van Ommen, T. D., and V. Morgan (1996), Peroxide concentrations in the Dome Summit South ice core, Law Dome, Antarctica, *J. Geophys. Res.*, *101*(D10), 15,147–15,152, doi:10.1029/96JD00838.
- Wang, X., C. L. Heald, D. A. Ridley, J. P. Schwarz, J. R. Spackman, A. E. Perring, H. Coe, D. Liu, and A. D. Clarke (2014), Exploiting simultaneous observational constraints on mass and absorption to estimate the global direct radiative forcing of black carbon and brown carbon, *Atmos. Chem. Phys.*, *14*(20), 10,989–11,010, doi:10.5194/acp-14-10989-2014.
- Warren, S. G., and A. D. Clarke (1990), Soot in the atmosphere and snow surface of Antarctica, *J. Geophys. Res.*, *95*(D2), 1811–1816, doi:10.1029/JD095iD02p01811.
- Weller, R., A. Minikin, A. Petzold, D. Wagenbach, and G. König-Langlo (2013), Characterization of long-term and seasonal variations of black carbon (BC) concentrations at Neumayer, Antarctica, *Atmos. Chem. Phys.*, *13*(3), 1579–1590, doi:10.5194/acp-13-1579-2013.
- Wolff, E. W., and H. Cachier (1998), Concentrations and seasonal cycle of black carbon in aerosol at a coastal Antarctic station, *J. Geophys. Res.*, *103*(D9), 11,033–11,041, doi:10.1029/97JD01363.
- Zhu, J., P. A. Crozier, and J. R. Anderson (2013), Characterization of light-absorbing carbon particles at three altitudes in East Asian outflow by transmission electron microscopy, *Atmos. Chem. Phys.*, *13*(13), 6359–6371, doi:10.5194/acp-13-6359-2013.

Appendix D. Permissions to reproduce figures

**JOHN WILEY AND SONS LICENSE
TERMS AND CONDITIONS**

Nov 12, 2016

This Agreement between Aja Ellis ("You") and John Wiley and Sons ("John Wiley and Sons") consists of your license details and the terms and conditions provided by John Wiley and Sons and Copyright Clearance Center.

License Number	3986821386568
License date	Nov 12, 2016
Licensed Content Publisher	John Wiley and Sons
Licensed Content Publication	Journal of Geophysical Research: Atmospheres
Licensed Content Title	A technology-based global inventory of black and organic carbon emissions from combustion
Licensed Content Author	Tami C. Bond,David G. Streets,Kristen F. Yarber,Sibyl M. Nelson,Jung-Hun Woo,Zbigniew Klimont
Licensed Content Date	Jul 24, 2004
Licensed Content Pages	1
Type of use	Dissertation/Thesis
Requestor type	University/Academic
Format	Print and electronic
Portion	Figure/table
Number of figures/tables	1
Original Wiley figure/table number(s)	Figure 2
Will you be translating?	No
Title of your thesis / dissertation	History and characterization of remote southern hemisphere black carbon aerosols during the Anthropocene
Expected completion date	Nov 2016
Expected size (number of pages)	250
Requestor Location	Aja Ellis 663 Maryland Ave PITTSBURGH, PA 15232 United States Attn: Aja Ellis
Publisher Tax ID	EU826007151
Billing Type	Invoice
Billing Address	Aja Ellis 663 Maryland Ave PITTSBURGH, PA 15232 United States Attn: Aja Ellis
Total	0.00 USD

TERMS AND CONDITIONS

This copyrighted material is owned by or exclusively licensed to John Wiley & Sons, Inc. or one of its group companies (each a "Wiley Company") or handled on behalf of a society with which a Wiley Company has exclusive publishing rights in relation to a particular work (collectively "WILEY"). By clicking "accept" in connection with completing this licensing transaction, you agree that the following terms and conditions apply to this transaction (along with the billing and payment terms and conditions established by the Copyright Clearance Center Inc., ("CCC's Billing and Payment terms and conditions"), at the time that you opened your RightsLink account (these are available at any time at <http://myaccount.copyright.com>).

Terms and Conditions

- The materials you have requested permission to reproduce or reuse (the "Wiley Materials") are protected by copyright.
- You are hereby granted a personal, non-exclusive, non-sub licensable (on a stand-alone basis), non-transferable, worldwide, limited license to reproduce the Wiley Materials for the purpose specified in the licensing process. This license, **and any CONTENT (PDF or image file) purchased as part of your order**, is for a one-time use only and limited to any maximum distribution number specified in the license. The first instance of republication or reuse granted by this license must be completed within two years of the date of the grant of this license (although copies prepared before the end date may be distributed thereafter). The Wiley Materials shall not be used in any other manner or for any other purpose, beyond what is granted in the license. Permission is granted subject to an appropriate acknowledgement given to the author, title of the material/book/journal and the publisher. You shall also duplicate the copyright notice that appears in the Wiley publication in your use of the Wiley Material. Permission is also granted on the understanding that nowhere in the text is a previously published source acknowledged for all or part of this Wiley Material. Any third party content is expressly excluded from this permission.
- With respect to the Wiley Materials, all rights are reserved. Except as expressly granted by the terms of the license, no part of the Wiley Materials may be copied, modified, adapted (except for minor reformatting required by the new Publication), translated, reproduced, transferred or distributed, in any form or by any means, and no derivative works may be made based on the Wiley Materials without the prior permission of the respective copyright owner. **For STM Signatory Publishers clearing permission under the terms of the [STM Permissions Guidelines](#) only, the terms of the license are extended to include subsequent editions and for editions in other languages, provided such editions are for the work as a whole in situ and does not involve the separate exploitation of the permitted figures or extracts**, You may not alter, remove or suppress in any manner any copyright, trademark or other notices displayed by the Wiley Materials. You may not license, rent, sell, loan, lease, pledge, offer as security, transfer or assign the Wiley Materials on a stand-alone basis, or any of the rights granted to you hereunder to any other person.
- The Wiley Materials and all of the intellectual property rights therein shall at all times remain the exclusive property of John Wiley & Sons Inc, the Wiley Companies, or their respective licensors, and your interest therein is only that of having possession of and the right to reproduce the Wiley Materials pursuant to Section 2 herein during the continuance of this Agreement. You agree that you own no right, title or interest in or

to the Wiley Materials or any of the intellectual property rights therein. You shall have no rights hereunder other than the license as provided for above in Section 2. No right, license or interest to any trademark, trade name, service mark or other branding ("Marks") of WILEY or its licensors is granted hereunder, and you agree that you shall not assert any such right, license or interest with respect thereto

- NEITHER WILEY NOR ITS LICENSORS MAKES ANY WARRANTY OR REPRESENTATION OF ANY KIND TO YOU OR ANY THIRD PARTY, EXPRESS, IMPLIED OR STATUTORY, WITH RESPECT TO THE MATERIALS OR THE ACCURACY OF ANY INFORMATION CONTAINED IN THE MATERIALS, INCLUDING, WITHOUT LIMITATION, ANY IMPLIED WARRANTY OF MERCHANTABILITY, ACCURACY, SATISFACTORY QUALITY, FITNESS FOR A PARTICULAR PURPOSE, USABILITY, INTEGRATION OR NON-INFRINGEMENT AND ALL SUCH WARRANTIES ARE HEREBY EXCLUDED BY WILEY AND ITS LICENSORS AND WAIVED BY YOU.
- WILEY shall have the right to terminate this Agreement immediately upon breach of this Agreement by you.
- You shall indemnify, defend and hold harmless WILEY, its Licensors and their respective directors, officers, agents and employees, from and against any actual or threatened claims, demands, causes of action or proceedings arising from any breach of this Agreement by you.
- IN NO EVENT SHALL WILEY OR ITS LICENSORS BE LIABLE TO YOU OR ANY OTHER PARTY OR ANY OTHER PERSON OR ENTITY FOR ANY SPECIAL, CONSEQUENTIAL, INCIDENTAL, INDIRECT, EXEMPLARY OR PUNITIVE DAMAGES, HOWEVER CAUSED, ARISING OUT OF OR IN CONNECTION WITH THE DOWNLOADING, PROVISIONING, VIEWING OR USE OF THE MATERIALS REGARDLESS OF THE FORM OF ACTION, WHETHER FOR BREACH OF CONTRACT, BREACH OF WARRANTY, TORT, NEGLIGENCE, INFRINGEMENT OR OTHERWISE (INCLUDING, WITHOUT LIMITATION, DAMAGES BASED ON LOSS OF PROFITS, DATA, FILES, USE, BUSINESS OPPORTUNITY OR CLAIMS OF THIRD PARTIES), AND WHETHER OR NOT THE PARTY HAS BEEN ADVISED OF THE POSSIBILITY OF SUCH DAMAGES. THIS LIMITATION SHALL APPLY NOTWITHSTANDING ANY FAILURE OF ESSENTIAL PURPOSE OF ANY LIMITED REMEDY PROVIDED HEREIN.
- Should any provision of this Agreement be held by a court of competent jurisdiction to be illegal, invalid, or unenforceable, that provision shall be deemed amended to achieve as nearly as possible the same economic effect as the original provision, and the legality, validity and enforceability of the remaining provisions of this Agreement shall not be affected or impaired thereby.
- The failure of either party to enforce any term or condition of this Agreement shall not constitute a waiver of either party's right to enforce each and every term and condition of this Agreement. No breach under this agreement shall be deemed waived or excused by either party unless such waiver or consent is in writing signed by the party granting such waiver or consent. The waiver by or consent of a party to a breach of any provision of this Agreement shall not operate or be construed as a waiver of or consent to any other or subsequent breach by such other party.

- This Agreement may not be assigned (including by operation of law or otherwise) by you without WILEY's prior written consent.
- Any fee required for this permission shall be non-refundable after thirty (30) days from receipt by the CCC.
- These terms and conditions together with CCC's Billing and Payment terms and conditions (which are incorporated herein) form the entire agreement between you and WILEY concerning this licensing transaction and (in the absence of fraud) supersedes all prior agreements and representations of the parties, oral or written. This Agreement may not be amended except in writing signed by both parties. This Agreement shall be binding upon and inure to the benefit of the parties' successors, legal representatives, and authorized assigns.
- In the event of any conflict between your obligations established by these terms and conditions and those established by CCC's Billing and Payment terms and conditions, these terms and conditions shall prevail.
- WILEY expressly reserves all rights not specifically granted in the combination of (i) the license details provided by you and accepted in the course of this licensing transaction, (ii) these terms and conditions and (iii) CCC's Billing and Payment terms and conditions.
- This Agreement will be void if the Type of Use, Format, Circulation, or Requestor Type was misrepresented during the licensing process.
- This Agreement shall be governed by and construed in accordance with the laws of the State of New York, USA, without regards to such state's conflict of law rules. Any legal action, suit or proceeding arising out of or relating to these Terms and Conditions or the breach thereof shall be instituted in a court of competent jurisdiction in New York County in the State of New York in the United States of America and each party hereby consents and submits to the personal jurisdiction of such court, waives any objection to venue in such court and consents to service of process by registered or certified mail, return receipt requested, at the last known address of such party.

WILEY OPEN ACCESS TERMS AND CONDITIONS

Wiley Publishes Open Access Articles in fully Open Access Journals and in Subscription journals offering Online Open. Although most of the fully Open Access journals publish open access articles under the terms of the Creative Commons Attribution (CC BY) License only, the subscription journals and a few of the Open Access Journals offer a choice of Creative Commons Licenses. The license type is clearly identified on the article.

The Creative Commons Attribution License

The [Creative Commons Attribution License \(CC-BY\)](#) allows users to copy, distribute and transmit an article, adapt the article and make commercial use of the article. The CC-BY license permits commercial and non-

Creative Commons Attribution Non-Commercial License

The [Creative Commons Attribution Non-Commercial \(CC-BY-NC\) License](#) permits use, distribution and reproduction in any medium, provided the original work is properly cited and is not used for commercial purposes.(see below)

Creative Commons Attribution-Non-Commercial-NoDerivs License

The [Creative Commons Attribution Non-Commercial-NoDerivs License](#) (CC-BY-NC-ND) permits use, distribution and reproduction in any medium, provided the original work is

properly cited, is not used for commercial purposes and no modifications or adaptations are made. (see below)

Use by commercial "for-profit" organizations

Use of Wiley Open Access articles for commercial, promotional, or marketing purposes requires further explicit permission from Wiley and will be subject to a fee.

Further details can be found on Wiley Online Library

<http://olabout.wiley.com/WileyCDA/Section/id-410895.html>

Other Terms and Conditions:

v1.10 Last updated September 2015

Questions? customercare@copyright.com or +1-855-239-3415 (toll free in the US) or +1-978-646-2777.



RightsLink®

[Home](#)
[Create Account](#)
[Help](#)


WILEY

Title: Bounding the role of black carbon in the climate system: A scientific assessment

Author: T. C. Bond, S. J. Doherty, D. W. Fahey, P. M. Forster, T. Berntsen, B. J. DeAngelo, M. G. Flanner, S. Ghan, B. Kärcher, D. Koch, S. Kinne, Y. Kondo, P. K. Quinn, M. C. Sarofim, M. G. Schultz, M. Schulz, C. Venkataraman, H. Zhang, S. Zhang, N. Bellouin, S. K. Guttikunda, P. K. Hopke, M. Z. Jacobson, J. W. Kaiser, Z. Klimont, U. Lohmann, J. P. Schwarz, D. Shindell, T. Storelvmo, S. G. Warren, C. S. Zender

Publication: Journal of Geophysical Research: Atmospheres

Publisher: John Wiley and Sons

Date: Jun 6, 2013

©2013 The Authors. Journal of Geophysical Research: Atmospheres published by Wiley on behalf of the American Geophysical Union.

[LOGIN](#)

If you're a **copyright.com user**, you can login to RightsLink using your copyright.com credentials. Already a **RightsLink user** or want to [learn more?](#)

Open Access Article

This article is available under the terms of the Creative Commons Attribution Non-Commercial No Derivatives License CC BY-NC-ND (which may be updated from time to time) and permits **non-commercial** use, distribution, and reproduction in any medium, without alteration, provided the original work is properly cited and it is reproduced verbatim.

For an understanding of what is meant by the terms of the Creative Commons License, please refer to [Wiley's Open Access Terms and Conditions](#).

Permission is not required for **non-commercial** reuse. For **commercial** reuse, please hit the "back" button and select the most appropriate **commercial** requestor type before completing your order.

If you wish to adapt, alter, translate or create any other derivative work from this article, permission must be sought from the Publisher. Please email your requirements to RightsLink@wiley.com.

[BACK](#)
[CLOSE WINDOW](#)

Copyright © 2016 [Copyright Clearance Center, Inc.](#) All Rights Reserved. [Privacy statement](#). [Terms and Conditions](#). Comments? We would like to hear from you. E-mail us at customercare@copyright.com

**JOHN WILEY AND SONS LICENSE
TERMS AND CONDITIONS**

Nov 12, 2016

This Agreement between Aja Ellis ("You") and John Wiley and Sons ("John Wiley and Sons") consists of your license details and the terms and conditions provided by John Wiley and Sons and Copyright Clearance Center.

License Number	3986121376220
License date	Nov 11, 2016
Licensed Content Publisher	John Wiley and Sons
Licensed Content Publication	Journal of Geophysical Research: Atmospheres
Licensed Content Title	Shapes of soot aerosol particles and implications for their effects on climate
Licensed Content Author	Kouji Adachi,Serena H. Chung,Peter R. Buseck
Licensed Content Date	Aug 14, 2010
Licensed Content Pages	1
Type of use	Dissertation/Thesis
Requestor type	University/Academic
Format	Print and electronic
Portion	Figure/table
Number of figures/tables	1
Original Wiley figure/table number(s)	Figure 5
Will you be translating?	No
Title of your thesis / dissertation	History and characterization of remote southern hemisphere black carbon aerosols during the Anthropocene
Expected completion date	Nov 2016
Expected size (number of pages)	250
Requestor Location	Aja Ellis 663 Maryland Ave PITTSBURGH, PA 15232 United States Attn: Aja Ellis
Publisher Tax ID	EU826007151
Billing Type	Invoice
Billing Address	Aja Ellis 663 Maryland Ave PITTSBURGH, PA 15232 United States Attn: Aja Ellis
Total	0.00 USD

TERMS AND CONDITIONS

This copyrighted material is owned by or exclusively licensed to John Wiley & Sons, Inc. or one of its group companies (each a "Wiley Company") or handled on behalf of a society with which a Wiley Company has exclusive publishing rights in relation to a particular work (collectively "WILEY"). By clicking "accept" in connection with completing this licensing transaction, you agree that the following terms and conditions apply to this transaction (along with the billing and payment terms and conditions established by the Copyright Clearance Center Inc., ("CCC's Billing and Payment terms and conditions"), at the time that you opened your RightsLink account (these are available at any time at <http://myaccount.copyright.com>).

Terms and Conditions

- The materials you have requested permission to reproduce or reuse (the "Wiley Materials") are protected by copyright.
- You are hereby granted a personal, non-exclusive, non-sub licensable (on a stand-alone basis), non-transferable, worldwide, limited license to reproduce the Wiley Materials for the purpose specified in the licensing process. This license, **and any CONTENT (PDF or image file) purchased as part of your order**, is for a one-time use only and limited to any maximum distribution number specified in the license. The first instance of republication or reuse granted by this license must be completed within two years of the date of the grant of this license (although copies prepared before the end date may be distributed thereafter). The Wiley Materials shall not be used in any other manner or for any other purpose, beyond what is granted in the license. Permission is granted subject to an appropriate acknowledgement given to the author, title of the material/book/journal and the publisher. You shall also duplicate the copyright notice that appears in the Wiley publication in your use of the Wiley Material. Permission is also granted on the understanding that nowhere in the text is a previously published source acknowledged for all or part of this Wiley Material. Any third party content is expressly excluded from this permission.
- With respect to the Wiley Materials, all rights are reserved. Except as expressly granted by the terms of the license, no part of the Wiley Materials may be copied, modified, adapted (except for minor reformatting required by the new Publication), translated, reproduced, transferred or distributed, in any form or by any means, and no derivative works may be made based on the Wiley Materials without the prior permission of the respective copyright owner. **For STM Signatory Publishers clearing permission under the terms of the [STM Permissions Guidelines](#) only, the terms of the license are extended to include subsequent editions and for editions in other languages, provided such editions are for the work as a whole in situ and does not involve the separate exploitation of the permitted figures or extracts**, You may not alter, remove or suppress in any manner any copyright, trademark or other notices displayed by the Wiley Materials. You may not license, rent, sell, loan, lease, pledge, offer as security, transfer or assign the Wiley Materials on a stand-alone basis, or any of the rights granted to you hereunder to any other person.
- The Wiley Materials and all of the intellectual property rights therein shall at all times remain the exclusive property of John Wiley & Sons Inc, the Wiley Companies, or their respective licensors, and your interest therein is only that of having possession of and the right to reproduce the Wiley Materials pursuant to Section 2 herein during the continuance of this Agreement. You agree that you own no right, title or interest in or to the Wiley Materials or any of the intellectual property rights therein. You shall have

no rights hereunder other than the license as provided for above in Section 2. No right, license or interest to any trademark, trade name, service mark or other branding ("Marks") of WILEY or its licensors is granted hereunder, and you agree that you shall not assert any such right, license or interest with respect thereto

- NEITHER WILEY NOR ITS LICENSORS MAKES ANY WARRANTY OR REPRESENTATION OF ANY KIND TO YOU OR ANY THIRD PARTY, EXPRESS, IMPLIED OR STATUTORY, WITH RESPECT TO THE MATERIALS OR THE ACCURACY OF ANY INFORMATION CONTAINED IN THE MATERIALS, INCLUDING, WITHOUT LIMITATION, ANY IMPLIED WARRANTY OF MERCHANTABILITY, ACCURACY, SATISFACTORY QUALITY, FITNESS FOR A PARTICULAR PURPOSE, USABILITY, INTEGRATION OR NON-INFRINGEMENT AND ALL SUCH WARRANTIES ARE HEREBY EXCLUDED BY WILEY AND ITS LICENSORS AND WAIVED BY YOU.
- WILEY shall have the right to terminate this Agreement immediately upon breach of this Agreement by you.
- You shall indemnify, defend and hold harmless WILEY, its Licensors and their respective directors, officers, agents and employees, from and against any actual or threatened claims, demands, causes of action or proceedings arising from any breach of this Agreement by you.
- IN NO EVENT SHALL WILEY OR ITS LICENSORS BE LIABLE TO YOU OR ANY OTHER PARTY OR ANY OTHER PERSON OR ENTITY FOR ANY SPECIAL, CONSEQUENTIAL, INCIDENTAL, INDIRECT, EXEMPLARY OR PUNITIVE DAMAGES, HOWEVER CAUSED, ARISING OUT OF OR IN CONNECTION WITH THE DOWNLOADING, PROVISIONING, VIEWING OR USE OF THE MATERIALS REGARDLESS OF THE FORM OF ACTION, WHETHER FOR BREACH OF CONTRACT, BREACH OF WARRANTY, TORT, NEGLIGENCE, INFRINGEMENT OR OTHERWISE (INCLUDING, WITHOUT LIMITATION, DAMAGES BASED ON LOSS OF PROFITS, DATA, FILES, USE, BUSINESS OPPORTUNITY OR CLAIMS OF THIRD PARTIES), AND WHETHER OR NOT THE PARTY HAS BEEN ADVISED OF THE POSSIBILITY OF SUCH DAMAGES. THIS LIMITATION SHALL APPLY NOTWITHSTANDING ANY FAILURE OF ESSENTIAL PURPOSE OF ANY LIMITED REMEDY PROVIDED HEREIN.
- Should any provision of this Agreement be held by a court of competent jurisdiction to be illegal, invalid, or unenforceable, that provision shall be deemed amended to achieve as nearly as possible the same economic effect as the original provision, and the legality, validity and enforceability of the remaining provisions of this Agreement shall not be affected or impaired thereby.
- The failure of either party to enforce any term or condition of this Agreement shall not constitute a waiver of either party's right to enforce each and every term and condition of this Agreement. No breach under this agreement shall be deemed waived or excused by either party unless such waiver or consent is in writing signed by the party granting such waiver or consent. The waiver by or consent of a party to a breach of any provision of this Agreement shall not operate or be construed as a waiver of or consent to any other or subsequent breach by such other party.

- This Agreement may not be assigned (including by operation of law or otherwise) by you without WILEY's prior written consent.
- Any fee required for this permission shall be non-refundable after thirty (30) days from receipt by the CCC.
- These terms and conditions together with CCC's Billing and Payment terms and conditions (which are incorporated herein) form the entire agreement between you and WILEY concerning this licensing transaction and (in the absence of fraud) supersedes all prior agreements and representations of the parties, oral or written. This Agreement may not be amended except in writing signed by both parties. This Agreement shall be binding upon and inure to the benefit of the parties' successors, legal representatives, and authorized assigns.
- In the event of any conflict between your obligations established by these terms and conditions and those established by CCC's Billing and Payment terms and conditions, these terms and conditions shall prevail.
- WILEY expressly reserves all rights not specifically granted in the combination of (i) the license details provided by you and accepted in the course of this licensing transaction, (ii) these terms and conditions and (iii) CCC's Billing and Payment terms and conditions.
- This Agreement will be void if the Type of Use, Format, Circulation, or Requestor Type was misrepresented during the licensing process.
- This Agreement shall be governed by and construed in accordance with the laws of the State of New York, USA, without regards to such state's conflict of law rules. Any legal action, suit or proceeding arising out of or relating to these Terms and Conditions or the breach thereof shall be instituted in a court of competent jurisdiction in New York County in the State of New York in the United States of America and each party hereby consents and submits to the personal jurisdiction of such court, waives any objection to venue in such court and consents to service of process by registered or certified mail, return receipt requested, at the last known address of such party.

WILEY OPEN ACCESS TERMS AND CONDITIONS

Wiley Publishes Open Access Articles in fully Open Access Journals and in Subscription journals offering Online Open. Although most of the fully Open Access journals publish open access articles under the terms of the Creative Commons Attribution (CC BY) License only, the subscription journals and a few of the Open Access Journals offer a choice of Creative Commons Licenses. The license type is clearly identified on the article.

The Creative Commons Attribution License

The [Creative Commons Attribution License \(CC-BY\)](#) allows users to copy, distribute and transmit an article, adapt the article and make commercial use of the article. The CC-BY license permits commercial and non-

Creative Commons Attribution Non-Commercial License

The [Creative Commons Attribution Non-Commercial \(CC-BY-NC\) License](#) permits use, distribution and reproduction in any medium, provided the original work is properly cited and is not used for commercial purposes.(see below)

Creative Commons Attribution-Non-Commercial-NoDerivs License

The [Creative Commons Attribution Non-Commercial-NoDerivs License](#) (CC-BY-NC-ND) permits use, distribution and reproduction in any medium, provided the original work is

properly cited, is not used for commercial purposes and no modifications or adaptations are made. (see below)

Use by commercial "for-profit" organizations

Use of Wiley Open Access articles for commercial, promotional, or marketing purposes requires further explicit permission from Wiley and will be subject to a fee.

Further details can be found on Wiley Online Library

<http://olabout.wiley.com/WileyCDA/Section/id-410895.html>

Other Terms and Conditions:

v1.10 Last updated September 2015

Questions? customercare@copyright.com or +1-855-239-3415 (toll free in the US) or +1-978-646-2777.
